Universität Bremen

marum

# Mud volcanism and fluid seepage at Venere mud volcano in the Calabrian Accretionary Prism (Central Mediterranean)

Dissertation

zur Erlangung des
Doktorgrades der Naturwissenschaften
Doctor rerum naturalium
(Dr. rer. nat.)

am Fachbereich Geowissenschaften
der Universität Bremen

vorgelegt von
**Markus Loher**

Bremen, September 2017

**Gutachter**

Prof. Dr. Gerhard Bohrmann
Universität Bremen
MARUM – Zentrum für Marine Umweltwissenschaften
Klagenfurter Strasse 2–4
28359 Bremen, Deutschland

Prof. Dr. Helmut Weissert
ETH Zürich (Swiss Federal Institute of Technology)
Sonneggstrasse 5
8092 Zürich, Schweiz

Datum des Kolloquiums: 13. Dezember 2017

Date of defense: 13 December 2017

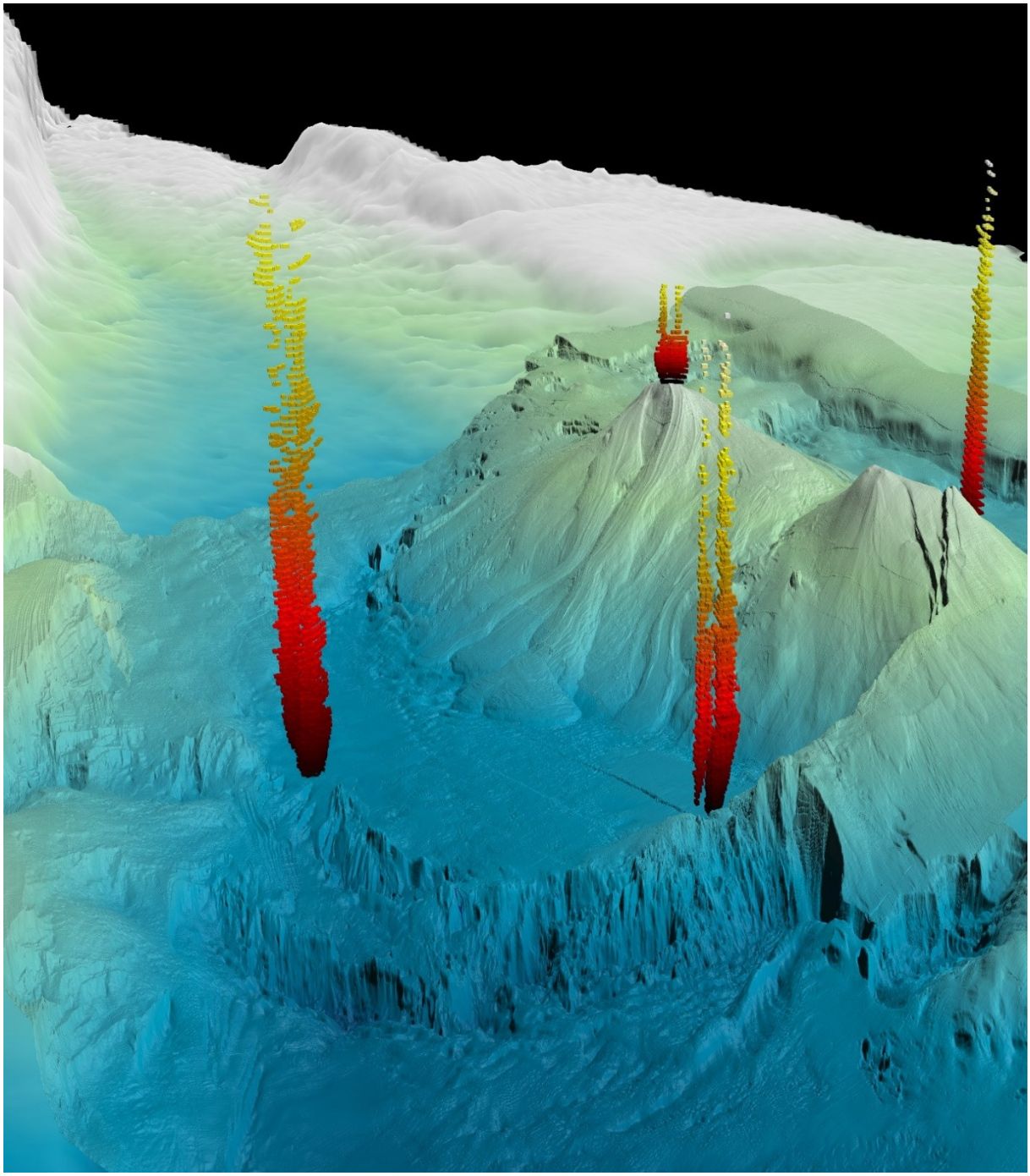

Perspective view (to the West) on Venere mud volcano in the Squillace Canyon at ~1600 m water depth in the Ionian Sea (Central Mediterranean). The twin cones are 100 m high and situated ~1200 m apart in a caldera. Gas flares (shown in red and yellow colors) rise from the western summit and from peripheral seeps along the caldera edge. Mudflows extend from the western summit and spread onto flat areas at the foot of the slope. High-resolution bathymetry, acquired by autonomous underwater vehicle MARUM-SEAL 5000, is draped on bathymetry obtained from RV METEOR.

## Preface

The oceans of the Earth still hold a wealth of hidden landscapes, since less than 20% (<72'400'000 $km^2$) of the global seafloor has been mapped at resolutions better than a few kilometers (e.g. Sandwell et al. (2014)). In contrast, the dwarf planet Pluto in the outer reaches of our solar system witnessed the arrival of NASA's New Horizons spacecraft on 14 July 2015. A flyby revealed the surface of Pluto (approximately 16'650'000 $km^2$) at a resolution of several hundred meters (Moore et al., 2016). Stunning images of ice-driven volcanoes reached Earth after a time of one third of my PhD project, which I carried out during three years (October 2014 to September 2017).

The cruises related to my PhD project involved the acquisition of roughly 100'000 $km^2$ of new seafloor maps. Among this large area is a patch of 29 $km^2$ in 1600 meters water depth in the Calabrian Accretionary Prism (Central Mediterranean), which has been mapped at resolutions better than 1 meter by an autonomous underwater vehicle. It reveals the twin-cones and caldera of Venere mud volcano in the Squillace Canyon. The possibility to zoom-in to such great detail and the clear evidence of ongoing fluid seepage make this one of the few deep-sea mud volcanoes where the recently-past development and ongoing activity can be studied. Furthermore, understanding fluid seepage at Venere mud volcano may represent a key to address outstanding questions regarding fluid generation and migration in the Calabrian Accretionary Prism and its effect on seafloor morphology. This led to the decision to make Venere mud volcano the main focus of my PhD studies and the findings of these investigations are presented in the following cumulative thesis. The results of this work contribute to the project "Geosphere-Biosphere Interactions" (GB) supported by the Deutsche Forschungsgemeinschaft (DFG) and the Research Center / Excellence Cluster "The Ocean in the Earth System".

While studying Venere mud volcano, I came to realize that the Roman god "Vulcanus" may not only have had his smithy under Mount Etna but also at the muddy forge of his wife "Venus".

## Table of contents

## List of Abbreviations

| | |
|---|---|
| AOM | Anaerobic Oxidation of Methane |
| AUV | Autonomous Underwater Vehicle |
| CAP | Calabrian Accretionary Prism |
| GBS | Gas Bubble Sampler |
| GHOZ | Gas Hydrate Occurrence Zone |
| GHSZ | Gas Hydrate Stability Zone |
| GIS | Geographic Information System |
| GC / GC-T | Gravity Core / GC equipped by temperature loggers |
| $C_{2+}$ | Hydrocarbons of higher molecular weight than methane |
| kHz | Kilohertz |
| LAPM | Large Area Photo Mosaicking (Tool) |
| mbsf | meters below sea floor |
| mbsl | meters below sea level |
| $C_1$ / $CH_4$ | Methane |
| MO | Methane Oxidation (aerobic) |
| MTL | Miniature Temperature Loggers |
| MV | Mud Volcano |
| MBES | Multibeam Echosounder |
| NDSF | Nile Deep Sea Fan |
| ROV | Remotely Operated Vehicle |
| Tg | Tera gram ($10^{12}$g) |
| USBL | Ultra-Short-Baseline |
| VPDB | Vienna Pee Dee Belemnite |
| VSMOW | Vienna Standard Mean Ocean Water |

General note: Most abbreviations will be introduced again at the beginning of the introduction of this thesis and again with each of the main manuscripts since they are aimed for a standalone format.

## Abstract

Cold seeps are the natural expression of focused upward flow and release of gases, liquids, solids, or a combination of components, which are sourced from subsurface sediments and are emitted at temperatures comparable to surface values. The involved fluids typically consist of hydrocarbon-rich gas or pore waters and they can support the development of chemosynthesis-based organisms and induce the precipitation of authigenic carbonate deposits. Mud volcanoes (MVs) are large cold seep systems, occur globally, and involve the mobilization and extrusion of mud breccia: a mixture of gas (predominantly methane), water, fluid-rich sediments and rock clasts.

Understanding the processes that generate, transport, and discharge fluids and solids at the geosphere-hydrosphere interface is important, since they are part of global material recycling, impact the development of submarine ecosystems, influence sediment dynamics and stability of the seafloor, and potentially point to the occurrence of energy resources. MVs have feeder systems that pierce kilometer-thick sedimentary columns. Studying the composition of seeping fluids and extruded solids can, therefore, provide insights into subsurface processes inaccessible for direct sampling. The driving mechanisms and amounts of discharging material from deep sea cold seeps and specifically from MVs are not well understood and poorly constrained. Although MVs do occur on land, they are most abundant in offshore locations characterized by tectonic compression and rapid sediment accumulation. In the Calabrian Accretionary Prism (CAP; Central Mediterranean), the occurrence of numerous of MVs has only recently been documented. However, open questions remain with regard to the nature of the fluids involved and ongoing activity, to how active the MVs really are, and to how they evolved over time. Therefore, the CAP is considered to be a frontier region for research on past and recent mud volcanism and fluid seepage.

This work has the aim of investigating the processes that govern the activity and evolution of submarine MVs and associated cold seeps by studying Venere MV, as an example. This MV is located within a deep-sea canyon at 1600 m water depth in a forearc basin of the CAP. The presented results and conclusions are based on data from two research cruises (RV METEOR M112 and RV POSEIDON POS499). They were obtained by multiple methods, including: Hydroacoustic seafloor and water column measurements by ship and an autonomous underwater vehicle (AUV); visual observations, photo-mosaicking, and geological sampling by a remotely operated vehicle (ROV); sediment coring techniques including cores taken under in-situ pressures. In addition, various analyses (e.g. stable isotope analyses, XRF scans, WDS analyses, etc.) were carried out post-cruise on selected samples.

A first study focusses on the overall structure of Venere MV including its caldera, the ongoing activity (mud breccia extrusion and gas release), the involved fluid sources, and the distribution of chemosynthetic ecosystems around the MV edifice. Two different but co-existing fluid discharge mechanisms can be characterized: 1) extrusion of mud breccia from a conduit at the summit, containing thermogenic methane and freshened pore waters

indicative of a deep-source (>3.5 km) and 2) hydrocarbon release at peripheral seeps hosting cold-seep ecosystems and authigenic carbonates along inward-dipping ring faults at the caldera edge. The results are argued to support a model of upward branching fluid discharge and to point to persistently high subsurface pore fluid pressures governing coeval gas release and extrusive activity.

A second study investigates the morpho-structural and spatio-temporal evolution of the twin-cone Venere MV and the surrounding seafloor of the canyon. The surface extents of mudflows are mapped and mudflow volumes are determined based on AUV-derived bathymetry and backscatter data. The burial of these mudflows by hemipelagic sediment indicate that they were emplacement between >4000 years ago and the present. Estimates of the extrusion rates range between 5000 and 47000 $m^3$/year. The interpretation of the seafloor morphologies, sediment deposits, and cold seep structures support the main conclusions that Venere MV experienced moderately extrusive but relatively continuous activity throughout the last centuries and that past sediment transport processes in the canyon affected its overall morphology.

A third study consists of detailed seafloor observations at four peripheral seeps of Venere MV showing different degrees of authigenic carbonate formation and settlement by chemosynthesis-based organisms such as filamentous microbial mats, vesicomyid clams, and tubeworms. Photo mosaics are used to classify different seafloor facies, sites of gas bubble release from soft sediments, flat carbonate pavements, mounded and ruptured carbonate domes, as well as crater-like collapse features. The observations indicate an evolution from plain to colonized seeps in soft sediments, to carbonate pavements that trap fluids, to ruptured but colonized structures, over decadal, centennial, and millennial timescales, respectively.

In conclusion, the ongoing activity and fluid sources of Venere MV and the evolution of its surface expression, including that of the peripheral cold seeps, have been studied in unprecedented detail. The state-of-the-art AUV- and ROV-based surveys have been complemented by systematic geological sampling and analyses of sediments and pore fluids. This work presents previously unknown details on geological, geochemical, and biological processes that govern mudflow extrusions and fluid seepage not only relevant to the CAP, but also to MVs and cold-seep systems globally.

## Zusammenfassung

Kalte Quellen sind natürliche Erscheinungen von fokussiertem, aufwärts gerichtetem Fluss und Austritt von Gasen, Flüssigkeiten, Feststoffen oder einer Kombination dieser Komponenten, aus dem sedimentären Untergrund. Die Austrittstemperaturen der Komponenten sind typischerweise vergleichbar mit der Umgebungstemperatur an der Oberfläche. Die involvierten Fluide bestehen grösstenteils aus kohlenwasserstoffreichem Gas oder Porenwasser. Diese ermöglichen, dass sich chemosynthetische Organismen entwickeln und zusätzlich, dass authigen gebildete Karbonate ausgefällt werden. Schlammvulkane sind grosse, global auftretende, kalte Quellen und gehen mit der Mobilisierung und dem Austritt von Schlammbreckzie einher, welche aus einer Mixtur aus Gas, Wasser, fluidreichem Sediment und Gesteinsfragmenten besteht.

Es ist wichtig, die Prozesse zu verstehen, welche zur Entstehung, zum Transport und zum Austritt der Fluide und Festkomponenten am Kontakt zwischen Geosphäre und Hydrosphäre führen. Diese sind nämlich Teil eines globalen Materialkreislaufs, beeinflussen die Entstehung von submarinen Ökosystemen sowie die Sedimentdynamik und Stabilität am Meeresboden und sind mögliche Anzeiger von Energieressourcen. Schlammvulkane haben Förderschlote, welche kilometerdicke Sedimentlagen durchqueren. Untersuchungen an der Zusammensetzung der austretenden Fluide und Festkomponenten können Einsicht in tiefreichende Prozesse geben. Allerdings sind die treibenden Mechanismen und die Menge von austretendem Material an kalten Quellen und besonders an Schlammvulkanen nicht gut verstanden und schlecht untersucht. Schlammvulkane kommen an Land vor aber im marinen Bereiche sind sie deutlich weiter verbreitet. Sie entstehen bevorzugt in Gebieten mit kompressiver Tektonik und in Regionen mit einer hohen Sedimentakkumulation. Im kalabrischen Akkretionskeil (zentrales Mittelmeer) wurde erst kürzlich eine grosse Anzahl Schlammvulkane dokumentiert. Allerdings gibt es noch offene Fragen in Bezug zur Zusammensetzung der Fluide, die in ihrer Entstehung und Aktivität beteiligt sind, wie aktiv die Schlammvulkane wirklich sind und wie sie sich im Laufe der Zeit entwickelt haben. Der kalabrische Akkretionskeil gilt deshalb als eine Region in der noch viel Neues über vergangene und jüngste Schlammvulkanaktivität und Fluidfluss erforscht werden kann.

Diese Arbeit hat zum Ziel, die Prozesse zu untersuchen, welche die Aktivität und die Entwicklung von submarinen Schlammvulkanen und den damit verbundenen kalten Quellen beeinflussen. Dies soll am Beispiel des Venere Schlammvulkans geschehen, der sich in einem Tiefsee-Canyon im Forearc-Becken des kalabrischen Akkretionskeils befindet. Die dargestellten Ergebnisse und Schlussfolgerungen basieren auf Daten von zwei Forschungsfahrten (RV METEOR M112 und RV POSEIDON POS499). Es wurden mehrere Methoden angewandt um die hier vorgelegten Resultate zu erzielen; unter anderen: hydroakustische Meeresboden- und Wassersäulenmessungen per Schiff sowie durch ein autonomes Unterwasserfahrzeug (AUV); visuelle Beobachtungen, Foto Mosaiks und geologische Probenahme durch ein ferngesteuertes Unterwasserfahrzeug (ROV); Sedimentkern-Techniken einschliesslich Kerne, die unter in-situ Druck genommen wurden;

und letztlich ausgewählte Messungen an den gesammelten Proben (z. B. stabile Isotopenanalysen, XRF Scans, WDS Analysen).

Eine erste Studie konzentriert sich auf die Gesamtstruktur des Venere Schlammvulkans einschliesslich seiner Caldera, der laufenden Aktivität (Ausfluss von Schlammbreckzie und Gasaustritte), der beteiligten Fluidquellen und der Verteilung der Chemosynthese-basierten Ökosysteme um den Schlammvulkan. Zwei verschiedene aber koexistierende Fluidaustrittmechanismen können charakterisiert werden: 1) Austritt von Schlammbrekzien aus einem Förderschlot am Gipfel des Schlammvulkans, welche thermogenes Methan und ausgesüsstes Porenwasser enthalten, was auf eine tiefe Quelle (>3,5 km) hinweist, und 2) Austritte von Kohlewasserstoffen bei randlichen, kalten Quellen mit chemosynthetischen Organismen und authigenen Karbonaten entlang von konzentrischen Bruchzonen am Rand der Caldera. Gestützt auf diese Ergebnisse ergibt sich ein konzeptionelles Modell in welchem sich der Fluidtransport gegen oben hin verzweigt und wobei dank anhaltendem, hohen Porendruck gleichzeitig Schlammbreckzie am Gipfel und Gas am Rand der Caldera ausgestossen werden.

Eine zweite Studie untersucht die morpho-strukturelle und räumlich-zeitliche Entwicklung der beiden Kegel vom Venere Schlammvulkan und des umliegenden Meeresbodens im Tiefsee-Canyon. Die Oberflächen der Schlammflüsse werden auskartiert und deren Volumina anhand von AUV-basierten Bathymetrie- und Rückstreuungsdaten bestimmt. Die Bedeckung dieser Schlammflüsse durch hemipelagische Sedimente deutet darauf hin, dass sie zwischen 4000 Jahren und der Gegenwart abgelagert wurden. Schätzungen der Extrusionsraten liegen zwischen 5000 und 47000 $m^3$/Jahr. Die Interpretation der Meeresbodenmorphologien, der Sedimentablagerungen und der kalten Quellen führt zu den folgenden Schlussfolgerungen: der Venere Schlammvulkan zeigte während der letzten Jahrhunderte einen mässigen aber relativ kontinuierlichen Schlammbreckzienaustritt und seine Gesamtmorphologie wurde durch Sedimenttransportprozesse im Canyon mitbeeinflusst.

Eine dritte Studie besteht aus detaillierten Meeresboden Beobachtungen an vier peripheren, kalten Quellen, die unterschiedliche Grade der authigenen Karbonatbildung und Besiedlung durch Chemosynthese-basierten Organismen zeigen, z.B. filamentartige, mikrobielle Matten, vesicomyide Muscheln oder Röhrenwürmer. Basierend auf Foto Mosaiks werden verschiedene Meeresboden-Typen klassifiziert. Es wird beschrieben, wo Gasblasen aus weichem Sediment austreten, und wo flache Karbonatplatten auftreten, domartige und zerbrochene Karbonathügel, sowie kraterähnliche Kollapsstrukturen auftreten. Die Beobachtungen deuten darauf hin, dass sich kalte Quellen folgendermassen entwickeln: Gasaustritt aus weichem Sediment wird über mehrere Dekaden durch Chemosynthese-basierte Organismen kolonisiert, dann bilden sich über Jahrhunderte erste Karbonatausfällungen, welche den Fluidfluss zu blockieren beginnen und letztlich entstehen über Jahrtausende die gewölbten Karbonatstrukturen, die allerdings unter dem hohen Überdruck zerbrochen und erneut kolonisiert worden sind.

In dieser Arbeit wurden die laufende Aktivität am Venere Schlammvulkan und die Entwicklung seiner Struktur, einschliesslich die der peripheren kalten Quellen, erfolgreich untersucht. AUV- und ROV-basierte Erhebungen wurden durch systematische, geologische Probenahmen und Analysen von Sedimenten und Porenflüssigkeiten ergänzt. Diese Arbeit präsentiert neue Einsicht in Prozesse, welche Schlammvulkanismus und Fluidaustritt massgeblich beeinflussen. Diese sind nicht nur für den kalabrischen Akkretionskeil von Bedeutung, sondern sind auch in einem globalen geologischen, geochemischen und biologischen, übergreifenden Kontext für Schlammvulkane und kalte Quellen relevant.

## Outline and contributions to manuscripts

This cumulative thesis focuses on high-resolution seafloor mapping at different spatial scales (regional to local) and visual imaging and to complement these datasets with geological sampling. The structure of this work aims to follow this approach by giving an introduction that summarizes generally relevant concepts of cold seeps and MVs (Chapter 1) and then focuses on mud volcanism in the Eastern Mediterranean and the Calabrian Accretionary Prism (CAP) as the main study region (Chapter 2). This is followed by a summary of outstanding questions and knowledge gaps that serve as the motivation (Chapter 3), and the methods and approaches that have been selected (Chapter 4), to investigate and address the mentioned research aspects. The first manuscript (Chapter 5) focuses on Venere MV as an exemplary case of an active structure in the CAP. This is followed by the second manuscript (Chapter 6) that investigates the development of Venere MV and the detailed seafloor structures surrounding it in a deep-sea canyon. An even more spatially focused study is presented in the third manuscript (Chapter 7), studying the evolution of cold-seep structures. These three manuscripts compose the main part of the cumulative thesis but two additional studies are presented still in a preliminary stage (Chapters 8, 9). The first is again a very spatially localized investigation of the mud extrusion from the summit of Venere MV. The second and last study, however, returns to a regional, CAP-wide context and presents an overview map of known and newly identified MVs across different morpho-structural zones of the prism. The thesis is concluded and research perspectives are presented in the final section (Chapter 10) followed by the acknowledgements (Chapter 11), a complete reference list (Chapter 12) and an appendix (Chapter 13).

Markus Loher is the main contributor to all chapters presented in this cumulative thesis and is responsible for the drafting of the articles, which are supported by contributions from selected co-authors. An author-based list of contributions is outlined in tabular form below.

**Manuscript I: Mud extrusion and ring-fault gas seepage – upward branching fluid discharge at the deep-sea Venere mud volcano (Central Mediterranean Sea)**

| Author name | Statement of contribution |
|---|---|
| Markus Loher | Principal author of this manuscript and all figures; conception and design of the study; data analyses and interpretation; gas hydrate stability calculations; AUV-dive planning (POS499) and bathymetry processing; support to gas analyses by Thomas Pape |
| Thomas Pape | Gas analyses (gas composition, stable carbon and hydrogen isotope ratios); intellectual contributions to manuscript (specifically to gas geochemistry) |
| Yann Marcon | ROV-dive planning and seabed investigations and sampling (M112); critical revision of manuscript |

| | |
|---|---|
| Miriam Römer | Hydroacoustic surveys (M112), AUV-dive planning (M112); water column data analyses (M112); critical revision of manuscript |
| Paul Wintersteller | AUV-dive planning and processing of bathymetry data (M112 + POS499); critical revision of manuscript |
| Daniel Praeg | ROV seabed investigations (M112); intellectual contributions to the manuscript (specifically to the geological setting and the proposed conceptual model) |
| Marta Torres | Pore water sampling and analyses (M112); intellectual contributions to the manuscript (specifically to pore water geochemistry) |
| Heiko Sahling | Co-chief scientist of cruise M112, ROV-dive planning, seabed investigations and sampling; critical revision of manuscript |
| Gerhard Bohrmann | Chief scientist of cruises M112 + POS499, conception and design of the study; intellectual contributions to the manuscript |

**Manuscript II: Mud volcanism in a canyon: Morpho-dynamic evolution of the active Venere mud volcano and its interplay with Squillace Canyon, Central Mediterranean**

| | |
|---|---|
| Markus Loher | Principal author of this manuscript and all figures; conception and design of the study; data analyses and interpretation; core descriptions; XRF and WDS analyses; AUV-dive planning and bathymetry processing (POS499) |
| Silvia Ceramicola | Core descriptions (POS499); intellectual contributions to the manuscript (specifically to the geological setting and the proposed evolutionary model) |
| Paul Wintersteller | AUV-dive planning and processing of bathymetry data (M112 + POS499); critical revision of manuscript |
| Gerrit Meinecke | AUV-handling, dive planning and data acquisition (M112 + POS499) |
| Heiko Sahling | Co-chief scientist of cruise M112; conception and design of the study; intellectual contributions to the manuscript |
| Gerhard Bohrmann | Chief scientist of cruises M112 + POS499, intellectual contributions to the manuscript |

**Manuscript III: Seafloor sealing, doming, and collapse associated to gas seeps and authigenic carbonate structures at Venere mud volcano, Central Mediterranean**

| | |
|---|---|
| Markus Loher | Principal author of this manuscript and all figures; conception and design of the study; data analyses and interpretation; photo mosaic assembly; carbonate sample preparation |
| Yann Marcon | ROV-dive planning and seabed investigations and sampling (M112); photo mosaic assembly; critical revision of manuscript |
| Thomas Pape | Isotope and mineralogical analyses of carbonates; critical revision of manuscript |
| Miriam Römer | Hydroacoustic surveys (M112), AUV-dive planning (M112); water column data analyses (M112); critical revision of manuscript |
| Paul Wintersteller | AUV-dive planning and processing of bathymetry data (M112 + POS499); critical revision of manuscript |
| Christian dos Santos Ferreira | AUV-bathymetry processing (M112); critical revision of manuscript |
| Marta Torres | Conception and design of the study; intellectual contributions to the manuscript and figures |
| Daniel Praeg | ROV seabed investigations (M112); intellectual contributions to the manuscript and figures |
| Heiko Sahling | Co-chief scientist of cruise M112; conception and design of the study; critical revision of manuscript |
| Gerhard Bohrmann | Chief scientist of cruises M112 + POS499, conception and design of the study; intellectual contributions to the manuscript and figures |

# 1. Introduction to cold seeps and mud volcanoes

## 1.1. Mud volcanoes and cold seeps

Cold seeps are geological structures that are characterized by the focused upward flow and release of solids or fluids (gases and liquids) or a combination of both, at temperatures comparable to those at the surface, in contrast to hydrothermal vents or magmatic systems (Parnell, 2002; Suess, 2014). Mud volcanos (MVs) are large expressions of cold seeps and focused flow of overpressured fluids drives the additional mobilization of solid material such as fluid-rich sediments and rock clasts, which are collectively extruded as mud breccia at the surface (Cita et al., 1981; Kopf, 2002; Deville and Guerlais, 2009; van Loon, 2010). MVs occur globally (Fig. 1.1), in terrestrial and shallow water settings (1100 estimated occurrences) as well as deep offshore environments ($10^3$–$10^5$ estimated occurrences), and have been found to be most common in submarine and tectonically active settings (accretionary prisms, convergent orogens, thrust belts), deep sediment basins, or delta regions (Milkov, 2000; Dimitrov, 2002; Kopf, 2002; Mazzini and Etiope, 2017).

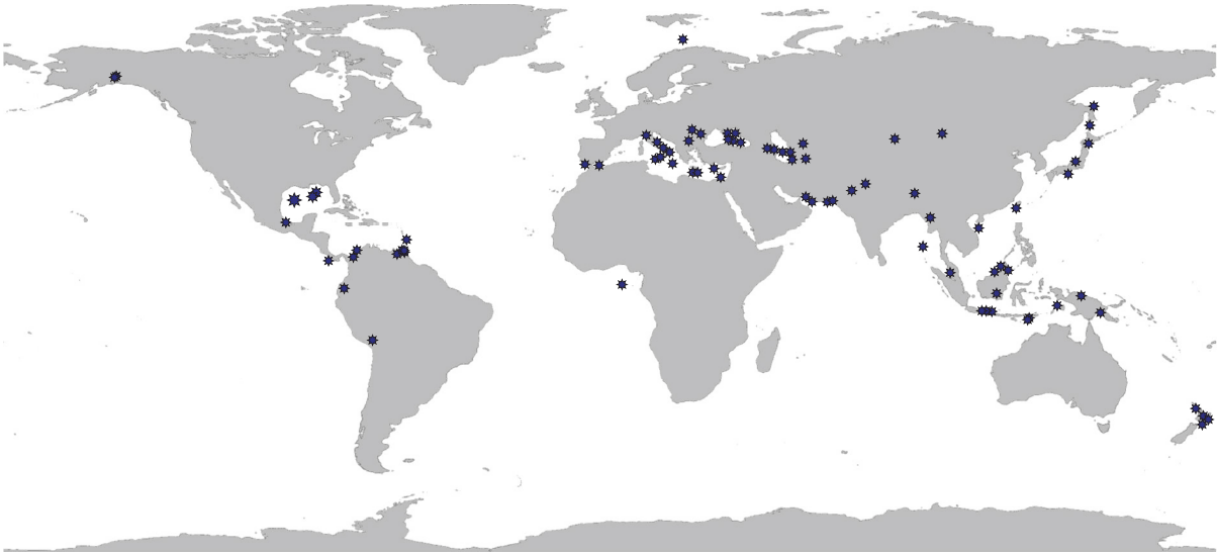

Figure 1.1. Distribution of main clusters of marine and terrestrial MVs around the globe (from Mazzini and Etiope (2017)).

Cold seeps are often characterized by the presence of authigenic carbonate deposits and host oasis-type ecosystems associated to the microbial oxidation of hydrocarbon-rich fluids (Paull et al., 1984; Hovland et al., 1987; Ritger et al., 1987; Sahling et al., 2002; Niemann et al., 2006; Himmler et al., 2015). The fluid that is released from MVs and cold seep structures has been found to consist predominantly of methane (Hovland et al., 1993; Kopf, 2003), a hydrocarbon gas of significant global warming potential (28 times that of the same mass of carbon dioxide when averaged over 100 years; (Lelieveld et al., 1998; IPCC, 2014)). If methane concentrations in the migrating fluids exceed saturation this may lead to the formation of gas as bubbles (Boudreau, 2012; Römer et al., 2012a) or, under adequately low temperatures and high pressures, to the formation of methane hydrate, a crystalline solid composed of gas and water (Bohrmann and Torres, 2006; Sloan and Koh, 2008; Pape et al.,

2011a). The release of gas bubbles (potentially coated by gas hydrate skins) results in specific hydroacoustic water column signatures of high intensity, referred to as flares, and indicate ongoing gas release (Greinert et al., 2006; Römer et al., 2012b).

The release of hydrocarbon-rich fluids may occur over widespread areas (Sahling et al., 2008b; Greinert et al., 2010; Skarke et al., 2014; Mau et al., 2017) or be localized to individual sites such as pockmarks and MVs (Sauter et al., 2006; Sahling et al., 2009; Hovland et al., 2010). Focused fluid flow activity can cause sediment deformation and instability (Dillon et al., 2001), dynamic processes of eruptive gas release (Prior et al., 1989; Leifer et al., 2006), subsurface mobilization, and transport of sediments across the sediment-water interface (MacDonald and Peccini, 2009; Perez-Garcia et al., 2009; Feseker et al., 2014; Loher et al., 2016). Understanding of the transfer mechanisms for volatiles, liquids, and fluid-rich sediments, as well as the underlying drivers and dynamics that govern fluid generation and migration is important to constrain processes occurring at the geosphere–hydrosphere interface, especially in the deep sea.

## 1.2. Processes and morphologies related to mud volcanism

Mud volcanism is primarily the result of focused fluid migration in the subsurface and the mobilization of sediment and the involved processes are schematically outlined in Fig. 1.2. Mud volcanism is driven by a combination of two main causes: 1) gravitative instability in the sediment column, such as a bulk density contrast between a low-density unit (e.g. a clay-rich mud) underlying a unit of relatively higher density (e.g. quartz-rich terrigenous deposits), and 2) overpressure, i.e. fluid pressures larger than the hydrostatic pressure, causing undercompacted conditions for subsurface sediments (Yassir, 1989; Brown, 1990; Kopf, 2002; Maltman and Bolton, 2003; Deville et al., 2010). In contrast, mud diapirism may result from the slow, upward-migration of buoyant material such as clay-rich sediment and does not necessarily pierce the overburden (Henry et al., 1990; Kopf, 2002). Increases in fluid pressure below impermeable barriers (e.g. a cap rock) can result from several processes: i) rapid sediment accumulation and compaction, ii) tectonic-stress (e.g. by compression and shortening; thrusting) and tectonic-overloading, iii) excess pore water generation by diagenetic reactions (mineral dehydration reactions such as clay transformations), iv) formation and migration of liquid or gaseous hydrocarbons, and v) gas hydrate dissociation (Higgins and Saunders, 1974; Yassir, 1989; Martin et al., 1996; Dimitrov, 2002; Kopf, 2002; Deville et al., 2003; Deville et al., 2010). The opening of vertical fluid migration pathways by fracture formation in the barrier can result from the generated overpressure directly (referred to as hydraulic fracturing) or can be triggered through tectonic stress, fault reactivation, or seismicity (Deville et al., 2010; Mazzini and Etiope, 2017). The upward migrating fluids incorporate rock fragments and fine grained sediments from the geologic sections through which they ascend until this fluid-rich sediment mixture – referred to as mud breccia – is extruded onto the surface (Cita et al., 1981; Camerlenghi et al., 1992; Dimitrov, 2002; Kopf, 2002).

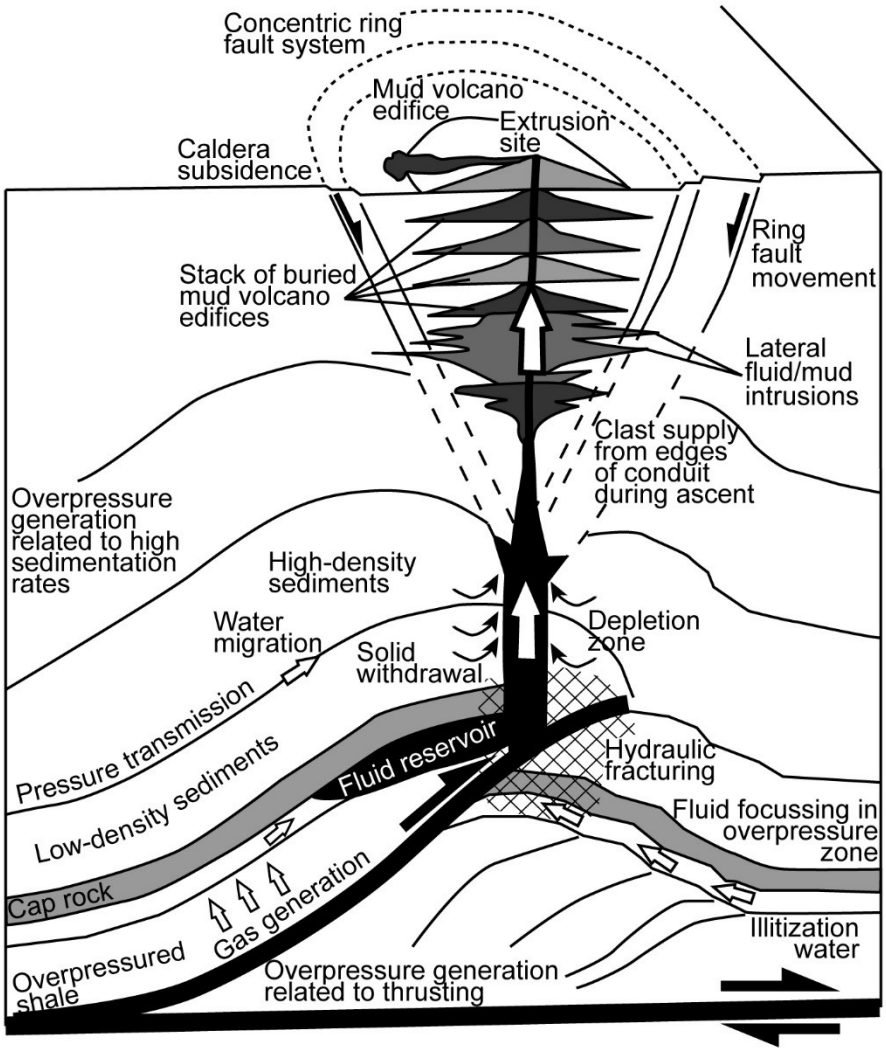


Fig. 1.2. A conceptual sketch of a MV and its plumbing system with general reactions and processes related to overpressure generation, fluid and solid material mobilization, pathway generation, material ascent and extrusion, and surface structures. For explanations see text; modified after Deville et al. (2010) and Mazzini and Etiope (2017).

Repeated mud breccia extrusion can lead to the build-up of MV edifices (Fig. 1.2) several kilometers in diameter and several hundred meters in height (Ivanov et al., 1996b; Dimitrov, 2002; Kopf, 2002; Kioka and Ashi, 2015). In turn, post-extrusive subsidence and caldera formation (Prior et al., 1989; Bonini, 2008; Evans et al., 2008; Mazzini et al., 2009b) have been argued to result from sediment mobilization and material withdrawal in the subsurface (Van Rensbergen et al., 2003), reductions in pore fluid pressures (deflation; (Fukushima et al., 2009)), and extrusive loading (Galindo-Zaldivar et al., 1996). MV calderas can form as so called summit calderas on top of the extrusive edifices (several meters to tens of meters in diameter; (Evans et al., 2008)) or can encompass the complete MV edifice (often measuring several kilometers in diameter, with up to tens of meters in relief; (Camerlenghi et al., 1995; Ivanov et al., 1996b)). Several authors have pointed out basic similarities between the surface expression of MVs and igneous volcanoes regarding the structure (e.g. shield- vs.

strato-volcanoes), types of eruptions (explosive vs. effusive; (van Loon, 2010; Tinivella and Giustiniani, 2012)), or the caldera formation (Bonini, 2008; Evans et al., 2008; Kopf, 2008). At magmatic volcanoes the development of sub-circular calderas is often linked to inward- or outward-dipping, concentric ring faults (e.g. Troll et al. (2002)). Similar peripheral ring fault systems (Fig. 1.2) have often been observed arranged concentrically around MVs (Prior et al., 1989; Neurauter and Bryant, 1990; Graue, 2000; Davies and Stewart, 2005; Mazzini et al., 2009b). Understanding the structural evolution of calderas and their subsidence mechanism may give insights on dynamics of material withdrawal from the subsurface (Robertson and Kopf, 1998), subsurface pressure variations (e.g. by degassing; (Henry et al., 1990; Camerlenghi et al., 1995)), or overburden loading and collapse (Praeg et al., 2009).

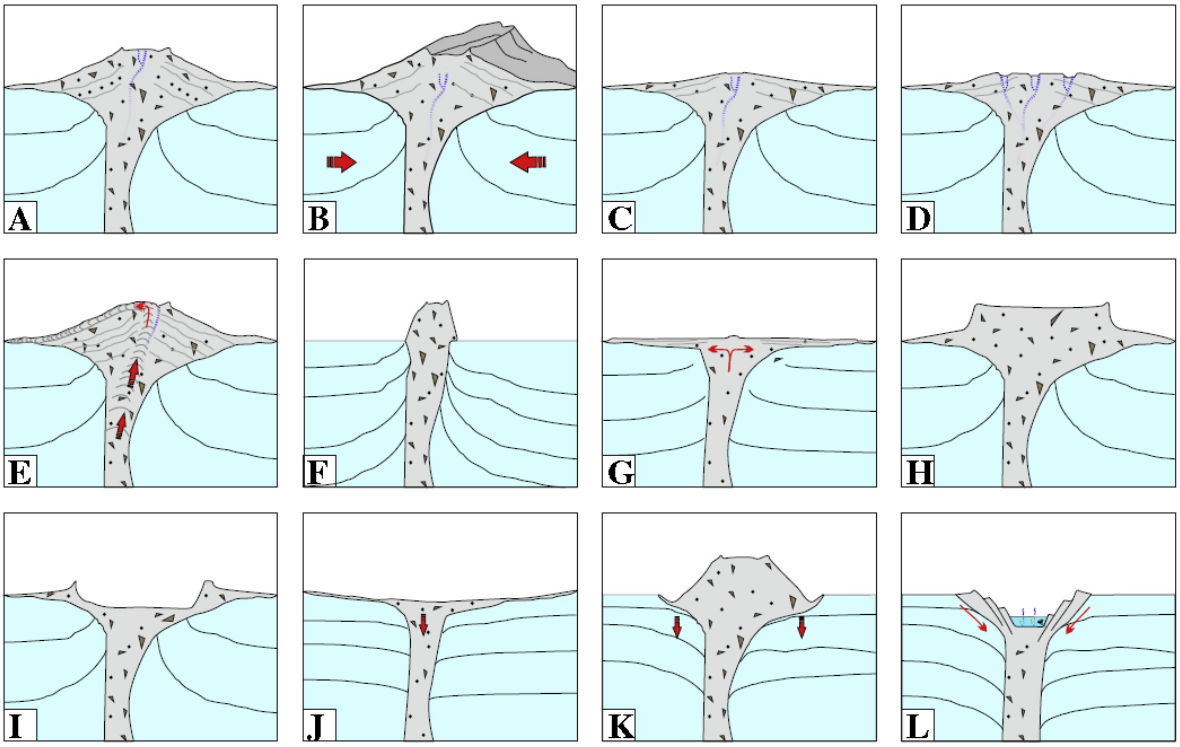


Fig. 1.3. Classification of MVs based on morphologies: (A) conical, (B) elongated, (C) pie-shaped, (D) multicrater, (E) growing diapir-like, (F) stiff neck, (G) swamp-like, (H) plateau-like, (I) impact crater-like, (J) subsiding structure, (K) subsiding flanks, (L) sink-hole type; from Mazzini and Etiope (2017).

The surface structure of MVs is described according to their overall positive (e.g. cones, domes) or negative (e.g. calderas) morphologies and an overview of various morphologies recognized to date is shown in Fig. 1.3 (see review by Mazzini and Etiope (2017)). Typical submarine MV structures range from pie-shapes with concentric mud breccia ridges (Dupré et al., 2008; Praeg et al., 2009) symmetrical cones with single or multiple sites of extrusion (Paull et al., 2015b), and negative or flat morphologies (Graue, 2000). The water-saturated conditions for offshore MVs suggest that extruded material can extend more laterally and mudflows are transported over greater distances than their terrestrial counterparts (Yusifov and Rabinowitz, 2004; Mazzini and Etiope, 2017). Furthermore, the topography surrounding a MV may influence its morphology significantly since extruded mud breccia tend to follow

along downslope pathways (Graue, 2000), and MV flanks can be subject to gravity-induced sedimentary destabilizations (Dupré et al., 2008; Roberts et al., 2011b). Whereas the morphology of onshore MVs is affected by weathering and surface erosion, offshore MVs have been found to be shaped by bottom currents, e.g. by deepening of subsiding rims and the formation of moats around the bases of the MV edifices (Vandorpe et al., 2016). The number of major extrusive centers or secondary seepage sites (also referred to as parasitic sites), and the overall morphology of the extrusions of submarine MVs can vary from irregular to symmetrical (Van Rensbergen et al. (2005a). Long elongate flows have been found to thin-out and become disconnected from their point of extrusion and accumulate at the base, whereas shorter and wider mud breccia flows may have come to rest along the slope of the MV edifice (Fig. 1.4). Large mudflow sheets or ridges and terraces are known from MVs which extrude material concentrically and form the so called mud pies (Dupré et al., 2008).

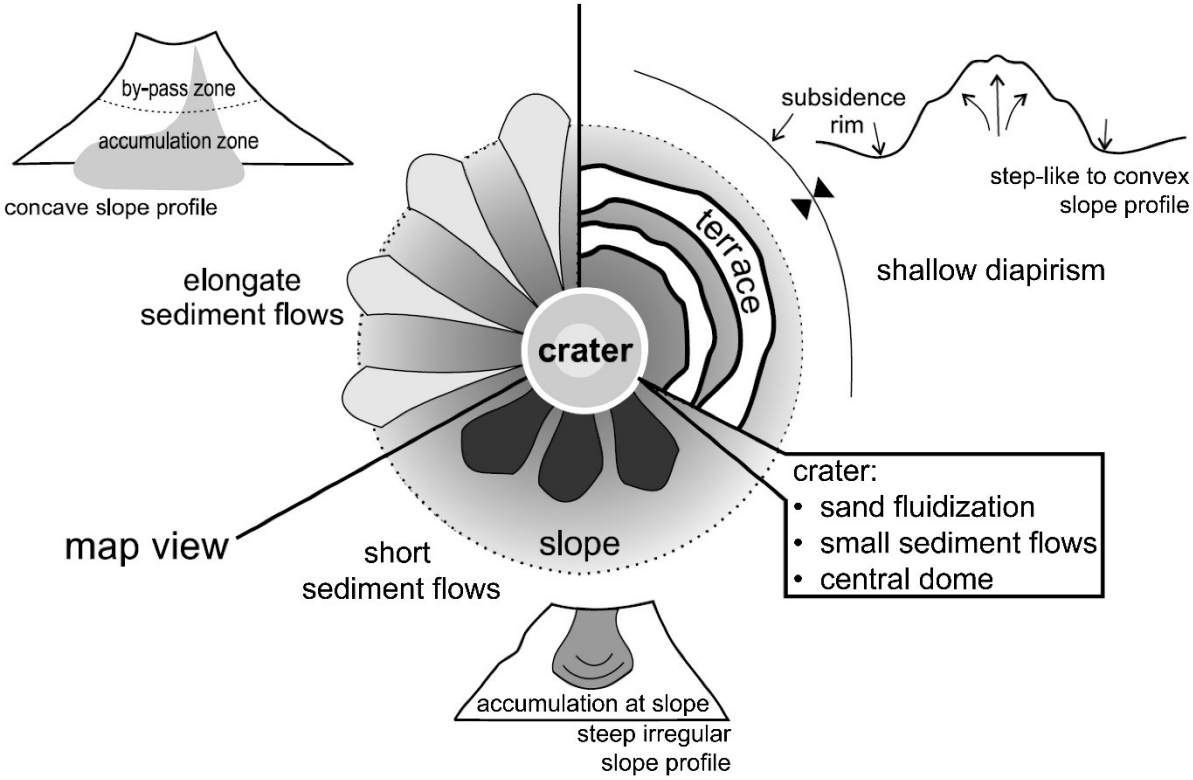


Fig. 1.4. Sketch drawing of typical extrusion types and corresponding map view morphologies of mudflows at MVs; modified after Van Rensbergen et al. (2005a).

Attempts to classify MVs based on their morphologies in the Mediterranean Ridge (Eastern Mediterranean) indicated a relationship to specific tectonic settings (frontal thrust, wedge-backstop, and backthrusts), the main active fault zones in the areas, the source, and the depth of extruded fluids or solids (Huguen et al., 2004; Huguen et al., 2005; Rabaute and Chamot-Rooke, 2007). In contrast, offshore MVs in the South Caspian Basin predominantly exist above anticlinal structures, but the occurrence of flat, concave, and convex edifices, or buried structures, do not show morpho-systematic trends in their distribution (Yusifov and

Rabinowitz, 2004). The factors determining the morphological expression of MVs has been argued to include the composition, frequency (i.e. the cyclicity of overpressure build-up) and intensity (i.e. the amount of overpressure and ascent velocity) at which mud breccia is extruded (Pettinga, 2003; Yusifov and Rabinowitz, 2004)) but also the conduit diameter (Lance et al., 1998; Kopf, 2002), and the depth from which the fluids and sediments are mobilized (Huguen et al., 2004; Paull et al., 2015b). It has been proposed that the size of a MV is related to the diameter of its conduit (i.e. larger structures have wider conduits), its age (cones evolve into plateaus), and that the shape is influenced by the rheological behavior (i.e. the viscosity) of the extruding mud breccia (Lance et al., 1998; Kopf, 2002; Paull et al., 2015b). The viscosity in turn depends on a range of factors and the most relevant factors influencing the height, width, and shapes to which MV systems can develop include: 1) the porosity (i.e. a more porous mud breccia can contain a higher fluid content); 2) the fluid content with respect to the sediment or clast content (i.e. a more fluidized mud breccia forms flatter structures); 3) mud breccia expulsion velocity (i.e. higher velocity causes higher shear-stress, a higher degree of fluidization, and a flatter structure); 4) pore fluid pressures (i.e. a higher subsurface overpressure generates a higher feature); 5) temperature (viscosity of the fluid decreases with increasing temperature); (Brown, 1990; Lance et al., 1998; Yusifov and Rabinowitz, 2004; Feseker et al., 2009a). The parameters influencing the consistency of the extruded material (Huseynov and Guliyev, 2004) may change throughout a single phase of MV activity (León et al., 2007) or gradually during its lifetime (Kopf et al., 2001). In addition, degassing and fluid loss of the mud breccia occurs as the material flows across the surface and results in an increase in viscosity with increasing distance from the MV. This process has been proposed to form steep ramparts at the edge of flat-topped mud pies (Paull et al., 2015b).

### 1.3. Gas hydrates at submarine mud volcanoes and seeps

Hydrates are crystalline solids that consist of cage-forming water molecules – also referred to as clathrates (Latin *clatratus* for cage) – with low molecular weight gas such as methane (structure I gas hydrate) or higher hydrocarbons (structure II gas hydrate) enclosed as “guest” molecules. Gas hydrates are present at continental margins or in the deep sea where methane concentrations in the sediments reach saturation and they are stable under specific high-pressure and low-temperature (P/T) conditions defining the phase boundary between hydrate and gas and the limit of the gas hydrate stability zone (GHSZ) depends on the prevalent temperature profile (Fig. 1.5; (Kvenvolden, 1988; Bohrmann and Torres, 2006; Sloan and Koh, 2008)). Sites of focused, methane-rich fluid migration at deep-marine cold seeps and MVs are therefore predestined for hosting shallow buried or exposed gas hydrates (Suess et al., 1999; Pape et al., 2010; Pape et al., 2011b) and typically form more massive but localized gas hydrate deposits compared to the accumulations found dispersed in sediments unaffected by seepage (Bohrmann and Torres, 2006).

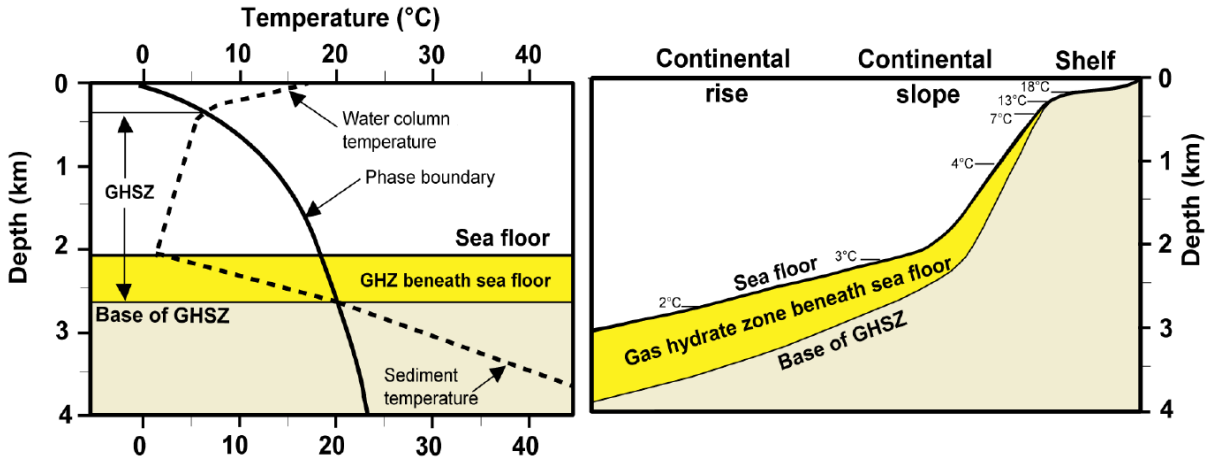


Fig. 1.5. Left: Calculated stability field of methane hydrate at normal seawater salinity, as defined by temperature and pressure (expressed as depth). The depths between where the temperature profile of the water and the subsurface (stippled line) intersect with the phase boundary (solid line) define the upper and lower limits of the gas hydrate stability zone (GHSZ). Right: Inferred thickness of gas hydrate in sediments of a stylized continental margin assuming a geothermal gradient of 28 °C/km. Typical bottom water temperatures are marked and range from 2–18 °C from the foot of the continental rise to the shelf, respectively; from Bohrmann and Torres (2006) (after Kvenvolden and McMenamin (1980)).

Gas hydrate deposits at these sites can undergo dissociation if changes in pressure (e.g. a drop in hydrostatic pressure (Kvenvolden, 1993)) or temperature (e.g. an increase in bottom water temperature (Kennett et al., 2000) or elevated fluid temperatures (Suess et al., 1999)) shift the ambient conditions of the hydrate deposit outside of the required P/T field. The presence of $CO_2$, $H_2S$, ethane, and propane (or a combination) in the fluid from which hydrate is formed, typically shifts the phase boundary to more stable conditions (higher temperatures at a given pressure). An increase in the concentration of other dissolved species such as $Na^+$ and $Cl^-$ ions in saltwater, however, lowers the stability of the hydrate (lower temperatures at a given pressure). On the other hand, gas hydrate formation inside the GHSZ is promoted if the solubility of methane in the fluid is lowered due to a higher salinity, i.e. if more other dissolved ions are present (Yang and Xu, 2007). Vice-versa it is more difficult to form gas hydrate from freshened fluids because more methane is needed to reach oversaturation. The occurrence and distribution of gas hydrates at submarine MVs (located in the GHSZ) is influenced by the methane supply as well as the heat flux from below and their respective changes during different phases (e.g. quiescence vs. eruptions) of MV activity. Gas hydrate decomposition may occur rapidly and locally at the extrusive center during phases of increased MV activity in case warm fluids are advected from the subsurface. In contrast, the base of the GHSZ may deepen in more distal regions away from the main conduit (Fig. 1.6) or during phases of low heat flux. Accordingly, gas hydrate may accumulate in areas or during times characterized by moderate MV activity (Pape et al., 2011b).

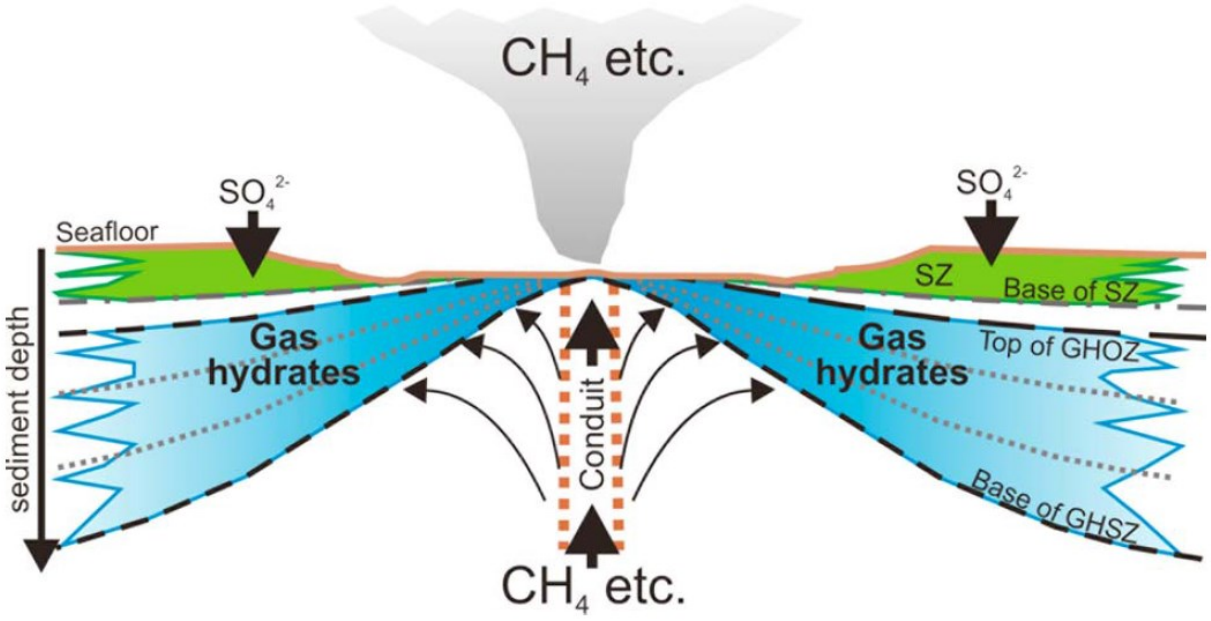


Fig. 1.6. Schematic cross section of a mud volcano with a central conduit that supplies warm fluids (and solids, not shown) including methane to the seafloor. The gas hydrate distribution (blue area), temperature isolines (grey stippled lines), and a sulfate zone (SZ, green), where sulfate infiltrates the sediments, are indicated. The supply of heat from below and the microbial consumption of methane in the SZ affect the base of the gas hydrate stability zone (GHSZ) and the top of the gas hydrate occurrence zone (GHOZ), respectively; from Pape et al. (2011b) (after Bohrmann and Torres (2006), Egorov et al. (1999), Ginsburg et al. (1999) following findings at the Håkon Mosby MV).

## 1.4. Gas release and mud extrusion at cold seeps

Cold seeps and MVs play a geologically relevant component in the global carbon and material cycle (Kopf et al., 2001; Etiope and Milkov, 2004; Kvenvolden and Rogers, 2005; Hong et al., 2013), influence ocean chemistry (Judd and Hovland, 2007; Mau et al., 2017) and sudden release of large amounts of methane from gas hydrate dissociation may even impact climate (Hesselbo et al., 2000; Padden et al., 2001; Dickens, 2003; Kopf, 2003; Archer, 2007). The natural release of gas from marine seeps has been estimated to contribute 31 to 48% of the annual global methane emissions from geological sources into the atmosphere (i.e. 53 +/-11 Mt/year; (Etiope et al., 2008; Etiope and Ciccioli, 2009)). Methane amounts emitted by an individual MV on land or in a shallow coastal area have been estimated to range on average from 300–2400 t/year (Dimitrov, 2002) or a slightly lower range of 10–1000 t/year (Etiope and Milkov, 2004). In the deep sea (>200 m water depth), an estimated 27 Mt of methane per year is released into the water from all MVs, of which most is assumed to become oxidized in the water column (Milkov et al., 2003).

Discharge of gas or mud breccia depends strongly on the type of activity at any given MV structure and the state of a MV can typically be classified as active, extinct, or buried. The active state is thought to be characterized by long phases (up to 95% of a MV lifetime) of quiescent fluid seepage, interrupted by short eruptive episodes (also referred to as catastrophic events), consisting of explosive or extrusive (or a combination) mud breccia

discharge, that essentially builds up the MV edifice (Kopf, 2002; Planke et al., 2003). Eruptive episodes have been observed predominantly at terrestrial MVs or in shallow offshore sites where mud volcanism can even cause the formation of (ephemeral) islands during vigorous eruptions (Delisle et al., 2002). It has been argued that MV activity is not only episodic but that fluid expulsion follows cyclic patterns at frequencies of decades for large and catastrophic events down to minutes for gas- and mudflows during quiescent phases (Deville and Guerlais, 2009). The catastrophic eruptions tend to be short lived (hours to several days; (Kopf, 2003)) but also long-lived (several years) extrusive activity is known e.g. from mudflows observed since 2006 (and currently still ongoing) at the sediment-hosted, hydrothermal Lusi structure in Indonesia (Miller and Mazzini, 2017). Whereas links between seismic events and the frequency of MV eruptions seem to exist in certain regions (e.g. Azerbaijan; (Mellors et al., 2007)) this may not be the case for other areas (e.g. Barbados; (Deville and Guerlais, 2009). Constraining a causal link between earthquakes and mud volcano activity may be possible in certain cases but is complicated by the fact that often there is insufficient knowledge about the threshold required to induce a MV eruption in the first place and the potential time delays between the seismic event and the eruption (Manga et al., 2009).

From studies of onshore MVs in Azerbaijan or Barbados, extrusion rates of gas-rich mud breccia have been reported. They range from tens to hundreds of $m^3$/day to short-lived (1–14 days) eruptions releasing 100’000 to 1’000’000 $m^3$/day (Deville and Guerlais, 2009; Roberts et al., 2011a). At the Håkon Mosby MV (Barents Sea) volumes of material outflow have been modeled and are thought to vary from 10’000 to 30’000 $m^3$/year (Kaul et al., 2006) whereas for the Milano and Napoli MVs (Eastern Mediterranean), rates of 2000 to 8000 $m^3$/year and 6000 to 15000 $m^3$/year for the respective mud breccia extrusion have been derived via the volumes and ages of the structures (Kopf, 1999; Wallmann et al., 2006). In contrast, activity during the quiescent phases does not show mud breccia extrusions but is restricted to the seepage of gas, liquids, and fluid-rich mud, lacking significant amounts of clasts. Discharge is often localized and typically occurs only at gryphons (parasitic cones limited to a few meters in size) or salses (fluid-rich mud pools; (Planke et al., 2003; Deville and Guerlais, 2009)).

## 1.5. Cold seep ecosystems

Marine cold seeps represent specific ecosystems where focused fluid flow supplies hydrocarbon-rich fluids, consisting predominantly of methane, from the subsurface into shallow-subsurface sediments (e.g. Mastalerz et al. (2009)). Most of the upward migrating methane in marine sediments is degraded by the anaerobic oxidation of methane (AOM) under anoxic conditions such as in deeper subsurface sediments, or oxidized aerobically by microbial processes in the oxic water column or in uppermost millimeters of sediment. AOM is an important process at cold seeps and occurs where the upward migrating methane encounters downward diffusing seawater-sulfate, which acts as the electron acceptor in the absence of oxygen. AOM involves the reaction of methane ($CH_4$) with sulfate ($SO_4^{2-}$) and

leads to the formation of hydrogen sulfide ($HS^-$), bicarbonate ($HCO_3^-$) and water ($H_2O$) according to the following net equation (Knittel and Boetius, 2009):

$CH_4 + SO_4^{2-} \rightarrow HS^- + HCO_3^- + H_2O$.

AOM has been found to be mediated by a consortium of sulfate reducing bacteria and anaerobic methane oxidizing archaea (Hinrichs et al., 1999; Boetius et al., 2000). In addition, it has been found that microorganisms from marine seeps can also make use of manganese or iron to oxidize methane and even gain more energy although at slower rates than by the sulfate-dependent AOM (Beal et al., 2009). The supply of methane, higher molecular-weight hydrocarbons, and sulfide, represents a source of carbon and metabolic energy for extensive micro- and macrofaunal, symbiotic or free-living, chemosynthesis-based organisms (Fig. 1.7; (Formolo et al., 2004; Dubilier et al., 2008; Rubin-Blum et al., 2017). For example, chemolithoautotrophic organisms including filamentous, sulfur-oxidizing bacteria (e.g. Beggiatoa) or chemosynthetic bivalves (hosting endosymbionts mostly in their gills) such as vesicomyid clams (e.g. Vesicomya, Calyptogena) and mytilid mussels (e.g. Bathymodiolus), or vestimentiferan tubeworms (hosting endosymbionts in their tubes), are typically associated with hydrocarbon seeps and mud volcanoes (Sibuet and Olu, 1998; Sahling et al., 2002; Joye et al., 2004; Olu-Le Roy et al., 2004; Marcon et al., 2014b; Rubin-Blum et al., 2014). These benthic organisms demand a constant supply of reduced compounds (i.e. methane or sulfide or both) in dissolved form and establish themselves in locations where the fluid flux corresponds to their relatively specific tolerance threshold. (Sahling et al., 2002). Shallow gas hydrates represent a constant source of dissolved hydrocarbons (mainly methane) as diffusion occurs between the hydrate and the methane-under-saturated water column and result in AOM and sulfide flux near the seafloor. In hydrocarbon seeps of the southern Gulf of Mexico it has been clearly observed for the first time that tubeworms are situated on top of gas hydrate outcrops. They are interpreted to act as ecosystem engineers and sustain a high rate of AOM and sulfide flux (Sahling et al., 2016) by their ability to release sulfate (taken up from the sea water) via their rhizosphere (the 5-10 cm thick layer at the posterior tube of the vestimentiferan tube worm; (Dattagupta et al., 2008)). The degradation of most of the methane in marine sediments by AOM is ineffective if fluid flow is too rapid or gas bubbles have formed because methane will largely bypass this so called microbial AOM-filter (Luff et al., 2004; Sommer et al., 2006). Furthermore, the colonization of a potentially suitable habitat by seep organisms is challenged in case frequent mudflows from MVs dislodge or bury the organisms (Roberts and Carney, 1997; Wallmann et al., 2006; MacDonald and Peccini, 2009; Feseker et al., 2014).

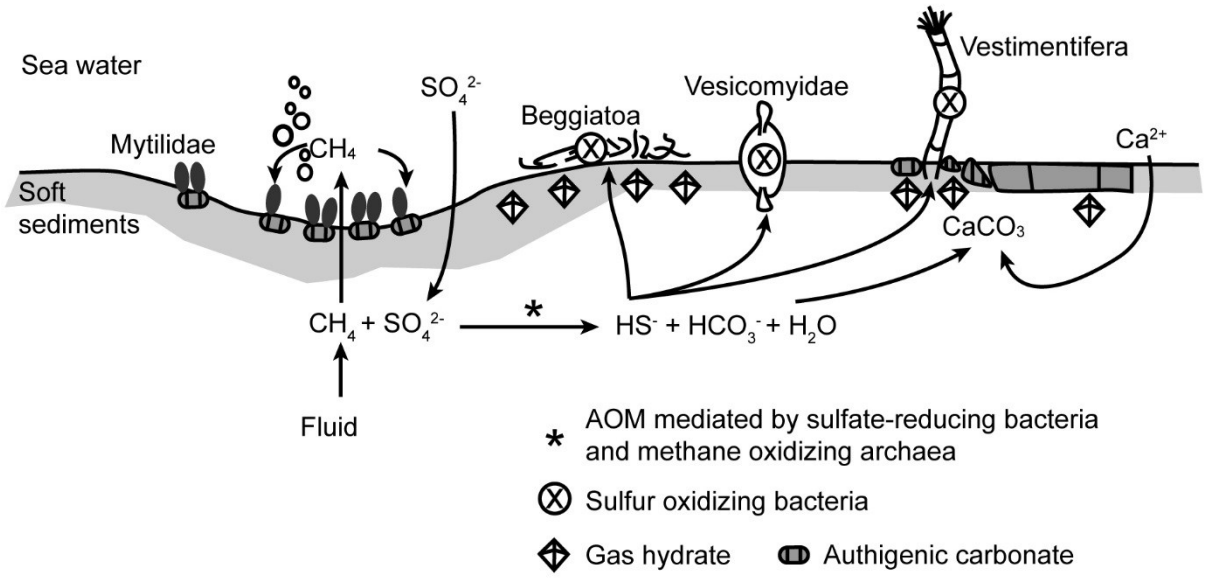


Fig. 1.7. Schematic drawing of the AOM reaction process. Methane is supplied by fluid flow or from shallow gas hydrates to the AOM consortia, which use seawater sulfate to produce hydrogen sulfide, bicarbonate and water. The utilization of methane by mytilid mussels and of sulfide by sulfur oxidizing bacteria forming filamentous mats (e.g. Beggiatoa) or living as endosymbionts in vesicomyid clams or vestimentiferan tubeworms is indicated. AOM increases pore water alkalinity and the bicarbonate reacts with seawater calcium to precipitate as authigenic carbonate that acts as substrate for certain organisms to establish (e.g. Mytilidae or Vestimentiferans) but also forms carbonate pavement sealing off the seafloor; modified after Sibuet and Olu (1998), Sahling et al. (2002), and Bayon et al. (2009).

AOM also causes to the precipitation and accumulation of authigenic carbonate, which is an additional process contributing to cold seep ecosystems. At high rates of sulfate reduction (up to 140 mmol/m$^2$/d; (Boetius et al., 2000)) there is an increase in bicarbonate ($HCO_3^-$) as a result of intensive AOM. This increases the alkalinity of the pore water and can react with calcium and magnesium in the seawater to precipitate as a variety of aragonite ($CaCO_3$), high-magnesium calcite ($MgCO_3$), or dolomite ($CaMg(CO_3)_2$) phases. The sulfate reduction exerts control on the composition of the precipitating phase as for example the presence of dissolved sulfate in pore waters has been found to be inhibiting towards high-magnesium calcite (Ritger et al., 1987; Aloisi et al., 2002; Luff and Wallmann, 2003). Authigenic carbonate formations can be localized and form small, disseminated nodules or concretions of a few centimeter, form decimeter-thick slabs, meter-high mounds, or pavements extending for several tens to hundreds of square meters (Aloisi et al., 2000; Gontharet et al., 2007; Himmler et al., 2011; Römer et al., 2014) or can even grow as chemoherms structures into the water column (Teichert et al., 2005).

Cementation by seep carbonates alters the seafloor surface structure to a hard substrate potentially with a high rugosity that can be detected hydroacoustically in backscatter data (Gay et al., 2007; Buerk et al., 2010). Importantly, the carbonate hardgrounds may provide stability and protection for seep-related fauna such as tubeworms (Sassen et al., 2004) or start to clog and eventually self-seal the available fluid migration pathways, effectively

shutting down further AOM and seepage (Hovland, 2002; Bayon et al., 2009). These carbonate deposits can thus be seen as indicators for past flow of hydrocarbon-rich fluids. The stable carbon isotope ($\delta^{13}C_{Carbonate}$) composition of authigenic carbonates typically reflects to some degree the $^{13}C$-depleted composition of the methane, which fueled its precipitation. The stable oxygen isotope ($\delta^{18}O_{Carbonate}$) composition on the other hand may be influenced by a combination of factors including the presence or absence of gas hydrate, the composition, temperature, and pH of the pore water from which the carbonate phase formed (Bohrmann et al., 1998; Teichert et al., 2005; Naehr et al., 2007; Himmler et al., 2011). Gas that is trapped in pores of authigenic carbonates, however, does not represent reliable archive for the original hydrocarbon composition from which the carbonates precipitated (Blumenberg et al., 2017).

## 1.6. Hydrocarbon sources and mud volcanism

Methane ($CH_4$) is the most common hydrocarbon gas in marine sediments (e.g. Hovland et al. (1993)) and focused methane seepage is characteristic for cold seeps with $CH_4$-concentrations in gases from MVs generally exceeding 80 vol-% (Kopf, 2002; Etiope et al., 2009). Methane generation in marine sediments occurs either by microbial degradation of organic matter (i.e. by methanogenic archaea) under anoxic conditions at temperatures <80 °C or by thermal decomposition of high molecular-weight organic matter or the cracking of oil at temperatures that may exceed 150 °C (Claypool and Kvenvolden, 1983; Quigley and Mackenzie, 1988; Clayton, 1991; Stolper et al., 2014). These temperature ranges indicate shallower burial depths (diagenesis) and more recent sediments for microbial methane production in comparison to thermogenic gas, which is typically associated with mature source rocks, within or after the “oil window” maturation level (catagenesis or metagenesis), and deep hydrocarbon reservoirs (Fig. 1.8; (Clayton, 1991; Floodgate and Judd, 1992; Mazzini and Etiope, 2017)). As a result, the processes and environments responsible for the hydrocarbon generation can be studied by differentiating microbial methanogenic pathways (i.e. acetate fermentation and carbonate reduction) from thermogenic degradation of organic matter (Whiticar, 1999; Etiope et al., 2009).

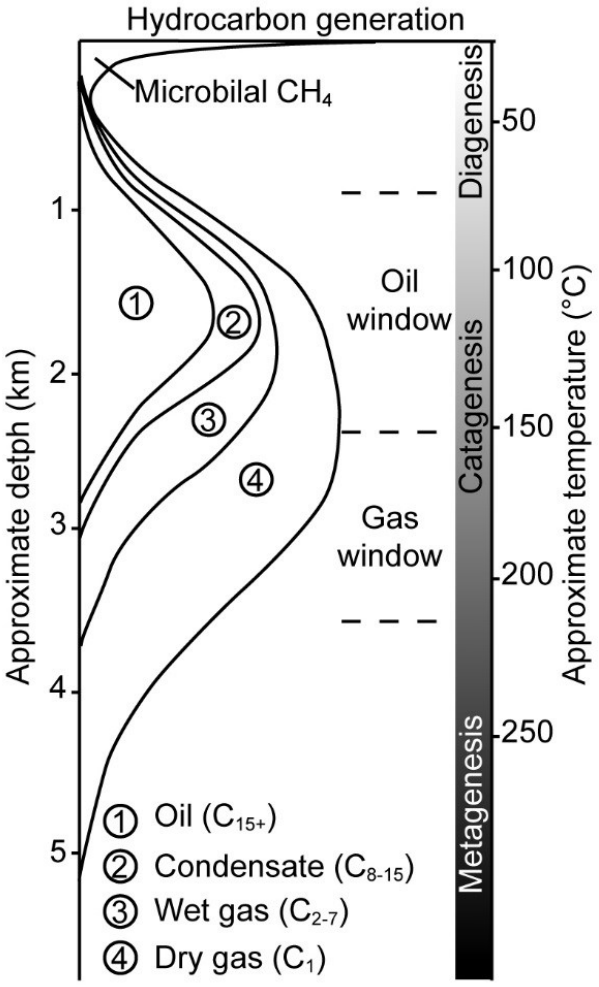


Fig. 1.8. Schematic hydrocarbon generation with depth; the depth scale varies with the geothermal gradient (modified after Floodgate and Judd (1992)). An approximate temperature range is given, based on the range of typical microbial and thermogenic gas formation (for sources see text), and the oil and gas windows are indicated.

Interpretations of the origin of hydrocarbon gases such as $CH_4$ (also referred to as $C_1$) or higher hydrocarbons such as ethane ($C_2$), propane ($C_3$), butane ($C_4$), etc., are typically based on the analysis of the stable carbon ($\delta^{13}C$) and hydrogen ($\delta D$) isotopes as well as the gas composition (i.e. the molecular ratio of $C_1$ vs. $C_{2+}$; (Bernard et al., 1977; Whiticar, 1999)). For example, microbial activity in methane production involves a strong kinetic isotope-fractionation effect, whereby the lighter $^{12}C$ isotope is preferentially targeted, and leads to more negative $\delta^{13}C$ of the produced methane. Specifically for methane, models to characterize the gas source are based on cross-plots of $\delta^{13}C$-$CH_4$ and $C_1/C_{2+3}$ (Bernard et al., 1977) or $\delta^{13}C$-$CH_4$ and $\delta D$-$CH_4$ (Schoell, 1983; Whiticar et al., 1986) as shown in Fig. 1.9. Following these diagrams, microbial methane is characterized by $C_1/C_{2+3}$ >1000, $\delta^{13}C$-$CH_4$ values <-60‰, and $\delta D$-$CH_4$ values of -170‰ to -250‰ for methane produced in marine sediments (i.e. following the carbonate reduction pathway). Methane with low $C_1/C_{2+3}$ ratios (< 100), with less depleted $\delta^{13}C$-$CH_4$ (>-50‰) and $\delta D$-$CH_4$ values (>-170‰) characterize the thermogenic methane source (Bernard et al., 1977; Whiticar et al., 1986)).

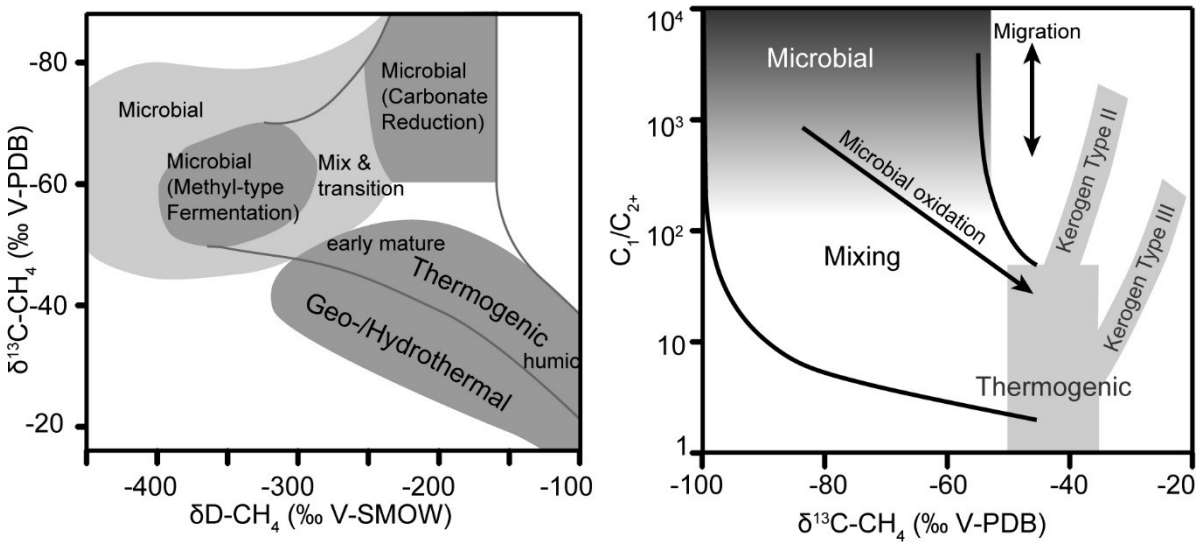


Fig. 1.9. Left: Carbon-hydrogen diagram for classification of microbial and thermogenic methane based on $\delta^{13}C\text{-}CH_4$ and $\delta D\text{-}CH_4$ stable isotope data (modified after Whiticar (1999)); Right: "Bernard" diagram for classification of hydrocarbon gas based on $\delta^{13}C\text{-}CH_4$ and $C_1/C_{2+3}$ information with addition of theoretical mixing lines and relative compositional effects of migration and oxidation (modified after Whiticar (1999)).

A compilation of data on methane by Etiope et al. (2009), sampled at numerous MVs on land, indicate that thermogenic methane is a common source of gas extruded within the MV and mud breccia. In terms of the $\delta^{13}C\text{-}CH_4$ vs. $C_1/C_{2+3}$ diagram, however, many samples plotted above the thermogenic and to the right of the microbial area, clearly outside of theoretical mixing lines, as e.g. defined by Whiticar (1999). Furthermore, in comparison to the gas reservoirs presumably feeding these MVs, the emitted gas was shifted towards lighter $C_1/C_{2+3}$ ratios. It is known that hydrocarbon-rich gas following a migration pathway leads to an enrichment in methane ($C_1/ C_{2+3}$ ratio increase, Fig. 1.9, right) that can again become enriched in the lighter $^{12}C$ (Prinzhofer et al., 2000). The geochemical gas signatures found at the MVs were interpreted to be the result of a molecular fractionation process related to differential adsorption of the gas onto the mud and differential solubilities of the gas in liquids. It is imagined that during the migration of the gas, similar to a "chromatographic effect", the compounds eventually emitted at the surface become enriched in methane (the lighter and smaller $C_1$ component) and the methane will be enriched in $^{12}C$).

A similar mechanism has also been proposed for MVs in Trinidad (Deville et al., 2003) and a comparison of the composition of gas released at the center of the Dashgil MV (Azerbaijan) with that released at the edge of the collapse caldera also showed differences that point to a fractionation effect during gas migration (Mazzini et al., 2009b). Etiope et al. (2009) further observed that during eruptions of the MVs (i.e. during phases of increased fluid flow), the emitted gas showed a composition more similar to that of the corresponding reservoir. At MVs in Barbados, the $C_{2+}$ has been documented to be higher at sites which experienced recent eruptions (Deville and Guerlais, 2009). This indicates that the MV plumbing system supplies material more directly from depth during eruptive activity, whereas during phases of quiescence or slow fluid flow, there is more time for gas-water-mud interactions and

adsorption. Differences in gas chemistry at contrasting seepage sites at a MV potentially give insight into variations of the transport mechanisms or pathways of the fluids and solids transported in the subsurface plumbing system.

## 1.7. Pore water chemistry of mud volcano sediments

Water ($H_2O$) is a regularly encountered pore fluid component in expelled mud breccia (e.g. Dählmann and De Lange (2003)). Three important sources that influence its composition in sediments affected by submarine mud volcanism (or fluid seepage in general) include the contribution of water: 1) entrapped in sediments during fast burial; 2) produced at depth during diagenetic reactions; 3) resulting from dissociation or formation of gas hydrate (Dählmann and De Lange, 2003; Kastner et al., 2014). The release of mineral-bound waters from clay dehydration reactions or gas hydrate dissociation adds fresh water to the sediments and causes a dilution effect of dissolved species such as chloride ($Cl^-$) with respect to $H_2O$ (i.e. causes a reduction in salinity; (Martin et al., 1996; Torres et al., 2004a; Kastner et al., 2014)). In contrast, gas hydrate formation excludes salt and leads to an increase in the $Cl^-$ concentration with respect to $H_2O$ in the remaining pore fluid (Torres et al., 2004b). If fluids are derived from evaporated seawater (Charlou et al., 2003) or if there is interaction with evaporite deposits in the subsurface (Huguen et al., 2009) this will also be reflected by an increased salinity (brine) in the pore water of the extruded mud breccia.

Diagenetic reactions at depth that cause pore pressure increase and a freshening (i.e. $Cl^-$ depletion) in fluids (Kastner et al., 2014) are known from cold seeps or MVs at a range of passive margins, such as at the Canadian Beaufort Sea (Paull et al., 2015b), erosive margins along Costa Rica (Hensen et al., 2004), or accretionary systems including Barbados (Le Pichon et al., 1990; Martin et al., 1996), Cascadia (Torres et al., 2004a), or the eastern Mediterranean (Dählmann and De Lange, 2003). Analyses on the composition of fluids obtained from MVs have revealed that the clay-mineral dehydration is an important source of pore water supply in mud breccia fluids (Mazzini and Etiope, 2017). The transformation of smectite to illite (illitization) typically takes place at ~60–150 °C (Kastner et al., 2014) and occurs at depths of several km (e.g. by assuming a linear geothermal gradient of 30 °C/km) and, therefore, provides a means to estimate the source depth for fluids associated to the MV system. An alternative dehydration reaction is the transformation of opal-A to opal-CT to quartz, which occurs at temperatures of ~10–100 °C. The dehydration of opal typically requires diatomaceous-ooze or radiolarians in the sediment as the source for the silica-opal (Dählmann and De Lange, 2003; Kastner et al., 2014).

## 1.8. Temperatures at cold seeps

Sediment temperature observations at cold seeps and MVs are helpful to characterize their activity. The ascent of subsurface material also transports heat and causes a temperature increase in near surface sediments affected by seepage. Although a precise temperature range for “cold” seeps is not defined, the term effectively differentiates against magmatic volcanic or hydrothermal systems and hot vents where emerging fluids are typically >60 °C and which occur in geologically different contexts (e.g. oceanic spreading centers at

divergent margins) and show much faster emission rates (Parnell, 2002; Haase et al., 2007). Cold seeps are typically characterized by sediment temperatures that are at maximum several tens of °C warmer (e.g. >40 °C at 10 m sediment depth at Isis MV; (Feseker et al., 2009a)) than sediments not affected by seepage (ca. 14 °C at 10 m sediment depth in the same study located in the warm Eastern Mediterranean). In case the background geothermal gradient is known for the study area, it is possible to estimate a source depth for material that is emitted at certain temperature. At best, these are minimum estimates, however, due to heat loss over time or distance during the material ascent or near-surface seawater infiltration, and should be cross-investigated via geochemical analyses of emitted gas or water (or both; (Feseker et al., 2009a; Feseker et al., 2009b)).

Elevated temperatures at cold seep sites may, however, not only result from the advection of warm subsurface material. The spontaneous formation of gas hydrate is an exothermic reaction and sediment temperatures at cold seep sites located within the GHSZ (i.e. if the necessary pressure and temperature conditions are met; see Fig. 1.5.) can be influenced by warmer values locally (Sahling et al., 2009). On the other hand, the dissociation of gas hydrate consumes heat and the occurrence or distribution of gas hydrate in a sediment core (retrieved on deck) can be investigated by looking for cold spots (temperature anomalies on the order of several degrees) with the use of an infrared camera (Weinberger et al., 2005; Bohrmann and Torres, 2006).

# 2. Study area

## 2.1. Tectonic and geological setting of the Calabrian Accretionary Prism

The Mediterranean Sea forms a contact area between the convergent African and Eurasian plates and continental-scale lithospheric subduction processes have strongly influenced the development of both the eastern and western Mediterranean basins since the Late Oligocene (Biju-Duval et al., 1977; Gueguen et al., 1998; Neri et al., 2009). Whereas remnants of Mesozoic oceanic crust (Neotethys) are likely present below the sedimentary infill of the Eastern Mediterranean (Granot, 2016), no Mesozoic oceanic crust is found in the Western Mediterranean basins. The Calabrian subduction zone in the central Mediterranean (Ionian Sea) is argued to represent one of the last remaining sites where oceanic crust of the Neotethys is involved in subduction today (Spakman, 1986; de Voogd et al., 1992). Based on tomographic studies of the subduction zones below the Apennines and Calabria it appears that a lateral slab tear has progressed southeastward from the northern Apennines across the central and southern Apennines and caused detachment of the downgoing slab (Wortel and Spakman, 2000). A slab tear is also argued to propagate from the west near Sicily, causing the onset of slab detachment at the Calabrian subduction zone (Fig. 2.1). These findings imply that the present-day subduction zone is limited to a narrow sector of Tethyan lithospheric material at the Calabrian subduction zone (Faccenna et al., 2001; Spakman and Wortel, 2004; Neri et al., 2009)).

The arcuate-shaped Calabrian subduction hinge developed by the progressive subduction of the African below the Eurasian plate coupled to the eastward retreat and the roll-back of the Ionian side of the subducting lithospheric slab during the last 30 Ma (Fig. 2.1; (Wortel and Spakman, 2000; Neri et al., 2009)). The slab retreat invoked the opening of the Tyrrhenian Sea basins in the backarc since the upper Miocene (ca. 10 Ma) generating the Vavilov basin during the Pliocene (4–3 Ma) and the Marsili basin in the Early-Mid-Plesitocene (2–1 Ma) in two rapid phases with extension rates of up to 50–70 mm/yr (Jolivet et al., 1999; Sartori, 2003; Faccenna et al., 2007; Polonia et al., 2011). During the eastward slab retreat across >300 km, the Calabria-Apennine subduction zone was fragmented and developed a narrow (ca. 200 km wide) and steeply dipping (~70°) plane dipping in NW direction (striking NE-SW) to >500 km depths (Faccenna et al., 2001; Neri et al., 2009). The present-day, arcuate shape of the Calabrian subduction zone has been attributed to a last phase of the slab retreat in combination with opposite vertical axis rotations between Sicily/Calabria (clockwise rotations) and the Southern Apennines (counterclockwise rotations; (Mattei et al., 2007)). It is assumed that subduction and slab retreat ceased between 1–0.5 Ma, causing a tectonic reorganization coinciding with the onset of km-scale uplift (on the order of 0.5–2 mm/yr) of Calabria and parts of the forearc basins (Westaway, 1993; Goes et al., 2004; Mattei et al., 2007; Zecchin et al., 2011). The uplift is argued to have substantially contributed to the morphology of the Calabrian-Ionian margin slopes. They are characterized by steeply incising riverbeds onshore (“fiumare”), that connect to numerous submarine canyons organized orthogonally to the coastline (Morelli et al., 2011; Gutscher et al., 2017).

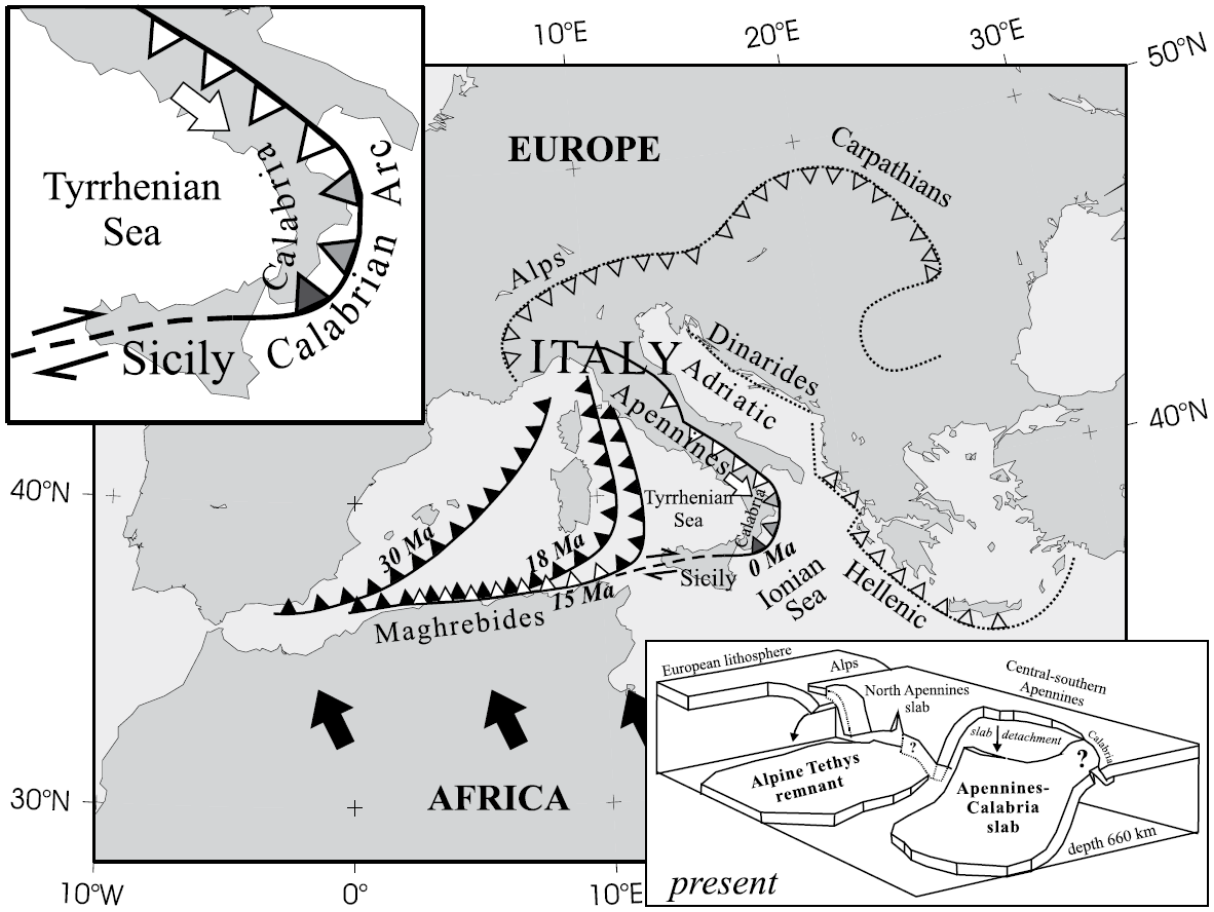


Fig. 2.1. Map of the Mediterranean region showing the Mediterranean plate boundary evolution during the last 30 million years; black arrows indicate the present plate motion of Africa with respect to Europe; curves with sawtooth patterns (pointing in direction of subduction) indicate the location of the western Mediterranean convergent boundary at different times; black, white, and grey sawteeth indicate, respectively, continuous, detached, or a doubtful (as for Calabria) situation of subducting slab; white arrow shows the inferred direction of lateral migration of slab detachment; Upper left inset: Map of the Calabrian Accretionary Prism area (here called Calabrian Arc) at a different scale; Lower right inset: 3D sketch of the geometry and geodynamic situation of the lithospheric slabs in the Alps, Apennines, southern Tyrrhenian Sea, and Calabria as derived and interpreted from positive upper mantle anomalies in tomographic data. A question mark indicates the doubtful situation of subduction beneath Calabria; from Neri et al. (2009) (after Wortel and Spakman (2000); Spakman and Wortel (2004)).

In the external part of the subduction zone, sediments were scraped off from the descending African plate and were accumulated into a thick wedge (up to 10 km) forming an accretionary complex. This wedge is referred to as the Calabrian accretionary prism (CAP). The CAP spans over 300 km from onshore Calabria at ~1900 m above sea level to the toe of the wedge at water depths of ~4000 m in the Ionian abyssal plain where it intersects with the Mediterranean Ridge (Fig. 2.2). To the southwest, the CAP is bordered by the Malta escarpment and by the Apulia escarpment to the northeast (Rossi and Sartori, 1981; Malinverno and Ryan, 1986; Minelli and Faccenna, 2010). The CAP can be separated in an Eastern Lobe and a Western Lobe, and the so called Ionian Fault has been identified at the limit between the lobes. The Ionian Fault arguably involves dextral strike-slip in the

northwestern portion but sinistral shear along the outer limit of the lobes (Polonia et al., 2011; Gutscher et al., 2017).

The overall geometry and deformational style was strongly influenced by the syn-accretionary deposition of evaporite units on the wedge and the undeformed frontal parts (Minelli and Faccenna, 2010) during the Messinian salinity crisis between 5.97 and 5.33 Ma (Hsü et al., 1973; Roveri et al., 2014). Several studies have analyzed the morpho-structural layout of the offshore to near-onshore CAP (e.g. Rossi and Sartori (1981), Minelli and Faccenna (2010), Polonia et al. (2011), Ceramicola et al. (2014b), Gutscher et al. (2017)), which can be summarized to consist of: 1) the Ionian abyssal plain, 2) the external (evaporitic) wedge also referred to as the post-Messinian wedge, 3) the internal (clastic) wedge also referred to as the pre-Messinian wedge, and 4) the forearc basins (offshore known as the Spartivento-Crotone basins) including the Calabrian slope and onshore land topography of Calabria (Fig. 2.2).

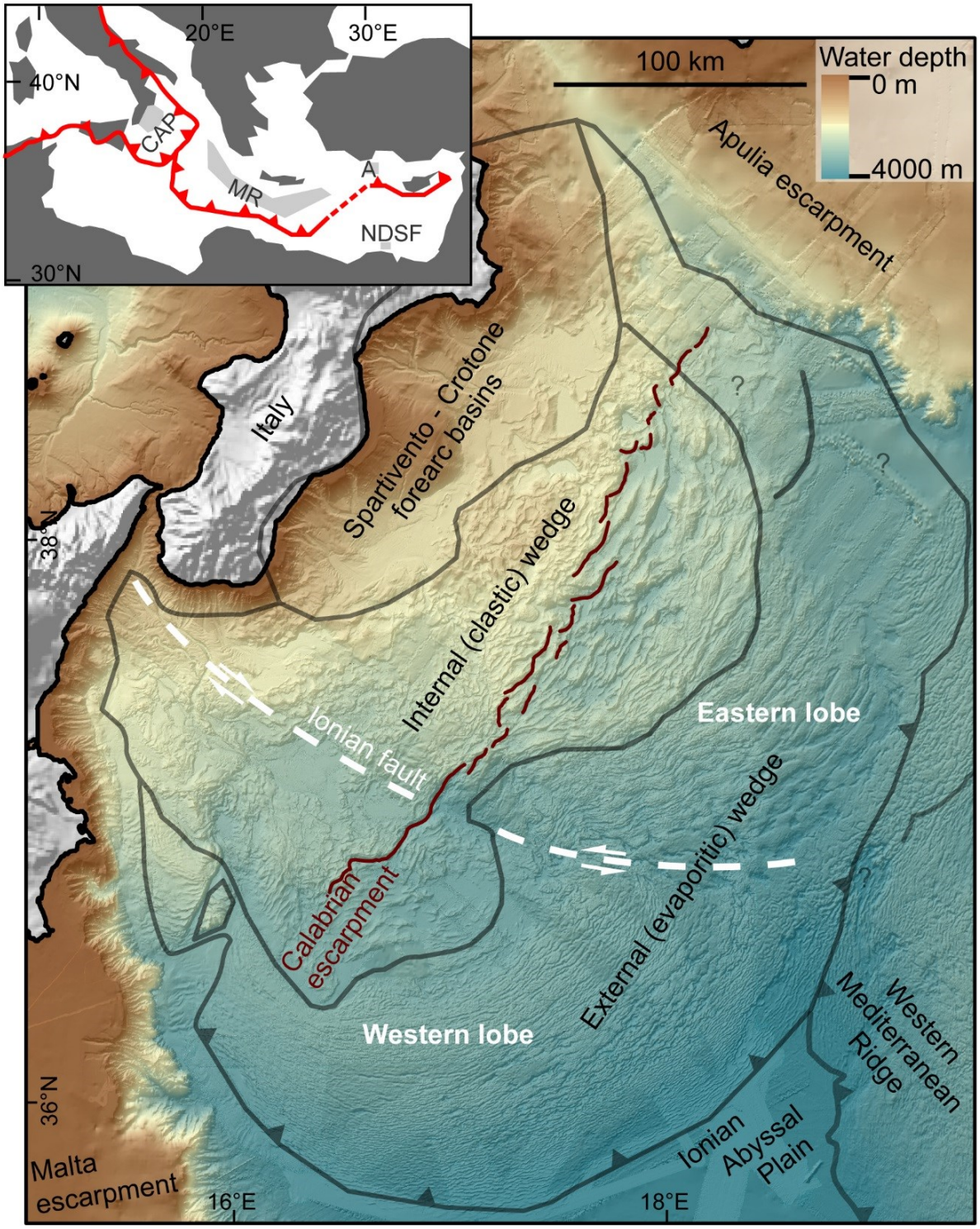


Fig. 2.2. Inset: The location of the Calabrian Accretionary Prism (CAP), Mediterranean Ridge (MR), Anaximander Mountains (A), and the Nile Deep Sea Fan (NDSF) and associated MV provinces (light grey areas; after Mascle et al. (2014)) in the Eastern Mediterranean region; major plate boundaries are indicated by red lines (sawteeth point in direction of subduction); Main figure: Bathymetry of the CAP with morpho-structural domains (each framed by a dark grey line) after Ceramicola et al. (2014b) and Gutscher et al. (2017); the Calabrian Escarpment separates the Internal wedge (see text) and the Ionian Fault straddles the boundary between an eastern and a western lobe; topography data of Italy from Ryan et al. (2009).

Metamorphic and sedimentary units of a Mesozoic-Cenozoic basement of the accretionary wedge is exposed in the onshore forearc basins. They are and overlain by sediments of up to Mid-Miocene (late Serravallian) age, including Messinian evaporites and Plio-Pleistocene units (Roda, 1964; Zecchin et al., 2003), which have also been drilled in nearshore wells (Capozzi et al., 2012). Seismic investigations suggest that the offshore Spartivento-Crotone forearc basins contain up to 2 km of Pliocene-Quaternary sedimentary infill with <500 m thick Messinian deposits (Minelli and Faccenna, 2010; Polonia et al., 2011). Capozzi et al. (2012) have proposed that the Messinian deposits likely consist of siliciclastic successions but it should be reminded that to date, the offshore forearc basins have never been drilled. Seawards, the internal wedge of pre-Messinian age is characterized by sets of ridges and basins of several hundred meters in relief that have been interpreted as a fold-and-thrust belt (Rossi and Sartori, 1981; Praeg et al., 2009). The most prominent ridge has been termed the Calabrian Escarpment and it marks the transition from an inner plateau and an outer, more rugged area. The fold-and-thrust belt morphologies are attributed to a series of out-of-sequence thrusts extending below the forearc basins and they document post-Messinian activity and deformation (Minelli and Faccenna, 2010; Polonia et al., 2011; Ceramicola et al., 2014b). The external, post-Messinian wedge is characterized by lower relief, referred to as a cobblestone morphology, which decreases progressively across the outer domain (Rossi and Sartori, 1981). The cobblestone morphology is attributed to underlying, evaporitic Messinian deposits that thicken seawards and have been identified to act as a basal décollement of the subduction zone. Indications of the northwest dipping, downgoing slab have been identified at the transition to the Ionian Abyssal plain (Minelli and Faccenna, 2010).

## 2.2. Mud volcanism in the Central and Eastern Mediterranean

The margins of northern Africa and southern Eurasia bordering the Eastern Mediterranean, host one of the world's highest abundance of currently recorded submarine MVs (Kopf, 2002; Foucher et al., 2009; Mascle et al., 2014). In the Central and Eastern Mediterranean the following offshore areas have been confirmed to contain major MV provinces: 1) the Mediterranean Ridge, 2) the Anaximander Mountains, 3) the Nile Deep Sea Fan (NDSF), 4) the Calabrian Accretionary Prism (CAP; Fig. 2.2).

The earliest studies of submarine mud volcanism in the Eastern Mediterranean have been conducted over 30 years ago. These pioneer studies cored (and introduced the new term) "mud breccia" for the first time at the Prometheus mud dome along the Mediterranean Ridge accretionary prism (Cita et al., 1981; Camerlenghi et al., 1992). Subsequent scientific drilling of the Napoli and Milano MVs revealed that extrusive activity occurred up to the last 1.2 Ma ago (Robertson et al., 1996). Systematic sidescan sonar investigations partially ground truthed by sediment cores revealed that 96% of all MVs on the Mediterranean Ridge occur in an area ca. 70 km wide forming a belt along the prism backstop. This MV belt seems to correspond to large regional shear zones resulting from strain partitioning due to oblique plate convergence between Africa and Eurasia (Rabaute and Chamot-Rooke, 2007).

The first (and so far only) occurrence of gas hydrates in the Mediterranean Sea could be confirmed at MVs in the Anaximander Mountains. Gas hydrates were initially sampled at the Kula MV (Woodside et al., 1998), and later also repeatedly at the Amsterdam, Kazan, Thessaloniki MVs (Lykousis et al., 2009; Pape et al., 2010). Given the generally high sea water salinity and temperature (e.g. 38.7 PSU and 13.8 °C at the CAP during 2014; (Bohrmann et al., 2015)) of the Mediterranean deep water masses, the gas hydrate stability, for example at the CAP, is reached in depths exceeding 1000 m (Fig. 2.3). This restricts the potential occurrence of gas hydrates in the Mediterranean to the deep basins such as at the Anaximander Mountains. Highly elevated gas concentrations, as found in the Anaximander Mountains MVs (Pape et al., 2010), are required for gas hydrates to occur at the seafloor or the near-surface sediments in the Mediterranean.

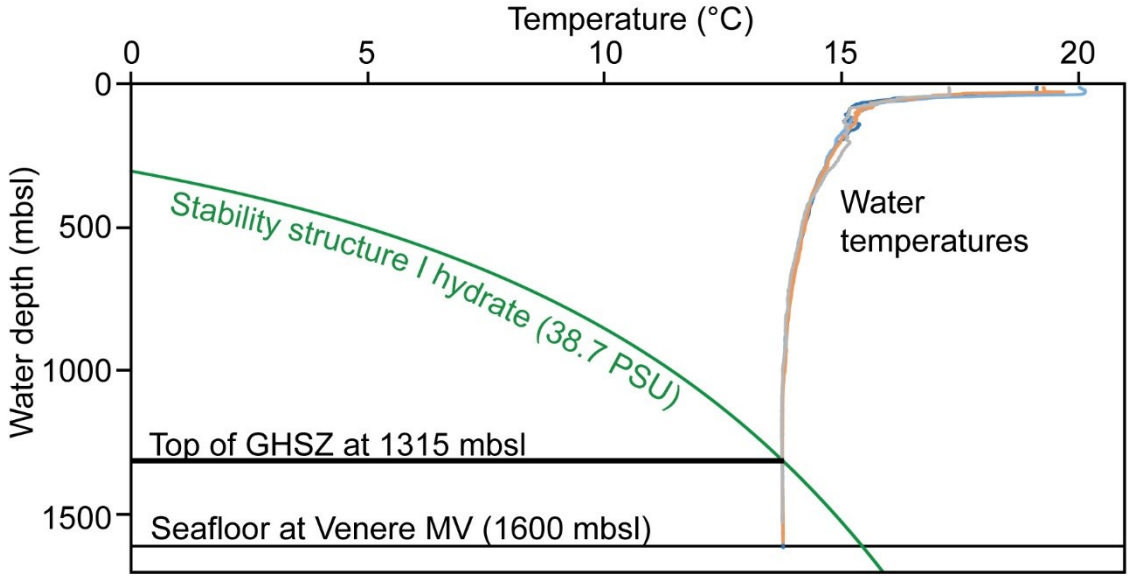


Fig. 2.3. Calculated stability field of methane hydrate (structure I) as defined by temperature and pressure (expressed as depth in meters below sea level (mbsl)) for salinity representative of the Mediterranean sea water encountered at Venere MV in the CAP. Based on the local water temperatures at Venere MV the top of the gas hydrate stability zone (GHSZ) could be determined; temperatures were measured by a conductivity-temperature-depth (CTD) probe, see Bohrmann et al. (2014), and the gas hydrate phase boundary was calculated with the program HWHYD (Masoudi and Tohidi, 2005).

The Egyptian continental margin hosts numerous cone-shaped MVs and kilometer-scale, gas rich mud pies at the eastern edge of the NDSF (Dupré et al., 2008). Of particular interest are a group of cone-shaped MVs within a large caldera structure located at the foot of the continental margin in the western reaches of the NDSF. The cones host summit calderas filled with highly saline brines and the seeping fluids have been interpreted to be sourced from within or below highly fractured Messinian evaporites (Huguen et al., 2009; Dupré et al., 2014). Brine lakes were also discovered on MVs in the Olimpi Field on the Mediterranean Ridge (Woodside and Volgin, 1996) but their salinity signature has been attributed to relict, evaporated pore water rather than dissolution of Messinian salt (Charlou et al., 2003). In fact, km-thick evaporite layers are seen as efficient traps for fluids and to prevent fluid flow to the seabed in the deep parts of the Mediterranean basins. Based on large-scale seismic

investigations, the distribution of most MV in the Mediterranean region has been found to correlate with sites where evaporites show reduced thickness, or are absent (within the seismic resolution; Fig. 2.4). The MV province located on the western edge of the NDSF represents an exception to this observation and may be related to specific source rocks underlying the Messinian evaporites (Kirkham et al., 2017) and the presence of growth faults and strongly fractured evaporites associated with that part of the African continental margin (Huguen et al., 2009; Mascle et al., 2014).

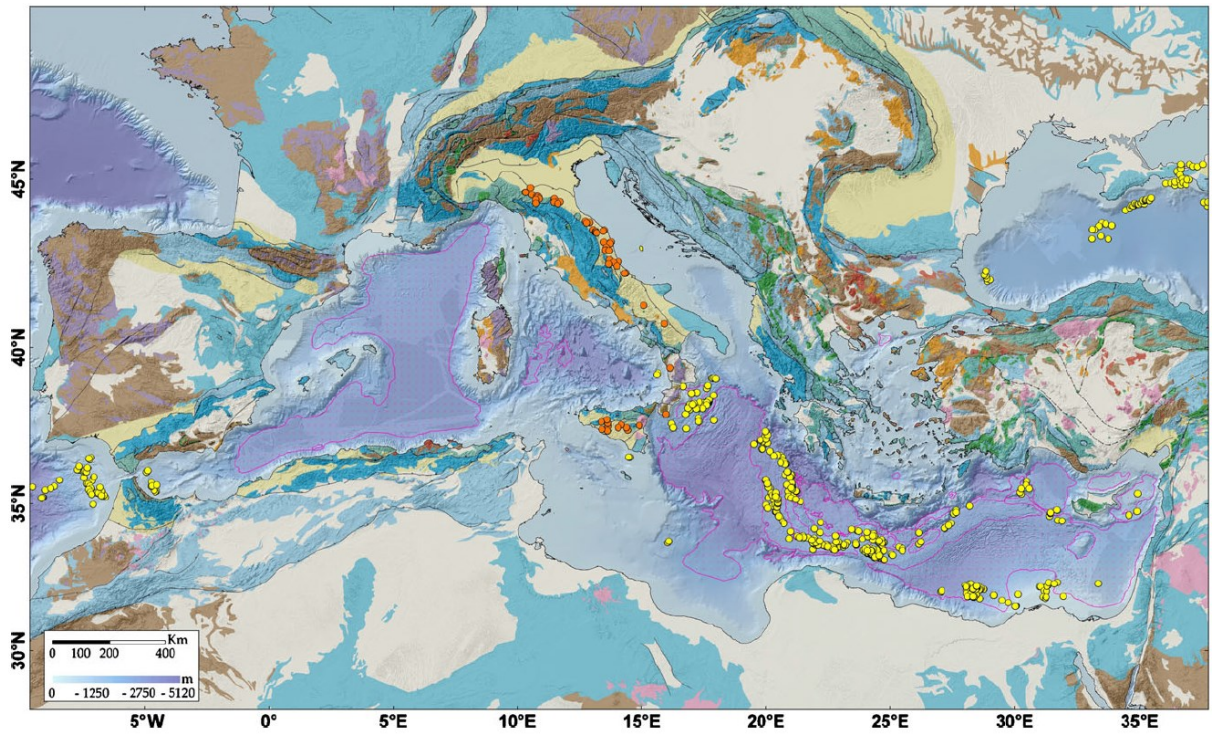


Fig. 2.4. Large-scale distribution of MVs (terrestrial MVs = orange dots; offshore MVs = yellow dots) and deep Messinian evaporite basins (pink lines) in the Mediterranean region, possibly the Earth's area most densely populated by MVs. Most occur where no thick Messinian evaporite deposits exist, with the exception of the northwestern Egyptian margin; from Mascle et al. (2014).

For the Central and Eastern Mediterranean it can be generally stated that MVs develop preferentially in association with compression such as in the Mediterranean Ridge accretionary prism (Limonov et al., 1996) but also along passive continental margin areas characterized by high sedimentation rates such as at the NDSF (Dupré et al., 2007). An underlying tectonic control with regard to MV distribution and extrusive activity has become apparent because most MVs so far identified in these areas show an association with structures such as thrusts or folds expressed morphologically on the seabed or in the shallow subsurface (Galindo-Zaldivar et al., 1996; Kopf, 2002). An active tectonic context, high sediment accumulation rates and an inhomogeneous distribution of Messinian evaporites also characterize the CAP, which is still considered a frontier area for MV research (Foucher et al., 2009). The occurrence of over 50 MVs has only recently been recognized (Praeg et al., 2009; Ceramicola et al., 2014b).

## 2.3. Mud volcanism in the Calabrian Accretionary Prism

In the CAP the first mud breccia containing lithic fragments of Upper-Cretaceous to Messinian age was recovered over 30 years ago in two sediment cores taken on top of a seismically chaotic body (Barbieri et al., 1982; Morlotti et al., 1982). These deposits were not recognized to originate from MVs but instead were interpreted to be the result of tectonic "chaoticization" (Morlotti et al., 1982) and have only recently been attributed to mudflows originating from the Sartori MV (Panieri et al., 2013). The likely presence of MVs in the CAP became apparent, however, during ground truthing and reassessment of large-scale sidescan surveys of the Mediterranean Ridge and a partial section of the CAP (Fusi and Kenyon, 1996; Sartori, 2003). To date, more than 50 MVs have been identified (the locations of the most relevant MVs for this study is shown in Fig. 2.5a) across the Spartivento and Crotone forearc basins as well as the pre-Messinian prism (Fig. 2.5b+c), with variable certainties based on the compilation of sediment cores, morphology, backscatter, and subbottom data (Ceramicola et al., 2014b). Several mud diapirs have been inferred from seismic data to occur below the forearc basins (Capozzi et al., 2012). Seawards of the Calabrian Escarpment (in the outer pre-Messinian prism), only one extrusive structure has been proposed to occur in addition to a site that may have been affected only by gas release in the past (Praeg et al., 2009; Panieri et al., 2013; Ceramicola et al., 2014b).

Seismic investigations have been conducted across the Madonna dello Iono MVs (forearc basin) and the Pythagoras MVs (near the Calabrian Escarpment; locations in Fig. 2.5a) and determined that extrusive activity started already 3 Ma ago. It is argued that the onset of mud volcanism corresponds with a major tectonic reorganization of the Calabrian subduction zone during the mid-Pliocene (Praeg et al., 2009). Systematic hydroacoustic surveys of the CAP revealed the general morphologies of numerous MVs and anomalous backscatter intensities could be attributed to sites of more recent mud breccia extrusion. Based on the burial depth of cored mud breccia deposits, an estimated sedimentation rate, and the corresponding backscatter intensity allowed to constrain overall MV activity during the last 56 ka, and within the last 12.5 ka in the forearc basins (Ceramicola et al., 2014b). Evidence of active fluid release at MVs or cold seeps in the CAP has been limited to observations made during ROV dives at the Madonna dello Iono MV, where seepage was indicated by elevated geothermal gradients in addition to the presence of reduced-appearing sediments and chemosynthetic tubeworms in a short core (Foucher et al., 2009).

The micropaleontological evidence of mud breccia clasts (e.g. from Madonna dello Iono, Pythagoras, or Sartori MVs) of up to Cretaceous age point to a source of mobilized material situated deep with the accretionary prism (Morlotti et al., 1982; Praeg et al., 2009; Panieri et al., 2013). Because a large number of MVs appear to be aligned along the Calabrian Escarpment or associated tectonic faults, the ascent of fluids from within the prism seems to be driven by the overall compressive regime of the CAP (Praeg et al., 2009; Gutscher et al., 2017). It has been suggested that the out-of-sequence thrusts provide preferential pathways for fluid migration (Polonia et al., 2011; Panieri et al., 2013). This, however, remains unclear because, with the exception of one structure, no MVs have so far been identified seawards of

the Calabrian Escarpment among the proposed out-of-sequence thrusts (Fig. 2.5c). MVs occur predominantly at the edges of the forearc basins or the inner pre-Messinian prism in areas where Messinian evaporites are absent or strongly thinned (Fusi et al., 2006; Ceramicola et al., 2014b).

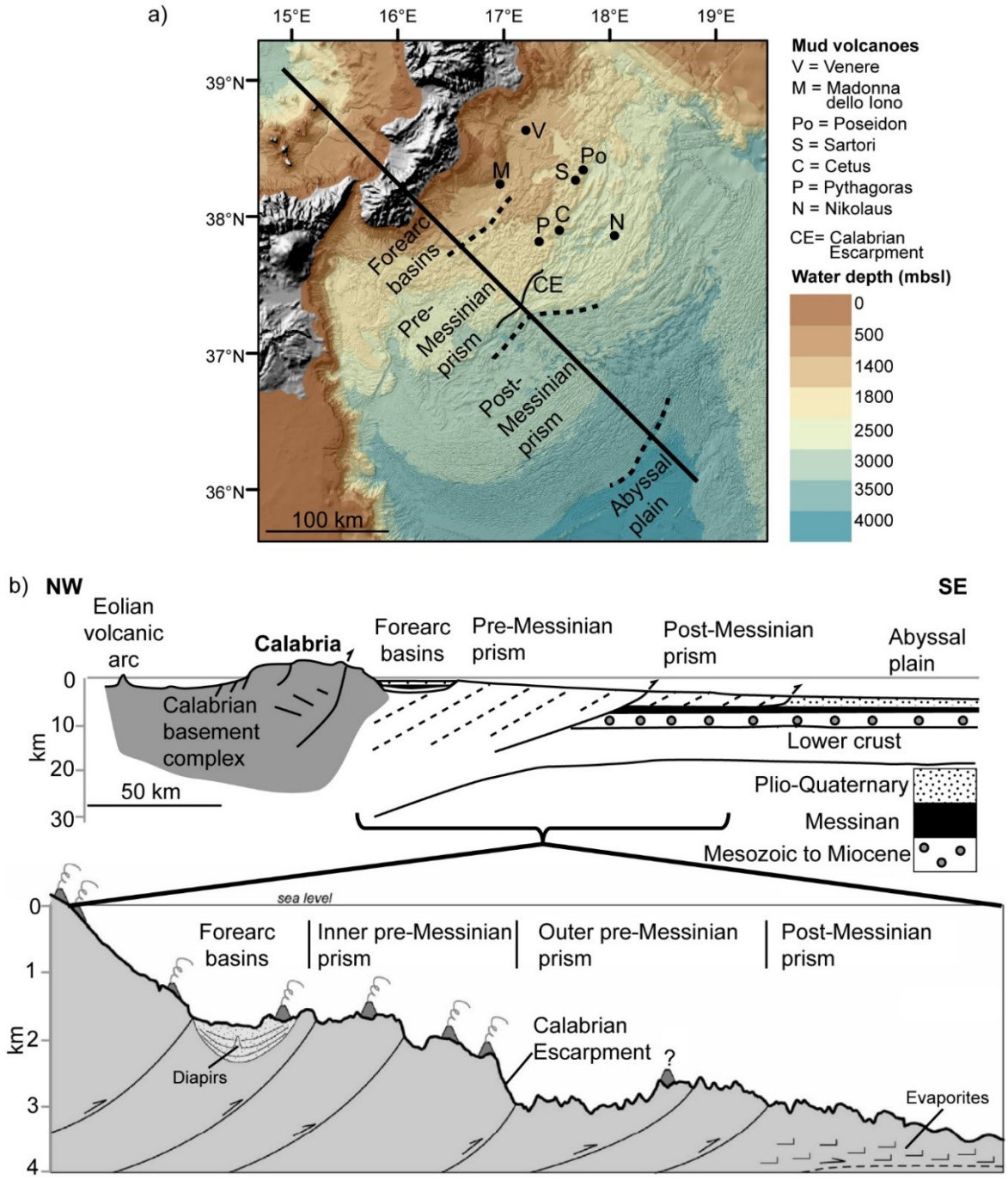


Fig. 2.5. a: Morpho-bathymetry of the CAP (note stretched color scale) and location of selected MVs in the forearc basin (Venere and Madonna dello Iono), the inner pre-Messinian prism (Sartori, Cetus, Pythagoras, Poseidon), and the outer pre-Messinian prism (Nikolaus); b: Schematic NW-SE cross-section from Tyrrhenian to the Ionian seas; see a) for nominal location; modified after Praeg et al. (2009)) and enlargement of the central part (modified after Ceramicola et al. (2014b)) with the MV distribution (projected) in relation to the structural zones; black lines with half-arrows indicate thrusts.

The main focus of this work is on the twin-cone Venere MV, which was identified for the first time and named by Ceramicola et al. (2014b), who recognized the overall morphology but no particular indications of ongoing seepage activity. It was during research cruise by RV METEOR M112 in 2014 that documented fresh appearing mud breccia extrusions and a flare at the MV summit and active gas bubble streams and chemosynthetic communities at peripheral seeps of the MV edifice (Bohrmann et al., 2015). Extensive and repeated hydroacoustic surveys across most of the MV structures initially identified across the CAP by Ceramicola et al. (2014b), indicated that Venere MV was the only structure characterized by gas emissions at that time. Considerable efforts including visual and hydroacoustic surveys, seafloor mapping, water column measurements, and geological sampling of fluids and solids were undertaken at Venere MV, to investigate this active structure. The gas emissions were monitored during repeated surveys over 31 days and the gas flares showed variability both in timing (episodic vs. continuous activity) and intensity (inactivity vs. flares of >250 m height). Bottom water samples from near the seafloor (0.5–2 meters) at flare sites were enriched in methane and showed concentrations of up to 566 µM. It was found, however, that this methane was rapidly oxidized in the higher water column at ca. 100 m above seafloor (Geprägs, 2016). Blumenberg et al. (2017) analyzed gas samples, that were collected at cold seeps along the periphery of the MV and have revealed a thermogenic origin based on the carbon stable isotope composition of methane ($\delta^{13}C\text{-}CH_4$ of -48.6‰ and -47.3‰) in addition to the presence of ethane ($\delta^{13}C\text{-}C_2H_6$ of -21.6‰ and -22.3‰) and propane ($\delta^{13}C\text{-}C_3H_8$ of -12.5‰ and -17.7‰).

The results from M112 included a bathymetric dataset derived from multibeam mapping by an autonomous underwater vehicle (AUV, MARUM-SEAL 5000) that partially covered Venere MV and the surrounding caldera (Bohrmann et al., 2015). The preliminary results obtained during M112 inspired a second research expedition by RV POSEIDON POS499 in 2016 to complete the AUV-based mapping and to complement the geological investigations by additional sediment cores (Bohrmann et al., 2016). The results and conclusions presented in this work are based on the data collected during both the M112 and the POS499 cruises.

# 3. Motivation and objectives

## 3.1. Overarching goal

The overarching goal of this work is to study mud volcanism and associated fluid seepage in a comprehensive geological context at the example of the active Venere MV in the CAP. The reviews provided in Chapters 1 and 2 indicate that a number of topics remain unsatisfactorily resolved with regard to the general functioning of cold seeps but also their association with fluid generation and migration in the CAP. The three main manuscripts presented in this cumulative thesis (Chapters 5, 6, 7) and the two additional studies (Chapters 8, 9) aim to address the aspects which are outlined in the following.

## 3.2. Open questions and aims of the three manuscripts

**i) Shed light on processes responsible for fluid generation, transport, and discharge.**

Processes that drive MVs occur at subsurface depths inaccessible for direct sampling. Analyzing fluids emitted at cold seeps or extruded within mud breccia of MVs, however, provides a way of learning about deep-seated crustal dewatering, hydrocarbon generation, and diagenetic reactions. The surface expression of mud volcanism and fluid seepage is related to the underlying plumbing system and the governing type of activity (eruptions vs. quiescent seepage). Whereas these aspects have been studied in case studies on land, they have rarely been investigated for submarine MVs. The potential implications of different fluid migration pathways for the distribution of cold seeps including the seep-associated fauna remain poorly known. In the CAP, the fluids involved in the mud volcanism have not been investigated so far even though it has been hypothesized that they are supplied from deep within the accretionary prism. The first study presents a new AUV-derived seafloor map at meter-scale resolution of Venere MV and makes use of hydroacoustic water column investigations and ROV surveys to locate gas emission sites and to document the area of most recent mud breccia extrusions. ROV observations and samples of sediments and fluids are used to characterize different discharge mechanisms and geochemical fluid analyses indicate the sources of fluids. Based on the geophysical, sedimentological, and geochemical datasets a conceptual model is proposed to explain the observed structure of Venere MV and the involved fluid sources. The results improve the understanding of the plumbing systems of submarine MVs and confirms the hypothesis that fluid origins are located deep below the forearc basins of the CAP.

**ii) Investigate the morpho-dynamic changes and the spatio-temporal evolution of the MV and potential interactions with processes in the surrounding channel.**

The morphologies of MVs (overall edifice, caldera, ring faults, etc.) result from mud breccia extrusion and represent a development of a MV over time. Thousands of submarine MVs are estimated to exist globally and the extrusion of mud breccia contributes to the cycling of gases, liquids, and solids from the subsurface into the hydrosphere. There is little information on the evolution of deep-sea MVs, few are mapped at resolutions that would render their detailed structures appropriately, and the age of structures revealed by mapping is generally poorly constrained. Furthermore, scarce quantitative information exists on the volumes and

amounts of mud breccia potentially extruded by individual MVs. In the CAP, it remains largely unclear if and how active the MVs are today and the timing of mud volcanism in the forearc basin has only been constrained loosely to within the past few millennia. The higher-resolution data available for Venere MV now allow to study the more recent and present-day extrusive activity, possibly representative of the past. Furthermore, potential interactions between Venere MV and a submarine canyon can be investigated. In the second manuscript, individual mudflows are identified on the AUV-derived bathymetry and backscatter data of Venere MV and their ages are estimated based on the amount of overlying hemipelagic sediment and the sedimentation rate, determined by sediment cores and tephrochronology. This allows to develop a three-stage evolutionary model for Venere MV, involving also processes in the surrounding submarine canyon, and to estimate volumes of extruded mud breccia. The findings constrain for the first time the morpho-dynamic and spatio-temporal evolution of surface structures observed at a deep-sea MV by AUV-based mapping. It reveals a more recent history of mud volcanism at Venere MV than was previously assumed based on only regional-scale investigations by other authors. The approximate volumes that are derived for mud breccia extrusion and methane emissions are valuable additions to the few estimates in previous literature.

**iii) Study the structure and development of cold seeps along the ring fault system.**

The seepage of hydrocarbon-rich fluids and the presence of gas hydrates can fuel chemosynthesis-based benthic communities with high species richness in remote deep sea areas. Little is known on these oases of life regarding their distribution and development within and around MVs and the fluid migration pathways they are associated to. Cold-seep structures, which are observed during visual investigations are often poorly documented and lack spatial and temporal context to each other. In the CAP, evidence of cold-seep ecosystems has been limited, but at Venere MV it is possible to study a large range of morphologically different structures and to investigate how such features may have developed. In the third manuscript, the structure and extent of cold-seep ecosystems around the periphery of Venere MV are documented for the first time. High-resolution photomosaics cover several entire structures and are complemented by ROV observations, analyses of carbonate samples, and AUV-derived backscatter data. Based on observed differences between the individual seep sites, the geological structure and biological colonization is investigated. A conceptual model is proposed to explain the structures and their development over different timescales. The results of this study expand previously existing models on the self-sealing nature of cold seeps and highlight the previously unknown diversity of cold-seep ecosystems and structures in the CAP.

### 3.3. Open questions and aims of the preliminary studies

Additional results have been obtained and are presented in their preliminary stage including tentative interpretations (Chapters 8 and 9). They aim to address the following aspects:

- **Investigations on the MV distribution in the CAP**

In the CAP, numerous MVs have been identified in the forearc basins and the inner pre-Messinian prism but their distribution within the fold-and-thrust belt remains poorly understood. Based on the obtained hydroacoustic data (bathymetry, backscatter, sub-bottom), the structure and distribution of previously confirmed or potentially new MVs is investigated. This work aims at a better understanding of MVs occurring along potential tectonic structures, their diversity in shapes and sizes, and their potential role for fluid flow in different morpho-structural domains of the CAP.

- **Revealing the structure of a submarine mud breccia flow**

Mud breccia extrusion by MVs is considered an important mechanism to transport fluids and solids from the subsurface and across the seafloor. The visual appearance and structure of such mudflows in the deep sea is largely unknown because seafloor investigations are often carried out by hydroacoustic mapping and visual observations are limited to individual images reported from ROV dives. This highlights a need for better visualization of MV mudflows and their sites of extrusion. A photomosaic of the extrusion site at the western summit of Venere MV was assembled and allows to investigate the surface morphology of a fresh mudflow for the first time. The resulting dataset provides a starting point to potentially unravel the way such mud-fluid-rock mixtures flow across the seabed and develop while dewatering and degassing modify the morphologies.

# 4. Methods and approaches

## 4.1. Detecting signs of seepage activity

A crucial part of cold seep investigations is the detection and localization of active gas emissions. This can be achieved by high-frequency echosounder systems that hydroacoustically ensonify the water column and reveal gas bubbles in the water column as flares (high backscatter signatures) resulting from the impedance contrast between the water and the free gas (Klaucke et al., 2006; Nikolovska et al., 2008; Römer et al., 2012a). Hydroacoustic multibeam echosounder (MBES) systems mounted on the hull of research vessels or deep-towed sidescan sonars are efficient tools to systematically map large study areas for bathymetry and seafloor backscatter (Fusi and Kenyon, 1996; Sahling et al., 2008b; Ceramicola et al., 2014b; Römer et al., 2017). Flares occurring in close association with high backscatter patches have proven reliable indicators of cold seep carbonates, associated fauna or free gas / gas hydrates just underneath the seafloor (Klaucke et al., 2006; Römer et al., 2014). Mud breccia extrusion from submarine MVs leads to the emplacement of mudflows visible in morpho-bathymetric and backscatter data of the seafloor, but over time the mudflows are buried by marine sedimentation as well as subsequent mudflows. Whereas mud breccia buried to depths of several hundred meters can be investigated by drilling (Robertson et al., 1996) or seismic surveys (Perez-Garcia et al., 2009; Praeg et al., 2009), at meter-scale depths they may be sampled by coring (Cita et al., 1981; Gennari et al., 2013) or mapped based on their elevated intensities in acoustic backscatter compared to surrounding sediments (Volgin and Woodside, 1996; Paull et al., 2015b).

Of particular interest are studies, which have revealed changes in seabed morphology related to MV activity by repeatedly mapping the same seafloor area (Foucher et al., 2010; Feseker et al., 2014). This requires state-of-the-art MBES technologies capable of mapping at meter-scale resolutions in contrast to the surveys conducted at tens of meters resolution by MBES systems mounted on the hull of research vessels. High-resolution surveys are increasingly possible through MBES systems mounted on AUVs or ROVs (Wynn et al., 2014; Paull et al., 2015a). In addition to documenting mud movements at MVs (Feseker et al., 2014), they have also lead to significant improvements in the understanding of the distribution of gas release sites around cold seeps (Körber et al., 2014; Römer et al., 2014), or of different mechanisms of mud breccia extrusion at MVs (Dupré et al., 2008; Paull et al., 2015b). However, complete surveys of submarine MVs that are supported by geological samples are scarce.

Access to and sampling of deep-sea cold seeps or mud volcanoes in remote localities, requires specialized tools and techniques such as ROVs and autoclave systems for fluid sampling under in-situ pressure, but also conventional tools such as sediment corers or conductivity-temperature-depth (CTD) probes. The results and conclusions presented in this work utilized a multi-method approach. This chapter will give an overview of general methodical principles focusing specifically on hydroacoustic data obtained by ship- and AUV-based surveying and ROV-based photo mosaicking. Details for all geological, geochemical,

and additional geophysical analyses carried out in context of the main manuscripts, are provided in the respective methods sections of each of the manuscripts. Additional information of more technical nature have previously been summarized in the cruise reports (M112: Bohrmann et al. (2015) and POS499: Bohrmann et al. (2016), available online at www.marum.de).

## 4.2. Hydroacoustic investigations

In this work, systematic hydroacoustic surveys by MBES were used to obtain bathymetry and backscatter maps of the seafloor across the CAP and to investigate the water column for potential flares by a ship-mounted system (Kongsberg EM122 operating at 12 kHz). In addition, an AUV-mounted system (MARUM AUV SEAL 5000 with a Kongsberg EM2040 operating at 300 kHz) was utilized to survey at 80 m above seafloor at Venere MV.

Echosounders emit acoustic waves at a specific frequency that are reflected from the targeted seafloor. Whereas the bathymetry (i.e. a depth value for a target-point below the vessel) is derived from the traveling time and phase, the backscatter intensity results from the amplitude (i.e. the amount of energy) of the returning waves. The resolution of both bathymetry and backscatter are strongly dependent on the frequency of the system and the water depth in which the system operates (Lurton and Lamarche, 2015).

The backscatter signal for any targeted seafloor can be compared to the reflective character of an object relative to incident light captured during the opening and closing of a shutter in the lens of a photographer. The backscatter signal represents an opto-acoustic record, averaged over time and across the footprint area of the beam (Lurton and Lamarche, 2015). In addition to the frequency, the backscatter signal (typically reported in dB) depends on the signal attenuation in the water column and sediments because it penetrates the seafloor to a certain degree (Fig. 4.1, left). This implies that also the physical composition of the seafloor, including surface rugosity and sediment properties, affect the returned backscatter intensity (Mitchell, 1993; Klaucke et al., 2010). Fig. 4.1 illustrates that the backscatter intensity of a buried, highly-scattering surface that is targeted by a high-frequency signal (300 kHz), is more strongly attenuated than a low-frequency signal (12 kHz) by the same overlying sediments.

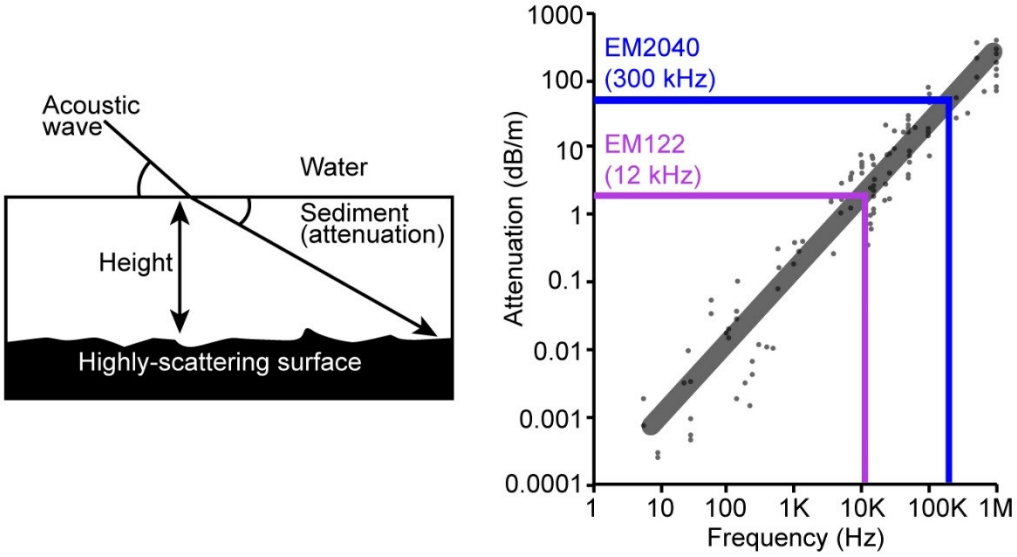


Fig. 4.1. Left: A highly-scattering (e.g. irregular and hard) surface overlain by attenuating soft sediment. The soft sediment reduces the intensity of the returned backscatter signal in proportion to its thickness (height) and in proportion to the attenuation rate (dB/m); Right: Plot of attenuation rates for different signal frequencies; the attenuation of a low frequency signal, such as the EM122 (mounted on the hull of RV METEOR), in soft sediment is much lower compared to the high-frequency signal of the EM2040 (mounted on the AUV utilized in this work); both figures modified after Mitchell (1993).

High backscatter intensities have been found associated to a range of irregular seafloor substrates including rock outcrops, carbonate hardgrounds, clast-rich mud breccia, and sediments charged by gas bubbles or even gas hydrate (Volgin and Woodside, 1996; Klaucke et al., 2006; Buerk et al., 2010; Eason et al., 2016). In contrast, soft hemipelagic sediments and strongly fluidized sediments such as in brine pools typically return lower backscatter intensities than the surrounding sediments (Woodside and Volgin, 1996; Sahling et al., 2009). Geological sampling (e.g. by sediment cores or ROV samples) is required to ground truth backscatter patterns before reliable interpretations of the observed structures are possible (Vogt et al., 1999).

The backscatter of a highly-scattering surface that is exposed at the seafloor decreases in intensity with increasing burial by sediments (Fig. 4.2). Such a behavior has been observed in cases where the seafloor was affected by fluid seepage and caused authigenic carbonate precipitation and biological activity, e.g. in the Congo Basin (Gay et al., 2007). Similarly, it has been possible to characterize progressively older mud breccia deposits at several MVs in the Eastern Mediterranean (Zitter et al., 2005).

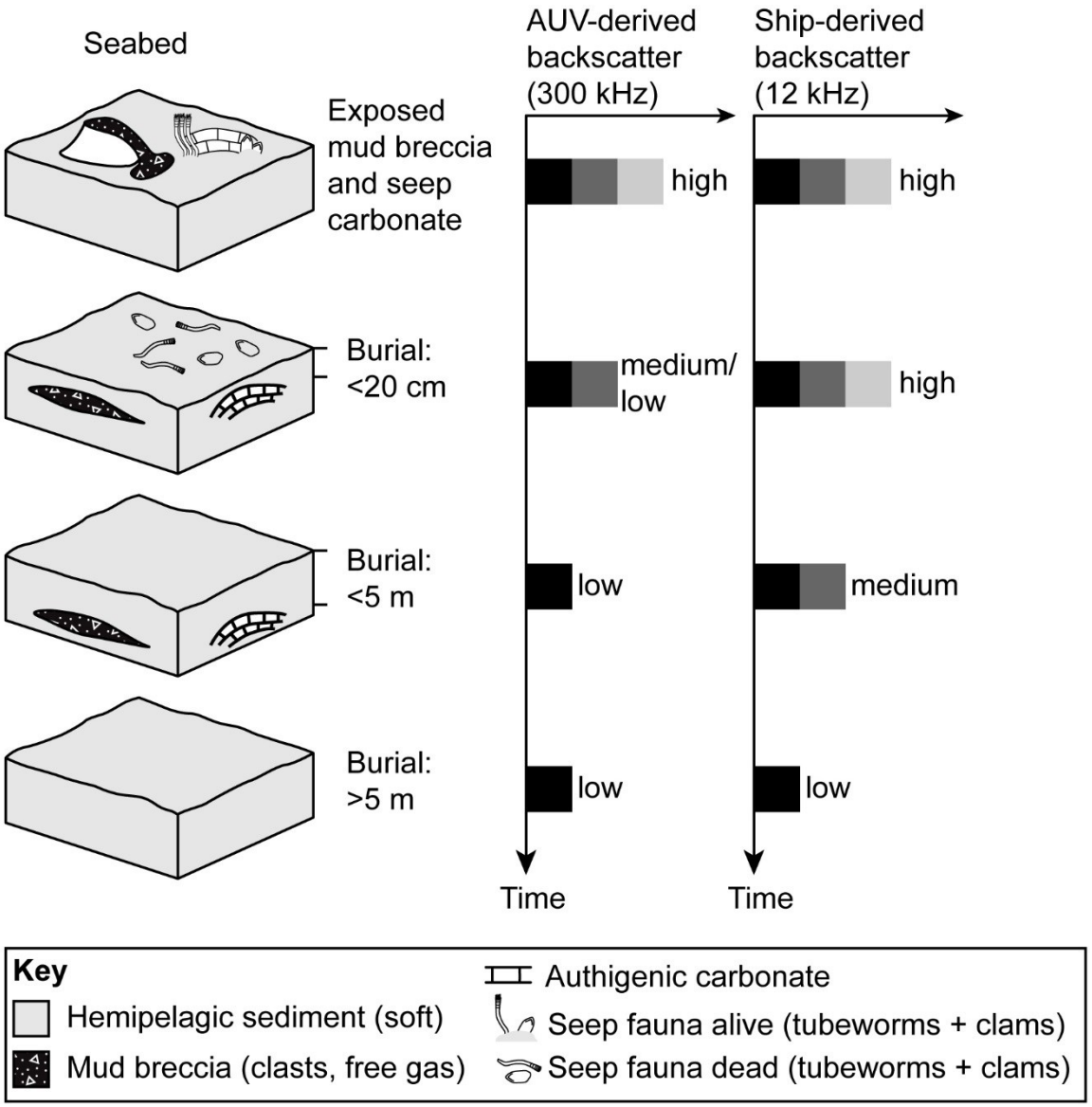


Fig. 4.2. Sketch illustrating the effect of increasing burial over time for the backscatter intensity (relative scale scale) of seep-influenced seafloor (i.e. highly-scattering carbonates and mud breccia deposits from a MV). Whereas the low-frequency signal (ship-derived backscatter) can reveal the subsurface up to several meters, the high-frequency signal (AUV-derived) is typically attenuated after several centimeters already but allows to differentiate younger deposits at a finer scale; modified after Gay et al. (2007).

For the manuscript presented in Chapter 6, a combination of hydroacoustic data and sedimentological ground truthing allowed a novel approach to investigate the activity of mudflow extrusions at Venere MV. A large number of mudflows was identified based on morphology and backscatter at Venere MV and the amount of hemipelagic sediment overlying the mud breccia could be systematically determined by sediment coring (Fig. 4.3). Based on the sedimentation rate it was possible to estimate the ages of emplacement (i.e. the onset of sedimentation on top) of individual mudflows and thus constrain the MV activity.

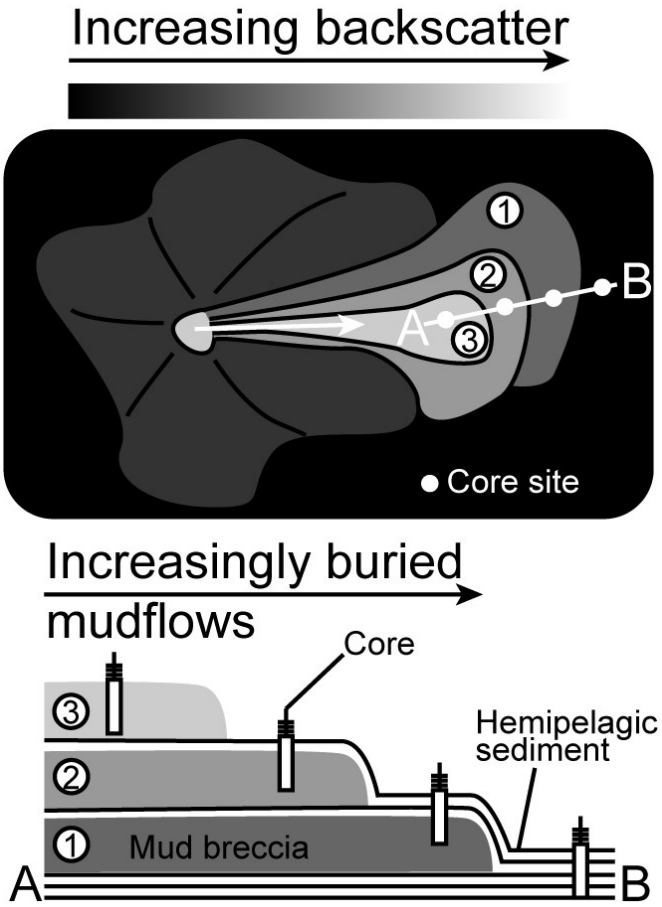


Fig. 4.3. Cartoon of a simplified, cone-shaped MV in backscatter map view (white arrow indicates flow direction from summit) and a group of stacked mud breccia deposits (1–3) shown in profile A–B in lower part. The study approach is to target each of the successive mudflows identified in backscatter data by a sediment core (white dots on profile line A–B) with the aim of investigating the amount of hemipelagic sediment overlying each mudflow.

## 4.3. Seafloor photo mosaicking

Understanding the overall structure of a cold-seep site can be challenging, given that the visibility in deep-sea is limited to the range of the ROV video cameras and lighting capabilities. More importantly, scientific findings in previously unexplored areas such as newly discovered cold seeps require visual documentation by video or photographic footage. Visualization of extended areas of the seafloor can be achieved by assembling several overlapping seafloor photos into a larger image referred to as a photo mosaic.

Photographic datasets for several photo mosaics were obtained during M112 during dedicated dives performed by MARUM ROV QUEST 4000m. The ROV moved in parallel lines (with one crossing-line for image rectification) and utilized a downward looking camera dedicated to photo mosaicking (Prosilica GT6600C). The ROV was set to fly at a constant elevation (1–5 m depending on coverage of each mosaic) above the seafloor to avoid strong image distortions. For the mosaic assembly a MATLAB toolbox called “Large Area Photo Mosaicking” (LAPM; (Marcon et al., 2013)) was utilized. This tool facilitates handling of large amounts of photos, allows the user to either employ an automated or manual detection of seafloor features (Fig. 4.4), and computes georeferenced mosaic tiles for direct import into a geographic information system (GIS).

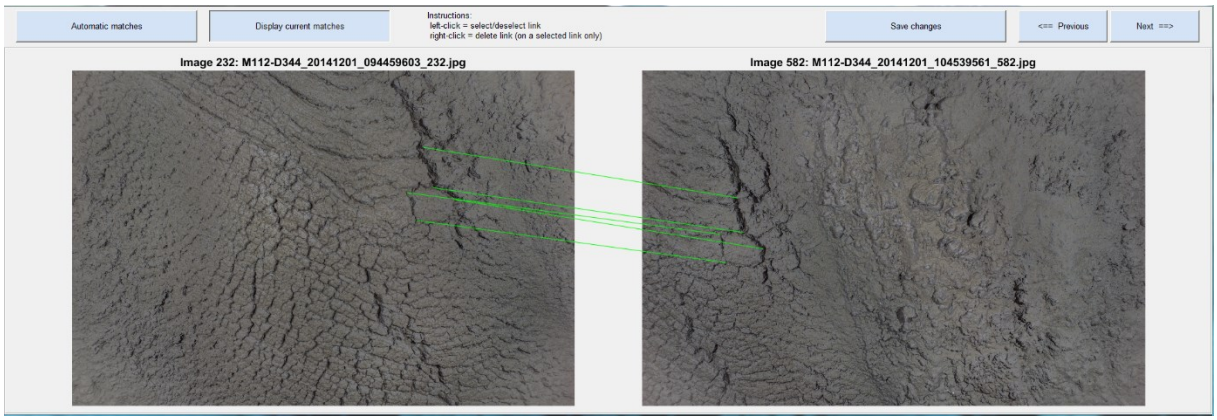


Fig. 4.4. The interface of the LAPM tool (Marcon et al., 2013) to detect and match seafloor features (green lines) on images obtained by a downward-looking camera as used during this work; these two images are part of a photomosaic of almost 700 pictures showing a recent mudflow at Venere MV (see Chapter 8).

## 5. Manuscript I: Mud extrusion and ring-fault gas seepage

# Mud extrusion and ring-fault gas seepage – upward branching fluid discharge at the deep-sea Venere mud volcano (Central Mediterranean Sea)

M. Loher[1,*], T. Pape [1], Y. Marcon [1,2], M. Römer[1], P. Wintersteller[1], D. Praeg[3], M. Torres[4], H. Sahling[1], G. Bohrmann[1]

**Under review in journal of Marine and Petroleum Geology.**

[1]*MARUM – Center for Marine Environmental Sciences and Department of Geosciences, University of Bremen, Klagenfurter Str., 28359 Bremen, Germany*

[2]*Alfred Wegener Institute, Helmholtz Centre for Polar and Marine Research, Am Handelshafen 12, 27570 Bremerhaven, Germany*

[3]*OGS (Istituto Nazionale di Oceanografia e di Geofisica Sperimentale), Borgo Grotta Gigante 42/c, Sgonico, 34010 Trieste, Italy; present address: Institute of Petroleum and Natural Resources, PUCRS, Av. Ipiranga, 6681, 90619-900 Porto Alegre, RS, Brazil AND Géoazur (UMR7329 CNRS), 250 Rue Albert Einstein, 06560 Valbonne, France*

[4]*College of Earth, Ocean, and Atmospheric Sciences, Oregon State University, 104 CEOAS Administration Building, Corvallis, OR 97331-5503, USA*

**corresponding author e-mail: mloher@marum.de*

Keywords: mud volcano; cold seep; gas flares; hydrocarbons; pore-water freshening; ring faults; mud breccia

## 5.1. Abstract

The Calabrian accretionary prism hosts a province of mud volcanoes, but little is known about their present-day activity, fluid sources or discharge mechanisms. Here we investigate Venere mud volcano, located at ~1600 m water depth in the Crotone forearc basin using hydroacoustic data acquired from a research vessel and an autonomous underwater vehicle, combined with seafloor data from a remotely operated vehicle, gravity and pressure cores. We show Venere mud volcano to be characterized by gas release from its summit and from peripheral sites that align with inward-dipping ring faults. At the summit, fresh mud breccia is up to 13 °C warmer than background sediments, and contains thermogenic hydrocarbons (methane $\delta^{13}C_{mean}$ = –38.6‰ V-PDB and $\delta D_{mean}$ = –146.2‰ V-SMOW) and pore waters depleted in chloride by up to five times ambient sea water values. These data are indicative of thermogenic organic matter degradation and mineral dehydration reactions and point to fluid sources at >3.5 km depth, i.e. below the forearc basin fill within the accretionary prism. Chemosynthetic communities are absent along fresh mudflows, despite methane concentrations that are 2.7 times above saturation values. Contrastingly, methane depleted in $^{13}C$ ($\delta^{13}C_{mean}$ = –47.1‰ V-PDB and $\delta D_{mean}$ = –172.9‰ V-SMOW) is emitted at the peripheral seeps which drives authigenic carbonate formation and sustains chemosynthetic ecosystems. However, neither mud breccia nor freshened fluids occur at these sites. We propose a conceptual model of an upward-branching plumbing system beneath the mud volcano in which a main conduit drives focused mud breccia extrusion and peripheral gas is released by dispersed flow along ring faults. We infer that coeval mud breccia extrusion, caldera collapse and hydrocarbon discharge at peripheral seeps are maintained by high subsurface pressures. Such a system may be generally applicable with implications for the distribution of chemosynthesis-based seafloor ecosystems around submarine mud volcanoes.

## 5.2. Introduction

Mud volcanoes (MVs) are geological structures created by the extrusion of sediments, water, and gases from a subsurface plumbing system that may extend to depths of kilometers. MVs are considered windows to the deep, as the composition of jointly expelled fluids and solids (called mud breccia) provide information on processes of crustal dewatering, hydrocarbon generation, and diagenesis. Mud volcanoes occur in a variety of plate tectonic settings, but are most common along convergent margins within accretionary wedges (Higgins and Saunders, 1974; Dimitrov, 2002; Kopf, 2002; Hensen et al., 2004; Pape et al., 2014; Hensen et al., 2015). Even though the estimate of up to $10^5$ submarine MVs outnumbers their onshore counterparts by up to two orders of magnitude (Milkov, 2000; Dimitrov, 2002), much of what we know regarding the processes of mud volcanism is based on studies of terrestrial MVs (Higgins and Saunders, 1974; Kopf, 2002) and less is known about the mechanisms leading to their formation on the seafloor and their impact on seafloor ecosystems.

Mud volcanism is episodic, whereby mud breccia outflow events can build extrusive edifices of up to several hundreds of meters in height and up to kilometer-scale widths (Kopf, 2002; Praeg et al., 2009; Kioka and Ashi, 2015; Mazzini and Etiope, 2017). Observations of terrestrial MVs suggest that, during longer quiescent phases, the activity of MVs is restricted

to secondary fluid pathways that expel mud and fluids at parasitic cones (<10 m high), gryphons (mud cones <3 m high) or salses (fluid-mud pools and gas seeps) (Planke et al., 2003). These features may be linked to extensional faults within the extrusive edifice, in some cases defining sub-circular calderas thought to result from post-eruptive subsidence (Evans et al., 2008; Mazzini et al., 2009b; Roberts et al., 2011a).

Submarine MVs are typically associated with hydrocarbon seepage, often with the presence of shallow gas hydrates (Stadnitskaia et al., 2008; Feseker et al., 2009b; Pape et al., 2010; Pape et al., 2011b), and are known to sustain chemosynthesis-based seafloor ecosystems (Suess, 2014). Advances in hydroacoustic imaging technologies and the use of autonomous underwater vehicles (AUVs) broaden our capabilities in identifying and investigating seafloor seep sites, which have in turn improved our understanding of submarine MV activity (Dupré et al., 2008; Foucher et al., 2010; Paull et al., 2015b), pockmark growth mechanisms (Marcon et al., 2014a; Sultan et al., 2014), and hydrocarbon seep ecology (Sahling et al., 2016). Remarkably little is known about the subsurface fluid migration pathways that control cold seep activity, the nature of fluid sources (i.e. deep vs. shallow), and the discharge volumes of volatiles within and around submarine MVs. Characterizing the composition of fluids discharged at MVs provides valuable insights into these outstanding issues as well as into the hydrogeological processes that drive mud volcanism and which occur at depths not readily accessible for direct sampling.

The eastern and central Mediterranean region hosts an exceptionally high density of MVs, the majority of which are located within the accretionary wedges of the Africa-Eurasia subduction zone (Calabrian accretionary prism, Mediterranean Ridge, Anaximander Mountains) and the Nile deep sea fan (Fig. 5.1a; (Mascle et al., 2014)). On the Mediterranean Ridge accretionary wedge mud breccia were first cored by Cita et al. (1981). At the Olimpi MV field, scientific drilling (Robertson et al., 1996) later revealed the mud breccia discharge processes (Kopf et al., 1998) and attributed a fluid source depth to ~3.5–7 km (Dählmann and De Lange, 2003). In the Anaximander Mountains region the presence of shallow gas hydrates, was attributed to gas release at MVs and as such these deposits are prone to decomposition during eruptive phases of mud volcanism (Woodside et al., 1998; Lykousis et al., 2009; Pape et al., 2010). Investigations of MVs in the Nile deep sea fan revealed a variety of extrusive processes (Dupré et al., 2007) including mud outflows and fluid seepage at submarine brine pools (Huguen et al., 2009; Dupré et al., 2014), used to infer migration from below and through fault-ruptured Messinian evaporite layers (Dupré et al., 2014). In the majority of MV provinces in the eastern Mediterranean, however, Messinian salt deposits are thought to act as seals to fluids ascending from depth so that MVs predominantly occur where salt deposits are absent, thin, or so far undetected in seismic data (Mascle et al., 2014).

In the central Mediterranean Sea, the inner Calabrian accretionary prism (CAP) has been shown to host a province of at least 54 extrusive features, most associated with seafloor backscatter signatures interpreted to indicate extrusive activity over the last glacial to

interglacial cycle (Ceramicola et al., 2014b). This includes Venere MV which lies in the Crotone basin (Fig. 5.1b) at ~1600 m of water depth along the axis of the Squillace Canyon (Fig. 5.1c). Gas-bearing sediments, visual observations of localized mud outflows, and a core containing tubeworms, provided the first indications of recent fluid and mud release on the CAP (Foucher et al., 2009).

MVs in the inner CAP are argued to have been erupting since ca. 3.5 Ma (early Pliocene), based on seismic profiles across two MVs associated with buried extrusive edifices over 1 km thick that interfinger with the upper part of the Plio-Quaternary succession and occupy subsidence depressions in lower Pliocene and older strata depressions (Praeg et al., 2009). Mud breccia from these and two other MVs contain material derived from strata ranging in age from Recent to as old as Late Cretaceous, indicative of fluid sources deep within the accretionary prism (Morlotti et al., 1982; Praeg et al., 2009; Panieri et al., 2013).

In this study we examined mechanisms of fluid seepage in relation to mud volcanism on the CAP, focusing on Venere MV. We considered hydroacoustic water column data, high resolution seafloor bathymetry, ROV observations, and samples of sediment and fluids obtained during campaigns in 2014-2016 (Figs. 5.1–3). Morphological and geochemical analyses of these data as well as direct seafloor observations allowed us to identify on-going seafloor extrusive activity and gas discharge from Venere MV and to obtain the first available information on the composition of fluids rising from sources within the CAP. We recognized distinct expressions of fluid discharge mechanisms at the summit versus surrounding ring-faults and linked them to the shallow plumbing system beneath Venere MV. Our findings support a conceptual model of coeval extrusion, faulting and gas seepage, in which subsurface fluid migration pathways are linked to different expressions of seafloor fluid discharge and ecosystem distribution.

## 5.3. Geological setting

The present-day CAP in the central Mediterranean Sea (Fig. 5.1a) results from the NW subduction of the African plate below the Eurasian plate during the Neogene and was associated with rapid SE rollback of an Ionian lithospheric slab (Malinverno and Ryan, 1986; Gueguen et al., 1998). The CAP can be divided into an external (post-Messinian) wedge that hosts evaporites and an internal (pre-Messinian) wedge, that is overlain by forearc basins (Spartivento-Crotone basins) containing up to 2 km of sediment (Fig. 5.1b; (Rossi and Sartori, 1981; Minelli and Faccenna, 2010; Polonia et al., 2011; Ceramicola et al., 2014b; Gutscher et al., 2017)). The inner pre-Messinian wedge is composed of accreted Mesozoic-Cenozoic units overlain by forearc basins; these are exposed onshore in southern Calabria and date back to the middle Miocene (late Serravallian; (Roda, 1964; Rossi and Sartori, 1981; Zecchin et al., 2015)). Messinian deposits including evaporites occur within the onshore Crotone forearc basin (Roda, 1964; Zecchin et al., 2003) and in nearshore wells (Capozzi et al., 2012). Seismic reflection profiles indicate stratified Messinian deposits locally up to 500 m thick within the offshore basins (Minelli and Faccenna, 2010), and diapir-like structures (Fig. 5.1b). The diapir-like structures were originally interpreted as halokinetic (Rossi and Sartori,

1981), but have been reattributed to shale mobilization from sub-Messinian intervals (Capozzi et al., 2012). The onshore Calabrian domain experienced rapid regional uplift during the late Pleistocene (Westaway, 1993), attributed to a tectonic reorganization ca. 0.8-0.5 Ma (Goes et al., 2004; Mattei et al., 2007) that affected the Crotone basin at ca. 0.45-0.4 Ma (Zecchin et al., 2011). Several canyon systems extend into the Crotone and Spartivento basins, incising the Calabrian-Ionian margin and creating retrogressive canyon head erosion, mass wasting processes and slope instabilities that constitute a potential geohazard for coastal areas (Morelli et al., 2011; Ceramicola et al., 2014a).

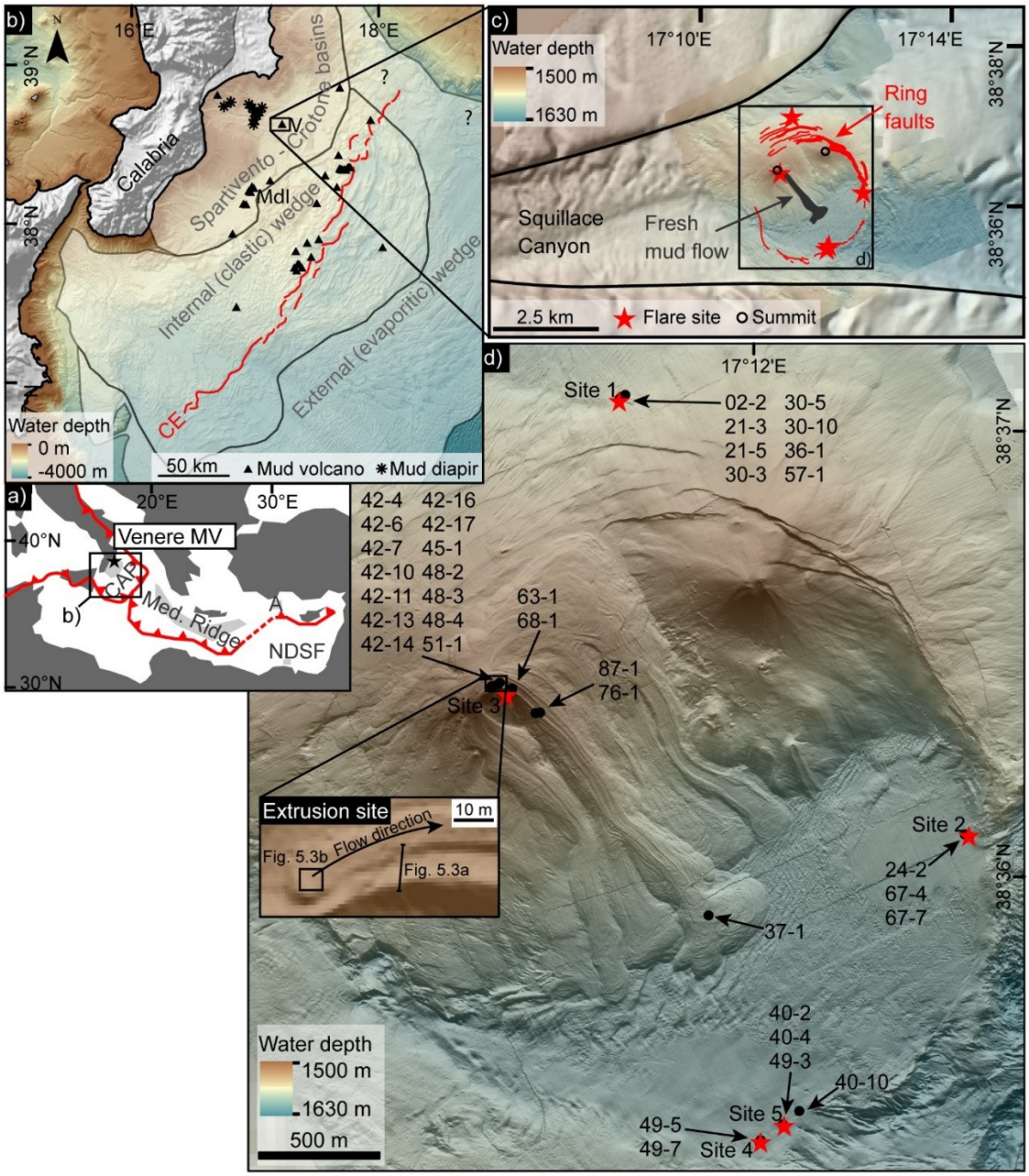


Figure 5.1. Maps of the study area; a: Location of Venere mud volcano (MV; star) in the Calabrian accretionary prism (CAP) relative to plate boundaries (red lines) with main mud volcano provinces (light grey shading, after Mascle et al. (2014)) in the eastern Mediterranean Sea (Med. Ridge = Mediterranean Ridge MVs, A = Anaximander Mountains MVs, NDSF = Nile Deep Sea Fan MVs); b: Topography of Italy (Ryan et al., 2009) and seafloor bathymetry (available at EMODnet, http://www.emodnet.eu/bathymetry) with morpho-structural zones of the CAP (CE = Calabrian Escarpment) and boundaries after previous interpretations, for references see text), locations of selected MVs (V = Venere MV, MdI = Madonna dello Iono MVs) after Ceramicola et al. (2014b), modified based on investigations during M112, and locations of shale diapirs (after Capozzi et al. (2012)); c: Map view of Venere MV in Squillace Canyon using autonomous-underwater-vehicle-based bathymetry draped over ship-derived bathymetric data (see box in b) for location); d: Close-up of c) (see box for location) with inset of the extrusion site of the most recent mudflow at the western summit, red stars mark the flare locations at Sites 1, 2, 4, 5 and near the western summit (Site 3), numbers indicate the last two GeoB identifiers of all sampling locations (s. Table 5.1 for detailed information).

## 5.4. Data and methods

Multi-disciplinary investigations of Venere MV were undertaken in 2014 and 2016 during R/V METEOR cruise M112 (Bohrmann et al., 2015) and R/V POSEIDON cruise POS499 (Bohrmann et al., 2016). Swath bathymetry data were collected using two Kongsberg multibeam systems, a ship-borne EM122 (12 kHz) in 2014 and an EM2040 (300 kHz) carried by the autonomous underwater vehicle (AUV) MARUM-SEAL 5000 in 2014 and 2016. Data were processed with MB-System (Caress and Chayes, 1996) and AUV-based data gridded to 1.6 m lateral and 0.1 m vertical resolution.

Cores (Table 5.1) of shallow sediments were acquired using both a conventional gravity corer and the Dynamic Autoclave Piston Corer (DAPC), that allowed for retrieval of cores under in-situ pressure (Abegg et al., 2008). Seafloor observations, sediment sampling with push cores and collection of gas bubbles in the water column were conducted using the remotely operated vehicle (ROV) MARUM QUEST 4000m during M112 (Bohrmann et al., 2015). Sediment temperatures were repeatedly measured at the western summit using miniaturized temperature data loggers (MTLs by ANTARES Datensystem GmbH in Germany) attached to a 5 m gravity core barrel. At peripheral seeps (Sites 1, 2, 4 and 5; Fig. 5.1d) as well as at the western summit (Fig. 5.1d), in-situ temperatures were measured with a 60 cm long probe (T-stick; RBR Ltd., Canada), inserted vertically into the sediment using the ROV (Feseker et al., 2012). Conductivity, temperature, and depth (CTD) measurements were recorded above each site by a Sea Bird Electronics SBE9plus probe.

Pore fluids were extracted from gravity cores and push cores (Table 5.1) using rhizon samplers. Sulfate and chloride concentrations were determined by ion-chromatography (“882 Compact IC plus 1” by Metrohm on a “Metrosep A Supp 5” column) with an analytical error below 0.4 % for both anions. Hydrocarbon data (Table 5.1) was generated from sediment retrieved by gravity coring using standard headspace techniques; from gas bubble sampling under in-situ pressures over the seeps using the ROV (Fig. 5.3c); and from the DAPC. Gas compositions and stable carbon and hydrogen isotope ratios were analyzed, as described in Römer et al. (2012a). Repeated analyses of standards gave a reproducibility for $C_1/C_{2+}$ ratios, stable carbon and hydrogen isotope ratios ≤2 %, 0.5 % and 1 %, respectively.

The gas hydrate phase boundary (Fig. 5.4a–c) was calculated with the program HWHYD (Masoudi and Tohidi, 2005). We used the molecular compositions of gases sampled in the mud breccia (western summit, near Site 3) and of free gas (bubble collection at peripheral seeps, Sites 1, 2, 4 and 5) as well as salinities of 10 PSU (freshened pore water values in fresh mud breccia) and 38.5 PSU (bottom water values at peripheral seeps, Sites 1, 2, 4 and 5). To determine the base of the gas hydrate stability zone (BGHSZ) temperature gradients (Table 5.1) were calculated from measured sediment temperatures and averaged gradients were used at sites where repeated measurements were carried out.

Table 5.1. Names, locations (WGS84), and water depths, of sample stations used in this study, together with results for gas chemistry (hydrocarbon composition, stable carbon isotopy, stable hydrogen isotopy), geothermal gradients, and pore water samples (full data available in supplementary data tables of Chapter 13.1); DAPC = Dynamic Autoclave Piston Corer, GBS = Gas bubble sampler; GC = Gravity corer; TS = T-stick; GC-HF = Gravity corer with T-loggers; PC = Push corer.

| GeoB-No. | Tool | Lat / N | Lon / E | Water depth (m) | Site | Gas chemistry | | |
|---|---|---|---|---|---|---|---|---|
| | | | | | | $C_1/C_{2+}$ | $\delta^{13}C$ (‰ VPDB) | $\delta D$ (‰ VSMOW) |
| 19257-1 | DAPC | 38°37.095' | 17°11.604' | 1561 | Seep, Site 1 | 1279 | -49 | -170.6 |
| 19224-2 | GBS | 38°36.096' | 17°12.571' | 1595 | Seep, Site 2 | 889 | -45.7 | -170.1 |
| 19249-5 | GBS | 38°35.429' | 17°11.960' | 1606 | Seep, Site 4 | 1216 | -46.7 | -176.0 |
| 19240-2 | GBS | 38°35.458' | 17°12.022' | 1607 | Seep, Site 5 | 1127 | -47.2 | -175.0 |
| 19251-1 | DAPC | 38°36.452' | 17°11.224' | 1497 | Venere W Summit | 92 | -39.5 | -141.6 |
| 19245-1 | GC | 38°36.455' | 17°11.223' | 1496 | Venere W Summit | - | -37.2 | -153.8 |
| 19268-1 | DAPC | 38°36.450' | 17°11.282' | 1500 | Mudflow | 103 | -41.1 | -150.4 |
| 19287-1 | DAPC | 38°36.394' | 17°11.361' | 1516 | Mudflow | 79 | -36.6 | -142.6 |
| 19263-1 | GC | 38°36.448' | 17°11.282' | 1500 | Mudflow | - | -41.3 | -149.3 |
| 19276-1 | GC | 38°36.393' | 17°11.348' | 1516 | Mudflow | - | -36.6 | -137.3 |
| 19237-1 | GC | 38°35.930' | 17°11.828' | 1594 | Mudflow | - | -37.9 | -148.5 |
| | | | | | | Temperature gradient | | |
| 19202-2 | TS | 38°37.084 | 17°11.593 | 1567 | Seep, Site 1 | 0.01 °C/m | | |
| 19221-3 | TS | 38°37.095 | 17°11.602 | 1568 | Seep, Site 1 | 0.16 °C/m | | |
| 19221-5 | TS | 38°37.094 | 17°11.600 | 1567 | Seep, Site 1 | 0.20 °C/m | | |
| 19230-3 | TS | 38°37.095 | 17°11.609 | 1568 | Seep, Site 1 | 0.31 °C/m | | |
| 19230-10 | TS | 38°37.102 | 17°11.630 | 1567 | Seep, Site 1 | 0.06 °C/m | | |
| 19267-7 | TS | 38°36.100 | 17°12.564 | 1596 | Seep, Site 2 | 0.18 °C/m | | |
| 19240-4 | TS | 38°35.457 | 17°12.021 | 1607 | Seep, Site 4/5 | 0.18 °C/m | | |
| 19249-3 | TS | 38°35.454 | 17°12.020 | 1607 | Seep, Site 4/5 | 0.22 °C/m | | |
| 19242-4 | TS | 38°36.453 | 17°11.223 | 1499 | Venere W summit | 14.92 °C/m | | |
| 19242-7 | TS | 38°36.453 | 17°11.223 | 1499 | Venere W summit | 15.39 °C/m | | |
| 19242-13 | TS | 38°36.454 | 17°11.225 | 1499 | Venere W summit | 14.66 °C/m | | |
| 19242-16 | TS | 38°36.457 | 17°11.226 | 1500 | Venere W summit | 15.54 °C/m | | |
| 19248-2 | GC-HF | 38°36.452 | 17°11.221 | 1500 | Venere W summit | 2.73 °C/m | | |
| 19248-3 | GC-HF | 38°36.452 | 17°11.223 | 1498 | Venere W summit | 2.51 °C/m | | |
| 19248-4 | GC-HF | 38°36.454 | 17°11.226 | 1495 | Venere W summit | 1.96 °C/m | | |
| | | | | | | Pore water | | |
| 19230-5 | PC | 38°37.095' | 17°11.609' | 1567 | Seep, Site 1 | s. supplementary data | | |
| 19236-1 | GC | 38°37.094' | 17°11.605' | 1557 | Seep, Site 1 | s. supplementary data | | |
| 19267-4 | PC | 38°36.100' | 17°12.563' | 1596 | Seep, Site 2 | s. supplementary data | | |
| 19249-7 | PC | 38°35.429' | 17°11.959' | 1606 | Seep, Site 4 | s. supplementary data | | |
| 19240-10 | PC | 38°35.486' | 17°12.074' | 1608 | Seep, Site 5 | s. supplementary data | | |
| 19242-6 | PC | 38°36.453' | 17°11.223' | 1499 | Venere W summit | s. supplementary data | | |
| 19242-10 | PC | 38°36.463' | 17°11.247' | 1502 | Venere W summit | s. supplementary data | | |
| 19242-11 | PC | 38°36.460' | 17°11.243' | 1502 | Venere W summit | s. supplementary data | | |
| 19242-14 | PC | 38°36.454' | 17°11.225' | 1499 | Venere W summit | s. supplementary data | | |
| 19242-17 | PC | 38°36.456' | 17°11.227' | 1500 | Venere W summit | s. supplementary data | | |
| 19245-1 | GC | 38°36.455' | 17°11.223' | 1496 | Venere W summit | s. supplementary data | | |

## 5.5. Results

### 5.5.1. Seafloor structures at Venere MV

Systematic hydroacoustic surveys during November and December 2014 (cruise M112) were performed across at least 50 of the extrusive features recognized by Ceramicola et al. (2014b) in the CAP, but encountered evidence of gas emissions into the water column (gas flares) only at Venere MV. This MV consisted of an eastern and a western cone located ~1200 m apart (Fig. 5.1d+Fig. 5.2a+b). Repeated hydroacoustic surveys over 31 days during M112 revealed temporally variable but generally persistent gas discharges from five sites: one slightly below the western summit (Site 3) and four peripheral to the MV cones (Sites 1, 2, 4, and 5; Fig. 5.2a+b).

AUV-based bathymetry data revealed that both cones of Venere MV were cut by concentric sets of inward-dipping scarps (Fig. 5.1d + Fig. 5.2a+b), visible as discontinuous morphological steps of 1 to >40 m and dips of 18–45°; both the relief and depth were greater in the east. The scarps defined a circular feature centered ~700 m SE of the western summit that offset seafloor features, including the eastern cone. These scarps are interpreted as extensional ring faults, defining a caldera up to 3 km in diameter. The locations of the four peripheral gas flares coincided with surface traces of the ring-fault system (Fig. 5.1d + Fig. 5.2). At the summit of the western cone (~1520 m water depth), the AUV bathymetric imagery showed mudflows to extend down the southern flank (Fig. 5.1d + Fig. 5.2a+b), for horizontal distances of up to ~1600 m from the summit (Fig. 5.1d+Fig. 5.2a+b). The mudflows formed elongate ridges (10–50 m wide) including subparallel furrows (up to 1 m deep) that formed prominent lobes where they spread out at the foot of the slope (~1620 m water depth). Smooth mudflows and lobes were observed at the eastern summit, where gravity coring revealed mud breccia draped by several decimeter of hemipelagic sediment cover.

ROV observations and sampling at the western summit identified the presence of fresh mud breccia flows that lacked the sedimentary cover present in areas adjacent to the most recent central mudflow (Fig. 5.3a). The extrusion site of these fresh mud breccia flows was observed at the top of the summit as a slightly elevated horseshoe-shaped feature about 3 m across with a central depression (Fig. 5.3b). ROV surveys of the mudflows at the western summit encountered no macroscopic indications of chemosynthetic communities (Fig. 5.3a+b). In contrast, ROV explorations of the four peripheral seeps (Sites 1, 2, 4, 5) confirmed sites of gas bubble emissions, settled by chemosynthetic organisms and surrounded by mounds and pavements of authigenic carbonate several decimeters thick (Fig. 5.1c+d+e).

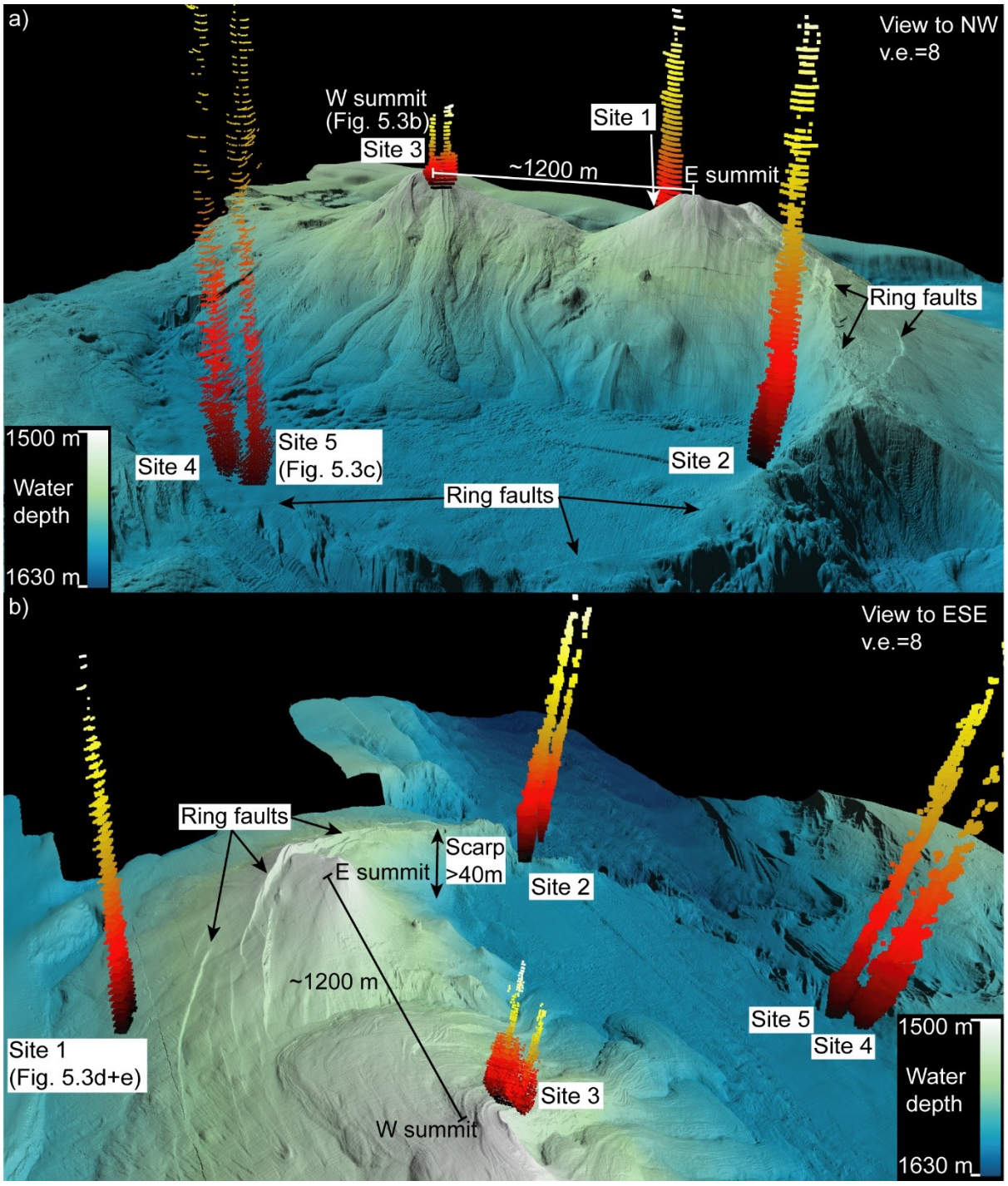


Figure 5.2. Bathymetry derived from autonomous underwater vehicle surveys showing perspective views of Venere MV (a: to NW; b: to ESE) and water column gas flares (red to yellow colors) extracted from hydroacoustic data. Hydroacoustic flares up to 260 m high are arranged along the periphery (Sites 1, 2, 4, 5). The most recent mudflow originates from the western summit and extends down to the caldera floor. In a), note the twin cones (E+W summit), ~1200 m apart, each up to 100 m high; in b), note that the ring faults are higher along the flanks of the eastern than the western cone.

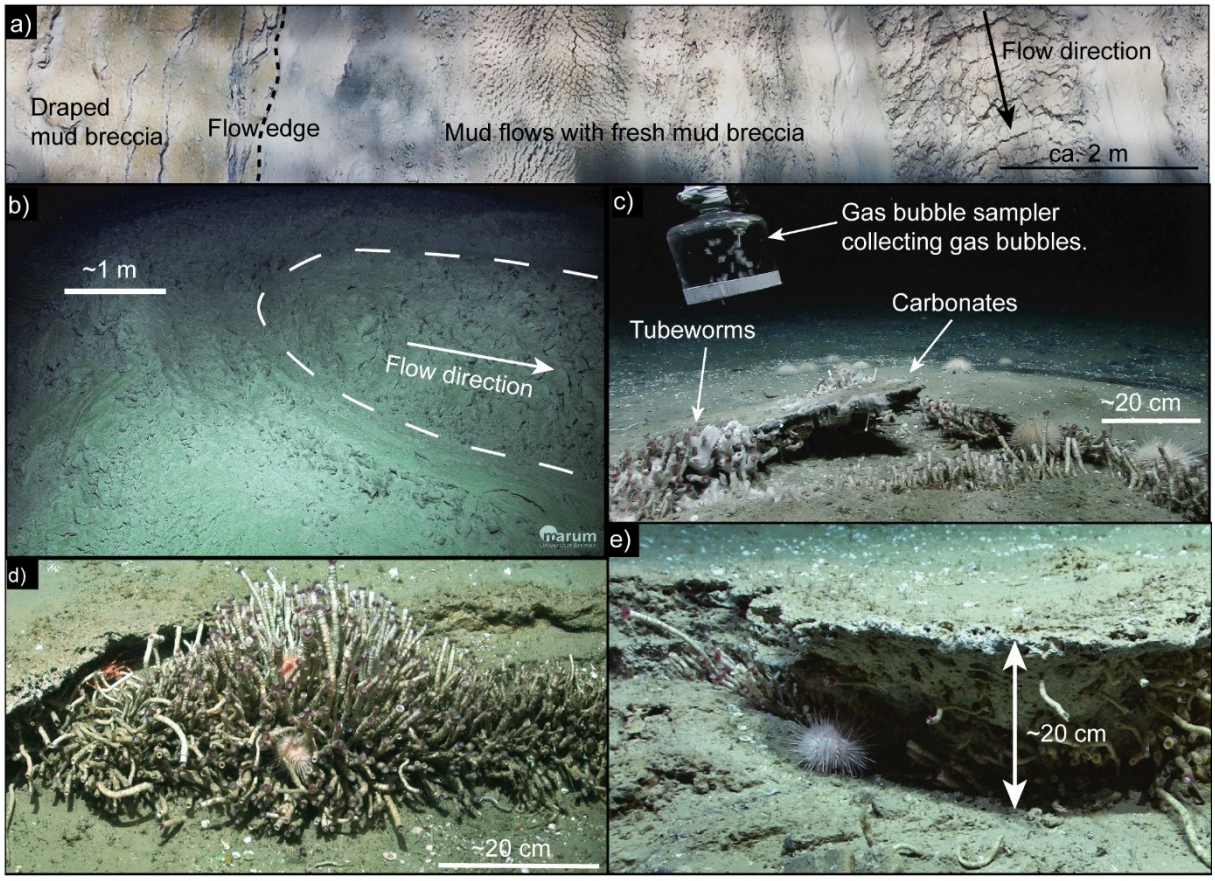


Figure 5.3. Seafloor photographs; a: ~10 m long transect across fresh (right) vs. older (left) mud breccia flows draped by hemipelagic sediments near the western summit (see inset of Fig. 5.1d for location); b: western summit of Venere MV showing elevated extrusive center at the origin of the most recent mudflow (see inset of Fig. 5.1d for location); c: authigenic carbonate crusts, cold-seep communities and sampling of gas bubbles at a peripheral seep (Site 5); d: tubeworm colony rooting in a fracture of authigenic carbonate crust at a peripheral seep (Site 1); e: cold-seep community and thick authigenic carbonate pavement at a peripheral seep (Site 1).

### 5.5.2. Mud breccia, gas, and fluids from the western summit of Venere MV

The mud breccia flowing down the western cone was characterized by mousse-like sediment textures resulting from gas bubbles within the mud, abundant gas pockets and decimeter-sized rock clasts. At the extrusion site on the western summit temperatures above 20 °C were repeatedly measured already <0.5 m below seafloor. The highest overall recorded temperature at the extrusion site was 26.8 °C, measured 30 cm from the tip of a 5 m gravity core barrel (GeoB19248-2), compared to an average of 13.8 °C for bottom water temperatures (Fig. 5.4a+b). Cores collected under pressure yielded 41.3 L of gas from the 11220 $cm^3$ of sediment retrieved, which translated to a volumetric gas-sediment ratio of 3.68. In addition to methane ($C_1$), heavier hydrocarbons such as ethane, propane, butane ($C_{2-4}$) and pentane ($C_5$) were detected in gas samples from the mud breccia. The ratio of methane to higher hydrocarbons ($C_1/C_{2+}$) in gas samples from the mud breccia ranged between 79 and 103 (Table 5.1). Assuming that methane ($CH_4$) constitutes 98.5 vol-% of the total gas released from the pressure core and using an average sediment porosity of 0.5 (determined

in samples from gravity core GeoB19245-1), the calculated average $CH_4$ concentration was 321.44 mmol/L pore water. This $CH_4$ concentration is about 2.7 times higher than the calculated in-situ $CH_4$ solubility (120.18 mmol/L pore water; temperature (T) at 2 meters below sea floor (mbsf) = 31.33 °C; salinity (S) = 10 psu). The stable carbon isotopic composition of the methane ($\delta^{13}C$-$CH_4$) ranged between –36.6 and –41.3‰ V-PDB (mean value of –38.6‰ V-PDB) and the stable hydrogen isotopic composition of the methane ($\delta D$-$CH_4$) between –137.3 and –153.8‰ V-SMOW (mean value of –146.2‰ V-SMOW; Table 5.1; Fig. 5.5a+b).

At the extrusion site on the western summit, fluids extracted from push cores in mud breccia outflows contained chloride concentrations that decreased in the upper 14 cm from ambient bottom water values of 618 mmol/L to as low as 128 mmol/L (Fig. 5.6a+b). Gravity core GeoB19245-1 from the extrusion site confirmed that low chlorinity fluids (lowest value of 125 mmol/L) extended down to 5 mbsf. In the area of Site 3 (Fig. 5.1d) no distinctive gas emission site was found and thus no seep-related sediments were sampled.

### 5.5.3. Gas emissions at peripheral seeps of Venere MV

Pore fluid samples obtained from peripheral seeps (Sites 1, 2, 4 and 5, Fig. 5.1d) had chloride concentrations close (<25 mmol/L difference) to bottom water values, to depths up to 2 mbsf (Fig. 5.6a). At all these sites we observed chemosynthetic macrofauna and abundant crusts of authigenic carbonates (Fig. 5.3c+d+e), indicative of a shallow zone of anaerobic methane oxidation, consistent with measured steep sulfate gradients and sulfate-methane transition at depths of <25 cm (Fig. 5.6b). The discharged gas at peripheral seeps (composed primarily of methane and ethane with trace amounts of butane and pentane, but lacking propane) had $C_1/C_{2+}$ ratios of 889–1216, while $\delta^{13}C$-$CH_4$ and $\delta D$-$CH_4$ ranged from –46.7 to –49.0‰ V-PDB (mean value of –47.1‰ V-PDB) and from –170.1 to –176.0‰ V-SMOW (mean value of –172.9‰ V-SMOW), respectively (Table 5.1; Fig. 5.5a+b). Averages of linear geothermal gradients (Table 5.1), obtained by repeated sediment temperature measurements at peripheral seeps, ranged from 0.15–0.20 °C/m (Fig. 5.4c). Using these gradients, the calculated base of the gas hydrate stability at the seeps could be located 8–10 m below the seafloor (Fig. 5.4a+c). Visual observations while sampling the seeps with the ROV suggested the presence of small amounts of gas hydrate associated with seepage along the ring faults.

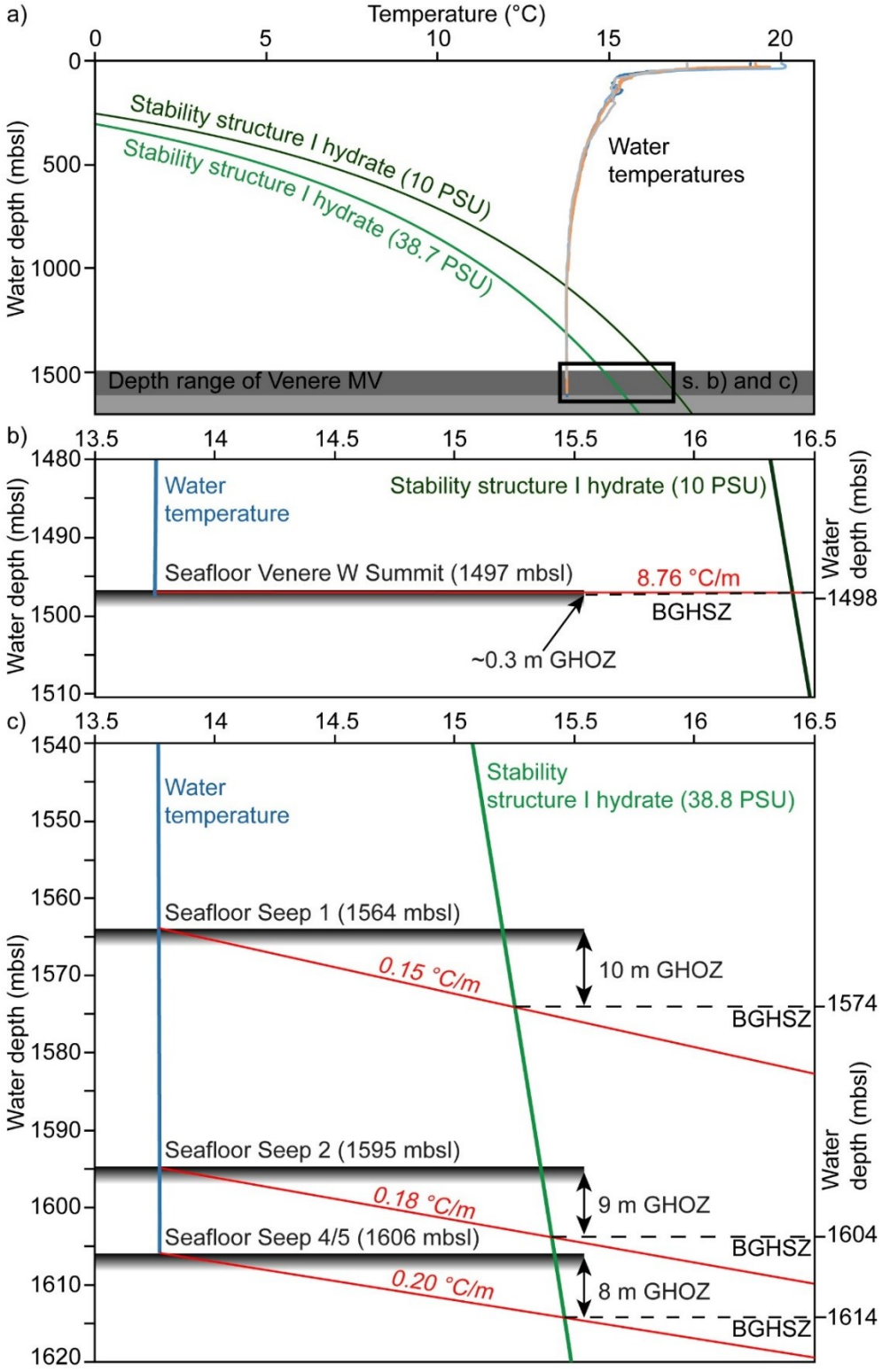


Figure 5.4. a: Calculated phase boundaries for structure I hydrates at Venere MV (mbsl = meters below sea level), b+c: enlargements of diagram shown in (a) with black stippled lines marking the base of the gas hydrate stability zone (BGHSZ) to define the gas hydrate occurrence zone (GHOZ), b) shows averaged, linear geothermal gradient at the western summit of Venere MV, note the steep temperature gradient indicating that gas hydrates are unlikely to be present at the summit (~0.3 m for GHOZ), c) shows averaged, linear geothermal gradients for peripheral seeps (Sites 1, 2 and 4/5).

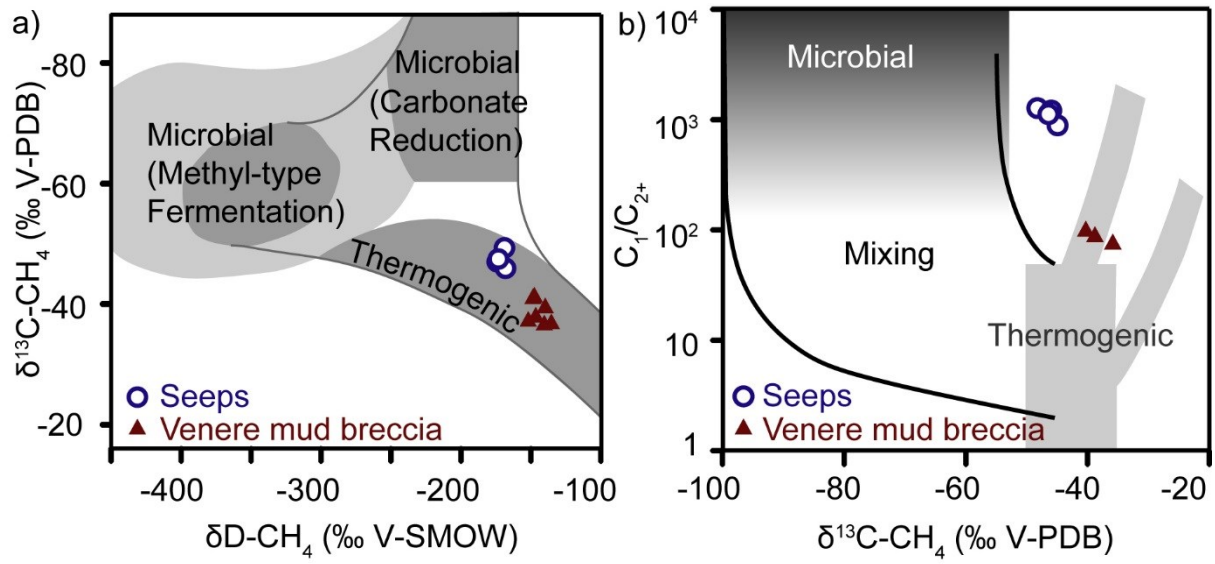


Figure 5.5. Molecular hydrocarbon and methane isotope composition of samples from Venere MV summit and mudflow (filled triangles) and peripheral seeps (circles, s. Table 5.1); a: Carbon-hydrogen diagram for classification of microbial and thermogenic methane modified after Whiticar (1999); b: "Bernard" diagram of $C_1/C_{2+}$ vs. $\delta^{13}C\text{-}CH_4$, (Bernard et al., 1977), showing the thermogenic, microbial, and mixed domains as proposed by Whiticar (1999).

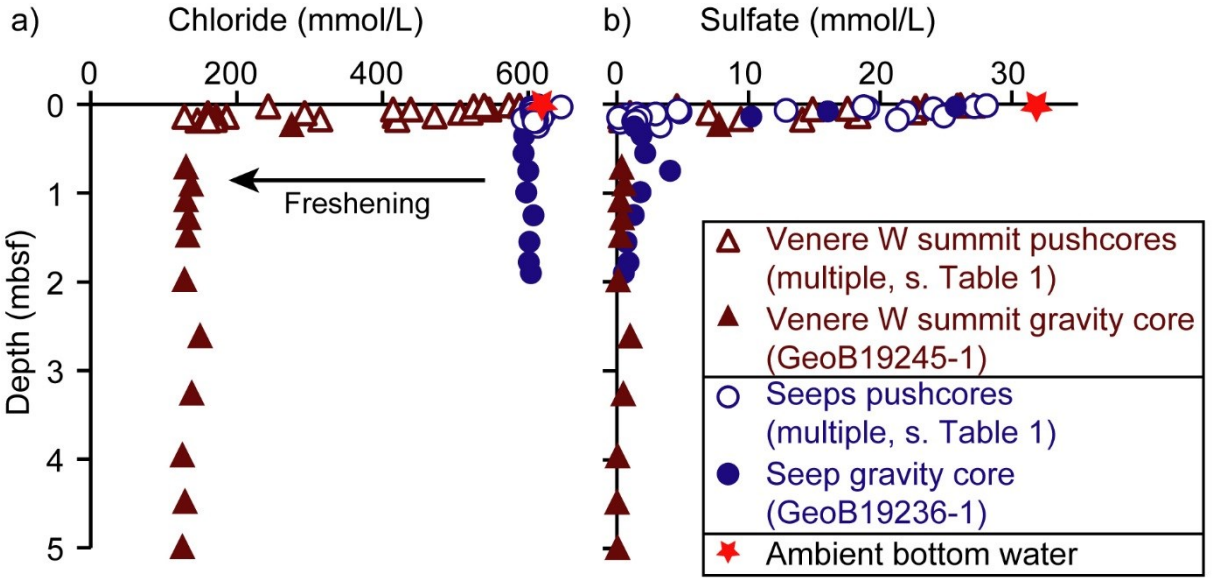


Figure 5.6. Pore water profiles of chloride (a) and sulfate (b) from gravity cores and push cores from both the western summit of Venere MV (triangles) and peripheral seeps (circles). Red star shows bottom seawater values of 618 mmol/L chloride and 32 mmol/L sulfate; mbsf = meters below sea floor.

## 5.6. Discussion

### 5.6.1. Mud breccia extrusion from Venere MV

Mud breccia extrusion from the western cone of Venere MV has resulted in mudflows that extended over 1.6 km from the summit to a lobe at the foot of the cone (Fig. 5.1d + Fig. 5.2a).

The structure of fresh mud breccia observed at the extrusion site (Fig. 5.3b) together with the lack of sedimentary drape on the most recent mudflow (Fig. 5.3a) suggested ongoing outflows. In-situ methane concentrations up to 2.7 times higher than $CH_4$ solubility measured in pressure cores indicated that a large fraction of the pore space in the fresh mud breccia was occupied by gaseous methane, consistent with mousse-like sediment textures observed in unpressurized gravity cores. Molecular compositions of hydrocarbons and isotopic compositions of methane indicated a thermogenic origin for hydrocarbons transported within the mud breccia of Venere MV (Fig. 5.5a+b; Whiticar (1999)); thermogenic hydrocarbons remained prevalent even in cores of mud breccia that had flowed over 1300 m downslope from the extrusion site (Fig. 5.1d, GeoB19237-1).

The sedimentary section of the offshore Crotone basin corresponds to at most 2 seconds in two-way travel time (TWT) – i.e. no more than 2 km – based on isochron maps derived from seismic data, with an estimated thickness of <1.5 km (<1.5 seconds TWT) at the location of Venere MV (Ambrosetti et al., 1983; Gennesseaux and Winnock, 1993; Minelli and Faccenna, 2010). Formation temperatures range from ~70 °C for the early thermogenic hydrocarbon generation to upwards of 150 °C for late thermogenic, methane-rich gas production systems (Claypool and Kvenvolden, 1983; Quigley and Mackenzie, 1988; Hunt, 1996). The eastern Mediterranean Sea is characterized by low heat flow from Tethyan crust, decreasing further within the inner Calabrian accretionary wedge (Chamot-Rooke et al., 2005). Venere MV lies midway between values as low as 0.013 °C/m offshore and 0.024-0.030 °C/m onshore (Pollack et al., 1991). Assuming a linear geothermal gradient of 0.020 °C/m at the location of Venere MV, the presence of thermogenic hydrocarbons in the outflowing mud breccia suggested a hydrocarbon source located at least 3.5 km (for 70 °C) but potentially even >7.5 km (for >150 °C) below the seafloor. This depth range corresponds to empirically determined burial depths for source rocks within the thermogenic window (e.g. Quigley and Mackenzie (1988)). Our hydrocarbon data did not unravel, however, whether a pressurized reservoir trapping these gases could exist at shallower depths (i.e. cooler temperatures) below Venere MV. Nevertheless, our data indicated that even at minimum formation temperatures, gas extruded within mud breccia at Venere MV was originally produced below the Plio-Quaternary forearc basin, i.e. within the accretionary wedge itself. A similar approach to estimate source depths of hydrocarbons is used by Pape et al. (2014), who investigated hydrocarbons expelled at marine MVs of the Kumano forearc basin in the Nankai accretionary prism and derived a comparable provenance for thermogenic hydrocarbons, i.e. old accreted sediments below the forearc-basin fill. In addition, our estimated source depths for thermogenic hydrocarbons at Venere MV, are consistent with evidence of upward migration of thermogenic hydrocarbons within the CAP at the Luna field (Mattavelli and Novelli, 1988). It is located in shallow water (<200 m) offshore Crotone, where isotopically heavy ($\delta^{13}C$-$CH_4$ of –35‰), dry thermogenic gas (>99% methane) within a reservoir at 1600-1750 m depth, is inferred to have risen from sources at >5000 m depth (Mattavelli and Novelli, 1988; Roveri et al., 1992).

Mud breccia flowing from the western summit of Venere MV are characterized by pore water freshening (Fig. 5.6a). The magnitude of chloride depletion, and the concave-down shape of the profiles revealed an upward advective aqueous component in the extruding mud, rather than freshening associated with gas hydrate decomposition (e.g. Torres et al. (2004a)). This was supported by sediment temperatures measured at the western summit, which translated to an average geothermal gradient of 8.76 °C/m showing that, at >30 cm below seafloor, mud breccia lies outside the gas hydrate stability zone (Fig. 5.4a+b). The pore water profiles were instead consistent with the extrusion of mud breccia containing fresh fluids, while concomitant steep sulfate gradients documented the advection of sulfate-depleted mud, suggesting recent outflows (Fig. 5.6b). We interpret the pore-water freshening to indicate fluid generation by mineral dehydration reactions, such as the transformation of smectite to illite, which take place at temperatures between ~60 and 150 °C (Kastner et al., 2014). Given the geothermal gradient of 0.02 °C/m (s. above), this temperature range translated to fluid sources at km-scale depths, comparable to those of the thermogenic hydrocarbon source. Pore-water freshening has also been observed in MVs in the Mediterranean Ridge, examined by scientific drilling, and has been attributed to mineral dehydration during smectite-illite transition at depths of 3.5–7 km, supported by oxygen isotopes in pore waters and geothermal gradients (Dählmann and De Lange, 2003).

We infer that a combination of thermogenic gas production and water release by mineral dehydration reactions, both taking place at km-scale depths within the CAP, contributed to the generation of overpressures that drive the upward migration of mud, water and gas to the seafloor. Additional driving forces for mud volcanism at accretionary settings typically involve a combination of gravitational loading, i.e. overburden, and tectonic stress which may increase pore pressures above hydrostatic and generate undercompacted conditions for subsurface sediments and overpressured pore fluids (Higgins and Saunders, 1974; Brown, 1990; Kopf, 2002; Maltman and Bolton, 2003). The onset of mud volcanism on the CAP has been proposed to be associated to a compressional tectonic stress field resulting from a tectonic reorganization in the mid-Pliocene that caused the release of overpressures from within the accretionary prism (Praeg et al., 2009). Fluids rising from depth have also been speculated to account for diapir-like features within the forearc basins (Ceramicola et al., 2014b), which seismic profiles suggest involve the mobilization of pre-Messinian shales (Capozzi et al., 2012). In the Crotone Basin, thin (<200 m) Messinian evaporites have been documented in onshore and nearshore wells (Capozzi et al., 2012), and suggested to be present across the deep offshore basins on seismic reflection profiles (Minelli and Faccenna, 2010). However, our data clearly indicated Venere MV to be characterized by the extrusion of mud breccia with freshened pore fluids, offering no evidence of interactions with Messinian evaporites during their rise from depth. One possibility is that Messinian deposits, if present in the sedimentary succession below the location of Venere MV, did not contain evaporites. Another possibility is that, over time, fluid migration through the plumbing system beneath Venere MV has removed any Messinian evaporites. Other studies in the eastern Mediterranean region have found that MVs preferably occur at sites where Messinian

deposits are thin or absent (Fusi et al., 2006; Polonia et al., 2011; Capozzi et al., 2012; Ceramicola et al., 2014b; Mascle et al., 2014), or cut by deep-seated faults with seafloor expressions where the faults act as fluid-migration pathways, such as at the western Nile deep sea fan (Dupré et al., 2014; Mascle et al., 2014).

### 5.6.2. Ring-fault gas emissions

The peripheral seeps of Venere MV are the first sites on the CAP from which extensive chemosynthesis-based communities in association with gas emissions and decimeter-thick authigenic carbonate deposits have been documented. Our seafloor observations and sampling of the peripheral seeps at Venere MV revealed anaerobic oxidation of methane in the shallow subsurface, which is consistent with a long-term (i.e. thousands of years) upward supply of dissolved methane (e.g. Bayon et al. (2009)). While the stable carbon and hydrogen isotopic signatures of methane collected at the peripheral seeps indicate a thermogenic methane source (Fig. 5.5a; Whiticar (1999)), the molecular ($C_1/C_{2+}$) data plot above the thermogenic and to the right of the microbial fields of hydrocarbons on the classification of Bernard et al. (1977) (Fig. 5.5b). Taking the methane being expelled in mud breccia at the summit of Venere MV as a potential thermogenic end-member, the samples lie far away from any theoretical mixing range with microbial end-members (Fig. 5.5; (Whiticar, 1999)). Several post-genetic processes could account for the observed gas compositions at the peripheral seeps: admixture of shallow microbial methane during fluid ascent; secondary microbial methane generation leading to drier gas with relatively more negative $\delta^{13}C\text{-}CH_4$ values (Pallasser, 2000; Head et al., 2003; Hong et al., 2013) and segregation effects during gas transport through porous, aqueous sediments (Prinzhofer et al. (2000) and sources therein). To geochemically constrain these processes, which may be controlling the gas compositions at the Venere seeps, requires measurement of the isotopic composition of higher molecular weight hydrocarbons and $CO_2$, which is beyond scope of this paper.

Gas discharge at peripheral sites was taking place along inward-dipping ring-faults, which encircled the deep-rooted conduit inferred to rise beneath the western summit. Given the geometry of the caldera (radius ca. 1.5 km, seafloor dips of the ring faults of up to 45°), the ring faults converged towards any conduit over horizontal and vertical distances of <2.5 km. We therefore argue that the gas being released at peripheral seeps and at the western summit came from a common source zone in the subsurface, but underwent upward divergence as it migrated through faults and microfractures of the ring-fault system. This is in agreement with the stable carbon and hydrogen isotopic signatures of methane (Fig. 5.5), which clearly indicated a thermogenic component (sensu Whiticar (1999); Fig. 5.5a) in gas discharged at the peripheral seeps of Venere MV, comparable to that within mud breccia extruded at the western summit. We argue that gas diverted from the central conduit experienced post-genetic processes during its migration along the <2.5 km long ring faults.

As shown for the sediment-hosted hydrothermal system of the Lusi site in Indonesia, divergent fluid migration along faults of collapsing calderas takes more time than focused flow along the main conduit resulting in changes in the composition of vented gases (Mazzini

et al., 2012). Similarly, longer distances and slower fluid flow of gas migrating along the ring-fault system of Venere MV most likely contributed to changes in gas composition observed at the peripheral seeps.

### 5.6.3. Upward-branching plumbing system

Based on our observations of prevailing seafloor morphologies and processes, and analyses of pore fluid (gas and water) compositions of samples from Venere MV, we propose a conceptual model of its plumbing system that inter-relates extrusive processes, ring-faulting, fluid seepage and seafloor ecosystems (Fig. 5.7).

Our results from pore fluids in mud breccia flowing from Venere MV provided the first direct evidence that MVs on the CAP are linked to fluid sources deep within the accretionary prism. Gas compositions and fresh pore waters point to thermogenic gas formation and pore water generation from mineral dehydration reactions at source depths of >3.5 km, beneath the <2 km thick (Minelli and Faccenna, 2010) infill of the Crotone basin. Our findings confirm inferences of deep sources for other MVs on the CAP based on mud breccia compositions (Morlotti et al., 1982; Praeg et al., 2009; Panieri et al., 2013) and are consistent with geochemical findings from MVs elsewhere along the Mediterranean accretionary system (Dählmann and De Lange, 2003). Overpressured fluids are assumed to force their way upward through hydraulic fracturing (pathway generation by overpressure) and fluidization (suspension of solids through fluid movement), which are argued to drive mud volcanism or mud diapirism in accretionary prisms (Brown, 1990; Deville et al., 2010).

At Venere MV, we propose that gas-rich pore fluids migrated upward along a conduit from within the accretionary prism and through the forearc basin to a source depth below the seafloor edifice of Venere MV. The maximum absolute temperature measured in fresh mud breccia at the summit (26.8 °C) indicated a maximum temperature difference of 13 °C compared to background sediments exposed to bottom water on the seafloor (13.8 °C). Assuming the background geothermal gradient of 0.020 °C/m (s. above), a minimum source depth of 650 m can be estimated. The source depth is inferred to correspond to a zone of critical pore fluid pressures in which ascending, overpressured fluids experience lower surrounding pressures that allows for lateral movement from the main conduit and intrusion into surrounding sediments (Fig. 5.7; cf. Deville et al. (2003)). We infer the ring faults at Venere MV to root in the zone of critical pore fluid pressures (Fig. 5.7) and respond to variations in pore pressures linked to fluid pulses from the deeper plumbing system. During episodic phases of high pore fluid pressures the ring faults facilitate the diversion of an overpressured gas phase to the periphery of the MV. In turn, variations in pore pressures may facilitate movement on the ring-faults (e.g. leading to caldera collapse). We note that the ring faults define an asymmetric caldera, with greater offsets to the east at greater distances from the western summit (Fig. 5.2b). This could reflect higher pore pressures along faults with longer extensions from the currently active conduit. These ideas are consistent with previous studies, proposing that calderas within or around MVs develop by near-surface reductions in pore fluid pressure or the evacuation of mud chambers (Planke et al., 2003;

Evans et al., 2008; Deville et al., 2010), either of which may be enhanced by extrusive loading.

The geothermal gradients at the summit of Venere MV (1.96–15.54 °C/m) were up to two orders of magnitude higher than those at the peripheral seeps (0.01–0.31 °C/m; Table 5.1). At the Haakon Mosby MV, Feseker et al. (2008) attributes anomalous temperatures in near-seafloor sediments to heat transport from depth by fluids or mud, migrating at different rates. Methane discharged along the caldera surrounding Venere MV provided clear evidence that the ring faults act as natural migration pathways for gas but not for mud breccia. A study from the giant Regab pockmark indicated that fluids may migrate laterally by dispersed flow through sediment pores, or by focused flow along sediment discontinuities (Marcon et al., 2014a). Given the longer migration distances and lower geothermal gradients for fluids discharged at the peripheral seeps, we suggest that in contrast to focused flow within the main conduit, the ring-fault system facilitates dispersed fluid flow along faults and microfractures.

Our model thus involves an upward-branching plumbing system (Fig. 5.7) in which high pore fluid pressures sustain coeval mud breccia extrusion, ring-fault activity and peripheral cold seep systems. Upward-branching systems have previously been inferred from observations of quiescent MVs in terrestrial settings, mostly associated with the seepage of muds rather than mud breccia flows (Mazzini et al., 2009b; Deville et al., 2010). Investigations of submarine MVs have documented faults bordering MV edifices in the Gulf of Mexico (Prior et al., 1989; Neurauter and Bryant, 1990), the Beaufort Sea (Paull et al., 2015b) and the western Mediterranean Sea where chemosynthetic fauna are documented at the rim of a MV caldera (Somoza et al., 2012). Our model links three forms of coeval activity – i.e. mud breccia extrusion, quiescent stage faulting, and fluid discharge – to high fluid pressures and suggests that upward-branching fluid migration pathways act as a control on cold seep functioning within submarine MVs. We propose that it exerts a previously unrecognized control on the distribution of seepage-dependent chemosynthesis-based oases of life and that this process may be more important than has been recognized to date at submarine MVs.

An upward-branching plumbing system is also suggested by the twin cones of Venere MV, each of which records mud breccia extrusion above a stable subsurface conduit (Fig. 5.7). This inference is based on the observation of a single caldera, and is consistent with observations at the Madonna dello Iono MVs where twin cones have been show to overlie a subsidence depression pointing to a single main conduit (Praeg et al., 2009). At Venere MV, our results showed that only one of the two conduits was extruding mud breccia at the time, while that beneath the eastern cone appeared to have been inactive, based on cores showing mud breccia to be buried beneath hemipelagic sediments up to several decimeter thick. The comparable height of the two cones suggested that, over longer timescales, the plumbing system beneath Venere MV is dynamic and switched between the two conduits, alternating or involving phases of coeval activity. Twin-coned MVs have been observed at

several other locations on the CAP (Ceramicola et al., 2014b), and occur elsewhere in the eastern Mediterranean Sea including in association with subsidence depressions (Mascle et al., 2014), suggesting that upward-branching drainage systems may be more common than has been recognized to date.

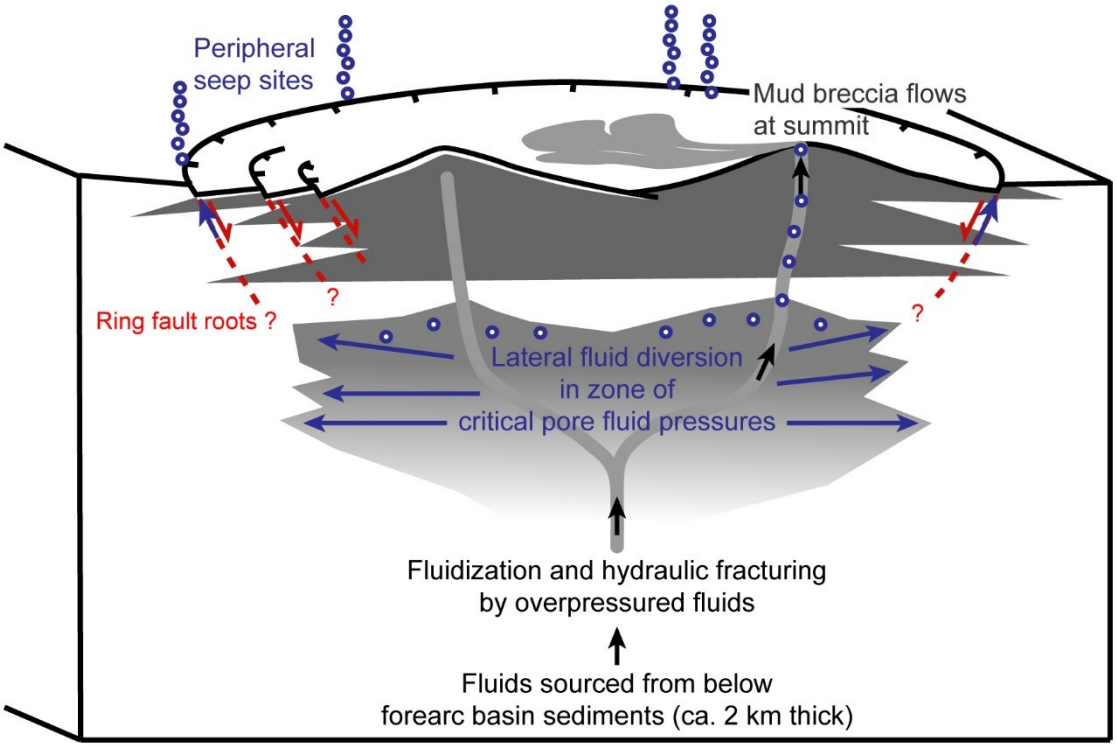


Figure 5.7. Conceptual model of Venere MV involving a conduit feeding gas-rich (blue circles represent free gas) mud breccia from the subsurface to the summit of a MV cone where mud breccia extrude and flow along the cone; dark grey wedges represent old buried mud breccia that build the cones and red stippled lines represent ring faults. Gas migration occurs along ring faults (short blue arrows along red stippled lines) and gas is discharged at peripheral seeps. We infer a zone of critical pore fluid pressures (light grey area) to accommodate mud and fluid release and caldera subsidence coevally (see text). Long blue arrows indicate lateral fluid diversion after the model of a MV plumbing system in Fig. 14 of Deville et al. (2003), see text). Fluid compositions point to sources below the ca. 2 km thick Plio-Quaternary filling of the forearc basin (see Minelli and Faccenna (2010)) while studies of other MVs on the CAP suggest mobilization of pre-Messinian deposits (Morlotti et al., 1982; Praeg et al., 2009; Panieri et al., 2013). Figure is not to scale but seafloor dips of the ring faults of up to 45° suggest comparable caldera depths and radius.

### 5.6.4. The active Venere MV – eruptive or quiescent?

Studying the eruption of MVs in deep-marine settings is in principle difficult, since eruptive episodes are typically short-lived and MVs may persist in a quiescent mode for 95% of their lifetime (Kopf, 2002). It has been suggested that, over the long-term, quiescent-phase activity regulates pressures and limits the build-up of pressures sufficient for eruptive activity (Mazzini and Etiope, 2017). At Venere MV, however, we observed the ongoing extrusion of mud breccia from a single main summit site, rather than muds from smaller, secondary, or parasitic cones as considered typical for quiescent-phase mud volcanism (e.g. Planke et al. (2003), Deville and Guerlais (2009)). Mud breccia extrusion at the summit was accompanied

by gas release along the ring-fault system, at sites supporting the development of chemosynthetic communities and precipitation of authigenic carbonate pavements. The growth of such cold-seep features indicates persistent methane seepage over thousands of years (Bayon et al., 2009). These findings point to a stable relationship between mud breccia flux through a conduit at the summit and gas escape along the ring-faults. We infer that this type of activity is caused by persistently high fluid pressures within the conduit and a subsurface zone of critical pore fluid pressures, which are sustained by gas and water supply from thermogenic organic matter degradation and diagenetic reactions at depth (Fig. 5.7). The coevality of mud breccia extrusion and gas release at peripheral seeps indicates that at the time of investigation, either Venere MV was in an 'eruptive' phase, or that its 'quiescent' activity involves the outflow of mud breccia volumes capable of forming kilometer-scale mudflows. Alternatively, Venere MV may be more aptly characterized as experiencing a phase of 'pressurized' activity, representative of an unknown proportion of its lifetime. 'Pressurized' activity may be defined by subsurface pore pressures high enough to drive coeval mud breccia extrusion, caldera collapse and fluid seepage. This form of activity may also characterize that of other MVs, challenging the binary characterization of eruptive versus quiescent activity.

## 5.7. Conclusions

Integration of data from hydroacoustic investigations, seafloor observations, and geological sampling at Venere MV allowed us to link morphological expressions of fluid discharge to processes occurring at depth and their impacts on ecosystem distribution. We provided the first data on the composition of fluids involved in mud volcanism on the Calabrian accretionary prism and identify two co-existing domains at Venere MV: 1) ongoing mud breccia outflows at a summit site, extrusion of thermogenic hydrocarbons, and freshened pore waters; and 2) advective seepage of methane fueling cold-seep communities at sites along peripheral ring-faults. Our data indicated that mud breccia and fluids discharging at the summit are generated by thermogenic organic matter degradation and mineral dehydration reactions occurring at depths of at least 3.5 km, below the Crotone forearc basin and within the accretionary prism itself. Freshened pore waters indicated that Messinian evaporites are either not present or have been removed by fluid migration from below Venere MV. We present an upward-branching plumbing system as a conceptual model for the activity of Venere MV. It involves mud breccia discharge at one or both of two main conduits that has led to the build-up of twin cones, accompanied by gas migration along a system of ring-faults that has led to the development of peripheral seeps. Coeval mud breccia extrusion, peripheral fluid release and caldera collapse are inferred to be sustained by high fluid pressures within and around the conduit as well as a zone of critical pore fluid pressures in which lateral fluid diversion occurs and which regulates variations in pore pressures resulting from fluid pulses from depth. Chemosynthetic communities and thick authigenic carbonates are limited to the peripheral seeps along the caldera and reveal that hydrocarbon discharge at these sites has been active and stable for several thousands of years. Given the abundance of submarine MVs but rare documentations of their eruptions, our data expanded

the understanding of active mud volcanism as well as seepage-dependent ecosystem distribution around MVs in the marine realm.

## 5.8. Acknowledgements

We thank the masters and crews of cruises RV METEOR M112 and RV POSEIDON POS499. The teams of the MARUM AUV SEAL 5000 and ROV QUEST 4000m are acknowledged. Marvin Lilley (at the ETH Zürich) is thanked for isotope cross-measurements on selected methane samples. We thank the Deutsche Forschungsgemeinschaft (DFG) and the Research Center / Excellence Cluster “The Ocean in the Earth System” for funding of expeditions M112 and POS499. Marta Torres acknowledges support through a fellowship from the Hanse Wissenschaftskolleg. Daniel Praeg acknowledges funding from the European Union’s Horizon 2020 research and innovation program under the Marie Skłodowska-Curie grant agreement No 656821 (project SEAGAS).

# 6. Manuscript II: Mud volcanism in a canyon

## Mud volcanism in a canyon: Morpho-dynamic evolution of the active Venere mud volcano and its interplay with Squillace Canyon, Central Mediterranean

Markus Loher[1], Silvia Ceramicola[2], Paul Wintersteller[1], Gerrit Meinecke[1], Heiko Sahling[1], Gerhard Bohrmann[1]

**Under review in Geochemistry, Geophysics, Geosystems.**

*[1]MARUM – Center for Marine Environmental Sciences and Faculty of Geosciences, University of Bremen, Klagenfurter Str., 28359 Bremen, Germany*

*[2]OGS (Istituto Nazionale di Oceanografia e di Geofisica Sperimentale), Borgo Grotta Gigante 42/c, Sgonico, 34010 Trieste, Italy*

Keywords: Mud volcano; Mud breccia; AUV; Submarine canyon; Tephra; Calabrian Accretionary Wedge

## 6.1. Abstract

Submarine mud volcanoes develop through the extrusion of methane-rich fluids and sediments onto the seafloor. The morphology of a mud volcano can record its extrusive history and processes of erosion and deformation affecting it. The study of offshore mud-volcano dynamics is limited because only few have been mapped at resolutions that reveal their detailed surface structures. More importantly, rates and volumes of extruded sediment and methane are poorly constrained. The 100 m high twin cones of Venere mud volcano are situated at ~1600 m water depth within Squillace Canyon along the Ionian Calabrian margin, Mediterranean Sea. Seafloor bathymetry, and backscatter data obtained by a ship-based system and an autonomous underwater vehicle (AUV) allow mapping of mudflows of the mud volcano and bedforms in the surrounding canyon. Repeated surveying by AUV document active mud movement at the western summit in between 2014 and 2016. Through sediment coring and tephrochronology, ages of buried mudflows are determined based on the sedimentation rate and the thickness of overlying hemipelagic sediments. An average extrusion rate of 27000 $m^3$/year over the last ~882 years is estimated. These results support a three-stage evolutionary model of Venere mud volcano since ~4000 years ago. It includes the onset of quiescence at the eastern cone (after ~2200 years ago), erosive events in Squillace Canyon (prior to ~882 years ago), and mudflows from the eastern cone (since ~882 years). This study reveals new interactions between a mud volcano and a canyon in the deep sea.

## 6.2. Introduction

A mud volcano (MV) results from the upward migration of mobilized subsurface sediments, gas, and water by focused fluid flow and the extrusion of a mixture of these components, referred to as mud breccia (Cita et al., 1981; Camerlenghi et al., 1992; Pape et al., 2010; Mazzini and Etiope, 2017). The surface morphology of a MV is therefore the direct result of repeated extrusions of mud breccia accumulating progressively over time. MVs typically develop into pie- or cone shaped edifices (Kopf, 2002; Planke et al., 2003) up to several kilometers wide and several hundred meters high (Ivanov et al., 1996b; Dimitrov, 2002; Kopf, 2002; Kioka and Ashi, 2015) and can induce surface subsidence by caldera formation (Prior et al., 1989; Bonini, 2008; Evans et al., 2008; Mazzini et al., 2009b). The rate and frequency of extrusions, and the amounts of hydrocarbons released remain poorly documented, especially for MVs located offshore in the deep sea (Dimitrov, 2002; Milkov et al., 2003; Etiope and Milkov, 2004; Feseker et al., 2014), where they potentially host shallow gas hydrates (Bohrmann et al., 2003; Stadnitskaia et al., 2008; Pape et al., 2010; Pape et al., 2011b). Investigating the morphological evolution of submarine MVs is important to try and assess their state of activity and estimate rates of mud breccia or fluid extrusion.

Seafloor mapping capable of resolving mud eruption events at deep sea MVs as subtle morphological changes over time (Foucher et al., 2010; Feseker et al., 2014) has only become possible due to the advent of multibeam echosounder systems mounted on remotely operated vehicles (ROVs; e.g. Kaul et al. (2006), Foucher et al. (2009)) or autonomous underwater vehicles (AUVs; (Wynn et al., 2014)). Apart from the pie-shaped Håkon Mosby MV, no other MV has so far been repeatedly mapped by AUV or ROV. In fact, of the estimated $10^3$–$10^5$ MVs occurring in deep sea environments (Milkov, 2000), high-resolution datasets are only available for the Amon, Isis, Chephren, and Cheops MVs in the Nile Deep Sea Fan (Dupré et al., 2008; Foucher et al., 2009; Dupré et al., 2014; Mascle et al., 2014), the Napoli MV in the Mediterranean Ridge (Mascle et al., 2014), and three MVs along the continental slope of the Canadian Beaufort Sea (Paull et al., 2015b). The majority of these structures are either pie-shaped structures (i.e. the Amon MV, Isis MV, Napoli MV, and all but one of the Canadian MVs) or flat-lying calderas (i.e. the Chephren and Cheops brine pools) Only Paull et al. (2015b) have documented a cone-shaped MV. Accordingly, understanding of the extrusive dynamics at cone-shaped MVs remains limited and investigations considering the age of structures visible in AUV-derived datasets and the recent evolution of MVs over time are lacking.

Mudflows are typically characterized by elevated backscatter intensities in sonar data (e.g. Zitter et al. (2005), Van Rensbergen et al. (2005b)), which is argued to result from a combination of surface scattering (depending on seafloor roughness) at the sediment-water interface and volume scattering (depending on the presence of mud breccia clasts or gas bubbles) in the shallow subsurface (Johnson and Helferty, 1990; Volgin and Woodside, 1996). Whereas the signal penetration and attenuation is strongly frequency dependent (Mitchell, 1993), the highest backscatter intensity for mudflows results where the mud breccia is exposed on the seafloor and decreases with increasing burial by soft and homogeneous

marine sediment (Zitter et al., 2005; Sahling et al., 2009). Visual observations of the seafloor surface may, therefore, not be able to fully resolve or ground truth backscatter variations (e.g. Paull et al. (2015b)) but requires sediment cores to investigate the shallow subsurface (Zitter et al., 2005). By dating of sediments overlying the mud breccia (Gennari et al., 2013) or according to the local sedimentation rate it has been possible to constrain the timing of extrusive activity of MVs on regional scales (Rabaute and Chamot-Rooke, 2007; Ceramicola et al., 2014b). Similarly, precise coring of mudflows at MVs mapped by AUV, may allow to reconstruct their extrusive dynamics and to constrain their morphological evolution over time.

Venere MV, discovered by Ceramicola et al. (2014b), is an active twin-cone MV with a subsidence caldera situated at ~1600 m water depth within the lower channel of Squillace Canyon along the Ionian Calabrian margin, Central Mediterranean Sea (Fig. 6.1 and 6.2). It was found by Loher et al. (in review (JMPG)), that fresh mudflows of distinct morphologies and lacking hemipelagic drape extend from the western summit. These types of extrusions were revealed for the first time as previous investigations of cone-shaped submarine MVs had only shown mudflows in sidescan data as narrow trails extending radially from the edifices (Ivanov et al., 1996b; Paull et al., 2015b). In addition to hydroacoustic water column anomalies (i.e. flares) at the western summit, gas release from peripheral seeps was detected in alignment with ring faults at the caldera edge. Fluids emitted with mud breccia consisted of thermogenic gases and pore water significantly depleted in chloride, that are argued to indicate thermogenic organic matter degradation and mineral dehydration reactions, respectively, and to point to fluids sourced at >3.5 km depth. It has been proposed that high subsurface pressures are required to sustain the extrusion of mud breccia at the MV summit and coevally drive gas release at the peripheral seeps through an upward-branched plumbing system (Loher et al., in review (JMPG)).

The main objective of this study is to investigate the age, evolution, and extrusive dynamics of the surface of Venere MV and the potential interaction of the MV edifice with sediment-transport processes along Squillace Canyon. Ship- as well as AUV-derived bathymetry and backscatter data, are complemented by subsurface profiles and 30 sediment cores for ground truthing. Seafloor maps provide insights into the morpho-dynamics of Venere MV and Squillace Canyon. Tephrochronology is applied to sediment cores and mapping of mudflows reveals the spatio-temporal evolution of the MV and allows to estimate the extrusion rates. Finally it is investigated if and how a MV edifice can alter the flow paths and dynamics of sediment transport processes in a canyon and vice-versa, their influence on the morphology of a MV.

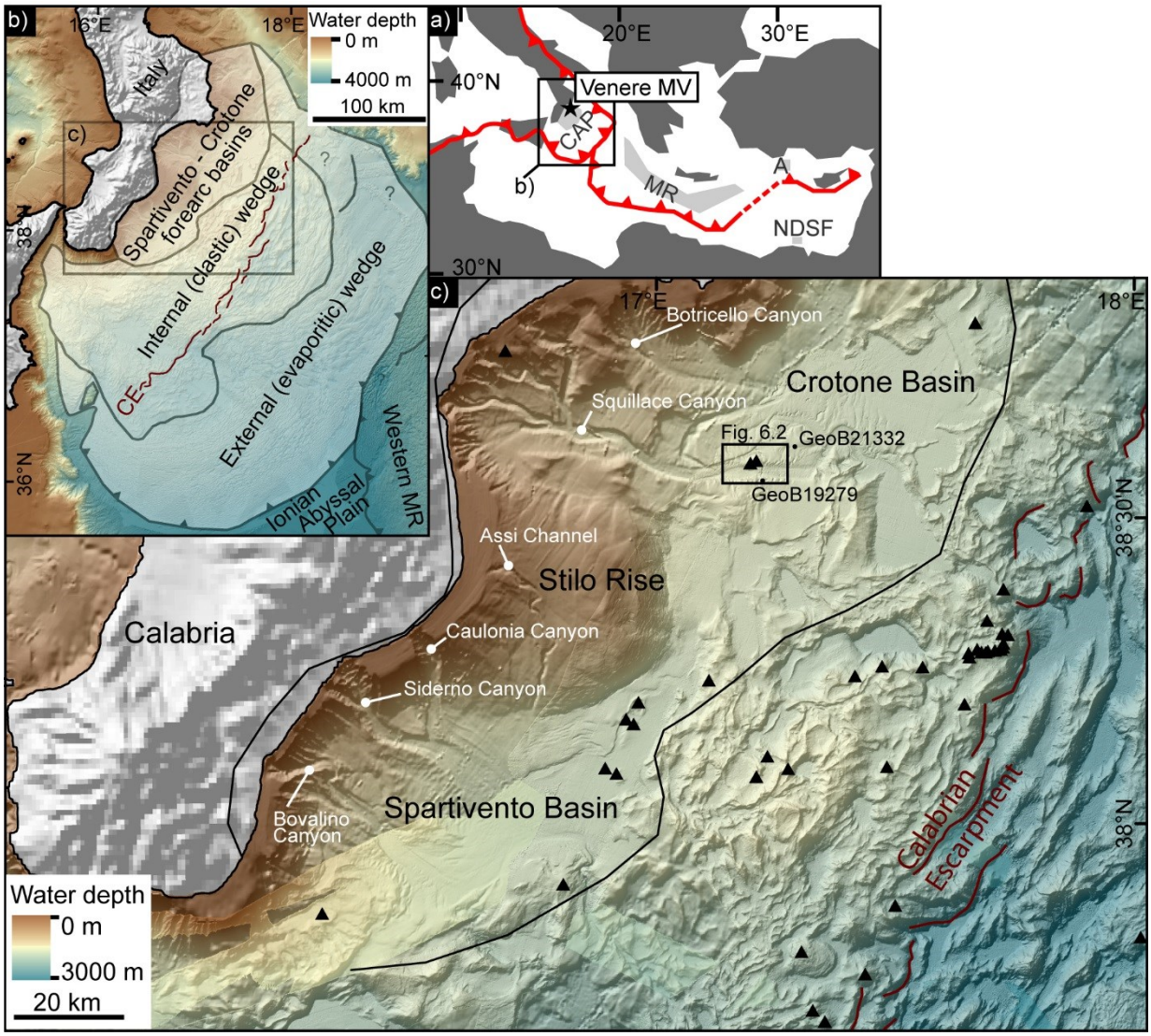


Figure 6.1. a: Map of the eastern Mediterranean region with location of Venere MV (black star) in the Calabrian accretionary prism (CAP) relative to plate boundaries (red lines); also shown are the Mediterranean Ridge (MR), Anaximander Mountains (A) and Nile Deep Sea Fan (NDSF) MV provinces (grey areas; after Mascle et al. (2014)). Black box represents extent of b: Morpho-structural domains (modified after previous interpretations, see text) of the CAP overlain on bathymetry map; CE = Calabrian Escarpment. Black box represents extent of c: Detailed bathymetric map of the Ionian-Calabrian margin showing the main submarine canyons (names in white), the locations of selected mud volcanoes (black triangles) and two gravity-core locations (black dots with GeoB-identifier); the black box indicates the extent of Fig. 6.2.

## 6.3. Regional setting and mud volcanism

The Calabrian Accretionary Prism (CAP; Fig. 6.1a and b) results from the northwest-oriented subduction of the Nubia plate below the Eurasian plate (Malinverno and Ryan, 1986; Gueguen et al., 1998; Faccenna et al., 2001; Rosenbaum et al., 2002; Neri et al., 2009). The CAP extends for more than 300 km from NE to SW and seaward from the Calabrian-Ionian coast towards the ca. 4000 m deep Ionian Abyssal Plain. The main morpho-structural domains of the CAP include the post-Messinian external wedge, the pre-Messinian internal

wedge, and the Spartivento–Crotone forearc basins (Fig. 6.1b; (Rossi and Sartori, 1981; Minelli and Faccenna, 2010; Polonia et al., 2011; Ceramicola et al., 2014b; Zecchin et al., 2016; Gutscher et al., 2017). In the pre-Messinian wedge a series of scarps, the most prominent of which is known as the Calabrian Escarpment (CE; Figs. 6.1b and c), has been interpreted as a fold-and-thrust belt, argued to be the result of several transpressive splay-faults (strike-slip faults and thrusts) indicating out-of-sequence movement and strain partitioning between the external and internal wedges (Cernobori et al., 1996; Praeg et al., 2009; Minelli and Faccenna, 2010; Polonia et al., 2011; Gutscher et al., 2017). In the forearc basins, Mesozoic-Cenozoic basement of the accretionary wedge is exposed onshore and overlain by sediments of up to Mid-Miocene (late Serravallian) age, including Messinian evaporites and Plio-Pleistocene units (Roda, 1964; Zecchin et al., 2003), which have also been drilled in nearshore wells (Capozzi et al., 2012). The offshore Spartivento-Crotone forearc basins contain up to 2 km of Pliocene-Quaternary sedimentary infill with <500 m thick Messinian deposits (Minelli and Faccenna, 2010; Polonia et al., 2011).

The Ionian-Calabrian margin has been experiencing rapid topographic uplift (on the order of 0.5–2 mm/yr) since 0.7–0.4 Ma (Westaway, 1993; Monaco and Tortorici, 2000; Catalano and De Guidi, 2003; Antonioli et al., 2006; Ferranti et al., 2007; Zecchin et al., 2011). The uplift influenced the geomorphological dynamics on- and offshore Calabria by forming steep coastal areas with riverbeds connecting to submarine canyon systems and sustaining sediment discharge across the Calabrian-Ionian margin. Submarine canyons along the Calabrian-Ionian margin (Fig. 6.1c) have been imaged on seismic lines (Capozzi et al., 2012) and their formation has been tentatively constrained to be younger than the Mid-Pleistocene (Coste, 2014), in accordance with the onset of regional uplift (Capozzi et al., 2012; Ceramicola et al., 2014a). Squillace Canyon, relevant to this study, is one of the largest submarine canyon systems along the Calabrian-Ionian margin. Near the coastline it consists of several tributary canyons, which converge to a main lower channel course at ca. 1150 m water depth and it extends seaward into the Crotone-Spartivento forearc basins to water depths of over 1800 m.

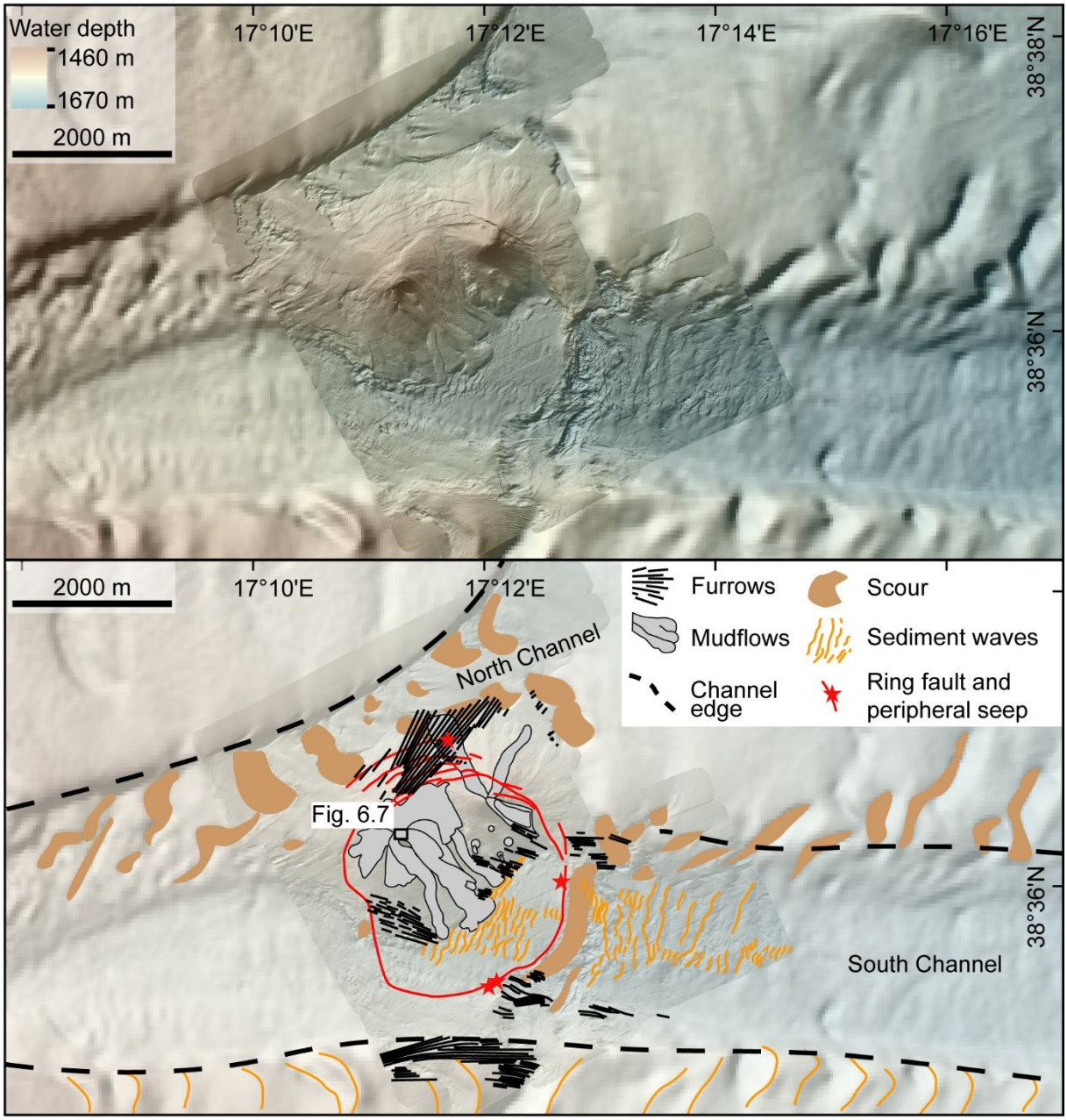


Figure 6.2. AUV-derived bathymetric map draped on ship-derived bathymetric map of the study area (upper panel) and interpreted structures (lower panel) including the investigated mudflows, sediment waves, scours, and furrows; see Fig. 6.1b for map extent; black box indicates extent of Fig. 6.7.

Hydroacoustic surveys across the CAP and sediment sampling have documented at least 53 submarine MVs occurring in the pre-Messinian domains and forearc basins of the CAP and only few in more seaward locations (Fig. 6.1c; (Ceramicola et al., 2014b; Bohrmann et al., 2015; Loher et al., in review (JMPG))). Several structures have been reported to show signs of recent mud breccia extrusion (Foucher et al., 2009; Praeg et al., 2009; Panieri et al., 2013; Ceramicola et al., 2014b) or fluid seepage (Foucher et al., 2009; Panieri et al., 2013) including a presumed flare at Catanzaro MV (Ceramicola et al., 2014b). Most extrusive features occur along tectonic lineaments such as transfer faults or thrusts, interpreted as post-Messinian out-of-sequence thrusts related to compressional or transpressive tectonics

of the CAP (Praeg et al., 2009; Minelli and Faccenna, 2010; Panieri et al., 2013; Ceramicola et al., 2014b; Gutscher et al., 2017). The onset of mud volcanism on the CAP is inferred to have originated >3 Ma ago (Late Pliocene; (Praeg et al., 2009)) and the study of mud breccia and microfossil assemblages indicated source materials as old as the Late Cretaceous for the Madonna dello Iono, Pythagoras and Sartori MVs (Morlotti et al., 1982; Praeg et al., 2009; Panieri et al., 2013). Regional backscatter mapping and subbottom profiles in combination with sediment coring at the Pythagoras, Madonna dello Iono, and Sartori MVs evidenced MV activity during the last 56 ka on the internal wedge, correlated mud breccia outflows to the last glacial maximum, and within the last 12 ka in the Crotone-Spartivento forearc basins (Praeg et al., 2009; Ceramicola et al., 2014b).

## 6.4. Methods

Data and samples used in this study were acquired during R/V METEOR cruise M112 in 2014 (Bohrmann et al., 2015) and R/V POSEIDON cruise POS499 in 2016 (Bohrmann et al., 2016). Swath bathymetry data were collected by a ship-based Kongsberg EM122 (12 kHz) system during cruise M112 and by a Kongsberg EM2040 (300 kHz) system mounted on autonomous underwater vehicle (AUV) MARUM-SEAL 5000 during M112 and POS499. Data processing was carried out with MB-System (Caress and Chayes, 1996) and bathymetry was made available through EMODnet (http://www.emodnet.eu/bathymetry). Ship-based data was gridded at 50 m lateral and meter-scale vertical resolution and AUV-derived data at 1.6 m lateral and decimeter-scale vertical resolution.

Gas emissions and sub-surface structures were investigated during M112 by a hull-mounted parametric sediment echosounder system (PARASOUND) operated at a primary frequency of 18 kHz used for gas bubble imaging in the water column and provided a parametric frequency of 4 kHz used for subbottom imaging. The software ATLAS PARASTORE was used for online data processing and plotting whereas the program SeNT (H. Keil, University of Bremen) was employed for basic data processing and plotting.

Sediment cores presented in this study were collected during cruises M112 and POS499 by a conventional gravity corer or by a mini-corer system equipped with up to four liners for short cores. Coring locations (precision on the order of several tens of meters), were chosen on top of the lobes of mudflows or in relatively flat and undisturbed seafloor areas. Measurements of magnetic susceptibility (MS) were conducted on gravity cores by a Bartington Instruments MS2 Magnetic Susceptibility System in 1 cm increments. Sediment cores were photographed and macroscopically described to investigate on the presence of mud breccia clasts larger than ca. 0.5 cm in relation to changes in lithology. Burial depths of mud breccia are reported as a range, accounting for uncertainties due to gradual or irregular contacts due to bioturbation or potential mixing by post-depositional gas release.

X-ray fluorescence (XRF) scans in 10 mm down-core step-size were carried out for core GeoB19234-1 (section 0-94 cm) with an XRF Core Scanner III (Avaatech Serial No. 12) at the MARUM–University of Bremen to provide elemental compositions reported in counts per step (cps). For the elements Al, Si, S, K, Ca, Ti, Mn, Fe the XRF scan was carried out at 10

kV with a current of 0.2 mA and 20 sec count time and for Br, Rb, Zr, Sr, Nb, Pb at 30 kV with a current of 1 mA with a count time of 20 sec.

Glass shards from a sieved (40 µm) and dried sediment sample extracted at 43–44 cm depth from Core GeoB19234-1 were mounted on epoxy resin and polished. Major element compositions of shards were determined at University of Bremen using a Cameca SX100 electron microprobe equipped with four wavelength-dispersive spectrometers (WDS) operating at 15 kV and utilizing a 4 nA defocused beam of 5 µm diameter. Accuracy was monitored by analyzing rhyolite and basalt glass standards (VG-568 and VG-A99; Jarosewich et al. (1980)) together with the samples (Table 13.12 in supplements Chapter 13.2).

## 6.5. Results

### 6.5.1. Sediment lithologies

In this study, gravity and mini-cores have been used to investigate the sediments on top and in the vicinity of Venere MV and Squillace Canyon. A total of 30 sediment cores have been described, including 6 gravity cores and 22 mini-cores from sites on the MV edifice or within the caldera (Fig. 6.3), and 2 gravity cores from sites unaffected by the MV (Fig. 6.1c).

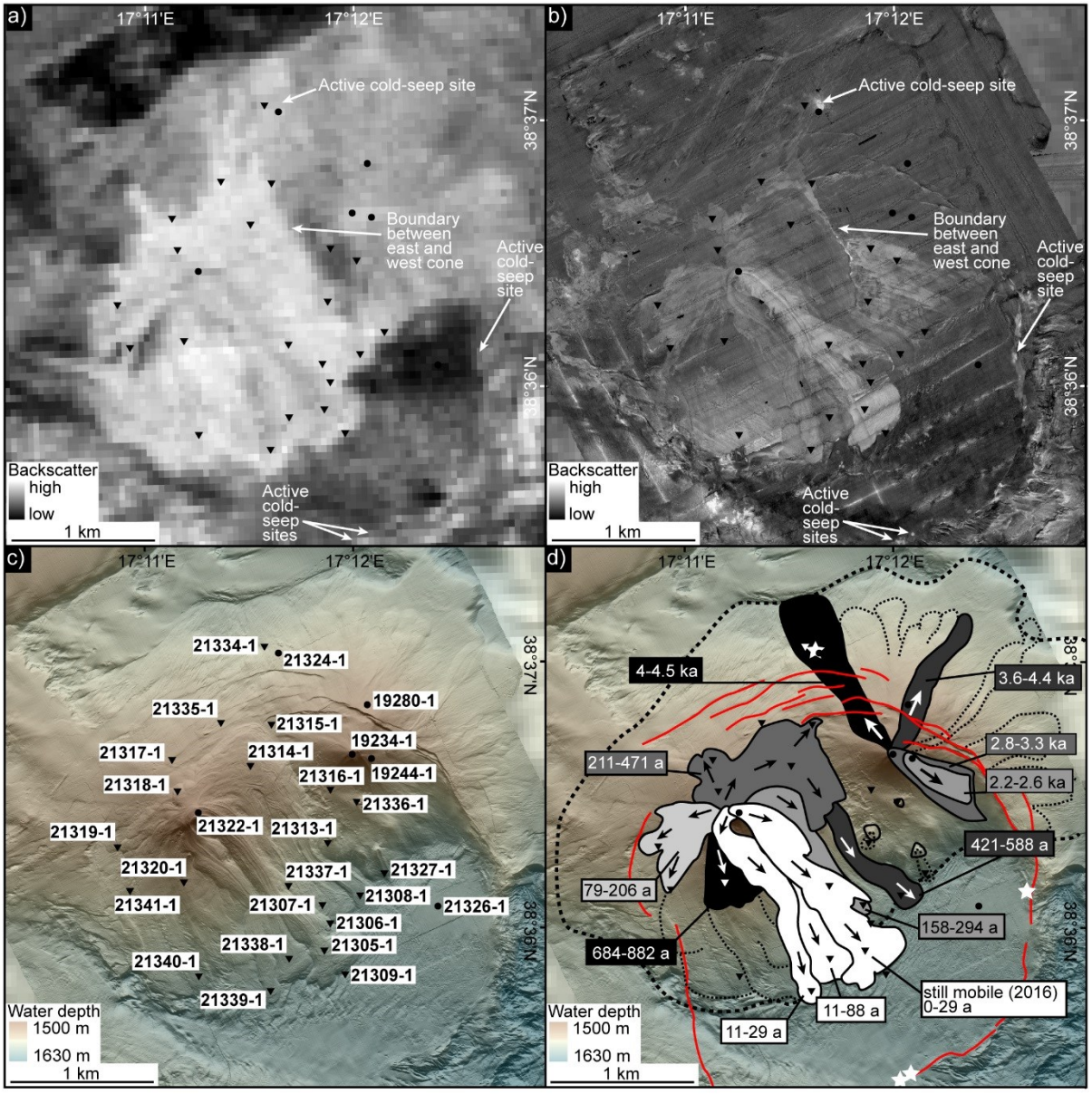


Figure 6.3. Maps of identical extent for Venere MV (a-d) indicating locations of mini-cores (triangles) and gravity cores (circles), numbers in c) refer to GeoB-identifier (see Table 6.1); a: ship-derived backscatter; b: AUV-derived backscatter draped on ship-derived backscatter; c: AUV-derived bathymetry draped on ship-derived bathymetry; d: same as c) with mapped mudflows (shaded gray) and age estimates (Table 6.1), ring faults (red lines), cold-seep locations (white stars), and estimated extents of mudflows not cored (stippled lines).

In Core GeoB19234-1 (Fig. 6.4a) the uppermost sediment consists of light yellowish or olive brown to grey, homogeneous (bioturbated) to faintly laminated, carbonate-bearing silty clay. XRF-based element ratios (Ti-normalized, Fig. 6.4a) showed an elevated Ca content, which resulted from biogenic carbonate components, compared to terrigenous contributions such as e.g. Zr. This lithology is identified as hemipelagic sediment very similar to hemipelagic sediments previously described for comparable settings on the CAP (Barbieri et al., 1982; Morlotti et al., 1982; Panieri et al., 2013).

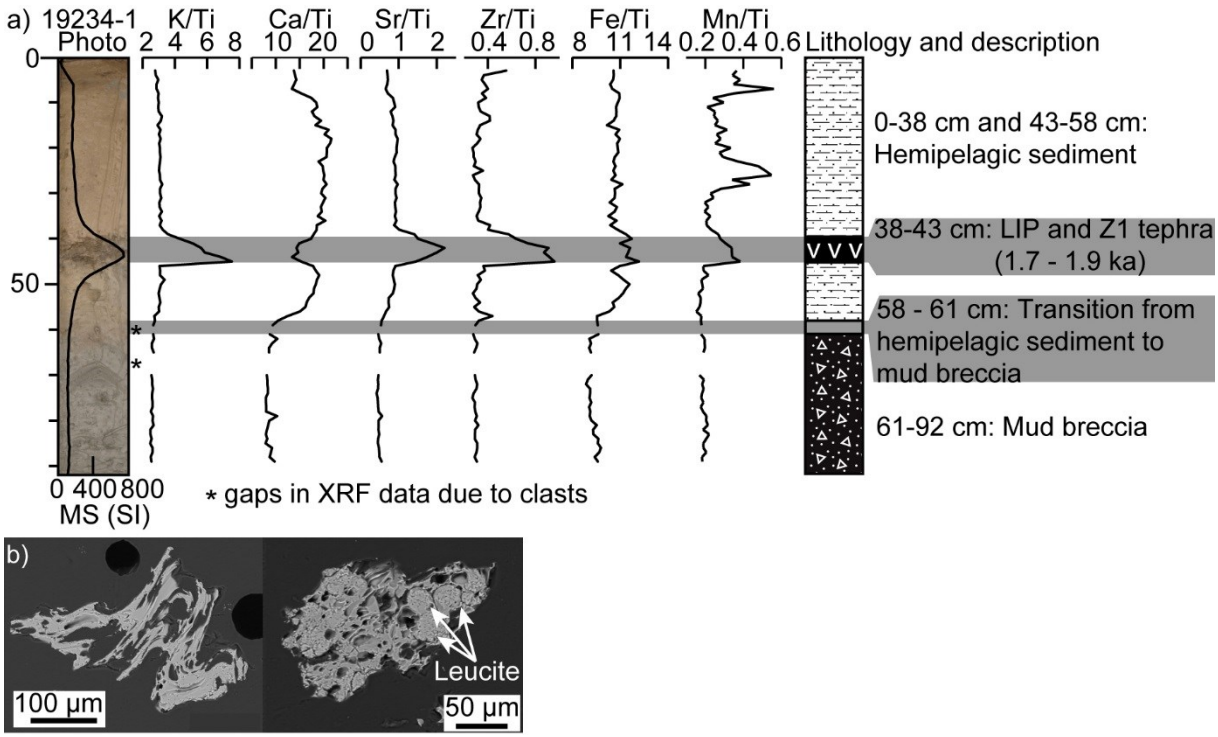


Figure 6.4. a: Magnetic susceptibility (MS) and XRF data (Ti-normalized) plotted against Core GeoB19234-1 photo (depth-scale in cm) with lithology and core description; ages for tephra (see text) are from Keller et al. (1978) and Paterne et al. (1988); b: Electron microscope images of glass shards (left: rhyolitic composition; right: phonolitic composition with leucite microcrysts, see Table 13.12 in supplements Chapter 13.2).

Most gravity- and mini-cores recorded hemipelagic sediment above mud breccia (Table 6.1; Figs. 13.1 and 13.2 in supplements Chapter 13.2). Mud breccia is characterized by a greenish grey, clay- and silt-rich matrix supporting poorly sorted, angular to subrounded rock clasts ranging from several mm to dm in size. Mousse-like textures of the matrix (resulting from high gas content) characterized cores with fresh mud breccia (GeoB21322, Fig. 6.5) whereas mud breccia was compact and massive in cores where it was overlain by several centimeters of hemipelagic sediment (Figs. 6.4a, 6.5, Figs. 13.1 and 13.2 in supplements Chapter 13.2). Clast lithologies included carbonates, sandstones, friable shale and marls. Contacts between mud breccia and overlying hemipelagic sediments were characterized by changes in color (from brownish to greyish), lithology and clast content (homogeneous silty clay to poorly sorted breccia) and transitions ranged from sharp to gradual (bioturbated) over up to 6 cm.

Dark grey to grey, homogeneous, silty to sandy sediments were encountered in mini-cores GeoB21309-1 (Fig. 6.5), 21316-1, 21334-1, and 21336-1 (Fig. 13.1 in supplements Chapter 13.2) and in gravity cores GeoB21324-1, 21326-1, 21332-1, and 19279-1 (Fig. 13.2 in supplements Chapter 13.2). Cores GeoB21332-1 and 19279-1 were characterized by several sandy intervals fining upward to silty clay. Cores GeoB21309-1 and 21326-1 from the MV caldera (Fig. 6.3), contained graded and irregular contacts between silt and massive

sand at 14 cm and 10 cm depth, respectively. These well sorted and normally graded silt and sand deposits were identified as gravity-flow deposits.

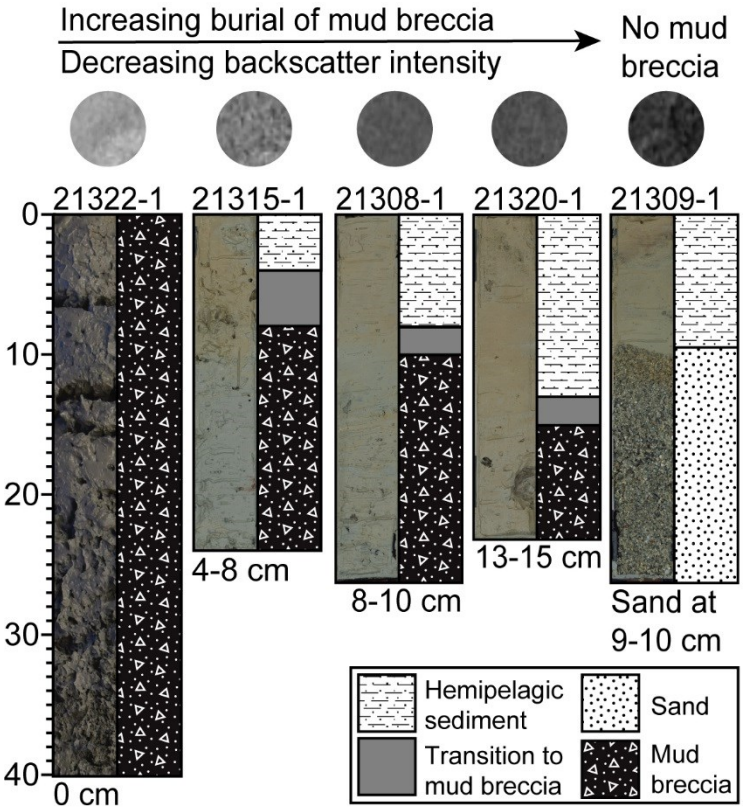


Figure 6.5. Core photo and lithology of sediment cores (numbers above cores are GeoB-identifiers) with corresponding backscatter (grey circles represent ca. 15 m radius of representative AUV-derived backscatter from the cored mudflows), exemplifying different amounts of mud breccia burial by hemipelagic sediment (numbers below cores indicate burial amount); note fresh mud breccia with mousse-like texture for Core GeoB21322-1 and sand instead of mud breccia in Core GeoB21309-1; depth axis in cm.

In Cores GeoB19234-1 (Fig. 6.4a), 19232-1, 19244-1, 19280-1, 21324-1 (Fig. 13.2 in supplements Chapter 13.2), 4 to 8 cm thick intervals of dark gray to brown, silty to fine-sandy sediment with clear basal contacts were present. In Cores GeoB19234-1, 19244-1, 19280-1 this intervals show a distinct peak in magnetic susceptibility (e.g. GeoB19234-1 in Fig. 6.4a). XRF analyses of Core GeoB19234-1 (Fig. 6.4a) document a lower Ca/Ti ratio than the hemipelagic sediments and higher Sr/Ti, Zr/Ti, Fe/Ti, Mn/Ti and K/Ti ratios than the mud breccia, comparable to XRF profiles across tephra layer Z1 by Polonia et al. (2015). Glass shards from Core GeoB19234-1 could be identified under the electron microscope (Fig. 6.4b) and WDS analyses revealed a phonolitic composition with leucite microcrystals for some of the glass shards but a rhyolitic composition for others (Table 13.12 in supplements Chapter 13.2). The phonolitic composition is comparable to the Z1 tephra (Polonia et al., 2015), which is known as a high-potassium phonolitic tephra, hosting leucite microcrysts in the glass matrix (Keller et al., 1978; Zanchetta et al., 2011). The Z1 tephra has been attributed to an eruption of Somma-Vesuvius in AD 79 (i.e. ca. 1900 years; (Keller et al., 1978; Zanchetta et al., 2011). The rhyolite glass analyzed additionally in shards here, showed a composition similar to a tephra layer analyzed by Paterne et al. (1988) (core KET8003 in Table 13.12 in supplements Chapter 13.2) dated at 1700 years. Tephra layers containing glass shards of different chemical compositions are known in this region and have been attributed to contemporaneous or amalgamated consecutive volcanic eruptions (Paterne et al., 1988). For the purpose of this study, an age range of 1700–1900 years is consistent with the identified

tephra layer. This results in sedimentation rates of 0.17–0.19 mm/year, averaged over the five cores where the tephra layer was identified. This sedimentation rate is comparable to previously determined sedimentation rates of the Spartivento forearc basin (0.18–0.26 mm/year (Ceramicola et al., 2014b)) and is clearly higher than values reported for the outer CAP (0.05–0.1 mm/year, (Kastens, 1984; Polonia et al., 2013)).

Sedimentological criteria such as color, lithology and occurrence of clasts >several mm in diameter, were applied to determine a depth range representing the amount of burial of mud breccia in cores that were taken on top of mudflows. Based on the sedimentation rates of 0.17–0.19 mm/year, the depth ranges were translated to minimum age ranges for the mudflows, corresponding to the onset of hemipelagic sedimentation on top of the mudflows. Respective core locations, burial depths and age ranges are summarized in Table 6.1. Core GeoB21306-1 was taken at the very edge of a mudflow and due to uncertainties of the exact core positioning, this core could not be reliably attributed to its corresponding mudflow. Cores GeoB21313-1, 21316-1, 21327-1, 21335-1, 21336-1, 21340-1 may not contain a complete hemipelagic section and their age estimates have not been further considered for establishing the stratigraphic order of mudflows (Fig. 6.3d, Table 6.2).

Table 6.1. GeoB-identifier and location data (WGS84) of sediment cores (MIC = mini-core; GC = gravity core) of this study and minimum–maximum depths of hemipelagic sediment cover on top of mud breccia and corresponding ages based on calculated sedimentation rates; no results for stations where no mud breccia deposits were cored.

| GeoB-No. | Type | Latitude (N) | Longitude (E) | Water depth (m) | Hemipelagic cover min. (cm) | Hemipelagic cover max. (cm) | Age min. (a)* | Age max. (a)** |
|---|---|---|---|---|---|---|---|---|
| 21305-1 | MIC | 38°35.930 | 17°11.814 | 1558 | 0.0 | 0.2 | 0 | 12 |
| 21306-1 | MIC | 38°36.033 | 17°11.845 | 1569 | 6.0 | 7.0 | 316 | 412 |
| 21307-1 | MIC | 38°36.103 | 17°11.810 | 1558 | 3.0 | 5.0 | 158 | 294 |
| 21308-1 | MIC | 38°36.134 | 17°11.992 | 1569 | 8.0 | 10.0 | 421 | 588 |
| 21309-1 | MIC | 38°35.837 | 17°11.911 | 1572 | - | - | - | - |
| 21313-1 | MIC | 38°36.334 | 17°11.842 | 1532 | 4.0 | 6.0 | 211 | 353 |
| 21314-1 | MIC | 38°36.631 | 17°11.481 | 1497 | 5.0 | 8.0 | 263 | 471 |
| 21315-1 | MIC | 38°36.780 | 17°11.575 | 1509 | 4.0 | 8.0 | 211 | 471 |
| 21316-1 | MIC | 38°36.535 | 17°11.861 | 1513 | - | - | - | - |
| 21317-1 | MIC | 38°36.661 | 17°11.104 | 1500 | 5.0 | 6.0 | 263 | 353 |
| 21318-1 | MIC | 38°36.547 | 17°11.127 | 1477 | 6.0 | 7.0 | 316 | 412 |
| 21319-1 | MIC | 38°36.341 | 17°10.832 | 1515 | 2.5 | 3.5 | 132 | 206 |
| 21320-1 | MIC | 38°36.199 | 17°11.148 | 1516 | 13.0 | 15.0 | 684 | 882 |
| 21327-1 | MIC | 38°36.214 | 17°12.111 | 1560 | 7.0 | 8.0 | 368 | 471 |
| 21334-1 | MIC | 38°37.083 | 17°11.561 | 1535 | - | - | - | - |
| 21335-1 | MIC | 38°36.795 | 17°11.343 | 1507 | 11.0 | 13.0 | 579 | 765 |
| 21336-1 | MIC | 38°36.488 | 17°11.986 | 1521 | - | - | - | - |
| 21337-1 | MIC | 38°36.179 | 17°11.649 | 1535 | 0.0 | 0.5 | 0 | 29 |
| 21338-1 | MIC | 38°35.901 | 17°11.644 | 1568 | 0.2 | 1.5 | 11 | 88 |
| 21339-1 | MIC | 38°35.785 | 17°11.551 | 1569 | 0.2 | 0.5 | 11 | 29 |
| 21340-1 | MIC | 38°35.843 | 17°11.209 | 1561 | 4.0 | 7.5 | 211 | 441 |
| 21341-1 | MIC | 38°36.175 | 17°10.886 | 1523 | 1.5 | 3.0 | 79 | 176 |
| 19234-1 | GC | 38°36.663 | 17°11.973 | 1505 | 53.0 | 56.0 | 2798 | 3304 |
| 19244-1 | GC | 38°36.648 | 17°12.062 | 1518 | 41.0 | 44.0 | 2165 | 2596 |
| 19279-1 | GC | 38°34.783 | 17°12.883 | 1560 | - | - | - | - |
| 19280-1 | GC | 38°36.851 | 17°12.048 | 1513 | 69.0 | 75.0 | 3643 | 4425 |
| 21322-1 | GC | 38°36.462 | 17°11.223 | 1474 | 0 | 0 | 0 | 0 |
| 21324-1 | GC | 38°37.053 | 17°11.627 | 1524 | 75 | 76 | 3960 | 4484 |
| 21326-1 | GC | 38°36.086 | 17°12.364 | 1570 | - | - | - | - |
| 21332-1 | GC | 38°38.039 | 17°17.512 | 1610 | - | - | - | - |

* based on minimum burial depth and sedimentation rate of 0.19 mm/a

** based on maximum burial depth and sedimentation rate of 0.17 mm/a

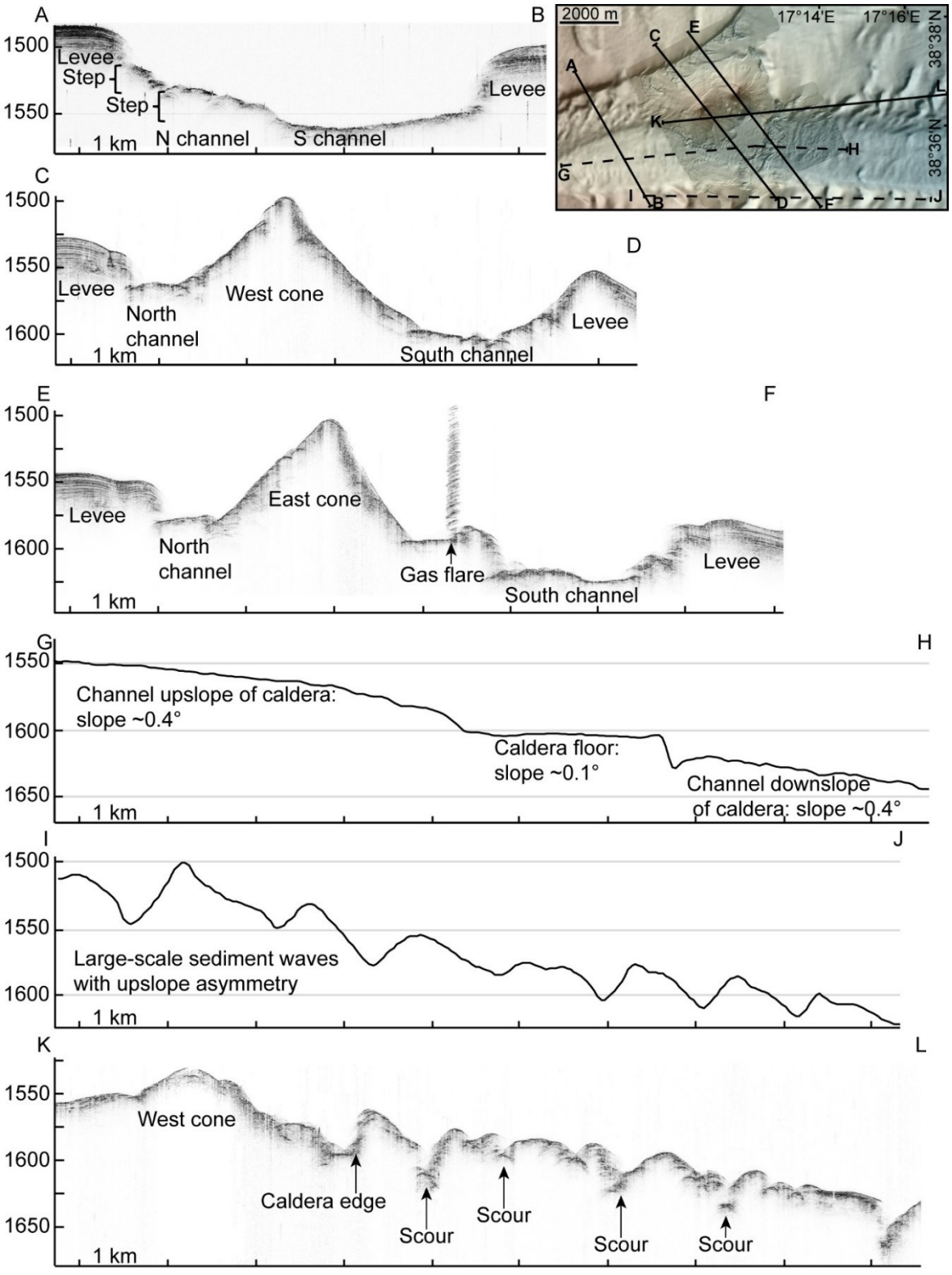


Figure 6.6. Subbottom profiles (PARASOUND) and bathymetric-topographic cross sections in the study (note index map with letters indicating the profiles); all profiles at the same scale with vertical exaggeration of ~15x.

### 6.5.2. Hydroacoustic results of Venere MV and surrounding Squillace Canyon

Venere MV consists of an eastern and a western cone, each ca. 100 m high, situated at the northern edge of a ca. 3000 m wide caldera defined by inward-dipping ring faults (Fig. 6.2). The main channel of Squillace Canyon bifurcates around Venere MV, forming a >70 m deep channel to the south and across the MV caldera and a <30 m deep channel to the north (Fig. 6.6, profile A–B). The channel levees are characterized by continuous and sub-parallel reflections in PARASOUND data (Fig. 6.6, profiles A–B, C–D, and E–F). The average slope of Squillace Canyon is ~0.4° in the southern channel and ~0.1° across the caldera of Venere MV (Fig. 6.6 profile G–H). The northern flanks of the MV cones are generally <10° steep compared to the southern flanks where slopes locally exceed 12° and 15°, respectively (Fig. 13.3 in supplements Chapter 13.2).

The MV surface shows elongate ridges (10–50 m wide; Fig. 6.7), subparallel ducts (up to 1 m deep), and tongue-shaped lobes (up to several hundred m wide and up to 15 m high; Fig. 6.8a) at horizontal distances of up to 1600 m from the summit (e.g. near the foot of the western cone; Fig. 6.2). These structures consist of exposed or buried mud breccia deposits forming mudflows. A comparison of AUV-derived bathymetry of the western summit from 2014 with that of 2016 documents the denudation of a ca. 10 m wide mound and the infilling of a ca. 2 m deep duct during this time interval (Fig. 6.7). Inward-dipping ring faults cut most mudflows along the eastern and northern slopes of the eastern cone. The lower area of the eastern cone is populated by three gryphons – i.e. parasitic cones of 4 to 8 m elevation and 60 to 150 m diameter (Figs. 6.2 and 6.8b).

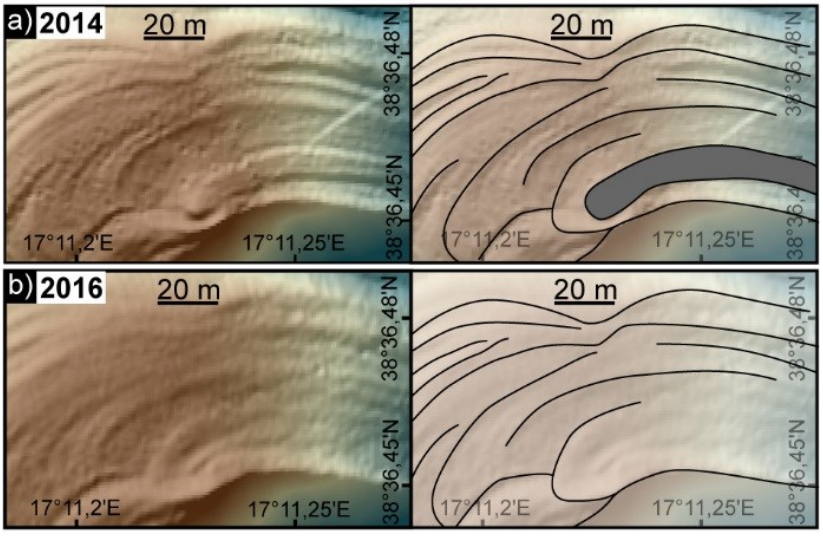


Figure 6.7. AUV-derived bathymetry map of the summit (~1500 m water depth) of the western cone of Venere MV (left) and line drawing of ridges and mudflows (right); see Fig. 6.2 for index of location; a: data from 2014, note a mudflow (ridge marked in grey) extending downslope from the central area; b: data from 2016, note the changed morphology of the mudflow compared to 2014.

Ship-derived backscatter data (Fig. 6.3a) show high intensities for the western cone (extent of ca. 5.0 km$^2$) and intermediate intensities for the eastern cone (extent of ca. 3.5 km$^2$), compared to sites of low intensity outside of Squillace Canyon. The total area of elevated

backscatter (ca. 8.5 km$^2$) matches in extent with the positive morphology of the MV edifice. Only mudflows at the western cone show elevated backscatter intensities in AUV-derived data (Fig. 6.3b) and cover ca. 2.0 km$^2$.

### 6.5.3. Bedforms in Squillace Canyon

Three types of bedforms have been identified in the vicinity of Venere MV: sediment waves, scours (crescent-shaped), and furrows (erosive lineations).

Sediment waves are positive bedforms with straight or crescentic crests mostly oriented perpendicular to the axis of Squillace Canyon. Large-scale sediment waves have heights of up to 30 m and wavelengths of over 1000 m. Their upslope-facing (stoss) slopes are generally steeper than their downslope facing (lee) slopes (i.e. they are upslope asymmetric; Fig. 6.6, profile I–J). Trains of large-scale sediment waves are found on the levees and shoulders of Squillace Canyon (Fig. 6.6, profile I–J; K–L). Medium-scale sediment waves show downslope-asymmetry with sinuous crests, 150–300 m wave lengths and 3–4 m wave heights (Fig. 6.8a, profile A–B; Fig. 6.9a, profile A–B). Trains of medium-scale waves extend from west to east across the caldera of Venere MV and their wavelength and wave heights decrease from 100 m to 40 m and from 3 m to less than 1 m, respectively (Fig. 6.8a, profile A–B). Small-scale sediment waves have wavelengths of 10–15 m, wave heights of 0.3–0.5 m and are often superimposed on top of medium-scale waves (Fig. 6.9a, profile A–B). Medium- and small-scale sediment waves are present inside the southern channel (Figs. 6.8a and 6.9a) and the caldera of Venere MV (Figs. 6.8a and b).

Scours are bedforms of negative morphology with crescent-shaped headwalls (Figs. 6.8c; 6.9a and b). They are up to 20 m deep relative to the surrounding seafloor, up to 800 m wide, 400 m long and exhibit a strong asymmetry with locally >30° steep lee slopes (Fig. 13.3 in supplements Chapter 13.2) and gently rising (1–5°) stoss slopes. The headwalls indicate upslope retrogressive erosion and expose truncated sediment beds. Erosion appears to have stripped away sediment along discrete layers forming small morphological steps or flat bottomed pits (Fig. 6.9b, profile C–D). Scours occur along the northern channel of Squillace Canyon (Fig. 6.2) with several crescent-shaped morphologies of more smoothed appearance, eroding into the northern flanks of Venere MV (Fig. 6.8c). A large-scale erosive scour also occurs along the south-eastern edge of the caldera rim of Venere MV (Fig. 6.9a) and stretches ~1300 m across the southern channel of Squillace Canyon. The negative morphology is ca. 400 m wide in downslope direction, forms a step in the channel profile of up to 35 m in height (Fig. 6.9a, profile A–B), which is locally >30° steep (Fig. 13.3). The lee slope and bottom of this scour are marked by smaller scours and a complex arrangement of furrows (Fig. 6.2).

Furrows are linear, erosional bedforms and are observed along the southern (Fig. 6.8a), southeastern (Fig. 6.8b) and northern flanks of Venere MV (Fig. 6.8c) as well as on the thalweg of the southern channel (Fig. 6.9a), and the southern shoulder of Squillace Canyon (Fig. 6.9c). The most pronounced furrows are found across the crest and lee slope of a large-scale sediment wave on the southern levee of Squillace Canyon (Fig. 6.9c). These furrows are continuous over several hundred meters, spaced 5 to 20 m, and have up to 1.5 m relief (Fig. 6.9c, profiles E-F and G-H). At the channel edge they terminate abruptly marking the collapse of the levee flank. In comparison, furrows found on the northern flank of Venere MV are lower (<1 m) and more discontinuous but spread out in downslope-divergent patterns (Fig. 6.8c). At the southern and southeastern flanks of the MV, furrows are more irregular but overprint buried mudflows (Figs. 6.8a and b). In backscatter data, areas marked by furrows along the MV flanks show areas of high backscatter intensities (Fig. 6.3b), which extend up along the cones to water depths matching the height of the southern levee of Squillace Canyon.

## 6.6. Discussion

### 6.6.1. Ground truthing of bathymetry and backscatter at Venere MV

Correlating backscatter intensities of mud breccia deposits with their burial depth has allowed to constrain extrusive activity of MVs over large regions, as studies on the CAP (Ceramicola et al., 2014b) or the Mediterranean Ridge (Rabaute and Chamot-Rooke, 2007) have demonstrated. For echosounders operating at 300 kHz, such as mounted on the AUV of this study, sediment penetration for the backscatter signal of ~20 cm can be estimated based on the signal-attenuation in marine sediments (Mitchell, 1993). All cores in this study (Figs. 13.1 and 13.2 in supplements Chapter 13.2) are of sufficient length to sedimentologically ground truth the AUV-derived backscatter and document the presence (or absence) of mud breccia deposits. Backscatter from the 12 kHz system, operated from the vessel, has a depth of detection of >2 m (Rabaute and Chamot-Rooke, 2007), and has revealed the extent of mudflows buried more deeply (e.g. 91 cm for GeoB21324-1). Local variations in backscatter intensities around MVs and cold seeps have previously been attributed not only to the thickness of sedimentary drape but also to rough or hard seafloor-surfaces such as crusts of authigenic carbonate, to clast content (grain size) as well as the presence of gas bubbles or gas hydrate in shallow sediments (Volgin and Woodside, 1996; Klaucke et al., 2006; Sahling et al., 2009; Römer et al., 2014; Paull et al., 2015b; Ceramicola et al., 2018). At Venere MV, cold-seep sites hosting authigenic carbonates have previously been documented from several sites along the periphery of the MV (Loher et al., in review (JMPG)) and are found to coincide with sub-circular patches of very high backscatter intensity in this study (Fig. 6.3b). The fresh mudflows at the western summit are characterized by high backscatter intensities and correspond to exposed mud breccia (lacking a hemipelagic sediment drape) with mousse-like sediment textures (Fig. 6.5), indicating the presence of gas bubbles (Loher et al., in review (JMPG)). Older mudflows lie stratigraphically deeper and are characterized by smoother morphological appearances with higher amounts of sedimentary drape and lower backscatter intensities relative to each other. Macroscopic core descriptions do not indicate

strong differences in mud-breccia clast content or grain size over the different mudflows. Instead, the mudflows show a general trend of decreasing backscatter intensity with increasing hemipelagic sediment cover (Fig. 6.5). It is concluded that predominantly the burial by hemipelagic sediment is influencing backscatter intensity when imaging mud breccia deposits.

### 6.6.2. Bedforms in Squillace Canyon and interactions with Venere MV

#### 6.6.2.1. Sediment waves and cyclic steps

The southern levee of Squillace Canyon is characterized by large-scale sediment waves showing parallel and continuous reflections (Fig. 6.6, profiles A–B, C–D, E–F) composed of gravity-flow deposits (GeoB19279-1). These sediment waves are attributed to repeated gravity-driven sediment transport events overspilling the channel levee, rather than to be the result of bottom currents. Similar sediment waves are known from other turbidite systems along submarine canyons (Normark et al., 2002), such as the Monterey Canyon (Normark et al., 1980), the Var turbidite system (Migeon et al., 2000), the Bounty Channel east of New Zealand (Carter et al., 1990), or the northern South China basin (Damuth, 1979). The overbank deposition of sediment onto the channel levees requires overspilling of a channelized flow (Peakall et al., 2000) whereby the upper, fine-grained sediment load of turbidity currents overspills the channel (Komar, 1973; Piper and Normark, 1983; Migeon et al., 2000). Contrastingly, medium- and small-scale waves (Figs. 6.8a and 6.9a) are present along the thalweg of the southern channel and the MV caldera, where they are composed of normally graded sand deposits (GeoB21309-1 and 21326-1). This implies transport and deposition of a coarse-grained sediment fraction inside the confinement of the channel (Migeon et al., 2000; Symons et al., 2016). Typically, such small-scale sediment waves result from density-stratified flows under confined settings, which deposit coarse sediments from dense basal layers (Symons et al., 2016). The medium- and small-scale sediment waves show downslope asymmetry (Fig. 6.8a, profile A–B and Fig. 6.9a, profile A–B), similar to so called cyclic steps (Taki and Parker, 2005; Symons et al., 2016). Cyclic steps may form during turbidity currents at a hydraulic jump (i.e. where a supercritical flow transitions to a subcritical state), with sediment deposition along the stoss side and erosion along the lee side of bedforms (Taki and Parker, 2005; Kostic et al., 2010). The change in slope from the gently dipping channel thalweg (0.4°) compared to the flat caldera floor (0.1°; Fig. 6.6, profile G–H) may have favored the development of hydraulic jumps. Decreasing wave-lengths and heights of these waves indicate a reduction in current speed and increased sediment deposition as flows traverse the caldera floor. At Venere MV, these processes are interpreted to have caused the partial infilling of the caldera and sediment ponding at the foot of the 11–42 m high eastern caldera edge (Fig. 6.6, profile K–L).

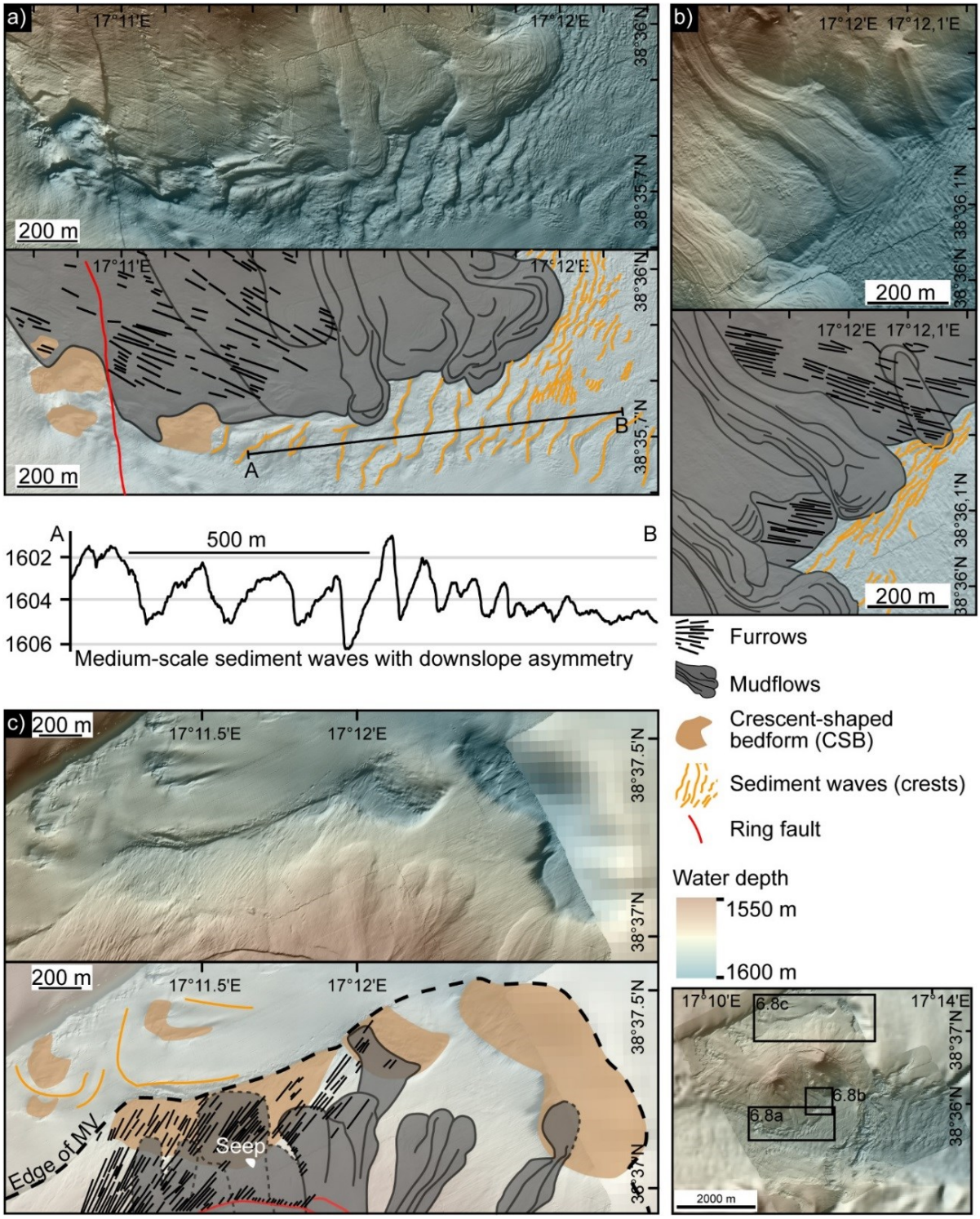


Figure 6.8. Detailed bathymetric maps and corresponding interpretations of seafloor structures to indicate the relative age relationships between bedforms, see index map in bottom right for locations; a: Mudflows with furrowed surfaces overlain by younger mudflows without furrows and bathymetric-topographic cross-section of sediment waves on the caldera floor; b: Mudflows with furrowed surfaces overlain by younger mudflows without furrows and sediment waves on the caldera floor; note gryphon-cone in upper right corner c: Scours, partially filled-in by mudflows, along the northern channel of Squillace Canyon and furrows cross-cutting mudflows along the northern slope of Venere MV.

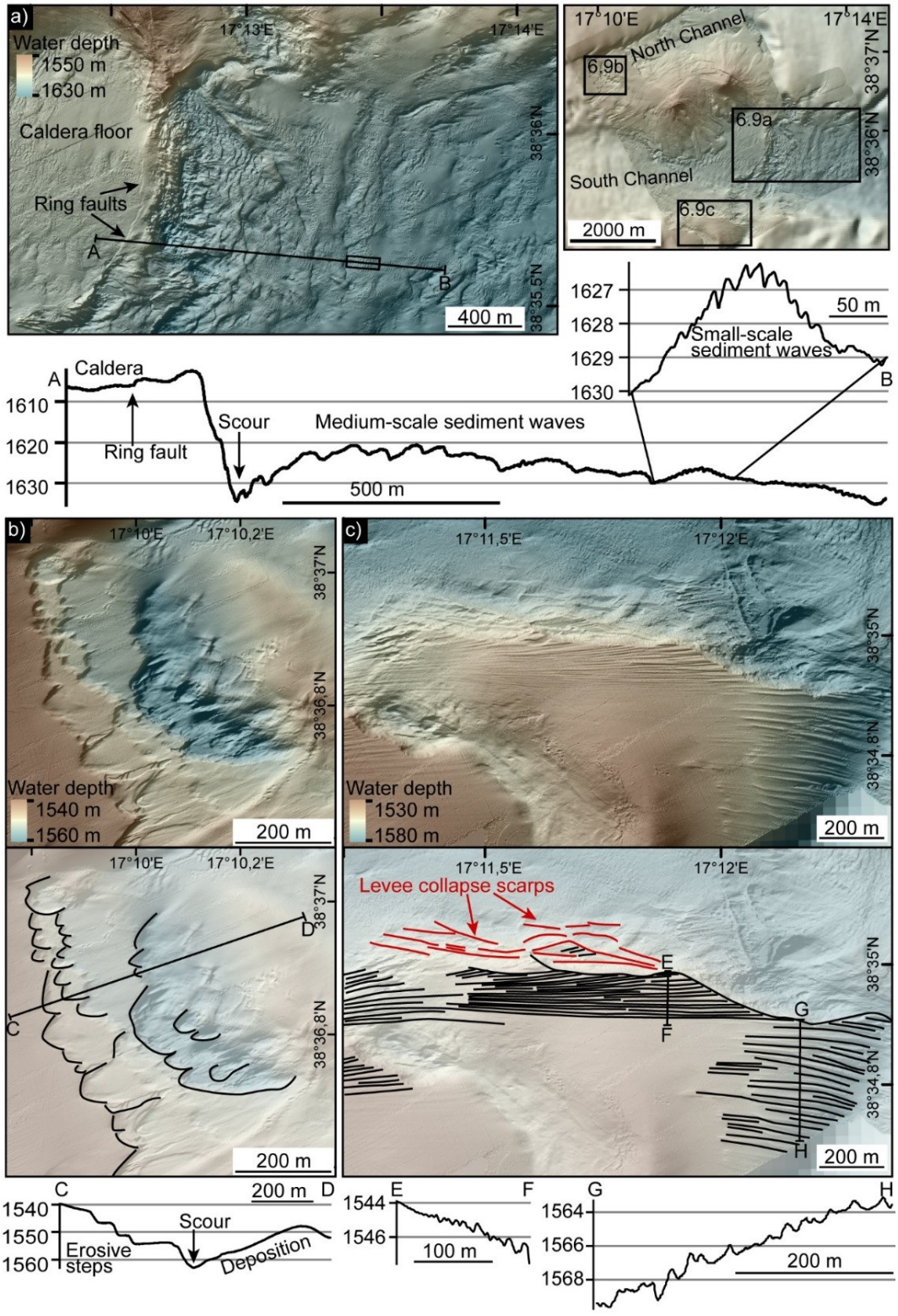


Figure 6.9. Detailed bathymetric maps, corresponding interpretations, and bathymetric-topographic cross-sections of seafloor structures in the study area, see index map on right side for locations; a: Scour at downslope edge of caldera giving way to medium-scale sediment waves, which are overprinted by small-scale sediment waves; b: Crescent-shaped scours (black lines mark headwalls) along northern channel of Squillace Canyon; c: Furrows (black lines) covering the southern levee of Squillace Canyon and scarps (red lines) from levee-flank collapse.

#### 6.6.2.2. Crescent-shaped scours

Bedforms of negative morphology with crescent-shaped headwalls (Figs. 6.8a, 6.9a and b), here referred to as scours, are characterized by erosive lee sides similar to cyclic steps (Cartigny et al., 2011; Paull et al., 2013; Symons et al., 2016). The formation of scours is disputed in the literature but it has been hypothesized that a continuum exists between depositional sediment waves, erosive or depositional cyclic steps, and cyclic scours as the most erosive endmember (Symons et al., 2016). Scours in the surrounding of Venere MV are interpreted to document the erosive capacity of gravity-driven processes transporting sediment through Squillace Canyon. Scours and sediment waves overprinting each other along the northern channel (Fig. 6.8c) indicate different generations of scour formation. Crescent-shaped bedforms have been found to remain at similar positions after successive sediment transport events (Paull et al., 2010) and can persist for thousands of years (Macdonald et al., 2011). Different generations of scours along the northern channel of Venere MV are interpreted to result from recurrent gravity-driven sediment transport events, which have spilled from the main channel into the northern channel. Overspilling flows are capable of forming trains of erosive and depositional cyclic steps outside of turbidite channels (Fildani et al., 2006; Lamb et al., 2008; Kostic, 2011). The overspilling of flows typically occurs at sharp bends or channel meanders, too strongly curved for the flows to traverse so that their upper parts abandon the channel (Peakall et al., 2000; Fildani et al., 2006; Lamb et al., 2008). In Squillace Canyon, however, the scours do not occur at a bend or major change in channel curvature. In contrast, it is inferred that the edifice of Venere MV at this location acts as an obstacle to the gravity-driven flow and facilitates bifurcation or partial deflection of turbidity currents to the northern channel.

The formation of seafloor scours can also result from the excavation of initial seabed defects by erosive flows or from hydraulic jumps, typically where there is a break in slope or where the flow can expand (Taki and Parker, 2005; Paull et al., 2010; Symons et al., 2016). The complex scour along the southern rim of the caldera of Venere MV (Fig. 6.9a) may have resulted from a combination of these mechanisms. Over time and continued extrusive activity at Venere MV, caldera subsidence was linked to movement along ring faults (Loher et al., in review (JMPG)). It is interpreted that the ring faults at the caldera edge presented an initiation zone for scour development. Gravity-driven sediment transport events may have partially filled the subsiding caldera and continued to erode the outer edge of the caldera, creating a morphological step (>30 m high, Fig. 6.9a, profile A–B) in the southern channel. Numerical simulations of turbidity currents cascading over a morphological escarpment have shown that the deposition of sand may not only occur at the toe of such a morphology but also along the upper edge (Ge et al., 2017). A hydraulic jump zone may develop at the toe, scouring sedimentary beds at the foot of the escarpment (Breda et al., 2007; Ge et al., 2017), a process similar to the formation of submarine plunge pools (Lee et al., 2002). This step in Squillace Canyon is inferred to promote a hydraulic jump in recurrent turbidity currents and the development of a complex scour extending along the caldera edge.

#### 6.6.2.3. Furrows

Furrows are interpreted to be the result of either bottom currents capable of reworking seafloor sediments (Posamentier and Kolla, 2003; Eddy Lee and George, 2004) or erosion during gravity-driven sediment transport processes (e.g. Migeon et al. (2001)). The most pronounced furrows are observed on the large-scale sediment waves at the southern levee of Squillace Canyon (Fig. 6.9c) and they are similar to other furrows on sediment waves in turbidity-current overbank deposits (Migeon et al., 2001; Trincardi et al., 2007). Their orientation parallel to the channel shows that they resulted from gravity-driven flows or currents traversing the overbank top along Squillace Canyon. Their expression is pronounced on the lee slopes of the waves, indicating that they resulted from flows or currents, which accelerated as the height of the sediment wave increased, inducing erosion or non-deposition on the crest and lee side of the wave where flow velocities typically are highest (Migeon et al., 2001).

Along the flanks of Venere MV (Fig. 6.8) furrows are shorter and more irregular than on the levee. It is inferred that erosive furrowing of the seafloor by gravity-driven flows confined to the channel caused these bedforms. It has been proposed that seafloor furrows can be created by coarse grained sediments or cohesive sediment blocks flushed along the canyon as bedload of flows (Flood, 1983, 1994; Canals et al., 2006; Lastras et al., 2009). The overall orientation of furrows around Venere MV indicates flow directions to the northeast and east along the northern slopes (Fig. 6.8c) and to the southeast and east along the southern slopes (Figs. 6.8a and b) of the cones. Divergent furrow patterns have been argued to indicate flow spreading in unconfined or overspilling gravity-driven flows (Migeon et al., 2001; Posamentier and Kolla, 2003). In this study, the most pronounced pattern of divergent furrows is observed along MV flanks in the northern channel (Fig. 6.8c). It is inferred that flows spilling from the main channel into the northern channel spread partially over Venere MV and that the MV edifice has acted as an obstacle for gravity-driven flows within Squillace Canyon and diverted them along its flanks. Furthermore, elevated backscatter intensities characterize these furrowed MV slopes, where the morphologies of mudflows are poorly preserved. MV flanks facing into the channel represent “cut slopes” during gravity-driven sediment transport processes. In contrast, mudflows along slopes facing downslope or away from the channels generally show better morphological preservation because they are less obliterated by erosive processes in Squillace Canyon. Erosion along the southern MV flanks could explain the asymmetric morphology and steeper southward slopes observed at the two cones (Fig. 6.6, profiles C–D, E–F; Fig. 13.3 in supplements Chapter 13.2).

### 6.6.3. Mud volcano dynamics

The volumes of the eastern and western MV cones could be estimated at ~0.083 $km^3$ and ~0.095 $km^3$, respectively, by calculating the volume between the seafloor bathymetry of 2016 and an inferred reference plane without the cones. The combined edifice volume (~0.178 $km^3$) is about half of the Touragay MV in Azerbaijan presumed to be one of the largest MVs on land (ca. 0.343 $km^3$; (Mazzini and Etiope, 2017)). The edifice volume only represents a

fraction of the total amount of material extruded during the lifetime of Venere MV, as total volumes (including buried deposits) are typically several orders of magnitude larger and have been found to be 0.1–3.3 $km^3$ for MVs in the Eastern Mediterranean (Kirkham et al., 2017), 3.4–14.6 $km^3$ for the Napoli and Milano MVs on the Mediterranean Ridge (Kopf, 1999) and >22 $km^3$ for one of the largest MVs in the Caspian Sea (Davies and Stewart, 2005).

The caldera of Venere MV is ca. 3000 m in diameter (Fig. 6.2) and its walls measure heights from 11–42 m in the east (Fig. 6.6, profile K–L) and <1 m in the south and west (Fig. 6.9a, profile A–B). Assuming an average and symmetric caldera subsidence on the order of 25 m and given the caldera diameter of ca. 3000 m, this conceptual caldera corresponds to a cylinder-shape with the same volume as the MV edifice. Due to compaction, loss of pore fluids upon extrusion, interbedded marine sediments, and caldera infilling, these estimates are subject to large uncertainties. Nevertheless, they suggest the same order of magnitude between subsurface sediment mobilization, edifice build-up, and caldera subsidence. Some of the extruded material may have been removed by episodic erosive processes occurring in Squillace Canyon. This is supported by the asymmetric shape of the MV-edifice (Fig. 6.6 profiles C–D, E–F) and the furrows along the southern and south-eastern flanks of Venere MV interpreted to result from gravity-driven sediment transport processes along Squillace Canyon, but additional sediment removal by bottom currents could have contributed to this effect.

Mudflow pathways clearly shifted direction several times throughout the last ~882 years at the western cone (Fig. 6.3d), covering all directions around the summit and ~40% of the total surface of the western cone. This is attributed to the fact that mudflows tend to follow the prevailing slopes (e.g. Graue (2000)), which may change through time. The cumulative volume of mudflows extruded during the last ~882 years was conservatively estimated at ~24 million $m^3$ (Table 6.2), by calculating the volume between the seafloor bathymetry of 2016 and an inferred reference plane underlying each flow. This volume corresponds to ~32% of the western cone (~0.095 $km^3$) or ~15% of the total edifice volume (~0.178 $km^3$) of Venere MV. The estimated amount of extruded material since ca. 206 years ago (comprising the flows of 0-29, 11-29, and 11-88 years in age, Fig. 6.3d) contributed ~10 million $m^3$ (Table 6.2), corresponding to ca. 12% of the western cone and ca. 5% of the total edifice of Venere MV in 2016.

Volume estimates of individual, catastrophic eruptions exist for studies of MVs on land with discharge on the order of several hundred thousand $m^3$ (Deville and Guerlais, 2009) to over one million $m^3$ of mud breccia (Dimitrov (2002) and sources therein). At Venere MV, the mudflows consist of multiple sheets of mud breccia stacked on top of each other. These composite mudflows suggest that material was extruded in pulses of moderate amounts, rather than in catastrophic, singular events. Venere MV may be similar to the “growing diapir-like” type of MVs where extrusive activity is thought to be continuous over time with moderate extrusion rates squeezing out tens of cm to several meters per year, due to persistently high overpressures in the subsurface (Mazzini and Etiope, 2017). Whereas the durations of the

extrusive events are not known for Venere MV, minimum rates of extrusion could still be estimated for mudflows at the western cone. This was achieved by assuming that mudflows were extruded consecutively (mudflow groups I-V in Table 6.2) and by considering the maximum age differences between groups of mudflows for which the emplacement ages had been determined (Table 6.2). The rates ranged from 5000 $m^3$/year to 47000 $m^3$/year with an average of 27000 $m^3$/year over the last ~882 years. These values are 2–3 orders of magnitude lower than estimates from the onshore Lusi structure (Indonesia) were during ca. eight years of eruptive activity >90 million $m^3$ of mud breccia (i.e. >10 million $m^3$/year; (Tingay, 2015)) resulted in an average of ca. 30000 $m^3$/day (with maximum rates of 170000 $m^3$/day (Mazzini et al., 2007)). Rates similar to Venere MV have been derived for the submarine Håkon Mosby MV, where volumes of mass outflow have been estimated to vary from 10000 to 30000 $m^3$/year (Kaul et al., 2006), or for the Milano and Napoli MVs with 2000 to 8000 $m^3$/year and 6000 to 15000 $m^3$/year (Kopf, 1999; Wallmann et al., 2006).

Assuming that methane constitutes 98.5 vol-% of the total gas in extruded mud breccia and a minimum gas-sediment ratio of 3.68 for surface near sediments of a fresh mudflow (Loher et al., in review (JMPG)) the minimum (i.e. 5000 $m^3$/year) and maximum (47000 $m^3$/year) mud breccia extrusion rates can be translated to methane volumes of 18100 $m^3$/year and 170000 $m^3$/year, respectively. This corresponds to minimum amounts of extruded methane of 12–114 t/year. Compared to estimates of methane emissions of 10–1000 t/year from individual MVs onshore (Etiope and Milkov, 2004), or 90–100 t/year for the Håkon Mosby MV (Ginsburg et al., 1999) the values of this study are of a similar order of magnitude but at the lower end of the range.

Ring faults forming the caldera have been shown to act as migration pathways for fluids and hydrocarbons, sustaining chemosynthetic life and causing the precipitation of authigenic carbonate crusts up to 20 cm thick, at several sites along the periphery of Venere MV (Loher et al., in review (JMPG)). This implies that the ring faults had to be developed prior to the onset of precipitation of the carbonates. Growth rates of authigenic carbonate at Venere MV are not known but numerical models of seeps on Hydrate Ridge, Cascadia Margin, have estimated growth rates at up to 5 cm/kyr for such structures (Luff and Wallmann, 2003). Assuming a similar growth rate, the precipitation of a 20 cm thick carbonate crust took at least 4000 years supporting the hypothesis that ring-fault related seepage occurred at least 4000 years ago. These estimates are similar to the ages of mudflows at the western cone (Fig. 6.3d, Table 6.1). It is hypothesized that throughout the last 4000 years at least, mud breccia extrusion co-existed with hydrocarbon seepage at the ring faults.

The mud breccia extrusion rates and methane fluxes estimated for Venere MV support results of burial depths and derived ages of mud breccia emplacement, which point to moderate extrusive activity, possibly persistent throughout the last ~882 years, compared to discharge estimates for calm periods of mud volcanism as e.g. compiled by Dimitrov (2002). These findings are in agreement with the conceptual model of activity at Venere MV proposed by Loher et al. (in review (JMPG)) who propose that high subsurface pore fluid

pressures maintained a pressurized state of the MV system and sustained continuous extrusive activity and discharge of mud breccia, gas and pore waters coevally. It is acknowledged that the extrusive dynamics of MVs can be governed by short term (days to years) of cyclic build-up of excess pore pressure at depth (Deville and Guerlais, 2009) but the results of this study indicate that an overall pressurized state of activity may be sustained over at least several hundred years.

Table 6.2. Groups of mudflows (I-V) in overall stratigraphic order with contributing sediment cores (GeoB-identifiers) and their age estimates. The maximum relative age difference between the mudflow groups could be determined. Minimum volumes for these mudflow groups were estimated based on the AUV-derived bathymetry data. Dividing the volume estimate by the respective age differences allows minimum order of magnitude estimates for the extrusion rates during the respective mud breccia outflows.

| Mudflow group | GeoB-No. of relevant cores | Age min. (a) | Age max. (a) | Mudflow group age (a) | Maximum age difference (a) between mudflow groups | Estimated volume ($*10^6$ $m^3$) | Estimated min. extrusion rate ($m^3$/a) |
|---|---|---|---|---|---|---|---|
| I) | 21322-1 | 0 | 0 | 0-88 | | | |
| | 21305-1 | 0 | 12 | | | | |
| | 21337-1 | 0 | 29 | | | | |
| | 21339-1 | 11 | 29 | | | | |
| | 21338-1 | 11 | 88 | | | | |
| | | | | | I-II: 206 | 10 | 47000 |
| II) | 21341-1 | 79 | 176 | 79-206 | | | |
| | 21319-1 | 132 | 206 | | | | |
| | | | | | II-III: 215 | 1 | 5000 |
| III) | 21307-1 | 158 | 294 | 158-294 | | | |
| | | | | | III-IV: 430 | 4 | 9000 |
| IV) | 21315-1 | 211 | 471 | 211-588 | | | |
| | 21317-1 | 263 | 353 | | | | |
| | 21314-1 | 263 | 471 | | | | |
| | 21318-1 | 316 | 412 | | | | |
| | 21308-1 | 421 | 588 | | | | |
| | | | | | IV-V: 671 | 9 | 14000 |
| V) | 21320-1 | 684 | 882 | 684-882 | | | |
| | | | | Sum: | I-V: 882 | 24 | Ø = 27000 |

### 6.6.4. Three-stage evolutionary model of Venere

Based on the stratigraphic order of mudflows and the relationships between bedforms, a three-stage evolutionary model of the surface expression of Venere MV and surrounding Squillace Canyon is proposed (Fig. 6.10).

#### 6.6.4.1. I) Extrusive activity at the eastern cone

At the time of the oldest mudflows documented in this study (4500–4000 years ago; Fig. 6.3d) the edifice of Venere MV is inferred to have consisted of the eastern and a smaller western cone (Fig. 6.10 part I). This is based on an estimate of the total minimum time required for the growth of the western cone (~0.095 $km^3$ at an averaged extrusion rate of 27000 $m^3$/year), resulting in an age of ~3500 years, and based on the extent of elevated backscatter intensities on the ship-derived data. Seafloor morphologies, backscatter intensities, and burial amounts of mudflows at the eastern cone document that mud breccia extrusion occurred in a phase of activity between ca. 4000 years ago until ca. 2200 years ago (Fig. 6.3d). This phase is similar in age to mudflows cored at two cones and the caldera of the Madonna dello Iono MVs (Praeg et al., 2009), with an estimated age of emplacement within the last 4800 to 2500 years (Ceramicola et al., 2014b). For the Pythagoras MV, located on the fold-and-thrust belt near the Calabrian Escarpment (Fig. 6.1c), the latest mud extrusions are indicated during 1400 to 3800 years by buried mudflows (Ceramicola et al., 2014b). These results suggest that MV activity in the CAP was coeval and distributed across numerous extrusive features.

Several seafloor depressions resembling denudated scours pre-date these mudflows (Fig. 6.8c). They are inferred to have resulted from gravity-driven sediment transport processes in Squillace Canyon eroding into the MV flanks. Subsurface sediment mobilization and edifice build-up, promoting surface loading, is inferred to have resulted in caldera subsidence and the development of ring faults. The disruption of surface-near sediments by the ring-faults may have promoted sediment scouring at the caldera edge (Fig. 6.9a) by recurrent gravity-driven sediment transport processes. The presence of authigenic carbonates and their thickness can be related to the duration and intensity of the hydrocarbon seepage (Buerk et al., 2010) and indicate that gas discharge at the peripheral seeps was already active during this phase (Fig. 6.10 part I). With the onset of a quiescent phase at the eastern cone after ca. 2200 years ago, fluid or minor mud breccia extrusions seems to have occurred at gryphons along the southern flank of the eastern cone. At the western cone, no mudflows of comparable age were recognized and it remains unclear if mud extrusion co-occurred at the western cone and was later completely covered by successive mudflows, or if the western cone was inactive during this phase.

#### 6.6.4.2. II) Sediment transport around the MV cones

Seafloor furrows from gravity-driven sediment transport processes along Squillace Canyon not only overprint buried mudflows at the western cone and the gryphons (Figs. 6.8b and c), but also seafloor underlying the oldest mudflows (684-882 years and 421-588 years, Fig. 6.3) at the western cone (Fig. 6.8a). This constrains the timing of at least some of the erosive

events to a phase after the last mudflows from the eastern cone and prior to the investigated mudflows at the western cone (Fig. 6.10 part II). Whereas evidence of repeated turbidite events at the Calabrian-Ionian margin have been linked to seismic shaking by earthquakes throughout the last two millennia (Polonia et al., 2015), this study did not resolve whether earthquake activity triggered mud breccia extrusion or increased fluid flow at Venere MV.

The southern channel is more deeply incised, than the northern channel (Fig. 6.6, profile A–B), suggesting this to be the predominant transport pathway of sediments along the lower section of Squillace Canyon. The orientation of furrows, trains of cyclic steps and sediment waves indicate that gravity-driven sediment transport processes were deflected around the flanks of the MV cones and that sediments were deposited in the MV caldera or spilled over the channel levees. Scours and furrows were observed cutting into the flanks of the MV (Fig. 6.8), eroding the edifice morphology asymmetrically (steeper towards the southern channel, Fig. 6.6, profiles C–D and E–F).

Cold seeps in an erosive environment in canyons offshore Nicaragua, have been found to consolidate slope sediments on mound structures by carbonate cementation, lack sedimentary cover, and be increasingly resistant to erosion (Buerk et al., 2010). A similar mechanism is envisaged for the peripheral seeps at Venere MV in order for them to persevere during the sediment transport events.

#### 6.6.4.3. III) Extrusive activity at the western cone

Whereas erosion potentially facilitated the release of overpressured fluids and mud breccia from below seafloor, it remains unclear when the onset of the most recent phase of activity at Venere MV occurred. At least, it consists of mud breccia extrusion from the western cone ~882 years ago until 2016 (Fig. 6.10 part III). These mudflows cover ca 40% of the surface of the cone, mainly along the steeper flank towards the south. Ages of the flows (Table 6.1) indicate consecutive extrusion events that formed composite flows. The morphologies, distribution, and estimated extrusion rates (Table 6.2) suggest continuous mud breccia extrusion throughout this phase and the extrusion of fresh mud breccia or at least the downslope movement of mobile material along a still active mudflow by 2016 (Fig. 6.7). Continued caldera subsidence is inferred to have caused movement at ring faults, offsetting surface-near sediments and mudflows along the periphery of Venere MV. The cold seeps along peripheral ring faults and the exposed thickness of authigenic carbonates document that mud breccia extrusion was accompanied by gas discharge (Fig. 6.6) during this phase. Furthermore, the occurrence of sand layers in sediment cores from the MV caldera suggest gravity-driven sediment transport processes at ca. 421-647 years ago (Table 6.1), i.e. during this phase. Sharply truncated furrows and collapse scarps at the southern edge of Squillace Canyon (Fig. 6.9c) indicate unstable channel flanks due to erosion of the levee edge, and widening of the channel.

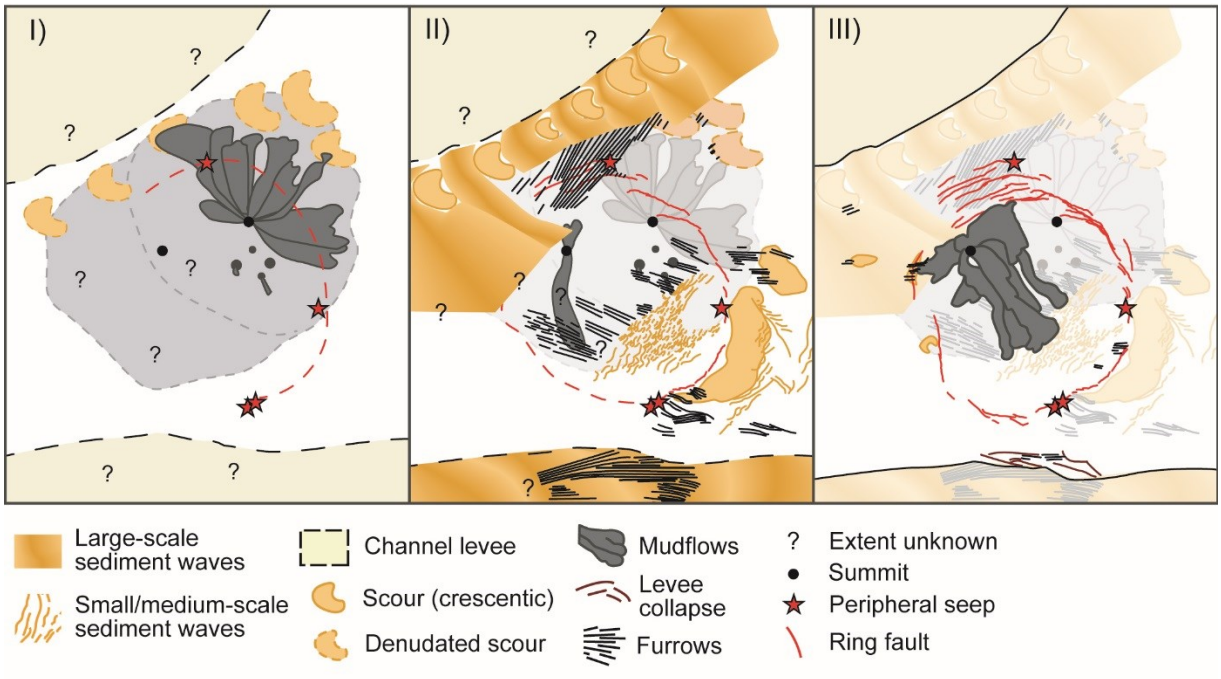


Figure 6.10. Three-stage evolutionary model of Venere MV and surrounding Squillace Canyon: I) Mud breccia extrusion at the eastern cone and peripheral seepage (ca. 4000-2200 years); II) Erosive processes at >882 years ago cause scours and seafloor furrows in old mudflows and the channel beds; III) Moderate but continuous mud breccia extrusion and peripheral gas release since ~882 at the western cone up to 2016.

## 6.7. Conclusion

Ship- and AUV-derived seafloor bathymetry and backscatter data, as well as sediment cores of Venere MV and Squillace Canyon, Central Mediterranean, have been analyzed. Interactions between mud volcanism (mud breccia extrusion, gas seepage, caldera subsidence and ring faulting) and erosive as well as depositional sedimentary processes (sediment wave-, scour- and furrow-formation) could be identified. The morphology of Venere MV shows signs of erosion by scour- and furrow-formation and sediment deposition on its flanks and in the caldera. Erosion and deposition were attributed to the repeated activity of gravity-driven sediment transport processes along Squillace Canyon. These observations support the interpretation that the twin-cone edifice of Venere MV obstructed and diverted gravity-driven flows, which were taking place within Squillace Canyon and facilitated the spilling of sediments across the channel levees. The presence of the MV edifice, caldera and ring faults are inferred to have influenced the flow-dynamics in the canyon by favoring the development of hydraulic jumps, e.g. at the edge of the MV caldera. Based on a tephra layer (1700–1900 years), sedimentation rates of 0.17–0.19 mm/year have been determined for the study area and constrain ages of hemipelagic sediments overlying mud breccia deposits. Cores of mudflows allowed investigating the extrusive activity of Venere MV and its evolution, summarized in a three-stage model spanning the last 4000 years. In the first stage, mudflows were extruded from the eastern cone and were accompanied by gas release at peripheral seeps throughout a phase of activity that lasted at

least since 4000 years ago until 2200 years ago. Activity ceased about 2200 years ago at the eastern cone and in the second stage, gravity driven sediment transport processes swept along Squillace Canyon. The third stage represents the last ~882 years of extrusive activity at the western cone, with gas release at peripheral seeps and mud movement persisting in between 2014 and 2016. It is estimated that MV growth on the order of 15% of today's total edifice volume occurred via mudflows during the last ~882 years at an average extrusion rate of 27000 $m^3$/year. Mud breccia extrusion at these rates coeval with caldera subsidence and gas release, are best explained by excess pore fluid pressures persisting in the subsurface plumbing system. Instead of violent, short lived eruptions, the activity at Venere MV consists of a state of pressurized activity sustaining moderate extrusions over timescales of hundreds of years. The fresh mudflows and ongoing gas release in 2016 suggest that Venere MV represents one of the most active MVs on the CAP even with respect to other MVs in the forearc basins.

## 6.8. Acknowledgements

We are grateful to masters and crews of cruises RV METEOR M112 and RV POSEIDON POS499. The team of the MARUM AUV SEAL 5000 is appreciated for their efforts during both cruises. The authors deeply appreciate the work by Miriam Römer for her help during the hydroacoustic acquisition and planning on board M112 and Christian dos Santos Ferreira for processing of multibeam data and the initial AUV map of Venere MV. Andreas Klügel (Fachbereich Geowissenschaften der Universität Bremen) is greatly thanked for the WDS analyses and his support in the tephra identification. Mark K. Brand is acknowledged for initial descriptions of mini-cores during his BSc thesis. For funding of cruises M112 and POS499 we thank the Deutsche Forschungsgemeinschaft (DFG) and the Research Center / Excellence Cluster "The Ocean in the Earth System". Data used are listed in the supplements (Chapter 13.2) and will be made available via Pangaea (https://www.pangaea.de).

# 7. Manuscript III: Seafloor sealing, doming, and collapse

## Seafloor sealing, doming, and collapse associated with gas seeps and authigenic carbonate structures at Venere mud volcano, Central Mediterranean

Markus Loher[1,*]; Yann Marcon[1,2]; Thomas Pape[1]; Miriam Römer[1]; Paul Wintersteller[1], Christian dos Santos Ferreira[1]; Marta Torres[3]; Daniel Praeg[4]; Heiko Sahling[1]; Gerhard Bohrmann[1]

**In preparation for submission to Geo-Marine Letters.**

*[1]MARUM – Center for Marine Environmental Sciences and Department of Geosciences at University of Bremen, Klagenfurter Str., 28359 Bremen, Germany*

*[2]Alfred Wegener Institute, Helmholtz Centre for Polar and Marine Research, Am Handelshafen 12, 27570 Bremerhaven, Germany*

*[3]OGS (Istituto Nazionale di Oceanografia e di Geofisica Sperimentale), Borgo Grotta Gigante 42/c, Sgonico, 34010 Trieste, Italy; present address: Institute of Petroleum and Natural Resources, PUCRS, Av. Ipiranga, 6681, 90619-900 Porto Alegre, RS, Brazil AND Géoazur (UMR7329 CNRS), 250 Rue Albert Einstein, 06560 Valbonne, France*

*[4]College of Earth, Ocean, and Atmospheric Sciences, Oregon State University, 104 CEOAS Administration Building, Corvallis, OR 97331-5503, USA*

**corresponding author e-mail: mloher@marum.de*

Keywords: mud volcano; cold seep carbonates; photomosaic; tubeworms; Calabrian Accretionary Wedge

## 7.1. Abstract

Sites of methane release at the seafloor are linked to the establishment of chemosynthesis-based ecosystems and the precipitation of authigenic carbonates. It has been proposed that cold seeps undergo self-sealing by carbonate growth, but little is known regarding their morphological evolution in relation to fluid migration pathways. In this study, multibeam micro-bathymetry and backscatter data are used together with photo mosaics, seafloor video observations, and samples to investigate structures resulting from gas seepage along faults peripheral to Venere mud volcano, in the central Mediterranean Sea. Sites of focused fluid flow are marked by gas bubble streams rising from the seafloor and the occurrence of chemosynthesis-based organisms (microbial mats, Vesicomyid clams, Vestimentiferan tube worms) over wider areas indicate anaerobic oxidation of methane. A range of carbonate structures is observed at these sites: 1) flat and extensive pavements, 2) mounds with disseminated nodules or cm-thick crusts, 3) fractured mounds with exposed, dm-thick crusts, and 4) seafloor depressions lined by dm-thick crusts. A conceptual model is proposed for the evolution of these peripheral seeps, in which plain seepage through hemipelagic sediments leads to the establishment of microbial mats on flat seafloor. It is followed over decadal timescales by the growth of pavements cemented by carbonates that seal the seafloor; over longer timescales (hundreds to thousands of years), subsurface pressure build-up leads to upward doming, fracturing and in some case to the collapse of carbonate mounds. Seepage through fractures allows re-sealing and provides habitats for colonization by chemosynthesis-based fauna. This scenario is suggested to be generally applicable to the development of ruptured mounds and collapse features described at other seepage sites, including in the eastern Mediterranean Sea.

## 7.2. Introduction

The migration, accumulation, and seepage of hydrocarbon-rich fluids in marine sediments at cold seeps have been linked to the development of a variety of seafloor morphologies, including flat pavements (Himmler et al., 2011; Römer et al., 2014), mounds (Bahr et al., 2007; Buerk et al., 2010; Römer et al., 2014; Koch et al., 2015), pockmarks (Judd and Hovland, 2007), and mud volcanoes (MVs; (Kopf, 2002)). Fluid flow at cold seeps involves the upward transport of methane in dissolved form or as gas bubbles where hydrocarbon concentrations exceed saturation (Boudreau et al., 2001; Römer et al., 2014). Dissolved methane is oxidized by microbes either aerobically near the sediment-water interface or anaerobically in the subsurface, typically using sulfate as the electron acceptor (Iversen and Jorgensen, 1985; Boetius et al., 2000). Anaerobic oxidation of methane (AOM) leads to an increase in dissolved sulfide, which in turn provides energy for chemosynthetic symbionts and allows the establishment of oasis-type ecosystems at cold seep sites (Paull et al., 1984; Sibuet and Olu, 1998; Boetius et al., 2000; Sahling et al., 2002; Niemann et al., 2006). AOM further increases the pore water alkalinity, promoting the precipitation of authigenic carbonates (Aloisi et al., 2000; Luff et al., 2004; Bayon et al., 2009; Himmler et al., 2011; Himmler et al., 2015). Methane-derived authigenic carbonate is characterized by $^{13}C$-depleated carbon isotope values and its presence in the sediment record documents

episodes of past fluid flow (Teichert et al., 2003; Formolo et al., 2004; Naehr et al., 2007; Bayon et al., 2009; Himmler et al., 2015).

Gas bubble emissions from the seafloor give rise to hydroacoustic high-backscatter signals in the water column, referred to as flares, that are reliable indicators of active seepage sites (Nikolovska et al., 2008; Philip et al., 2016; Römer et al., 2016). Sites of seafloor fluid discharge may also be identified as distinctive positive or negative morphologies that result from sediment deformation or extrusion or a combination (Dillon et al., 2001; Buerk et al., 2010; Römer et al., 2012a; Ceramicola et al., 2014b; Römer et al., 2014), although not all cold seep expressions have distinct morphologies (Suess et al., 1999; Klaucke et al., 2006; Römer et al., 2012b). However, the most common expression of seepage, i.e. carbonate crusts, biological communities, the presence of free gas or gas hydrates at or near the seafloor, as well as mud breccia outflows, are typically characterized by anomalous backscatter signatures in swath sonar data (Volgin and Woodside, 1996; Klaucke et al., 2006; Gay et al., 2007). Accurate mapping of seepage-influenced seafloor morphologies requires state-of-the-art echosounder technologies, typically mounted on autonomous or remotely operated underwater vehicles (AUVs or ROVs; (Römer et al., 2012a; Mascle et al., 2014; Pierre et al., 2014; Römer et al., 2014; Paull et al., 2015a; Philip et al., 2016; Römer et al., 2016)). In deep-sea settings, visual documentation of the mapped extent of seepage structures and sites of fluid emission is available from only a few studies (e.g. Jerosch et al. (2007) or Marcon et al. (2014a)) and is restricted to narrow strips or spots, for example where video sleds have been towed across large targets (Greinert et al., 2002; Mazzini et al., 2008; Naudts et al., 2008; Sahling et al., 2008a; Sahling et al., 2008b; Naudts et al., 2010; Panieri et al., 2017).

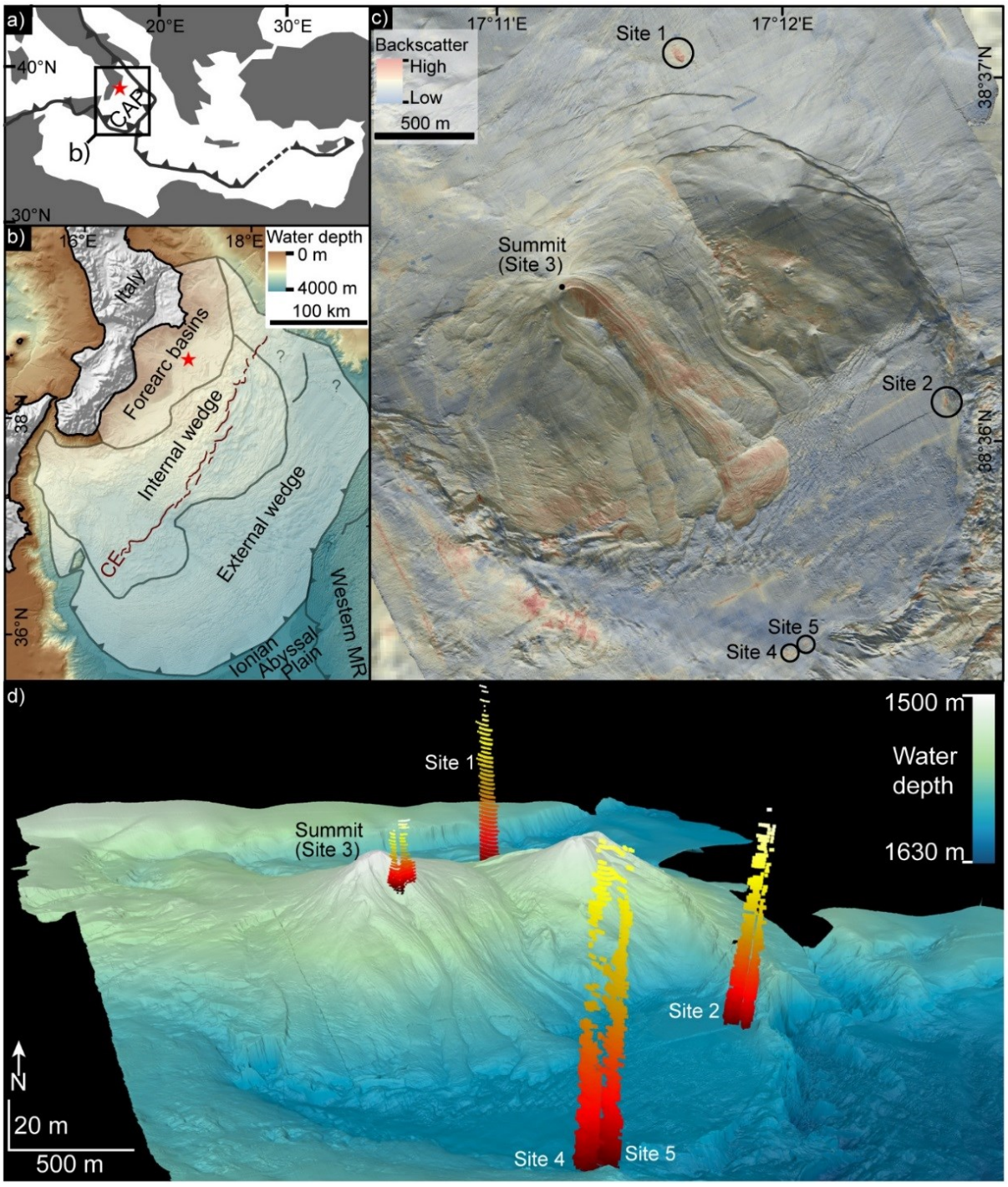


Figure 7.1. a: Location of the Calabrian Accretionary Prism (CAP) within the central to eastern Mediterranean subduction system (teethed lines indicate plate boundaries); b: Location of Venere MV (red star) on the inner CAP relative to its main morpho-structural zones (CE = Calabrian Escarpment; see text for references); bathymetry from EMODnet, www.emodnet.eu/bathymetry), topography of Italy (Ryan et al., 2009); c: AUV-derived backscatter draped on bathymetry of Venere MV and locations of peripheral seeps (Sites 1, 2, 4, 5) investigated in this study; Site 3 (black dot) marks the western summit of Venere MV (not investigated here); d: Perspective view of Venere MV (based on AUV-derived bathymetry) with hydroacoustic anomalies in the water column (flares in red-yellow colors) corresponding to Sites 1–5.

The precipitation of carbonate reduces the permeability of sediments (Luff and Wallmann, 2003; Bahr et al., 2007) and over time has the potential to seal fluid migration pathways (Hovland, 2002; Bayon et al., 2009). Sediment permeability can also be reduced by the formation of gas hydrates (Sassen et al., 2004; Römer et al., 2012a), which may form within the upper hundreds of meters below seafloor where the required pressure, temperature, and salinity conditions are met and where pore fluids are oversaturated in methane (Kvenvolden, 1988; Bohrmann et al., 1998; Egorov et al., 1999; Ginsburg et al., 1999; Pape et al., 2010; Pape et al., 2011b; Römer et al., 2012a). The rapid growth of gas hydrates in response to a supply of hydrocarbon-rich fluids may modify migration pathways and lead to hydrate dissolution due to localized methane undersaturation, a process argued to contribute to sediment deformation and pockmark formation (Sultan et al., 2014). Dissolution of gas hydrates in near-surface sediments provides a diffusive methane supply towards the water column, which is undersaturated in methane (Egorov et al., 1999; Sahling et al., 2002; Sassen et al., 2004). Hydroacoustic observations of gas flares at the edges of high backscatter patches has been inferred to indicate gas bubble release at the edges of carbonate pavements (Naudts et al., 2008; Naudts et al., 2010; Römer et al., 2014) or shallow gas hydrate accumulations (Römer et al., 2012a) which form a seal above the main fluid migration pathway. Persistent fluid flow and trapping of gas below carbonate-seal structures may cause pore fluid pressures to rise, leading to brittle deformation and fracturing (Bahr et al., 2010). Such a process could account for the common observation of cold-seep organisms along fractures in carbonate pavements (e.g. Römer et al. (2012a)). Several studies have proposed an evolutionary scheme for the self-sealing mechanism of cold seeps (Hovland, 2002; Bayon et al., 2009) or in which seal formation is followed by fracturing (Bahr et al., 2010) and subsequent pockmark formation (Hovland et al., 1987; Matsumoto, 1990; Marcon et al., 2014a). Testing of such an evolutionary scheme remains limited by the lack of a detailed understanding of the spatial distribution and variability of seafloor features in cold seep settings supported by systematic visual documentation and ground-truthing.

In this study, submarine cold seep environments are explored both visually and hydroacoustically at examples resulting from gas seepage at Venere MV, located in the Calabrian Accretionary Prism (CAP) in the central Mediterranean Sea (Fig. 7.1a). Seepage structures are examined at high spatial resolution, using photo-mosaics and seafloor observations made with remotely-operated vehicles (ROVs), complementary to multibeam bathymetric and backscatter datasets obtained using autonomous underwater vehicles (AUVs) in 2014 and 2016 (Loher et al., in review (JMPG)). These observations are ground-truthed by geological sampling and compositional and isotopic analyses of carbonate material. Our findings provide new insights into the development of cold-seep environments and allow us to propose a conceptual model for their evolution over decadal to millennial timescales, of general applicability to deep-sea settings.

## 7.3. Background

### 7.3.1. Geological setting

The CAP lies above the Eurasian-African subduction zone (Fig. 7.1a) and its Neogene development is the result of the SE rollback of a NW-dipping Tethyan lithospheric slab that has undergone fragmentation and narrowing to its present width of 300 km (Malinverno and Ryan, 1986; Dewey et al., 1989; Gueguen et al., 1998). Subduction has slowed to plate convergence rates of 2-5 mm/year following a tectonic reorganization c. 0.8-0.5 Ma (Devoti et al., 2008; D'Agostino et al., 2011), which also marked the onset of km-scale uplift of Calabria (Westaway, 1993; Monaco and Tortorici, 2000; Antonioli et al., 2006; Zecchin et al., 2011). The CAP consists of an accreted thrust-stack of pre-Mesozoic metamorphic basement and Mesozoic-Cenozoic strata (Gueguen et al., 1998; Van Dijk et al., 2000; Iannace et al., 2007), overlain by forearc basins that contain strata dating back to the Miocene (Roda, 1964; Rossi and Sartori, 1981; Zecchin et al., 2015). Landward of the Ionian abyssal plain, the CAP can be subdivided into three main morpho-structural domains (Fig. 7.1b): 1) an outer post-Messinian wedge (hosting Messinian evaporites), 2) an inner pre-Messinian wedge (hosting mainly clastic sediments), and 3) forearc basins both offshore Calabria, and uplifted onshore (Rossi and Sartori, 1981; Minelli and Faccenna, 2010; Polonia et al., 2011; Ceramicola et al., 2014b; Gutscher et al., 2017). Regional unconformities within the onshore basins have been traced offshore on seismic profiles and are interpreted to record prism-wide tectonic reorganizations linked to episodic subduction zone retreat in the mid-Pliocene and in the Pleistocene (Zecchin et al., 2012; Zecchin et al., 2015).

At least 53 MVs have been identified across the internal CAP and within its forearc basins the majority located within the inner wedge and the forearc basins (Ceramicola et al., 2014b; Loher et al., in review (JMPG)). Numerous MVs occur in association with post-Messinian out-of-sequence thrust faults mapped across the CAP or within the forearc basins (Praeg et al., 2009; Minelli and Faccenna, 2010; Ceramicola et al., 2014b; Gutscher et al., 2017). Mud volcanism in the CAP is suggested to have been triggered by a mid-Pliocene tectonic reorganization (ca. 3.5 Ma ago; (Praeg et al., 2009)), while high acoustic backscatter signatures from most MVs on the CAP implies them to have extruded mud breccia within the last 56 ka (Ceramicola et al., 2014b). Evidence of active gas seepage in the CAP is so far limited to MVs located in the forearc basins (Foucher et al., 2009; Praeg et al., 2009; Ceramicola et al., 2014b; Loher et al., in review (JMPG)).

### 7.3.2. Venere MV

At Venere MV (discovered by Ceramicola et al. (2014b)) mud breccia extrusion and gas release has been documented (Loher et al., in review (JMPG)) and confirmed by repeated, AUV-based bathymetric mapping (Loher et al., in review (G3)). Venere MV consists of a twin-cone edifice rising ~100 m from the seafloor in ~1600 m water depth (Fig. 7.1c+d). Loher et al. (in review (JMPG)) describe the extrusion of warm mudflows from the summit of the western cone, consisting of exposed mud breccia with gas-rich, mousse-like sediment textures. Pore water in the mud breccia contain chloride concentrations strongly depleted

relative to ambient bottom water values and consistent with clay-mineral dehydration reactions at kilometer-scale depths as a fluid source. Venere MV is characterized by inward dipping ring faults defining a sub-circular subsidence caldera up to 3 km in diameter (Fig. 7.1c+d). Four peripheral seeps have been identified along these ring faults based on the release of gas bubbles into the water column, the presence of authigenic carbonates, and chemosynthesis-based ecosystems (Loher et al., in review (JMPG)). Gas analyses documented thermogenic gas for both the gas extruded via mudflows at the summit and the peripheral seeps. The ring faults branch upward and away from the central conduit in shallow depths and are inferred to provide migration pathways for gas rising from depth (Loher et al., in review (JMPG)). The extrusion of mudflows from the western summit has occurred throughout the last phase of activity at Venere MV (i.e. at least the last ~880 years) at average extrusion rates estimated at 27000 $m^3$/year (Loher et al., in review (G3)). Extrusion of mudflows, together with gas release at peripheral seeps, points to persistently high subsurface pore fluid pressures and subsidence-induced ring faulting governing the ongoing activity at Venere MV. This MV is located within the gas hydrate stability zone but the extruded mud breccia at its western summit is too warm to support gas hydrate formation, with temperatures in the upper 5 m measured to be up to 13 °C warmer than the surrounding seafloor. In contrast, despite elevated geothermal gradients of up to 0.15–0.20 °C/m, the peripheral seeps lie within the stability zone and contains potential gas hydrate occurrence zones of 8–10 m below the seafloor (Loher et al., in review (JMPG)).

## 7.4. Data and methods

Combined swath-bathymetry and backscatter data, seafloor observations, carbonate samples, and photo mosaics of cold seepage sites at the periphery of Venere MV were obtained during RV METEOR cruise M112 and RV POSEIDON cruise POS499. Swath-bathymetry and backscatter data were obtained with a Kongsberg EM122 (12 kHz) ship-borne system and an EM2040 (300 kHz) system mounted on autonomous underwater vehicle (AUV) MARUM-SEAL 5000. Data processing was carried out with MB-System. AUV-derived bathymetry was tied to the ship-borne swath bathymetry by setting anchor points at prominent morphological features using the navigation adjustment tool (MBnavadjust; Caress and Chayes (1996)). Seafloor observations, sampling, and photographic acquisitions were conducted using the remotely operated vehicle (ROV) MARUM QUEST 4000m. Photo mosaics were obtained from altitudes 1–5 m above seafloor and compiled based on smoothed ultra-short baseline (USBL) navigation data of ROV Quest with the LAPM tool (Marcon et al., 2013). Seafloor positioning by USBL has an estimated accuracy better than 10 m (Bohrmann et al., 2015). Offsets between seafloor structures visible in bathymetric data and photo mosaics have been rectified by manually applying horizontal shifts (10–50 m) to the final mosaics in Global Mapper® software.

A total of 6 carbonate samples from Sites 1, 4, and 5 (Fig. 7.1c) were analyzed (Table 7.1 for coordinates of sample). The carbonate samples were cleaned and dried before being cut into slabs. Sub-samples (ca. 1-2 $cm^3$) were ground to powder (<20 µm) in an agate mortar. X-ray diffraction (XRD) analyses on the powder were carried out on a Philips X'Pert Pro MD X-ray

diffractometer (PANalytical, Eindhoven, The Netherlands; Cu-$K_\alpha$ tube; k = 1.541; 45 kV, 40 mA) by the Institute of Crystallography, University of Bremen (Dr. C. Vogt). XRD-patterns were obtained from 3–85° 2θ using a step size of 0.016° 2θ and a time step of 100 s. Standard deviations for bulk mineral determinations typically range from +/-1% for carbonates, +/-2% for quartz, and +/-5–10% for clays (Vogt et al., 2002). The shift in the d-spacing of the (104) reflection was used to calculate the content of magnesium ($Mg^{2+}$) in carbonate minerals following standard equations by Goldsmith et al. (1961) and Lumsden (1979). For simplicity, low-magnesium-calcite (<5 mol-% $MgCO_3$) is referred to as calcite and high-Mg-calcite (>5 mol-% $MgCO_3$) is referred to as Mg-calcite.

Table 7.1. Site information (coordinates in WGS84) of carbonate samples, δ18O values averaged per sample in VPDB and VSMOW, calculated equilibrium temperatures (T) and the difference from present-day bottom water T, and calculated equilibrium δ18O values for aragonite precipitation and the difference from present-day bottom water δ18O.

| Site | GeoB-No. | Latitude (N) | Longitude (E) | Water depth (m) | $\delta^{18}O$ values averaged per sample (‰ VPDB) | $\delta^{18}O$ values averaged per sample (‰ VSMOW)* | Calculated equilibrium T (°C) for aragonite precipitation from a fluid with $\delta^{18}O$=1.5‰ VSMOW* | T-difference (°C) to present-day bottom water (T=13.8 °C) | Calculated equilibrium $\delta^{18}O$ (‰ VSMOW) of fluid precpitating aragonite at T=13.8 °C** | Difference in $\delta^{18}O$ (‰ VSMOW) of fluid to present-day bottom water ($\delta^{18}O$=1.5‰ VSMOW) |
|---|---|---|---|---|---|---|---|---|---|---|
| 1 | 19205-2 | 38°37.103 | 17°11.620 | 1556 | 1.9 | 32.8 | 15.8 | 2.0 | 1.1 | -0.4 |
| 1 | 19230-8 | 38°37.081 | 17°11.629 | 1564 | 2.5 | 33.4 | 13.0 | -0.8 | 1.7 | 0.2 |
| 1 | 19230-9 | 38°37.082 | 17°11.629 | 1564 | 2.5 | 33.4 | 13.0 | -0.8 | 1.7 | 0.2 |
| 4 | 19252-4 | 38°35.428 | 17°11.971 | 1606 | 1.4 | 32.3 | 17.6 | 3.8 | 0.6 | -0.9 |
| 4 | 19252-13 | 38°35.428 | 17°11.950 | 1606 | 2.2 | 33.1 | 14.1 | 0.3 | 1.4 | -0.1 |
| 5 | 19240-5 | 38°35.457 | 17°12.021 | 1607 | 1.8 | 32.8 | 15.9 | 2.1 | 1.0 | -0.5 |

*Friedman and O'Neil 1977
**Patterson et al. 1993

A handheld micro-drill was used to obtain powdered sub-samples for isotopic analyses. Analogous to the procedure reported by Himmler et al. (2015) the carbonate powder was completely reacted to carbon dioxide (by 100% phosphoric acid at 75° C) and injected into a "Finnigan MAT 251" mass spectrometer to analyze stable carbon and oxygen isotopes at MARUM – Center for Marine Environmental Sciences and Department of Geosciences at University of Bremen (Dr. H. Kuhnert). Reproducibility of the analyses was checked against repeated measurements of an internal standard (Solnhofen limestone, calibrated with the NBS19 standard) and results of $\delta^{13}C$ and $\delta^{18}O$ are reported in per mill (‰) relative to Vienna-Pee Dee Belemnite (V-PDB; standard deviations are 0.04‰ for both $\delta^{13}C$ and $\delta^{18}O$). Equilibrium $\delta^{18}O$ isotopic compositions of the fluids as well as temperatures from which the carbonates may have precipitated were calculated according to experimental fractionation equations (Patterson et al., 1993) following standard approaches for authigenic carbonates as detailed by Bohrmann et al. (1998) and Han et al. (2004).

## 7.5. Results

### 7.5.1. Hydroacoustic character of the peripheral seeps

Ship-borne and AUV-borne multibeam hydroacoustic data document sites of gas release to the water column at Sites 1–5 (Fig. 7.1d; (Loher et al., in review (JMPG))). Visual observations were undertaken at Sites 1, 2, 4, and 5, all located along the ring-fault system of Venere MV (Fig. 7.1d). These peripheral seeps coincide with areas of increased

backscatter intensity (Fig. 7.1c), and show variability with respect to their size, morphology, and the location of gas bubble release.

Site 1, on the northern flank of Venere MV, is ca. 80 m long and >50 m wide and is the only seep with a positive morphology, rising up to 1 m above surrounding areas of flat seafloor on AUV-borne bathymetry (Fig. 7.2a). The site consists of a central area of high backscatter surround by a diffuse halo of intermediate backscatter, from which gas bubble emissions to the water column were observed (Fig. 7.2a+b). Very high backscatter intensities are associated with several elongate mounds 0.5–1 m high and ca. 10 m long. Site 2 lies on the eastern rim of Venere MV (Fig. 7.1c+d), at the foot of a ca. 40 m high scarp of the ring-fault system (Fig. 7.3a). It coincides with an irregular, ovoid patch of elevated backscatter up to 130 m long and 50 m wide (Fig. 7.3b), of lower overall intensity than Site 1 and gas bubble release was documented from the central area of the patch from a site with moderate backscatter intensity. Sites 4 and 5 both lie on the southern edge of the caldera about 120 m apart (Fig. 7.1c+d). Site 4 consists of an irregular patch of high backscatter up to 50 m in north-south direction and 80 m wide, while Site 5 to the NE consists of a circular backscatter patch 30 m across (Fig. 7.4a). Gas bubble release occurred from several sites within the elevated backscatter area at Site 4 and from the very center for the circular patch at Site 5.

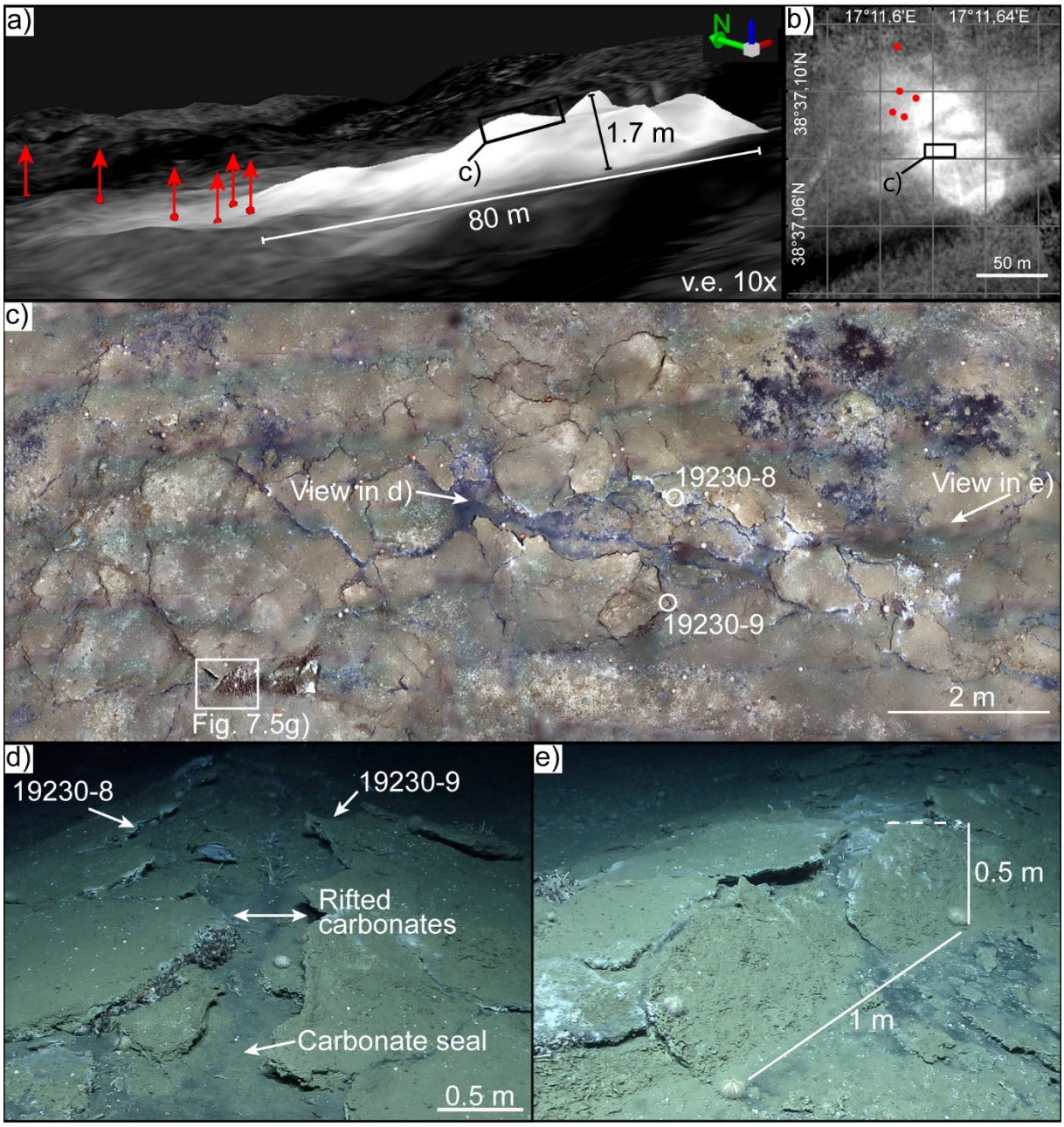


Figure 7.2. Site 1 (location in Fig. 7.1); a: Perspective view of AUV-borne multibeam bathymetry draped with backscatter (white is higher) and the location of hydroacoustically detected gas bubble emissions (red arrows); b: Map view of AUV-borne backscatter and gas bubble emission sites (red dots); c: Photomosaic (see a+b for extent) of ruptured mound, note carbonate slabs with black sediment between; carbonate sample numbers are indicated; d+e: seafloor photos showing updomed carbonate slabs (see c) for orientation).

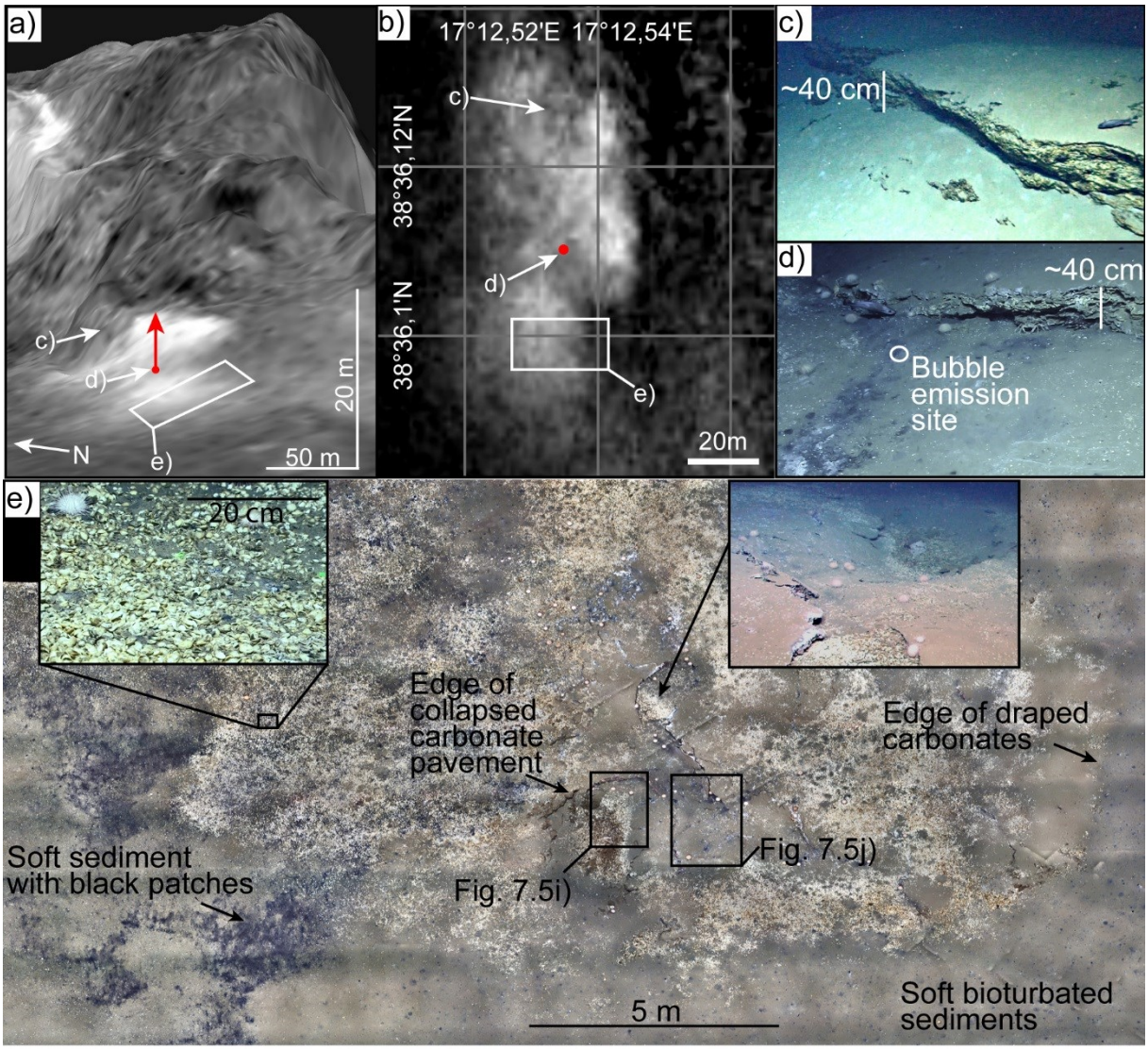


Figure 7.3. Site 2 (location in Fig. 7.1); a: Perspective view of AUV-borne bathymetry draped with backscatter (white is high) and hydroacoustically-detected gas bubble emission site (red arrow); b: Map view of backscatter (white is high) and gas bubble emission site (red dot); c: Photo of massive carbonate outcrop in northern part of site 2 (location in b); d: photo of gas bubble site among outcropping carbonates in central site 2 (location in b); e: Photomosaic (see a+b for extent) of extensive carbonate pavement (note correspondence of right edge of draped carbonate with onset of lower backscatter in b); inset at left shows close-up of seafloor littered with Vesicomyid clam shells, inset at right shows seafloor depression lined by carbonates.

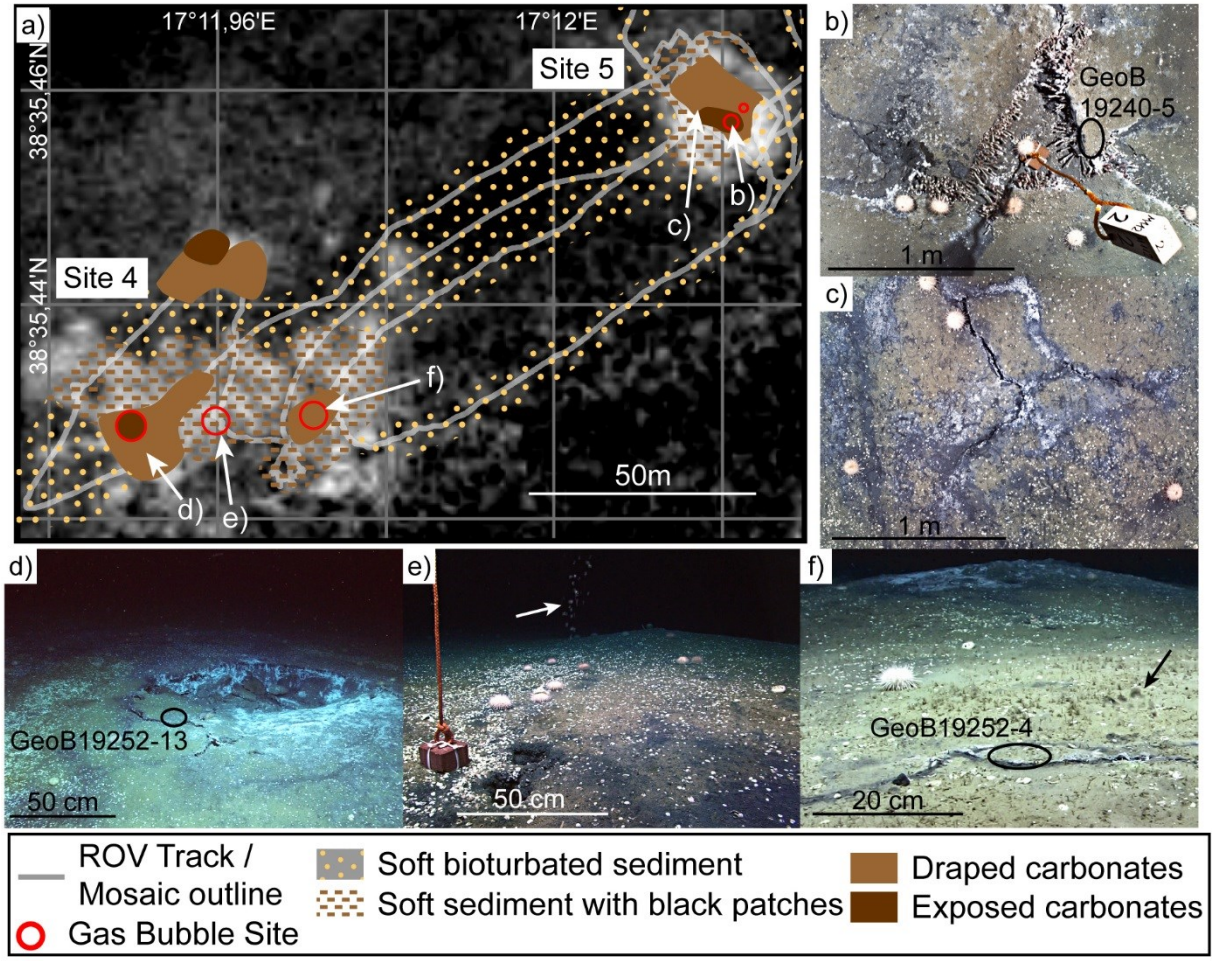


Figure 7.4. Sites 4 and 5 (location in Fig. 7.1); a: Map view of AUV-borne backscatter (white is high) superimposed with seafloor categories mapped along the ROV track and the location of a photomosaic at Site 5; gas bubble sites are visual observations; b: Detail of photo mosaic at Site 5 showing a ruptured mound releasing gas bubbles (see also supplementary video 13.4) and tubeworms underneath the carbonate slabs; c: Detail of photomosaic at Site 5 showing white microbial mats between carbonate pavements next to the ruptured mound; d: Collapse structure at Site 4; e: Gas bubbles (white arrow) rising from black sediment (note push-core holes next to red marker) and partially sealed mound in the background; f: Gas bubble release (black arrow) from a fracture in carbonate pavement (black circle marks GeoB-No. of carbonate sample) with partially sealed carbonate mound (note white microbial mats on top).

### 7.5.2. Visual observations of peripheral seeps

Visual observations of the seep sites during ROV investigations and from photomosaics allow the distinction of five categories of seafloor (Fig. 7.4+5): 1) soft bioturbated hemipelagic sediments (Fig. 7.5c); 2) soft hemipelagic sediments with patches (cm to m in diameter) of black sediment and white filamentous mats (<50 % coverage; Fig. 7.5d; 7.6a+b); 3) soft hemipelagic sediments populated by dense (>50 % coverage) filamentous white mats (Fig. 7.5e and 7.6d); 4) hard carbonates overlain by dusting of hemipelagic sediments and/or large numbers of shells and tubeworm (tube) remains (Fig. 7.3c+d, 7.4c, 7.5f+h-j, 7.6c); 5) hard carbonates exposed at seafloor including chemosynthesis-based organisms in fractures (Fig. 7.4b, 7.5g, 7.6e-g). Categories 4 and 5 both included cracks or ruptures in the carbonates, often infilled by black sediments, that made it possible to identify pavements even below a thin (few mm to cm) hemipelagic cover (Fig. 7.4c, 7.5j, 7.6c). Carbonate pavements exposed or thinly mantled by sediments (category 4 and 5) reached extents of several tens of square meters (Fig. 7.4a, 7.5a+b). An increased degree of bioturbation was consistently observed at transitions between hemipelagic sediments and areas with black patches or buried carbonates (Fig. 7.5f). Shell detritus (Fig. 7.3e), predominantly of Vesicomyid clams (genus Isorropodon of 1-2 cm size), was observed to litter the seafloor in areas of black patches and buried carbonates. Vesicomyid clams presumed to be alive were observed along crawl paths in black patches of soft sediment (Fig. 7.6a). In addition, sites of gas bubble release were documented at all of the peripheral seep structures (Fig. 7.4a, 7.5a+b).

At Site 1 gas bubbles were observed at three sites (Fig. 7.5a) to rise from mm- to cm-sized holes in the black sediment patches or, where these were covered by dense aggregations of filamentous mats, in their immediate vicinity (centimeters to decimeters away). Intense bubble streams were observed to evacuate sediment grains and form cm-scale mounds of black sediment around the emission holes. Gas trapped inside a bubble sampler spontaneously formed gas hydrate (Fig. 7.6h) and upward-floating flakes of white material, assumed to be gas hydrate, were repeatedly observed during or after push-core sampling (see supplement videos 13.1 and 13.2). Gas bubble streams or pulses were also observed to rise from holes in an area of bioturbated hemipelagic sediment ca. 10 m across that contained no other seepage features. All three gas ebullition sites were located at the north-eastern edge of the high-backscatter area (Fig. 7.2b, 7.5a), which was seen to correspond to carbonate crusts forming positive morphological structures. Photomosaics at Site 1 (Fig. 7.2c) reveal a ca. 5 m wide, 20 m long and up to 1 m high mounded ridge, composed of upward convex carbonate slabs (Fig. 7.2d+e). At the apex of the structure the carbonates appear ruptured and rifted apart, with black sediments within the ruptures and within fractures along the flanks of the structure. No gas bubble emissions were observed from these carbonates. White microbial mats were recognized along the edges of the ruptures, while in cracks between carbonate slabs bush-like colonies of tubeworms (Vestimentiferan tubeworms of the genus *Lamellibranchia*) were observed, inferred to root below the slabs (Fig. 7.2d+7.6g). Vesicomyid clams and their shell remains are observed in the soft substrate (black sediment) between the carbonates and around the ridge structure.

Site 2 is characterized by authigenic carbonate pavements, clam shells, patches of white filamentous mats, and several clusters of tubeworms surrounded by hemipelagic sediments containing black patches (Fig. 7.3e+7.5b). A gas bubble stream was observed to rise from a patch of black sediments a few dm west of an outcrop of carbonates (Fig. 7.3d+7.5b+h). The top of the carbonates was draped by hemipelagic sediments and black patches (few cm in diameter), which disappeared a few meters further east. An area consisting predominantly of carbonate pavement extended to the south. In a central area, cm to dm-thick carbonate plates formed an irregular crater-like seafloor depression of >5 m extent and ca. 1 m depth (Fig. 7.3e). Along the ruptures between the plates, white microbial mats and live tubeworms were observed (Fig. 7.5h-j). The floor of the crater was covered by shells, empty tubeworm tubes, and anthropogenic litter (Fig 7.3e+7.5i). In this southern area, the photomosaic in Fig. 7.3e shows a close relationship between what is proposed to be the edge of carbonates buried below hemipelagic sediments and the edge of the high backscatter patch (Fig. 7.5b).

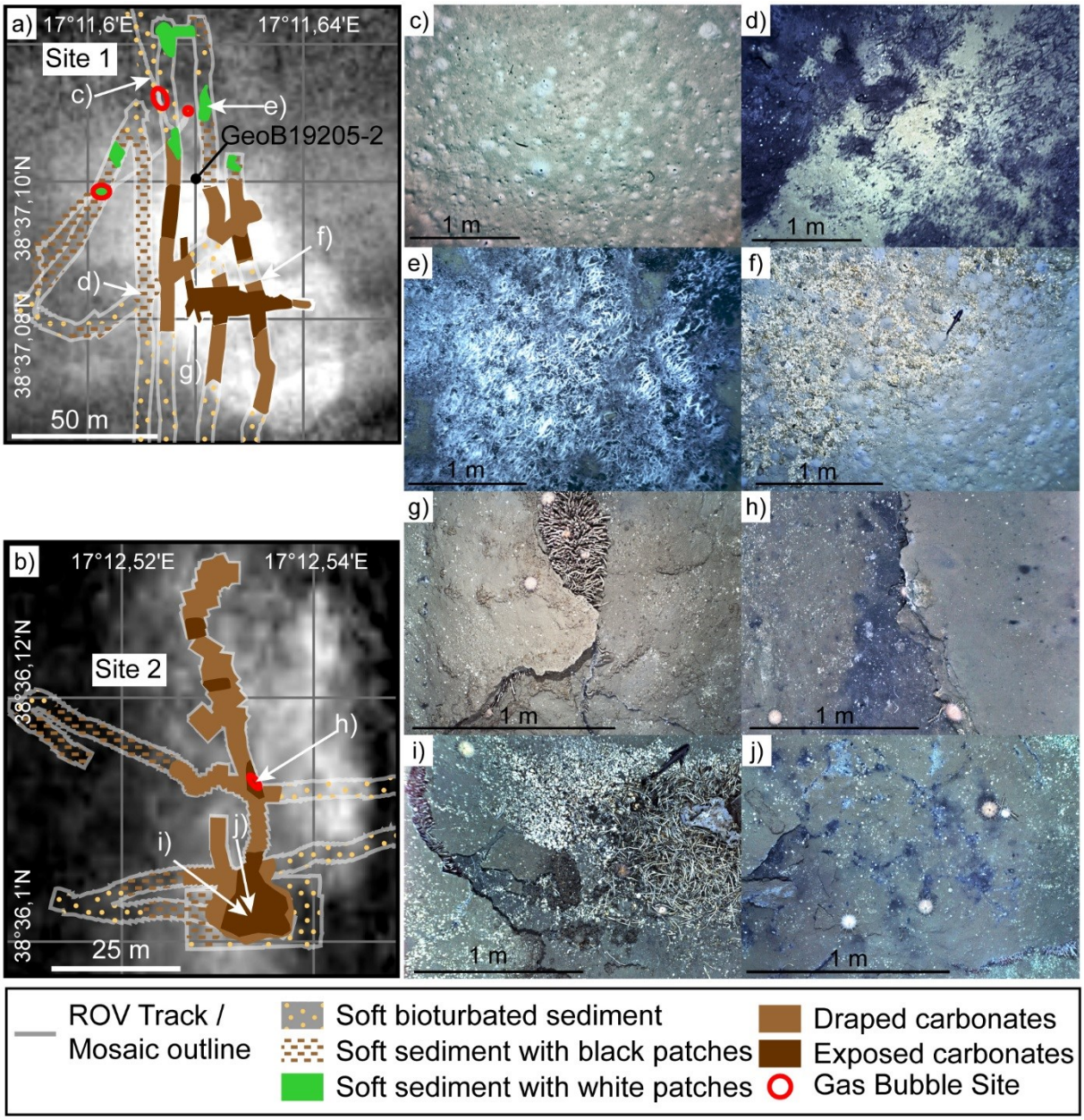


Figure 7.5. Sites 1 and 2 (location in Fig. 7.1); a+b: Map views of Sites 1+2 with AUV-borne backscatter (white is high) superimposed with seafloor categories mapped along the ROV tracks and the locations of photomosaics, at Site 1 a carbonate sample obtained by gravity corer is shown by its GeoB number; gas bubble sites are visual observations; c-j) Details from the photomosaics (white arrows in a+b) illustrating the different seafloor categories that have been mapped; see text for detailed explanations.

Site 4 includes two mounds 1.5–2.5 m in diameter and ca. 0.5 m high (Fig. 7.4e+f). The mounds were partly covered by dense accumulations of loose carbonate pieces (few cm diameter), hemipelagic sediments, and white filamentous mats associated with black sediments. Microbial mats are evidence of AOM and indicate that methane- or sulfide-rich fluid is transported through disseminated carbonate pieces or through pores in cm-thick carbonate crusts. One of the mounds was mechanically ruptured by inserting a temperature lance, causing the release of bursts of gas bubbles and schlieren (flow disturbances by inhomogeneous transparent media in fluid, e.g. Karpen et al. (2004)) from the penetrated area, indicating a pressurized fluid in the subsurface (see supplementary video 13.3). Cracks in the carbonate pavement at the edge of the mounds hosted clusters of small Vestimentiferan tubeworms and few microbial mats, as well as with weak gas bubble streams at two sites (Fig. 7.4a). In addition, a crater-like seafloor depression was found (Fig. 7.4d), similar in size to that at Site 2. It consisted of slabs of broken carbonate up to dm thick, which appeared to have collapsed from a formerly continuous seafloor pavement. Pulses of gas bubbles were observed to be recurrently released from a site among the carbonate pieces, while white filamentous mats covered the edges of the crater and carbonate slabs. No living tubeworms or empty tubes were observed within this crater. Around the area of Site 4, the onset of soft sediments with black patches (seafloor category 2) correlates with the edge of elevated backscatter (Fig. 7.4a).

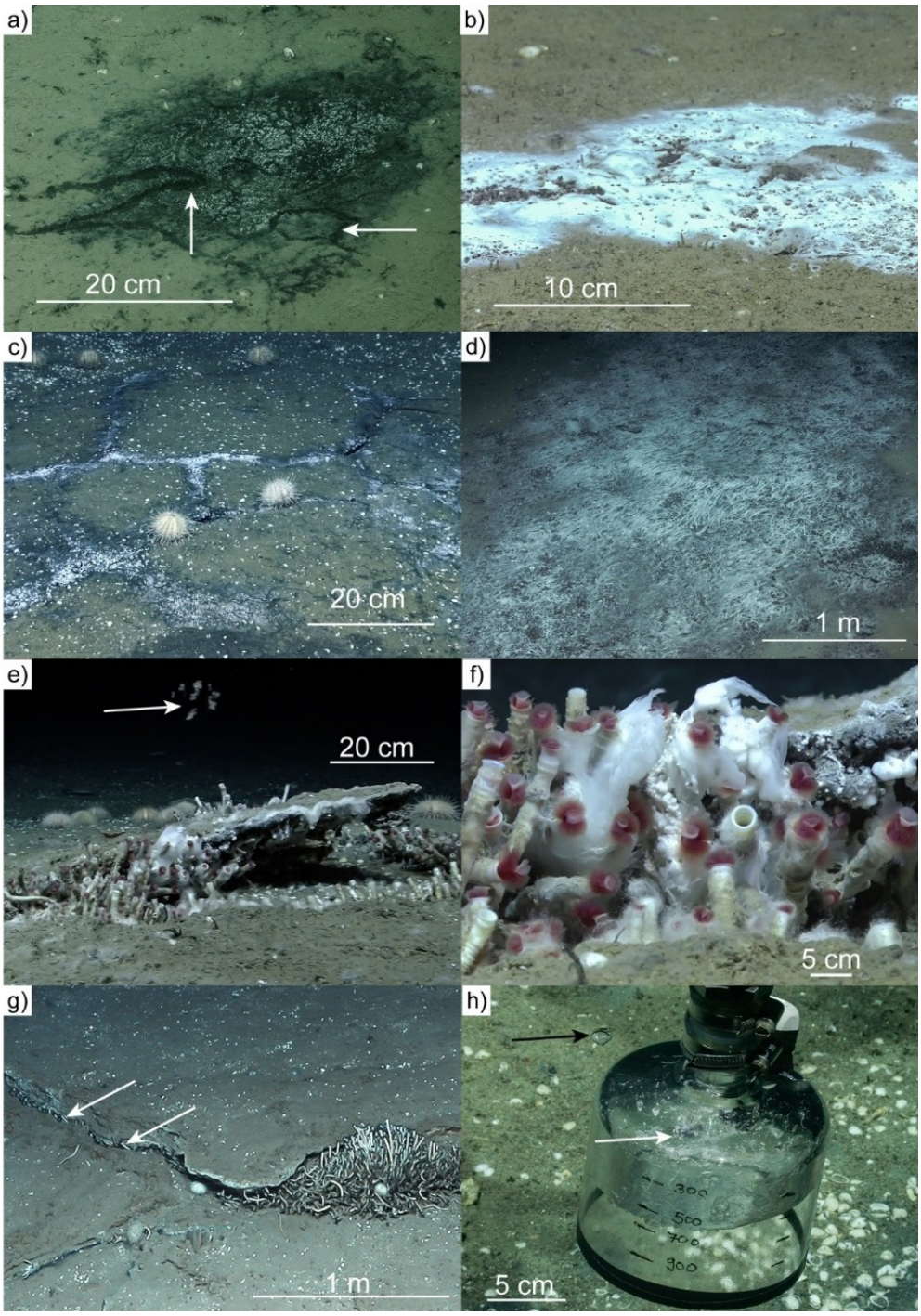


Figure 7.6. Seafloor photographs; a: Patch of black sediment with few white microbial mats, note crawl paths (white arrows) of presumably live Vesicomyid clams, location at N rim of high backscatter at Site 1; b: Small patch of intense, white microbial mat on soft sediment (location near Site 5); c: Carbonates draped by a bit of hemipelagic sediment with black sediment populated by white microbial mats along fractures (location near Site 5); d: Large patch of filamentous, white microbial mats on soft sediment (location of Fig. 7.5e); e: Gas bubble release at Site 5 (location as Fig. 7.4b and supplementary video 13.4) with white microbial mats and tubeworm colonies rooting below carbonate outcrop; f: Close-up of Vestimentiferan tubeworms in e); g: Large tube worm colony (location as Fig. 7.5g) along fractures (white arrows) rooting below thick carbonate slabs; h: Gas (note bubble at black arrow) which is trapped inside in a gas bubble sampler forms gas hydrate (white arrow; location at Site 1).

At Site 5 gas bubble pulses were observed from a circular mound ca. 2 m wide and 0.5 m high with ruptured carbonate slabs at the apex (Fig. 7.6e). The pulsating release of gas bubbles was seen to relate to the presence of a carbonate slab, which formed a ledge that temporarily retained gas bubbles beneath it (see supplementary video 13.4). White filamentous mats covered the ledge and a bush-like colony of tubeworms appeared to root underneath it. The carbonate pavement at the foot of the mound was densely covered by shell remains, forming a ring around the mound. A few meters towards the east, the seafloor gave way to carbonates buried by smooth hemipelagic sediments. To the southwest of the gas bubble site, the exposed or slightly buried carbonate pavements (categories 4 and 5) give way to soft sediments with black patches (seafloor category 2) and finally to soft bioturbated sediments (seafloor category 1) inherently with a change from high to low backscatter Fig. 7.4a).

### 7.5.3. Mineralogy and petrography of carbonate samples

#### 7.5.3.1. Samples from Site 1

Sample GeoB19205-2 was collected at the edge of a high backscatter area (Fig. 7.5a), while samples GeoB19230-8 and GeoB19230-9 were collected from up-turned carbonate slabs at a mound-like feature (Fig. 7.2c+d). In all three samples, carbonate is the most abundant mineral fraction, predominantly in the form of aragonite (53–60 wt-%) with lesser amounts of non-carbonate minerals including quartz and mica (Table 7.2). Visually samples GeoB19205-2 and GeoB19230-9 consist of dark grey microcrystalline cement (estimated 50-70%), light grey lithified hemipelagic sediment (estimated 50-30%) and few cm-sized voids and cemented mud clasts (Fig. 7.7). Shells of *Idas Modiolaeformis* are present on the surface of the carbonate samples (Fig. 7.7a). Sample GeoB19230-8 consists predominantly (up to 75%) of brownish semi-lithified hemipelagic sediment and areas of dark grey microcrystalline cement (estimated <25%; Fig. 7.7). There are several large pores 1-2 cm wide, cemented tubeworm-tube remains as well as light grey cemented mud clasts. There is a high content of shells (the bivalve *Idas Modiolaeformis* and the Vesicomyid clam genus *Isorropodon* could be identified) imbricated as a horizontal layer at the upper side of the sample. Stable oxygen isotope ($\delta^{18}O$) values of the carbonates are positive and range between 1.5 and 3.1‰, and stable carbon isotope ($\delta^{13}C$) values range from -27.1 to -16.8‰ (Table 7.3).

Table 7.2: Bulk-rock mineralogy from XRD analyses of carbonate samples.

| Site | Sample | Aragonite | Calcite | | Mg-calcite | | Quarz | Illite | Others |
|---|---|---|---|---|---|---|---|---|---|
| | | wt-% | wt-% | mol-% Mg | wt-% | mol-% Mg | wt-% | wt-% | wt-% |
| 1 | 19205-2 | 53 | 4 | 0 | 1 | 15 | 20 | 0 | 22 |
| 1 | 19230-8 | 60 | 4 | 0 | 1 | 13 | 14 | 0 | 21 |
| 1 | 19230-9 | 53 | 6 | 0 | 1 | 13 | 27 | 0 | 13 |
| 4 | 19252-4 | 50 | 2 | 3 | 1 | 17 | 15 | 0 | 32 |
| 4 | 19252-13 | 17 | 6 | 2 | 2 | 17 | 20 | 27 | 28 |
| 5 | 19240-5 | 34 | 2 | 1 | 1 | 15 | 32 | 0 | 31 |

### 7.5.3.2. Samples from Sites 4 and 5

Sample 19252-4 from Site 4 was collected from a fracture in a carbonate pavement in the vicinity of a sealed mound (Fig. 7.4f). The most abundant mineral fraction is carbonate (53%, predominantly aragonite at 50%), followed by lesser amounts of non-carbonate minerals including quartz, mica, sanidine, and anhydrite (Table 7.2). Sample GeoB19252-13 from Site 4 was collected at a crater-shaped depression (Fig. 7.4d). The predominant mineral phase is illite (27%) with relatively high amounts of silicates (20% quartz) and a low carbonate content (17% aragonite). Sample GeoB19240-5 from Site 5 was collected at a ruptured mound (Fig. 7.4b) and consists mainly of carbonate (37%, predominantly aragonite at 34%) but also contains a large fraction of silicates. Visually, samples GeoB19252-4, GeoB19252-13, and GeoB19240-5 are porous and consist mainly of brownish semi-lithified hemipelagic sediments (estimated 60-75%), dark grey microcrystalline cement (25-40%; Fig. 7.7). Cemented tubes of the Vestimentiferan *Lamellibranchia* as well as shells of the bivalve *Idas Modiolaeformis* and the Vesicomyid clam genus *Isorropodon* (Fig. 7.7b) could be identified. Samples GeoB19252-4 and GeoB19252-13 show layers of imbricated shells and biogenic remains 1-2 cm below the sample surface. The $\delta^{18}O$ values of these samples range from -0.7 to 2.9‰, and $\delta^{13}C$ from -24.7 to -11.4‰ (Table 7.3).

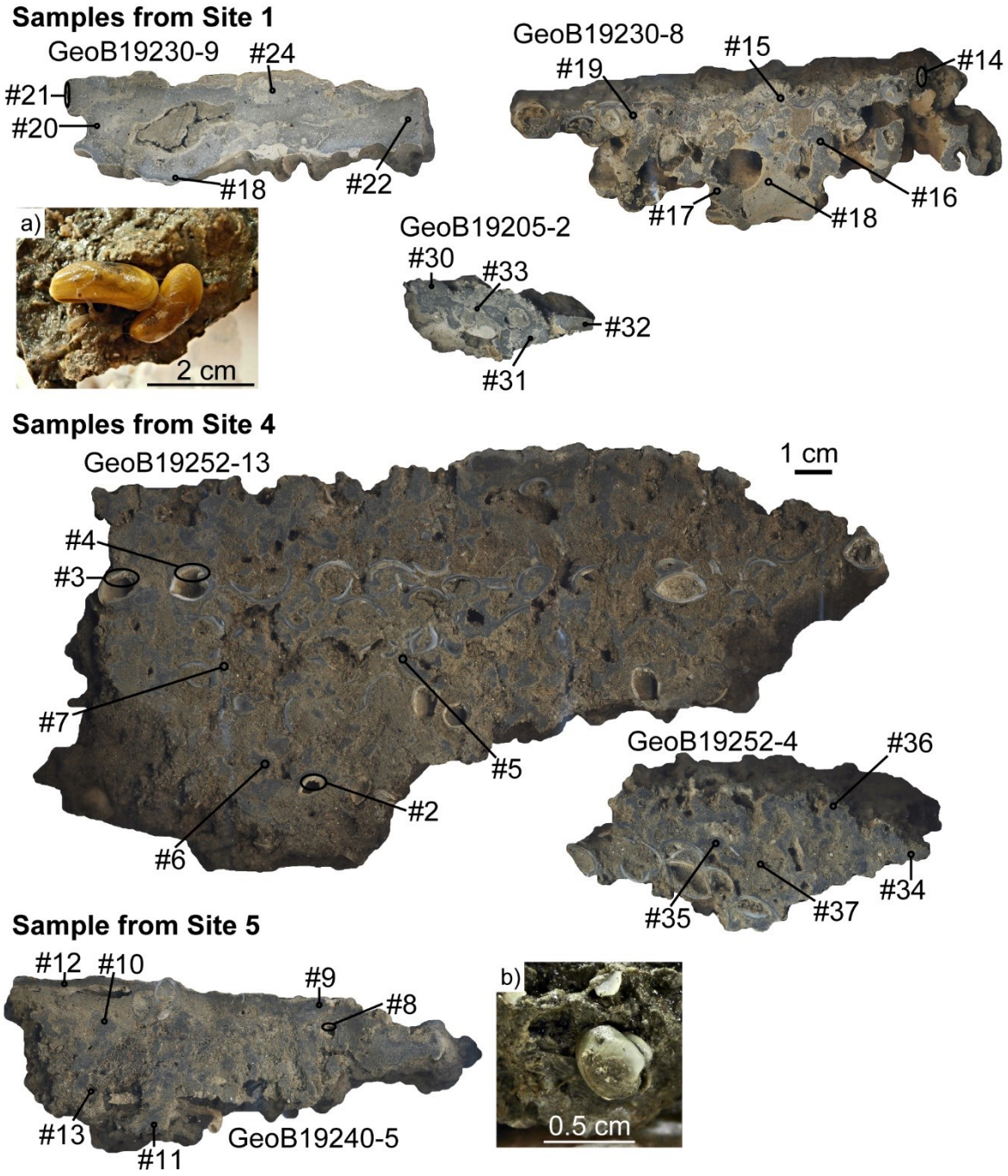


Figure 7.7. Authigenic carbonates from Sites 1, 2, 4 and 5 (note GeoB sample number) with locations and numbers of sub-sample (#) obtained using a micro-drill; inset a: Photograph of Idas Modiolaeformis identified on outside of sample GeoB19230-9; inset b: Photograph of Vesicomyid clam identified on the outside of sample GeoB19240-5.

Table 7.3. Sub-samples of authigenic carbonates obtained by micro-drill ordered by site location and sample number (see Fig. 7.7 for photographs), with corresponding δ13C and δ18O values and comments on macroscopic appearance.

| Sample-No. | GeoB No. | Site | $\delta^{13}C$ ‰ VPDB | $\delta^{18}O$ ‰ VPDB | Comment |
|---|---|---|---|---|---|
| 30 | 19205-2D | 1 | -25.28 | 2.21 | microcrystalline cement (dark grey) |
| 31 | 19205-2D | 1 | -21.16 | 1.47 | microcrystalline cement (dark grey) |
| 32 | 19205-2D | 1 | -25.08 | 2.03 | microcrystalline cement (dark grey) |
| 33 | 19205-2D | 1 | -16.83 | 1.70 | semi-lithified sediment or mud clast (light grey - brown) |
| 20 | 19230- 9B | 1 | -23.40 | 2.06 | microcrystalline cement (dark grey) |
| 21 | 19230- 9B | 1 | -27.08 | 3.13 | fibrous cement (white) |
| 22 | 19230- 9B | 1 | -24.90 | 2.36 | microcrystalline cement (dark grey) |
| 23 | 19230- 9B | 1 | -23.97 | 2.44 | microcrystalline cement (dark grey) |
| 24 | 19230- 9B | 1 | -25.81 | 2.35 | semi-lithified sediment or mud clast (light grey - brown) |
| 14 | 19230-8 | 1 | -20.71 | 2.84 | fibrous cement (white) |
| 15 | 19230-8 | 1 | -26.73 | 2.27 | microcrystalline cement (dark grey) |
| 16 | 19230-8 | 1 | -24.17 | 2.21 | microcrystalline cement (dark grey) |
| 17 | 19230-8 | 1 | -23.64 | 2.59 | microcrystalline cement (dark grey) |
| 18 | 19230-8 | 1 | -21.66 | 2.49 | fibrous cement (white) |
| 19 | 19230-8 | 1 | -21.99 | 2.44 | microcrystalline cement (dark grey) |
| 2 | 19252-13 B | 4 | -24.70 | 2.91 | fibrous cement (white) |
| 3 | 19252-13 B | 4 | -16.14 | 2.51 | fibrous cement (white) |
| 4 | 19252-13 B | 4 | -19.98 | 2.44 | fibrous cement (white) |
| 5 | 19252-13 B | 4 | -19.17 | 2.45 | microcrystalline cement (dark grey) |
| 6 | 19252-13 B | 4 | -21.37 | 2.20 | microcrystalline cement (dark grey) |
| 7 | 19252-13 B | 4 | -12.65 | 0.82 | semi-lithified sediment or mud clast (light grey - brown) |
| 34 | 19252-4 | 4 | -21.09 | 2.01 | microcrystalline cement (dark grey) |
| 35 | 19252-4 | 4 | -13.59 | 2.66 | microcrystalline cement (dark grey) |
| 36 | 19252-4 | 4 | -23.68 | 1.78 | microcrystalline cement (dark grey) |
| 37 | 19252-4 | 4 | -11.36 | -0.67 | semi-lithified sediment or mud clast (light grey - brown) |
| 8 | 19240-5 A | 5 | -24.09 | 2.53 | fibrous cement (white) |
| 9 | 19240-5 A | 5 | -22.12 | 1.90 | microcrystalline cement (dark grey) |
| 10 | 19240-5 A | 5 | -23.18 | 2.31 | microcrystalline cement (dark grey) |
| 11 | 19240-5 A | 5 | -20.17 | 1.73 | microcrystalline cement (dark grey) |
| 12 | 19240-5 A | 5 | -21.31 | 1.84 | microcrystalline cement (dark grey) |
| 13 | 19240-5 A | 5 | -17.14 | 0.69 | semi-lithified sediment or mud clast (light grey - brown) |

## 7.6. Discussion

### 7.6.1. Fluid sources contributing to authigenic carbonate compositions

Authigenic carbonates record the stable carbon isotopic signature of the total dissolved $CO_2$ (DIC) pool at the time of precipitation (Naehr et al., 2007). The DIC pool can comprise a mix of sources, including seawater (e.g. a typical value for eastern Mediterranean deep seawater of $\delta^{13}C$ ~1.2‰; (Pierre, 1999)), oxidized organic matter ($\delta^{13}C$ ~ –23‰), oxidized methane (or higher hydrocarbons) depleted in $^{13}C$ (ranging from $\delta^{13}C$ values of –110 to –30 ‰; (Aloisi et al., 2000; Formolo et al., 2004; Naehr et al., 2007), and fluids enriched in $^{13}C$ due to $CO_2$ reduction deep in the methanogenetic zone (Mozley and Burns, 1993; Kopf et al., 1995; Greinert et al., 2001; Stakes et al., 2002; Orphan et al., 2004). Accordingly, authigenic carbonates may show high variability in their stable isotope compositions (e.g. Greinert et al. (2001)). However, all samples collected from the peripheral seeps at Venere MV show

depleted values of $\delta^{13}C$ in a relatively narrow range –11.4‰ to –27.1‰ VPDB (Fig. 7.8). These values are consistent with methane as an important carbon source during precipitation of the predominantly aragonitic (Table 7.2) authigenic carbonates. This is inferred to take place shallow sediment depths during microbially mediated AOM, with lesser contributions from DIC dissolved in seawater and the oxidization of marine organic matter. These values are similar to $\delta^{13}C$ values of less than –5‰ reported in authigenic carbonates from sites of methane seepage on a number of continental margins (e.g. Naehr et al. (2007)), as well as from sites of mud volcanism within the eastern Mediterranean Sea including the Mediterranean Ridge and the Anaximander Mountains (Aloisi et al., 2000; Himmler et al., 2011) and the Nile Deep Sea Fan (Gontharet et al., 2007).

The oxygen isotope composition of authigenic carbonate is controlled by several factors, including the composition and temperature of the pore fluid from which precipitation occurs, as well as the mineralogy of the carbonate that forms. As a first approximation, the theoretical $\delta^{18}O$ values of aragonite and Mg-calcite (i.e. with 12 mol-% $MgCO_3$) should amount to, respectively, 3.3‰ and 2.9‰ VPDB (Friedman and O'Neil, 1977; Grossman and Ku, 1986; Aloisi et al., 2000; Gontharet et al., 2007), under the assumption that precipitation occurred from eastern Mediterranean bottom waters in present-day conditions (of temperature, pH, and $\delta^{18}O$). The averages of the oxygen isotope compositions for each sample in this study range of $\delta^{18}O$ from 1.4 to 2.5‰ VPDB (Table 7.1). These values are more depleted in $^{18}O$ (Fig. 7.8), indicating that the fluid source was either significantly warmer or more depleted in $^{18}O$ (or a combination of these effects). Exposed carbonates at sites of methane seepage may experience lower pH values during AOM activity (Himmler et al., 2011), which has been argued to result in heavier $\delta^{18}O$ values (Zeebe, 2001; Han et al., 2004). The depleted $^{18}O$ signals recorded here, suggest that changes in fluid pH values did not significantly affect the stable oxygen isotopes of the studied samples.

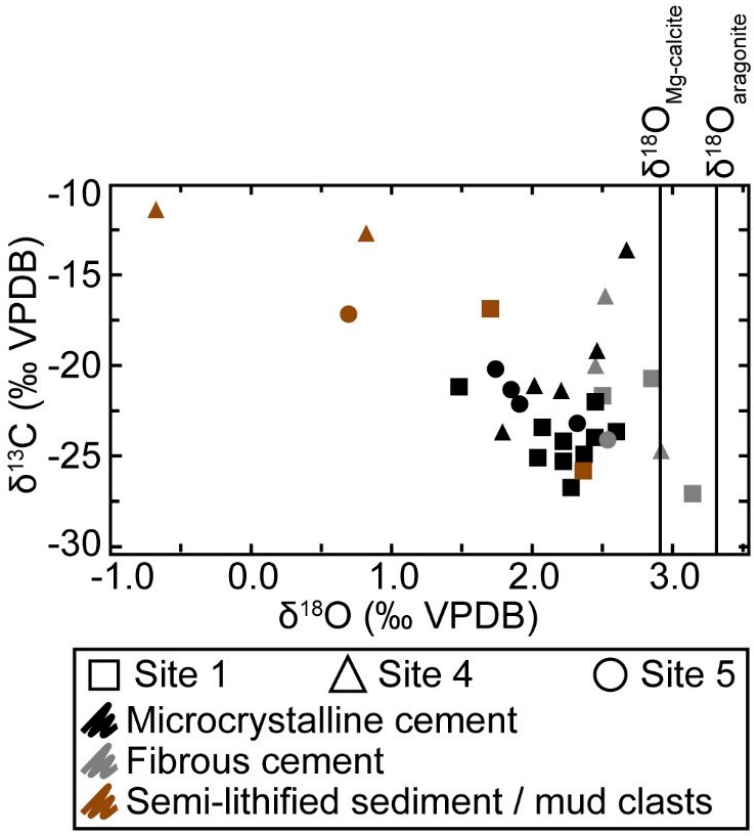


Figure 7.8. Carbon and oxygen isotopic compositions of carbonate samples from Sites 1, 4 and 5, color coded according to the macroscopic appearance of the carbonate phase; vertical lines represent the theoretical $\delta^{18}O$ value of calcium carbonates (aragonite and Mg-calcite with 12% $MgCO_3$ content) calculated on the assumption of precipitation in isotopic equilibrium with present-day Mediterranean bottom water (see text for references).

Aragonite is the predominant carbonate-forming component in all samples (Table 7.2). The temperatures of the precipitating fluid were estimated (Table 7.1; see methods section) by assuming authigenic aragonite crystallization in equilibrium with the present-day regional bottom water $\delta^{18}O$ value of 1.5‰ VSMOW (Pierre, 1999). Most of the samples (from Sites 1, 4 and 5) require fluid temperatures that are higher than the current bottom water by 0.3–3.8 °C, while two samples (both from Site 1) require fluid temperatures that are lower by 0.8 °C. Advection of warm subsurface fluids at the peripheral seeps of Venere MV is indicated by geothermal gradients that are elevated relative to regional values, and lie in the range of 0.15–0.2 °C/m (Loher et al., in review (JMPG)). Corresponding subsurface temperatures imply that, for most samples, aragonite precipitation might have occurred several meters below seafloor. However, this does not account for the two carbonate samples from site 1 that require lower temperatures. Bottom water temperatures in the eastern Mediterranean Sea were up to 5 °C colder during the last glacial maximum (LGM) and water masses characterized by 1.5‰ increased $\delta^{18}O$ values (Aloisi et al., 2000). Given that all carbonate samples were collected close to or exposed at the seafloor, it is unlikely that they record either burial to reach higher temperatures or precipitation during times of cooler bottom waters. Alternatively, carbonate precipitation could have occurred from a fluid

that had a temperature close to values measured today (i.e. 13.8 °C; (Loher et al., in review (JMPG))) but of a different $\delta^{18}O$ isotopic compositions.

The oxygen isotope ratios of the water from which aragonite in the different samples may have precipitated has been calculated, assuming a temperature of 13.8 °C (Table 7.1; see methods section). The results for most samples from sites 1, 4 and 5 suggest a composition depleted in $^{18}O$ by 0.1 to 0.9‰ VSMOW, compared to the present-day bottom water $\delta^{18}O$ value of 1.5‰ VSMOW, while two samples from Site 1 indicate a fluid source slightly enriched in $^{18}O$ by 0.2‰ VSMOW. The water cage of gas hydrate preferentially incorporates the heavier oxygen isotope, causing the residual fluid source to be depleted in $^{18}O$ (Ussler and Paull, 1995). In contrast, the release of cage water from gas-hydrate dissociation leads to enrichment in $\delta^{18}O$ of up to +3‰ (Davidson et al., 1983; Hesse et al., 1985; Bohrmann et al., 1998). The weak enrichment calculated for the fluids at Site 1 do not indicate a significant contribution from gas hydrate dissociation, whereas the more depleted signals may point to the formation of small amounts of gas hydrate.

### 7.6.2. A conceptual model of seep evolution

#### 7.6.2.1. Stage A - “plain seepage”

In this study, the initial stage of a cold-seep (Stage A of Fig. 7.9) is inferred to be characterized by the continuous or pulsating release of gas bubbles from bioturbated hemipelagic sediments with no additional seepage indications. This is comparable to the “plain seepage” described by Hovland (2002). The initial establishment of a physicochemical micro-environment that supports AOM, occurs by microbial colonization of bubble pathways in the subsurface (Hovland, 2002; Treude et al., 2005). Where methane oversaturation occurs with respect to the pore water, diffusion processes allow methane gas bubbles to grow and expand, leading in turn to the fracturing of sediments and the creation of pathways for the upward migration of bubbles (Martens and Berner, 1974; Boudreau, 2012). Strong advective gas flow may largely bypass the microbial AOM-filter so as to release methane to the overlying water (Luff et al., 2004; Sommer et al., 2006). Initial precipitation of AOM-induced carbonate and the onset of settlement by chemosynthesis-based organisms such as microbial mats may hamper fluid flow and causes methane to spread into and charge surrounding sediments (Hovland, 2002).

#### 7.6.2.2. Stage B - microbial mats and first colonization by seep-organisms

The next stage of an evolving seep (stage B in Fig. 7.9) is characterized by black patches of reduced (anoxic) sediment (e.g. Fig. 7.5d) that are partially or fully covered by filamentous microbial mats (Fig. 7.5e+7.6a, b, d) and contain pieces of authigenic carbonate. After anoxic conditions have been established in the subsurface (stage A), chemosynthesis-based organisms may start to emerge on the seafloor and microbial mats such as filamentous, sulfur-oxidizing bacteria (e.g. Beggiatoa) may spread (Sassen et al., 1993; Hovland, 2002)). Since all peripheral seeps at Venere MV lie within the gas hydrate stability zone (Loher et al., in review (JMPG)), it is inferred that any gas permanently trapped in pores or underneath carbonates will form gas hydrate at least in small amounts (see supplement videos

13.1+13.2). In addition, soft sediments constitute a habitat for mobile Vesicomyid clams (Fig. 7.6a). This type of chemosynthesis-based macrofauna typically roots in soft sediments to access AOM-derived sulfide with its foot (Sahling et al., 2002). Gas rising in soft cohesive sediments may stall by spreading horizontally in zones of decreased lateral fracture toughness (Boudreau, 2012) and can start to deform the seafloor by increasing pressure (Barry et al., 2012) due to fluid accumulation. This exerts an additional buoyancy force in the subsurface (Koch et al., 2015). In this study, however, seafloor doming was not observed at sites associated with plain seepage, nor where soft sediments occurred with microbial mats or black patches. Instead, seafloor mounds were observed where carbonate crusts partially or completely paved the seafloor (Fig. 7.4a+e+f).

#### 7.6.2.3. Stage C - self-sealing and mound formation

Stage C (Fig. 7.9) is associated with extensive carbonate pavements and (partially) sealed mounds (Fig. 7.4e+f). In-tact carbonate crusts form a seal at the sediment-water interface, preventing the release of hydrocarbon-bearing fluids and the downward diffusion of seawater sulfate, and thus inhibit AOM and further carbonate precipitation. The carbonates represent a physical and chemical barrier e.g. for Vesicomyid clams who live partially embedded in soft sediments. The large numbers of empty clam shells littering the surface of the carbonate pavements (e.g. Fig. 7.3e) may be explained by progressive carbonate cementation and exclusion of the clams from their habitat (Bohrmann et al., 2015).

The cementation of surface or shallow-subsurface sediments is known to result in the blockage and the diversion of fluid migration pathways at seeps (Hovland, 2002; Marcon et al., 2014a). Authigenic carbonate can precipitate as individual cemented nodules up to several cm in diameter (Aloisi et al., 2000; Gontharet et al., 2007), or form mm to dm thick crusts that extend as seafloor pavements over areas of $10^0$-$10^2$ $m^2$ (Gontharet et al., 2007; Himmler et al., 2011; Römer et al., 2014). Carbonates may form mounds of varying height from meters (Gontharet et al., 2007; Römer et al., 2014; Himmler et al., 2015) to several tens of meters (Buerk et al., 2010), or grow vertically upward into the water column as chemoherms (Teichert et al., 2005). As demonstrated by Luff et al. (2004), the presence of dispersed carbonate pieces may significantly lower sediment porosity and cause fluid retention and overpressure generation in the shallow subsurface.

The formation of gas hydrate can also result in a sealing effect for fluid migration (Römer et al., 2012a). Doming by gas hydrate formation has been argued to require high gas hydrate saturations (Hovland and Svensen, 2006; Koch et al., 2015; Sahling et al., 2016) and the rapid formation of gas hydrate near the seafloor is commonly associated with the presence of brines, as salts are excluded from the clathrate cage (Torres et al., 2004b; Torres et al., 2011). Temperature gradients at the peripheral seeps allow for a thin (<10 m) gas hydrate stability zone, but chloride profiles do not indicate gas-hydrate related pore water freshening (Loher et al., in review (JMPG)). The oxygen isotopic results of this study (Fig. 7.8) could be explained by hydrate formation, but visual observations suggest the presence of only disseminated flakes of gas hydrate (see supplement videos 13.1+13.2). Therefore, it is

inferred that while gas hydrates are forming locally within the seepage sites, they do not account for the development of the dome-shaped structures. However, the slow dissolution of gas hydrate may act as a buffer and continue to release methane-rich fluids even in case the underlying fluid supply ceases (Sahling et al., 2008a; Foucher et al., 2009). Such a mechanism can sustain AOM until the local gas hydrate reservoir is depleted or fluid flow resumes from depth.

The mounds observed in this study are interpreted to represent the surface locations of pathways for the upward migration of fluids. Permeability reduction in response to the formation of carbonates (and locally of gas hydrates) is inferred to generate overpressure and exert a buoyancy force by which the seafloor is deformed. The mounds most likely contain a mixture of hydrocarbon-rich pore water, free gas, and possibly small amounts of disseminated gas hydrate underneath the carbonate pavement. Gas spreads laterally underneath this seal and emanates as gas bubbles from cracks or along the edge of the carbonate pavement up to several meters from the mounds (Fig. 7.4f). Continued fluid supply enhances overpressures in surface-near sediments, and the resulting buoyancy force leads to the seafloor deformation by up-doming of sediments and carbonates within them that are incompletely annealed.

#### 7.6.2.4. Stage D - ruptured carbonate mounds

At Stage D (Fig. 7.9), fluid release occurs at discrete ruptures in carbonate crusts, in the form of free as well as dissolved gas. Peripheral seep sites at Venere MV, characterized by ruptured carbonate mounds with decimeter-thick crusts and significant numbers of chemosynthesis-based organisms (Fig. 7.2d, 7.5g, 7.6e), are interpreted to represent the most mature stage of the peripheral seeps at Venere MV. The established chemosynthesis-based communities and ongoing gas bubble emissions indicate persistent subsurface fluid supply at all the peripheral seeps (Fig. 7.4+7.5). Buoyancy-driven fracturing occurs when fluid pressures can break through the overburden carbonate seal and fluid can escape through the break overcome.

The mound at Site 1 hosts at least two generations of carbonates (Fig. 7.2d+e): slabs that were rifted apart by up-doming of the seafloor, and carbonate slightly draped by hemipelagic sediment that sealed the seafloor in the central part between the rifted slabs. The inferred process of rupturing and re-sealing is likely to have occurred repeatedly and contributed to the convex-up shape of the mounds, with younger carbonate slabs underplating the overlying ones. Seal-and-break mechanisms have also been argued to explain the formation of pockmarks (Matsumoto, 1990; Hovland, 2002; Marcon et al., 2014a). The observations in this study, however, indicate that under persistent methane seepage and AOM, ruptures in mounds or pavements may be sealed again without necessarily undergoing collapse. The ruptured carbonate mounds described here resemble seepage structures observed by Römer et al. (2014) on the Nile Deep Sea Fan. Those structures are larger and higher, but similarly consist of ruptured authigenic carbonates with gas bubble emissions from the fractures and chemosynthesis-based organisms at the fractures along the edges of the

structure. We suggest, that the observations of Römer et al. (2014) support a similar dynamic for the evolution of seeps as that we propose for the peripheral seeps of Venere MV during stage D.

The fractures in the carbonate mounds clearly allow seawater sulfate to infiltrate the subsurface of the mounds, providing an electron acceptor source for AOM. This also supports the re-establishment of chemosynthesis-based organisms such as Vesicomyid clams and tubeworms along the fractures in the carbonates (Fig. 7.6g). This scenario is supported by observations of ruptured mounds where microbial mats cover the edges of carbonate crusts, Vestimentiferan tubeworms root below the mounds in the cracks (Fig. 7.5g+7.6e-g; supplementary video 13.4), and Vesicomyid clams inhabit the softer sediments that accumulated in between carbonate slabs. Vestimentiferan tubeworms depend on sulfide fluxes that are thought to be an order of magnitude higher than those e.g. for Vesicomyid clams (Sahling et al., 2002; Cordes et al., 2003; Sahling et al., 2005). It has been found that tubeworms are capable of fueling or self-enhancing AOM by releasing seawater sulfate through their tubes at their root-like extensions (Cordes et al., 2005) and that they can contribute to carbonate formation (Marcon et al., 2014b) whereby they may get cemented into the carbonate crusts (Luff et al., 2004). In this study, the occurrence of large colonies of Vestimentiferan tubeworms at ruptures in the mounds and the presence of their encrusted remains in carbonate samples (GeoB19230-8; Fig. 7.7), are interpreted as signs of intensive AOM and persistent supply of hydrocarbon-rich fluid underneath the mounds. The carbonate fractures constitute a strongly localized habitat where microbial consortia and seep-typical macrofauna can flourish, profiting from protection and stability provided by cementation of the carbonate crusts extending above or around them.

#### 7.6.2.5. Stage E - collapse craters

Another type of seafloor structure (Stage E in Fig. 7.9) resulting from rupturing of the carbonate pavement is seen where the carbonate-paved seafloor has collapsed and formed convex-down, crater-like depressions (Fig. 7.3e+7.4d). In marine sediments, different mechanisms have been proposed to account for the formation of pockmarks during gas ebullition (Judd and Hovland, 2007) either through sediment loss and non-deposition (King and MacLean, 1970; Hovland et al., 1984) or through subsurface sediment mobilization and fluid flow (Maltman and Bolton, 2003; Reusch et al., 2015; Loher et al., 2016). At the peripheral seeps of Venere MV, neither the crater morphology nor the seafloor surrounding the craters indicate a sediment expulsion event. Instead, the arrangement of broken slabs of carbonate that line the inside of the sub-circular craters suggest an inward collapse and down-sagging of the seafloor. Collapse without the removal of subsurface sediment requires the presence of a subsurface void. Overpressure due to the accumulation of fluids below an impermeable seal can result in compaction of the pore space, for example by gas invasion into the sediments causing a rearrangement of grains (Hantschel and Kauerauf, 2009; Jain and Juanes, 2009). The formation of seafloor depressions can also occur through compaction, which has been shown in numerical models where subsurface overpressure resulted in the mobilization of sediments and large settlements (up to 35% reduction in

volume) in the remolded sediments occurred when overpressure dissipated (O'Regan et al., 2015). Alternatively, it has been proposed by Matsumoto (1990) that persistent fluid flow underneath a carbonate crust can undermine the carbonate formation and induce their collapse and fragmentation. The craters observed in this study are interpreted to result from rupturing of a carbonate pavement due to a small-scale fluid accumulation beneath it. The subsequent release of fluid, either slowly or suddenly, caused the overpressure to dissipate, the buoyancy force to recede, and the carbonates to collapse under their own weight.

Similar to the process described by Bahr et al. (2010), it is assumed that breaking of carbonates occurs by brittle deformation as progressive cementation increases the rigidity of sediments. Samples obtained from the ruptured mound at Site 1 (GeoB19205-2; GeoB19230-8; GeoB19230-9) show massive cement with little incorporation of hemipelagic sediments (Fig. 7.7; Table 7.2). In contrast, the sample from the collapse crater near Site 4 (GeoB19252-13) contains abundant hemipelagic sediment, is not highly cemented and crumbles easily. A more homogeneous cementation as in the samples from Site 1 is interpreted to result in a stronger carbonate slab whereas incorporation of hemipelagic sediments and biogenic remains gives rise to a weaker carbonate pavement. A stronger, more stable carbonate at Site 1 would explain why the mound did not collapse upon rupturing, whereas a collapse-crater formed near Site 4. Intermittent gas bubble release, microbial mats, and tubeworm colonies (Fig. 7.3e+7.4d) are clearly signs of ongoing seepage at the collapsed craters. Whether this represents residual seepage from the rupturing event, the dissolution of residual gas hydrate, or a younger reactivation of the underlying fluid migration pathway, remains unclear.

### 7.6.3. Timescales of cold-seep evolution

Whereas the processes of AOM and associated carbonate precipitation at cold seeps are relatively well understood, little is known about the timescales of their development. U-series have previously been successfully used to date cold-seep carbonates (Teichert et al., 2003; Bayon et al., 2009), but this procedure requires non-trivial correction procedures where detrital sediment such as clays are incorporated during the cementation process (Bayon et al., 2009). Absolute dating of carbonates is beyond the scope of this study and may be difficult given the heterogeneous composition of the carbonates (containing e.g. significant amounts of illite, see GeoB19252-13, Table 7.2) lacking massive cement phases. Nevertheless, the temporal evolution of the seeps studied here can be constrained by order-of-magnitude estimates based on seafloor observations and seep-related processes described in the literature and suggests the interaction of processes operating over a range of timescales, from decades to millennia, as illustrated in Fig. 7.9.

The establishment of a microbial AOM community in sediments and the growth kinetics of microbial mats are thought to be relatively slow (Knittel and Boetius, 2009), with modeling of bioenergetic reactions by Dale et al. (2008) indicating that a steady-state AOM biomass can be reached on the order of 60 years after a change in advective flow. Accordingly, it is estimated that it takes several tens of years from the onset of seepage in hemipelagic

sediment (i.e. plain seepage as in stage A, Fig. 7.9) to formation of black sediments and colonization by chemosynthesis-based organisms, assuming a constant supply of hydrocarbon-rich fluid. In this study this includes the establishment of extensive (several $m^2$) white microbial mats on the seafloor and settlement by macrofauna (Stage B in Fig. 7.9). In reality growth rates may vary significantly, as the typically localized or patchy distribution of microbial mats or macrofauna such as clams, mussels, and tubeworms at cold seeps depends strongly on the amount and intensity of methane seepage and sulfide production (Sahling et al., 2002). Nevertheless, similar estimates have been obtained from hydrocarbon seeps in the Gulf of Mexico, at water depths ca. 1000 m shallower than Venere MV, where chemosynthesis-based communities have been found to take tens of years to reach maturity (Nix et al., 1995; Smith et al., 2000). This is less than the lifespan of Vestimentiferan tubeworms such as of *Lamellibranchia sp.* which in established colonies can reach 100–150 years (Fisher et al., 1997; Southward et al., 2011). At Venere MV, the mature tubeworm colonies observed at Sites 1 and 4 along ruptures in the carbonates are therefore inferred to be at least tens to hundreds of years old, in turn implying the fractures they populate to be of similar age. This is consistent with numerical models showing that disseminated carbonate pieces or crusts of few centimeter thickness take at least several centuries to develop (Luff et al., 2004), while the growth of massive (dm-thick) authigenic carbonate crusts may take place over longer timescales, at rates of up to 5 cm/kyr (Luff and Wallmann, 2003; Bayon et al., 2009). Ruptures and visibly exposed carbonate crusts of >20 cm thickness were observed at several locations at the peripheral seeps of Venere MV, indicating that seepage has persisted throughout the last thousands of years (Loher et al., in review (G3)).

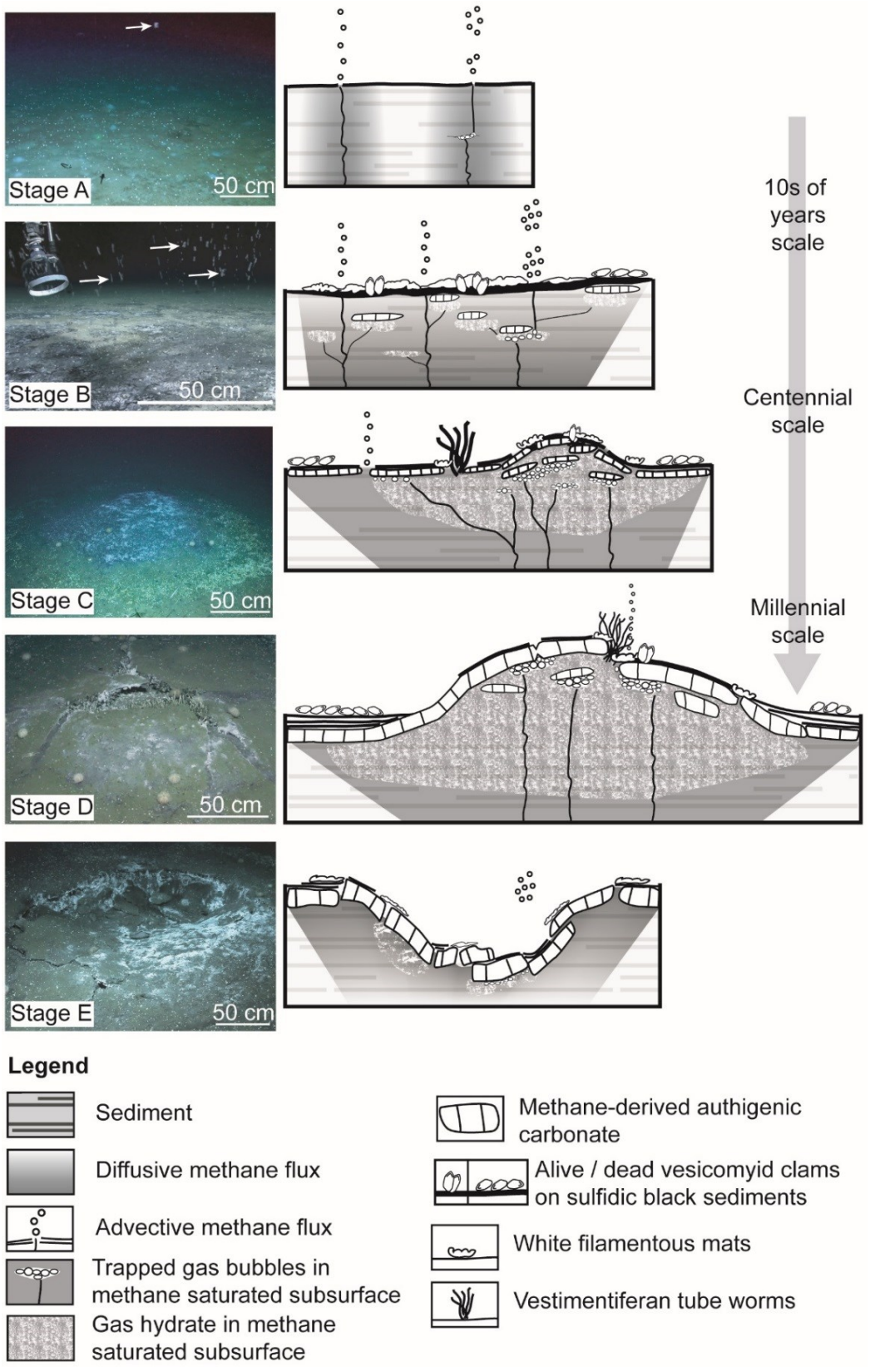


Figure 7.9. Conceptual evolutionary model for the carbonate structures and chemosynthesis-based communities observed at the peripheral seeps of Venere MV. White arrows in seafloor photos point to rising gas bubbles.

## 7.7. Conclusions

Detailed acoustic and visual investigations of submarine fluid seeps located along ring-faults peripheral to Venere MV allow the recognition and categorization of a range of seafloor expressions of gas seepage. At all sites, high acoustic backscatter is seen to correspond to authigenic carbonate deposits, of varying morphology and structure, indicating methane to be the predominant carbon source. The carbonates are colonized by chemosynthesis-based organisms known to be associated with microbially mediated AOM driven by methane supply from below. Sites of gas bubble release from the carbonates or surrounding hemipelagic sediments indicate localized methane oversaturation and focused fluid flow to by-pass the microbes performing AOM. All sites investigated in this study lie within the gas hydrate stability zone, free gas trapped within a sampling tool in the water column spontaneously formed hydrate and putative flakes of gas hydrate were observed to rise from seabed sediments during sampling. Gas is presumed to form hydrate locally in the subsurface, but seafloor structures are attributed primarily to self-sealing and fluid overpressures in response to carbonate precipitation. The varied expressions of seepage observed are used to propose a conceptual model for the evolution of seep settings, involving five possible stages:

A) Plain seepage through bioturbated, hemipelagic sediments, with gas bubble release from small orifices.

B) Black patches and filamentous microbial mats develop within sediments hosting disseminated carbonate pieces or thin crusts, and localized gas bubble release. Persistent seepage over several tens of years is required for this development stage.

C) Carbonate pavements partly seal the seafloor, but diffusive fluid migration and gas bubble release through cracks and at the edges of the pavements sustains microbial mats and the development of chemosynthesis-based communities, gas trapping due to carbonate growth, and potentially due to gas hydrate formation, contribute to pressure build-up and the formation of mounded morphologies on the seafloor. Persistent seepage over hundreds of years is required to reach this stage.

D) Carbonate mounds develop, comprising dm-thick, fractured but strongly cemented slabs. Fractures result from brittle failure in response to subsurface pressure build-up, and allow seawater rich in sulfate to infiltrate and sustain chemosynthesis-based organisms such as tubeworms which root beneath the carbonate slabs. Carbonate cementation may re-seal the mounds. Mound development is estimated to require several thousand years.

E) Collapse depressions lined by fractured carbonate slabs may also develop, due to release of trapped gas on development of fractures. Colonization by chemosynthesis-based organisms indicates resumed seepage within several tens to hundreds of years.

This model for the evolution of cold seeps is suggested to apply to other structures observed in the eastern Mediterranean Sea, which resemble those at Venere MV. Changes in fluid flow, gas accumulation and pressure release are the three factors inferred to control the evolution of seafloor expression of seepage, in the case of Venere MV primarily in response

to carbonate precipitation and secondarily in response to gas hydrate formation and dissolution. The results of this study help to interpret seep sites encountered during visual seafloor exploration and highlight the extent and dynamics of seafloor mounds or craters formed in association with gas release from marine sediments.

## 7.8. Acknowledgements

The authors are grateful for the efforts of the masters and crews of cruises RV METEOR M112 and RV POSEIDON POS499. The teams of the MARUM AUV SEAL 5000 and ROV QUEST 4000m are also thanked for their efforts during both cruises. Jonas Brünjes is acknowledged for the sample preparation and initial description of the carbonates during his BSc thesis. The Deutsche Forschungsgemeinschaft (DFG) and the Research Center / Excellence Cluster “The Ocean in the Earth System” are thanked for funding of expeditions M112 and POS499. Marta Torres acknowledges support through a fellowship from the Hanse Wissenschaftskolleg. Daniel Praeg acknowledges funding from the European Union’s Horizon 2020 research and innovation program under the Marie Skłodowska-Curie grant agreement No 656821 (project SEAGAS).

# 8. The structure and morphology of a mudflow from Venere Mud Volcano (Central Mediterranean)

## 8.1. Introduction

Marine cold seeps are sites on the seafloor where typically the focused upward flow and release of methane-rich fluids occurs (e.g. by gas ebullition). They are often associated with oasis-type chemosynthesis-based faunal communities and authigenic carbonate deposits (Suess, 2014). Mud volcanoes (MVs) are considered to be a specific type of seepage structure whereby the focused flow of subsurface fluids leads to the additional mobilization, transport, and discharge of solids (i.e. soft sediments and rock clasts). Such a three-phase (gas-water-sediment) mixture is referred to as mud breccia and it is typically discharged as a mudflow onto the seafloor (Cita et al., 1981; Mazzini and Etiope, 2017). Most of the methane advected towards the seafloor is degraded microbially when electron acceptors such as oxygen for aerobic methane oxidation (MO) or sulfate for anaerobic oxidation of methane (AOM) are able to penetrate into the sediments from the seawater (De Beer et al., 2006). Rapid fluid seepage and the extrusion and emplacement of methane-rich but sulfate-poor mudflows can challenge the colonization by cold-seep organisms that depend on AOM in two ways: 1) chemically, due to the lack of electron acceptors such as sulfate in the fresh mud breccia (Loher et al., in review (JMPG)) or their inability to penetrate due to rapid upward fluid flow (Luff and Wallmann, 2003; De Beer et al., 2006); and 2) physically due to burial, dislodgement, or destabilization of the organisms by the movement of the mudflow or subsequent eruptions (Roberts and Carney, 1997). Whereas it is difficult for cold-seep ecosystems to develop near the active extrusive centers of MVs, they have been found on old mudflows (Olu-Le Roy et al., 2004; Huguen et al., 2005; Jerosch et al., 2007; MacDonald and Peccini, 2009) as well as at peripheral sites of fluid release (Olu-Le Roy et al., 2004; Loher et al., in review (JMPG)).

It has been proposed that MV eruptions are episodic (Kopf, 2002; Deville and Guerlais, 2009) and for example in Azerbaijan MV eruptions have been observed to only persist for a few hours or days (Planke et al., 2003). The expression of slow extrusions and fluid-mud discharge have been predominantly documented from terrestrial MVs during quiescent phases of activity. Dense mud plugs are squeezed out in bulk mass at several cm/day and show fractures and extrusion striations (Planke et al., 2003; Roberts et al., 2010). Emission of high-viscosity muds tend to form elongate flows that move downslope fastest at the center and slow down at the sides as they spread out in lobes. When the mud sheets are deposited they typically dry up and mud cracks develop in slab-like patterns (Hovland et al., 1997). At offshore MVs, visual observations of the surface of MV mudflows are limited to individual photos showing similar cracks and striations to the terrestrial examples (Dupré et al., 2007) or mud breccia ridges and crevasses (Zitter et al., 2005). The behavior and expression of mudflows remain largely unexplored and areally comprehensive visualization of such structures are lacking.

## 8.2. Objectives and methods

This study presents the results of optical surveys across a site of recent mud breccia extrusion at the summit of Venere MV (Central Mediterranean) and morpho-structural analyses of the entire mudflow based on acoustic data. Photographic footage has been assembled to a photomosaic of >400 $m^2$ and presents a unique dataset of an extrusion site of a MV adjoining mudflows a deep-sea environment. In particular, the results allow new insights on the potential flow behavior and material transport processes of MVs.

Seafloor bathymetry and backscatter data were obtained with a Kongsberg EM122 (12 kHz) ship-based system and an EM2040 (300 kHz) system mounted on autonomous underwater vehicle (AUV) MARUM-SEAL 5000. Visual seafloor observations were conducted using the remotely operated vehicle (ROV) MARUM QUEST 4000m. The photo mosaic consists of almost 700 individual seafloor images, which were acquired from altitudes 1–2 m above seafloor and based on smoothed ultra-short baseline (USBL) navigation data of the ROV (estimated accuracy is better than 10 m; (Bohrmann et al., 2015)). The LAPM tool (Marcon et al., 2013) was utilized for compilation of the mosaic by using the automatic feature detection function as well as by setting tie points manually.

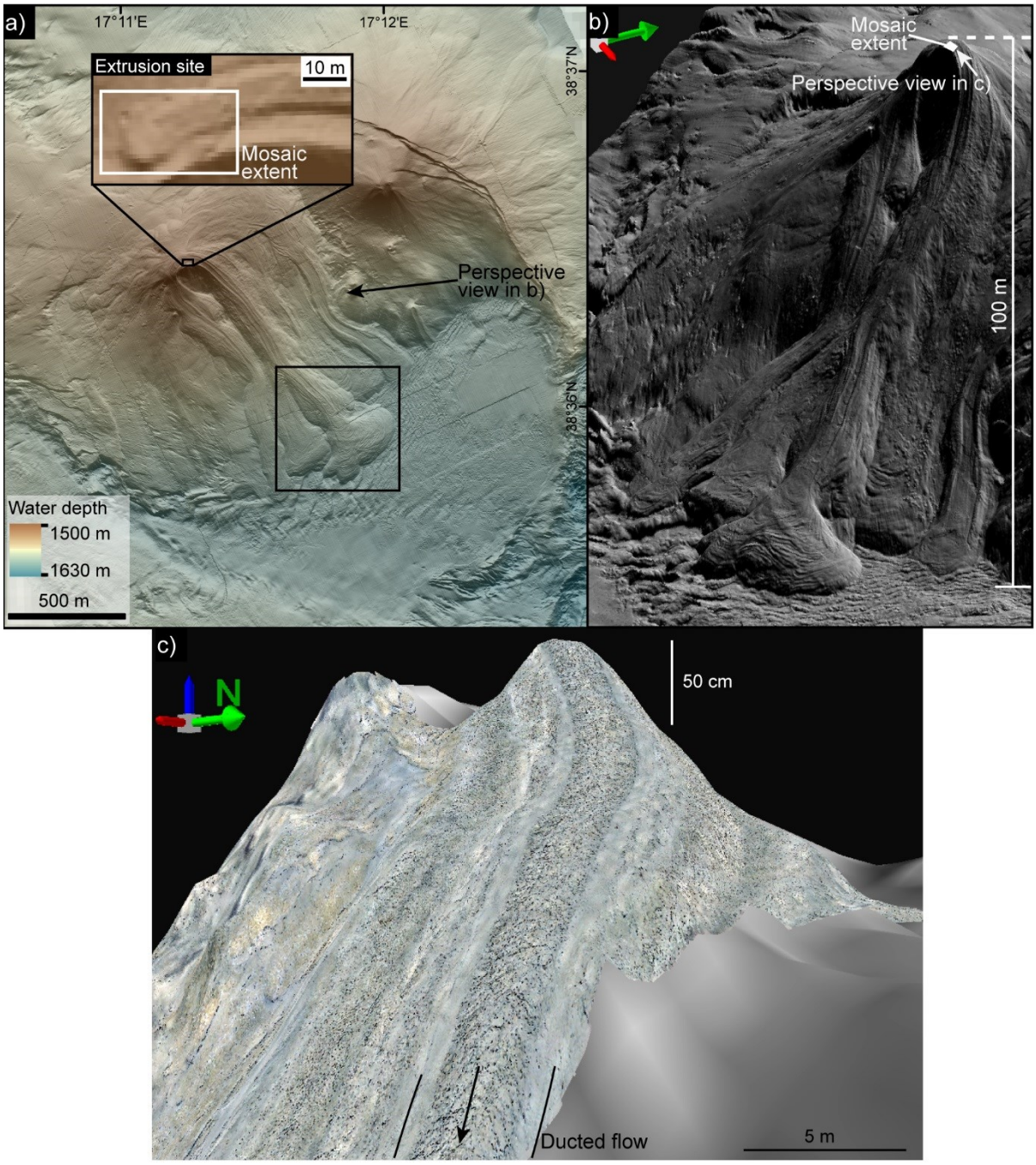


Figure. 8.1. a: AUV-derived bathymetry showing Venere MV (two cones and caldera); at the western summit the extrusion site is shown (inset) and the black box shows the extent of Fig. 8.2; b: 3D-perspective view (hillshade with illumination from NW) of the western cone of Venere MV showing the most recent mudflow in the foreground: channelized section extends from the summit to the floor of the caldera where the lobate section begins at the break in slope inherent with a widening of the flow; c: Photomosaic of the most recent mudflow at the extrusion site draped on AUV-borne bathymetry (v.e. ~10x; note extent and location indicated in a) and b)).

## 8.3. Morphologies of a recent mudflow

The most recent mudflow at Venere MV extends from the western summit (Fig. 8.1) and is emplaced along the southern flank of the MV. This flow is over 1.6 km long and can be subdivided into: 1) a channelized section in the upper part and along the MV slope and 2) a lobate section at the foot of the MV edifice (Fig. 8.2). Its site of origin is crescent-shaped, ca. 3 m across, in the summit area of the western cone (Fig. 8.1a). The central part of the exposed mudflow is domed convex-up and consists of irregular, angular bodies (up to several dm in size) of light grey mud breccia separated by crevasses (several cm to dm deep) oriented orthogonal as well as parallel to the flow direction (Fig. 8.3a+b). These bodies show sets of fractures and joints and their flat-top surfaces are often covered by flow-parallel (cm-scale) striations (Fig. 8.3c). The edges of the flow are marked by ridges of smooth mud breccia (up to 0.5 m high) deposited on the sides and bordering older generations of mudflows with fine-scale fracture networks and striations in regular patterns (Fig. 8.3d+e). Outside of the mudflows, light grey mud breccia is exposed underneath an olive-brown surface where elongated, downslope-extensional fractures occur (Fig. 8.3a+b).

The channelized mudflow terminates at the foot of Venere MV and transitions to zone of deposition consisting of several tongue-shaped, partly amalgamated lobes of material (Fig. 2). The lobes consist of stacked sheets of material, whereby they terminate in parallel ridges (resembling contours) visible in the ramped frontal parts of the lobes.

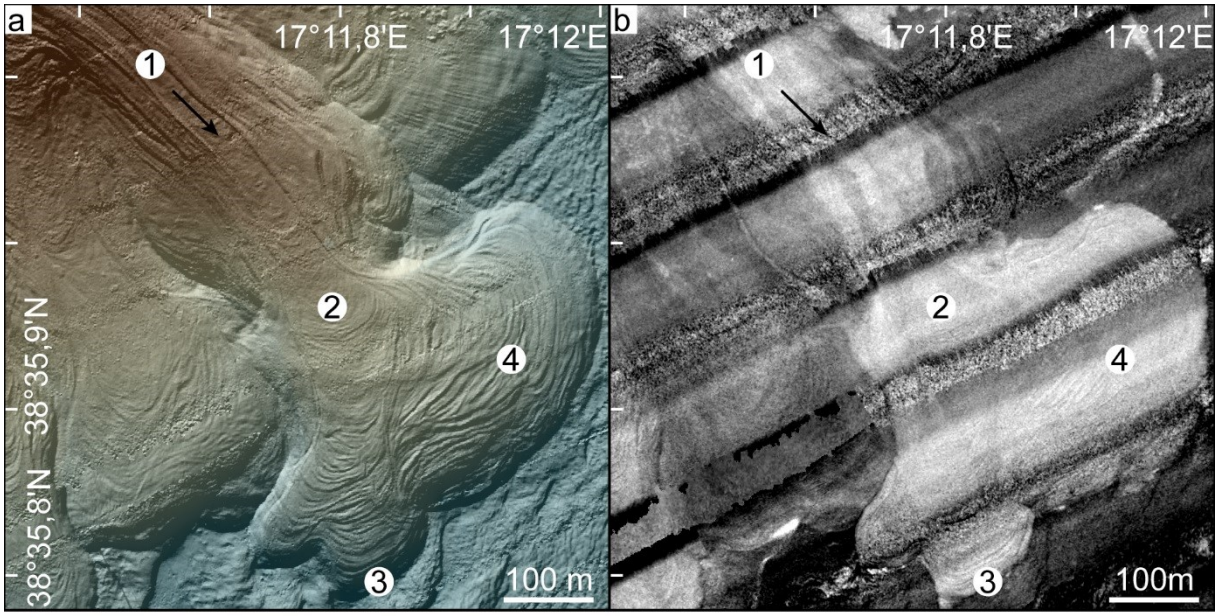


1) Channelized part of mudflow
2) Transition to lobe-shaped mudflow
3) Frontal ramp of mudflow
4) Ridges in sheets of the mudflow

Figure 8.2. Bathymetry (a) and backscatter (b); light colors represent higher backscatter) of lower section of the most recent mudflow (see Fig. 8.1 for location), black arrow indicates downslope flow direction.

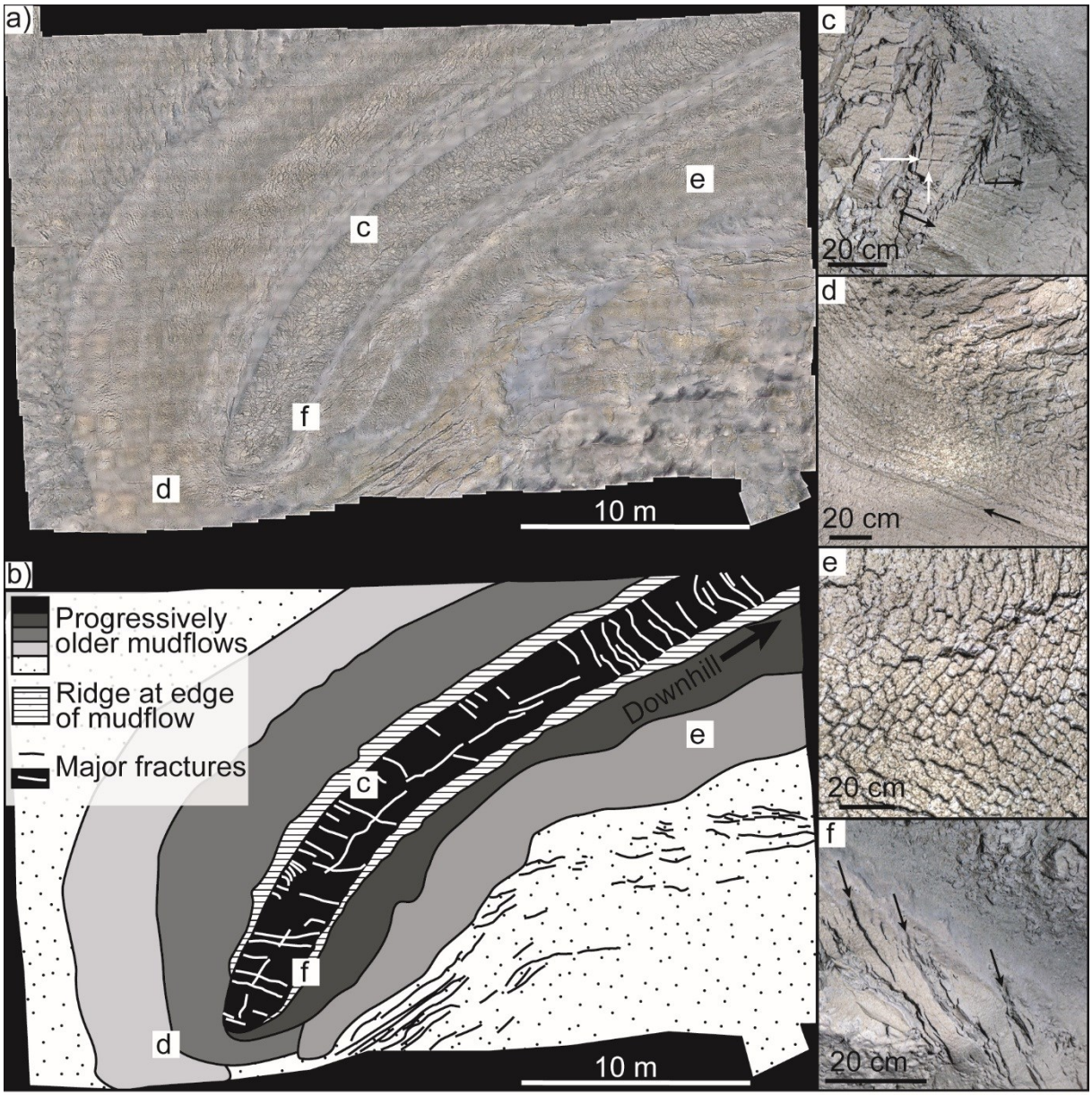


Fig. 8.3. a: Photomosaic of the extrusion site and mudflow (for extent see Fig. 8.1); b: Interpretation of a) showing different generations of mudflows; c: intact, angular blocks of mud breccia rafted on top of the flow (white arrows point to orthogonal fractures, black arrows point to striations on top of the mud breccia blocks); d: Striated and finely textured mud breccia with slight dusting of hemipelagic sediments; e: Polygonal fractures in mud breccia surface; f: Shear fractures along the mudflow edge (black arrows indicate en-échelon arrangement).

## 8.4. Discussion of mudflow structures

The observed mudflows at Venere MV indicate that the mud breccia was extruded as a cohesive mass that generated viscous gravity-driven flows. The surface morphology of Venere MV documents that mudflows can stack-up and become amalgamated where fresh material has moved along the pathways of previous mudflows or where they spread over the surface of pre-existing deposits. This is in contrast to the types of flows previously known from cone-shaped submarine MVs, where sidescan backscatter investigations have revealed

narrow, radial flows of mud breccia flows at cone-shaped edifices (Ivanov et al., 1996a; Paull et al., 2015b). The photomosaic draped onto the bathymetry reveals that levee-like ridges can be formed by the deposition of material at each side-wall of the mudflows, which results in a duct for the flow (Fig. 8.1c). Furthermore, recurrent mudflows are extruded from a narrow area at the summit of Venere MV. This points to stable conduits within the seafloor edifice of conical MVs, capable of supplying mud breccia for hundreds if not thousands of years, as indicated by mudflows mapped and dated across the cone of Venere MV (Loher et al., in review (G3)). This observation substantiates previous modelling results of conical mud volcanoes, which suggested that mudflows extruded from conical MVs that are near their maximum height, should be thin and fluid rich and may, therefore, flow to the foot of the structure (e.g. Murton and Biggs (2003)).

Meter-scale fractures occur on the surface of the most recent mudflow (Fig. 8.3a+b). They are interpreted to result from tensional forces induced on the mud breccia by the spreading of material laterally (e.g. outward from the convex-up, central bulge of the mudflow) or by the gravity-induced downslope motion of material. The gravity-driven mudflows move faster in steeper terrain and the down-slope section of the cohesive mudflow exerts a tensional stress on the upper section – i.e. promotes crevasses orthogonal to the flow direction. The fastest moving portion of MV mudflows is typically at their center whereas movements are slower at the edges (Hovland et al., 1997). Additional fractures at the edge of the mudflow (Fig. 8.3f) are interpreted to result from the effect of friction between the mobile mud breccia and the unmoving material at the edge or underneath the flow. These fractures and the ridges observed in the mudflow-lobes at the foot of the cone, respectively, are similar to crevasses typically observed in glaciers (see examples on http://www.swisseduc.ch/glaciers/ (26/09/2017)) and the furrow and ridge morphologies known from rock glaciers (e.g. Kääb and Weber (2004), Frehner et al. (2015)). There, crevasses and ridges result from either extending or compressive flow, respectively, when changes in slope occur or through different rates of movement within the flow (Nye, 1952; Vornberger and Whillans, 1990; Harper et al., 1998).

A similar mechanism for the formation of fractures is known from plastic materials moving at differential rates to each other. It has been observed that fluids or sediments moving at faster rates underneath an overlying sediment layer (e.g. a cohesive bed of clay) lead to the detachment of sediment bodies (Shanmugam, 2000; Paull et al., 2013). In this case, the fractures propagate through the cohesive surface layer to the top of the faster moving material in the interior of the flow, similar to crevasse-formation in glacier flow (Nye, 1952). At the mudflow of Venere MV a similar behavior could be expected in case the movement of the flow was faster in the interior (i.e. depths of several cm to dm given the depth of the fractures) than in the surface material. This implies that there can be differential rates of movement within a single mudflow, in turn influencing its surface expression. Subsurface movement of mud breccia and fracture formation could explain the exposure of fresh mud breccia on the seafloor of apparently inactive MV systems, without the requirement of a violent eruption (as

proposed e.g. for the Pythagoras MV by Foucher et al. (2009)), through the injection of fluid-rich mud breccia underneath a slow or stationary package of cohesive mud breccia.

On a dm-scale, the most recent mudflow shows a network of orthogonal fractures that cross-cuts its surface both orthogonal and parallel to the flow direction into flat-topped, angular bodies of mud breccia (Fig. 8.3c). Loss of volatiles and the infiltration of seawater into pore space may support the formation of such cracks in surface-near mud breccia down to the cm-scale. The orthogonal arrangement of the fracture network (Fig. 8.3c+e) may be the result of a desiccation process similar to patterns observed in dry and cracked mudflows of terrestrial MVs (Hovland et al., 1997). Extrusion striations seen on the surface of the flat-topped bodies remain preserved even several meters away from the extrusion site (Fig. 8.3c). These cm-scale striations resemble slightly larger striations previously observed at MVs offshore (see Fig. 11, photo e) by Dupré et al. (2007)) and on land (see Fig. 4D in Planke et al. (2003)). In MVs of Azerbaijan, such deposits have been interpreted to result from the slow but continuous extrusion of viscous, plastic mud breccia at rates of several meters/year (Guliyev and Feizullayev, 1997; Planke et al., 2003; Mazzini and Etiope, 2017). Their mechanism of extrusion has been compared to the squeezing of “toothpaste” from a tube (Hovland et al., 1997; Roberts et al., 2011b). At Venere MV, the striated and angular blocks of mud breccia appear as intact bodies rafting in the center of the mudflow again an indication that subsurface material might flow faster than the cracked and desiccated surface layer.

In the manuscripts I and II (Chapters 5 and 6), the ongoing extrusive activity and mud movement at the summit of Venere MV have been demonstrated. The freshly extruded mud breccia appears devoid of chemosynthesis-based macrofauna in contrast to the methane-charged sediments and carbonate mounds at the peripheral seeps (e.g. manuscript III in Chapter 7). This phenomenon has previously been described at other MVs (Wallmann et al., 2006) and is attributed to the lack of sulfate in the mud breccia as the terminal electron acceptor which is typically required by the organisms performing AOM. Furthermore, mud movements across benthic ecosystems can cause significant disturbance and challenges the settlement of seep fauna (Roberts and Carney, 1997; MacDonald and Peccini, 2009; Feseker et al., 2014). In this study it cannot be resolved if any cold-seep ecosystems have been disturbed or covered by the emplacement of the studied mudflow.

## 8.5. Conclusion and outlook

This is one of few studies which present a high-resolution visual documentation of a recently extruded mudflow of a deep-sea MV. The high-resolution seafloor images from photomosaics provide a better spatial context for understanding the dimensions of seafloor morphologies than single seafloor photos. In addition, the preliminary analysis and interpretation of mudflow structures reveals analogies to glacial morphologies and indicates a complex flow behavior potentially involving differential motion and frictional forces between fresh and old deposits or differences in the mud breccia composition (clast-rich vs. fluid-rich).

Comparisons with model experiments of fluid and sediment flows or geotechnical investigations on sediment (mud breccia) samples may provide further insights for the flow behavior (rheology), flow speed (e.g. mud flowing on an inclined plane), or the spreading behavior of mud breccia (e.g. on the flat caldera floor). A range of temperature profiles are available from the summit site as well as of more distal mudflows (Bohrmann et al., 2015) and their analysis and interpretation may further help to better differentiate between younger (warmer) or older (colder) flows and their respective morpho-dynamic behavior.

# 9. Mud volcanoes across the Calabrian Accretionary Prism – mapping morphology and backscatter

## 9.1. Summary

This chapter presents an updated inventory of MVs in the CAP following the initial study of Ceramicola et al. (2014b). Confirmed and inferred MVs are analyzed and mapped based on their morpho-acoustic characteristics and different categories of mud constructions have been identified. Examples of previously known and newly identified MVs are shown based on the available bathymetry and backscatter obtained during cruise M112 (Bohrmann et al., 2015). The MV distribution across the different morpho-structural domains of the CAP is re-assessed and the relationship between MVs and tectonic structures is investigated. In preparation for a potential future submission to a peer-reviewed journal, the following paragraphs present a general introduction including some open questions with regard to the MV distribution in the CAP. For general tectonic setting and geological background the reader is referred to Chapter 2 of the thesis.

## 9.2. Introduction

The margins of northern Africa and southern Eurasia bordering the eastern Mediterranean Sea, host one of the world's highest abundance of currently recorded submarine mud volcanoes (MVs; (Kopf, 2002; Foucher et al., 2009; Mascle et al., 2014)). Several MVs have been found at the Nile Deep Sea Fan (Dupré et al., 2007) but they are most abundant in tectonic settings experiencing compression such the Mediterranean Ridge, the Anaximander Mountains, or the Calabrian Accretionary Prism (CAP; (Limonov et al., 1996; Woodside et al., 1998; Ceramicola et al., 2014b; Mascle et al., 2014)). Specifically the CAP is a little explored area (Foucher et al., 2009) and the occurrence of 54 MVs has only recently been recognized (Praeg et al., 2009; Ceramicola et al., 2014b).

MVs can show characteristic seafloor morphologies typically resulting from mud breccia extrusions that lead to the build-up of edifices, cause subsidence and form a caldera (Evans et al., 2008), or involve a combination of both positive and negative morphologies (e.g. Van Rensbergen et al. (2005a)). Recent or fossil mudflows may be indicated by elevated backscatter intensities due to either (or a combination of) their irregular surface, high clast content, or the presence of free gas in the pore space of the mud breccia (Volgin and Woodside, 1996). Whereas ship-based seafloor bathymetry and backscatter data have revealed the location, general shape, and extent of many MVs on the CAP, most are rendered at resolutions insufficient to study their detailed morphology and associated mudflows. However, understanding the surface expression of MVs is important as it can give insights into their most recent phases of activity and the dynamics by which they emit fluids and mud breccia (e.g. Dupré et al. (2008), Feseker et al. (2014)). In many cases, however, the morphological diversity of MVs neighboring each other in a similar tectonic setting has remained speculative (Huguen et al., 2004; Paull et al., 2015b).

In the Eastern and Central Mediterranean including the CAP, a large number of MVs have been found associated to folds or thrusts at (or near) the seafloor (Fusi and Kenyon, 1996;

Galindo-Zaldivar et al., 1996; Kopf et al., 1998; Praeg et al., 2009). This substantiates findings from other regions that overpressure generation and release by focused fluid flow is favored by tectonic compression (Higgins and Saunders, 1974). Praeg et al. (2009) argue that compressive stress is not actually favorable to vertical fluid migration and likely neither to mud breccia ascent. Fluids may, however, use existing fractures or faults as migration pathways (e.g. during phases of overpressure release by fault-failure; (Bonini, 2007)) or self-generate pathways by hydrofracture in case overpressure is high enough to overcome the fracture toughness of the surrounding sediment (Deville et al., 2010). Alternatively, strike-slip faults have been found to significantly lower the threshold for the generation of critical pore fluid pressures that are capable of causing sediment fluidization (Mazzini et al., 2009a) and appear to represent efficient pathways even for deep-seated crustal fluids (Hensen et al., 2015).

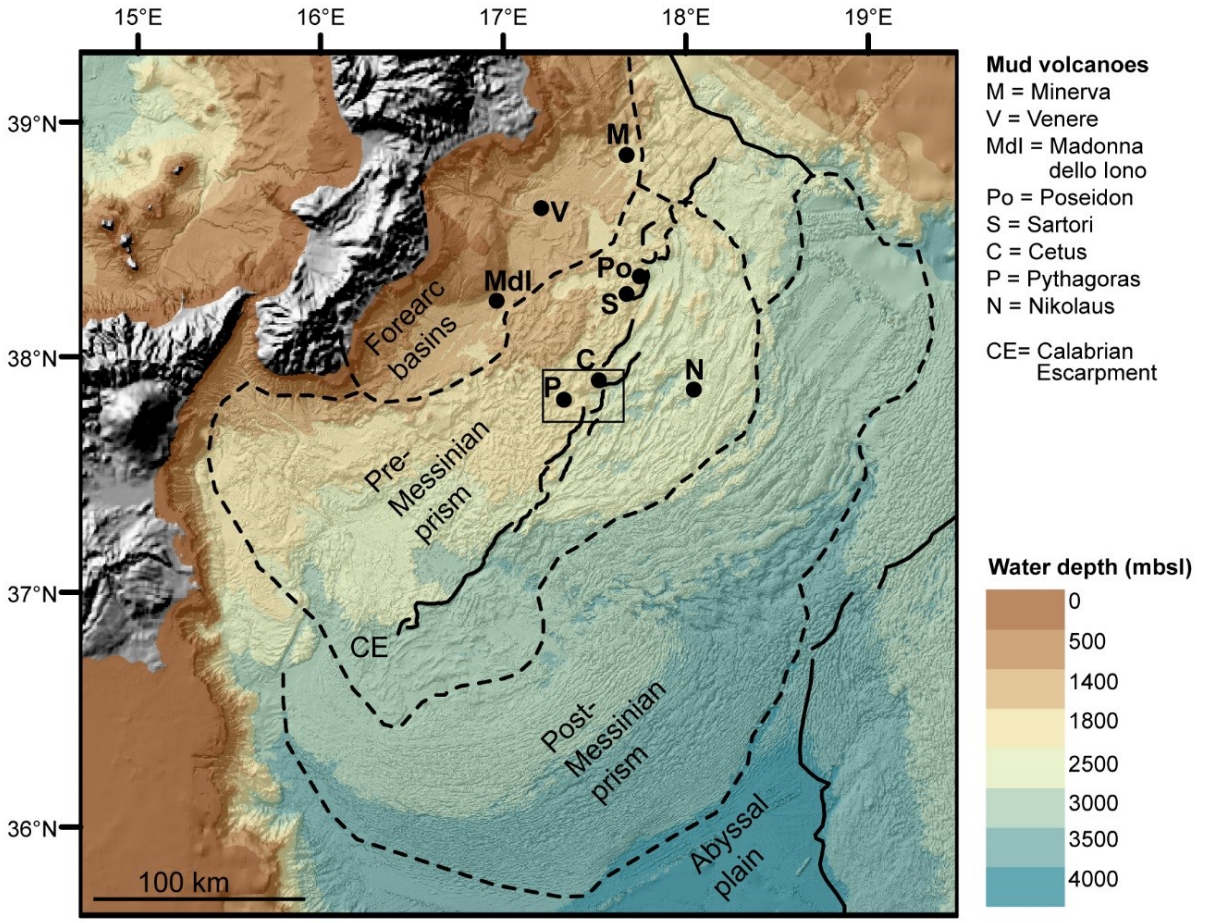


Fig. 9.1. Bathymetry of CAP (note stretched depth scale to accentuate morpho-structural zones, which are drawn in stippled black lines after Ceramicola et al. (2014b)) and location of named MVs (some are shown in more detail in Fig. 9.3) in the forearc basin, along the Calabrian Escarpment (inner pre-Messinian prism) and one MV in the outer pre-Messinian prism (Nikolaus MV); black box indicates extent of Fig. 9.2.

In the CAP it has been proposed that mud volcanism was triggered by post-Messinian out-of-sequence thrusts (Polonia et al., 2011; Panieri et al., 2013; Ceramicola et al., 2014b) and a number of MVs are found associated with structural features such as thrusts or transpressive

faults at the inner deformation front (Praeg et al., 2009; Panieri et al., 2013; Gutscher et al., 2017). There remain, however, open questions regarding the distribution of MVs seawards of the Calabrian Escarpment in the outer part of the pre-Messinian prism (Fig. 2.5; (Ceramicola et al., 2014b)). This morpho-structural domain of the CAP is strongly affected by out-of-sequence thrusting (Minelli and Faccenna, 2010; Polonia et al., 2011). The presence (or absence) of MVs in this part of the CAP could support (or challenge) the hypothesis that the out-of-sequence thrusts act as preferential fluid migration pathways from deep within the CAP. Furthermore, a number of MVs appear to be located several km landwards of the largest out-of-sequence thrusts, the so called Calabrian Escarpment, rather than at the thrust plane outcrop and their exact structural context remains unclear (Ceramicola et al., 2014b).

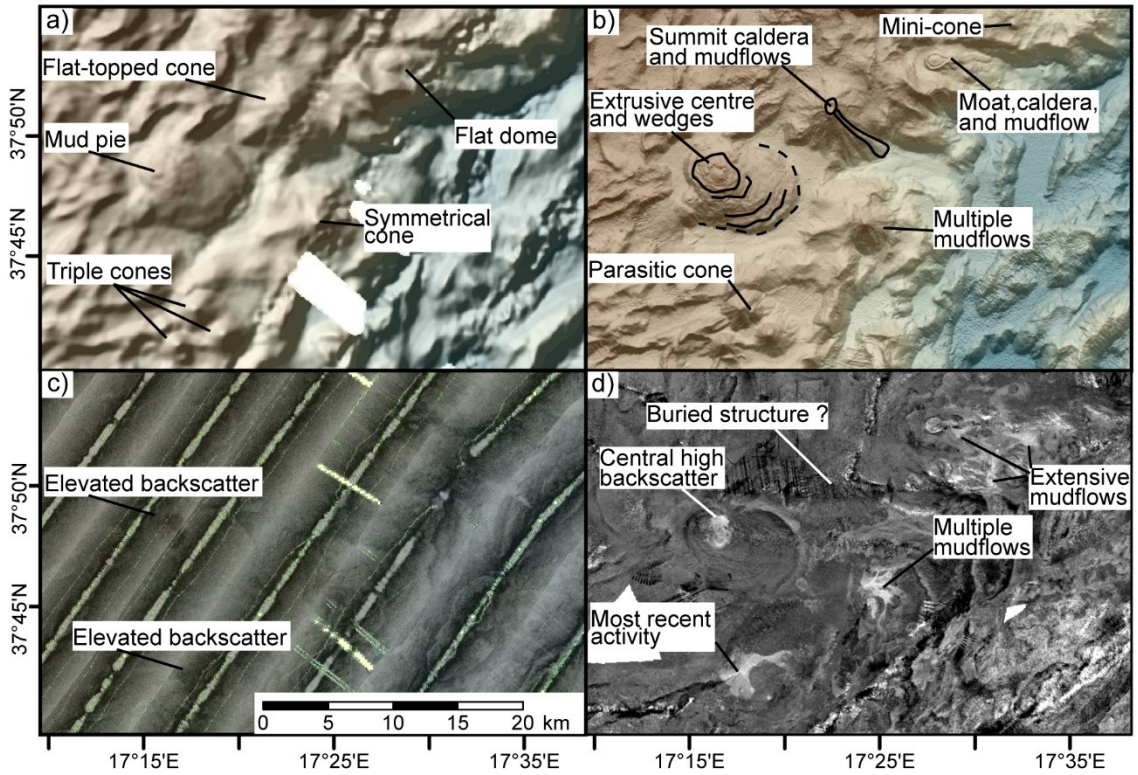


Fig. 9.2. Comparison of seafloor bathymetry (a) and b)) and backscatter (c) and d)) from 2005/2009 (a) and c); (Ceramicola et al., 2014b)) and new data from 2014 (b) and d; (Bohrmann et al., 2015)); all four panels show the same geographical extent; note that in the new data it is possible to identify individual mudflows and structures clearly based on morphology and backscatter where previously these may have been insufficiently resolved.

## 9.3. Approach and results of mud volcano mapping

This study uses hydroacoustic characteristics (bathymetry and backscatter) to investigate potentially new MVs or re-evaluate those already proposed by Ceramicola et al. (2014b). Whether an observed morphology or backscatter anomaly can be attributed to an extrusive structure such as a MV is ultimately only proven by seafloor sampling, i.e. by sediment cores containing mud breccia. However, the resolution of the seafloor bathymetry and backscatter data available for the study area has been greatly increased (Fig. 9.2) during the surveys of cruise M112 in 2014 (Bohrmann et al., 2015) compared to the previously available data (Ceramicola et al., 2014b).

A selection of four MVs are shown in the 3D-panels of Fig. 9.3 to exemplify a range of morphologies and structures that have been described in the new dataset. Only the Sartori MV had previously been known and the Poseidon, Cetus, and Nikolaus MVs have been newly identified based on their morphology and high backscatter intensities (sediment cores exist additionally for Poseidon and Cetus MV but these are not discussed here, see Bohrmann et al. (2016)):

- Sartori MV is a pie-shaped MV with extensive (apparently far flowing) mudflows visible in the backscatter only. The far-flowing behavior strongly contrasts with extrusions that must have formed the main pie.
- Poseidon MV is a mound or pie-shaped MV located at the SE end of a chain of MVs referred to as the MV Ridge situated at the Calabrian Escarpment. Mudflows can be seen to have flowed down the escarpment over horizontal distances of >6 km.
- Cetus MV is a well-defined, pie-shaped structure surrounded by a moat and ridge feature. A major mudflow (visible morphologically and in backscatter) extends downslope at the Calabrian Escarpment along the foot of a steep wall. Parasitic mounds appear to populate the surrounding (caldera?) of Cetus MV. On top of the wall, a small cone-shaped MV is situated. This mini-cone is classified as an individual MV since.
- Nikolaus MV is a cone-shaped structure with a summit caldera. Mudflows are clearly visible in backscatter data and they extend downslope into a deep basin over several kilometers horizontal distance.

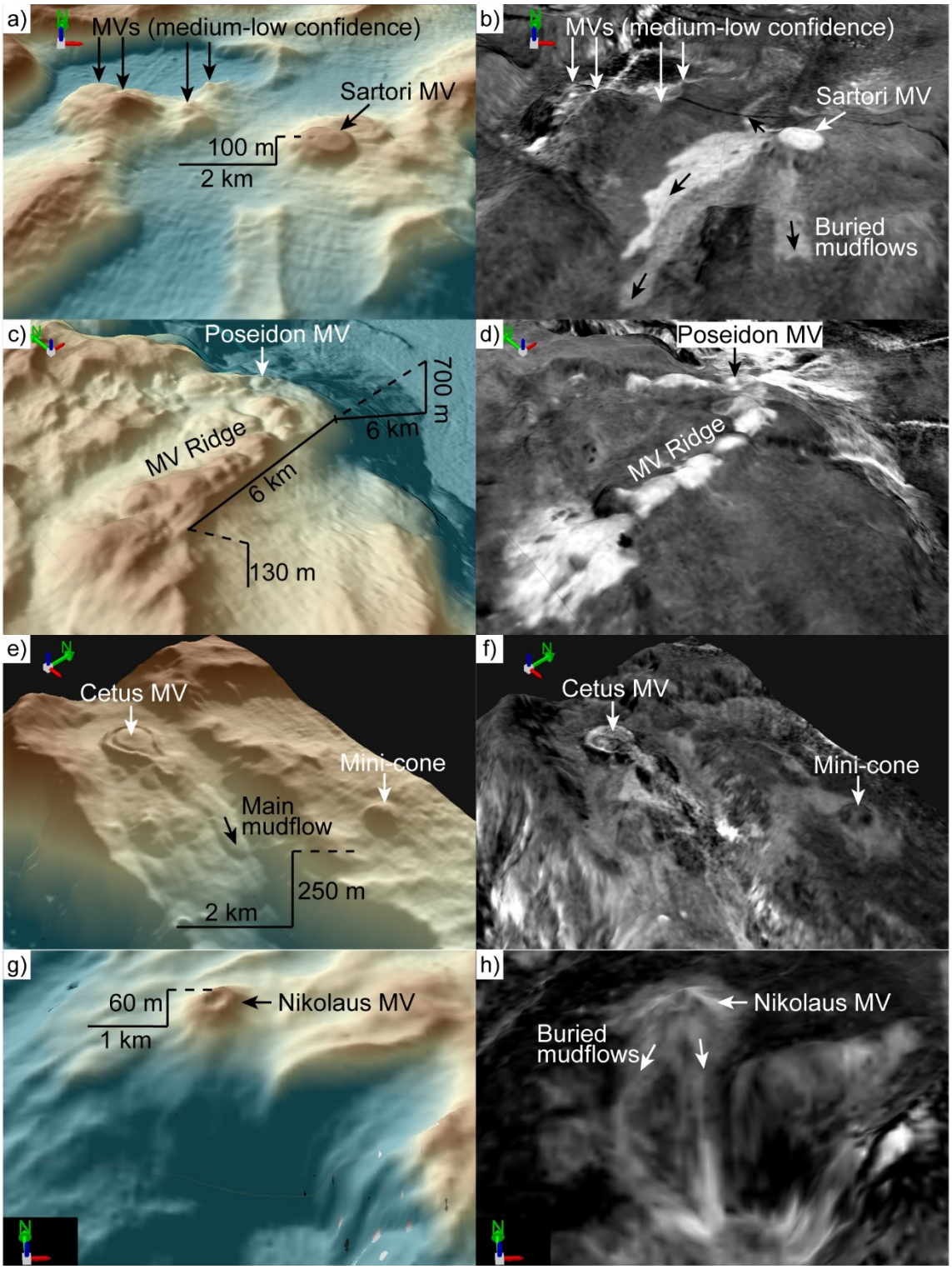


Fig. 9.3. 3D-views of MVs (bathymetry on left side) and backscatter (on right side); a-b: Sartori MV which had been previously identified and named by (Ceramicola et al., 2014b); c-d: Poseidon MV as one MV of the so called MV Ridge; e-f: Cetus MV and a mini-cone MV in close proximity; g-h: Nikolaus MV identified and named during M112 as the first clearly identified MV seawards of the Calabrian Escarpment; locations of the respective MVs can be found in Fig. 9.1.

Bathymetry and backscatter data was manually examined in a geographic information system (GIS) and ambiguous morphological patterns or high backscatter patterns (elevated above the surrounding seafloor) were considered. This resulted in a range of potential features as candidates of MV structures. From these, three groups of MVs have been classified based on the following criteria:

- **Confirmed MVs** – Structures which have either been confirmed to consist of mud breccia by coring (i.e. Venere MV (both cones), Madonna dello Iono MVs (both cones and a dome inside the caldera), Pythagoras MV, Sartori MV, Poseidon MV) or which show clear morphologies such as mudflows, calderas, moats, or extrusion sites in bathymetry or backscatter; examples of confirmed MVs are shown in Fig. 9.3.
- **MVs with high confidence** – Structures that show morphologies resembling the confirmed MVs or which are characterized by distinct patterns of elevated backscatter but lack distinguishable mudflows (or vice-versa). This category also contains a number of potential MVs as parasitic (secondary) extrusive sites of larger (confirmed) MVs; examples of MVs identified with high confidence are shown in Fig. 9.4 b-d.
- **MVs with medium or low confidence** – Structures characterized by a seafloor morphology (often small and close to the limit of resolution, i.e. 50 m) or by elevated backscatter lacking a clearly defined extent or shape; examples of MVs identified with medium to low confidence are shown in Fig.9.4 e+f.

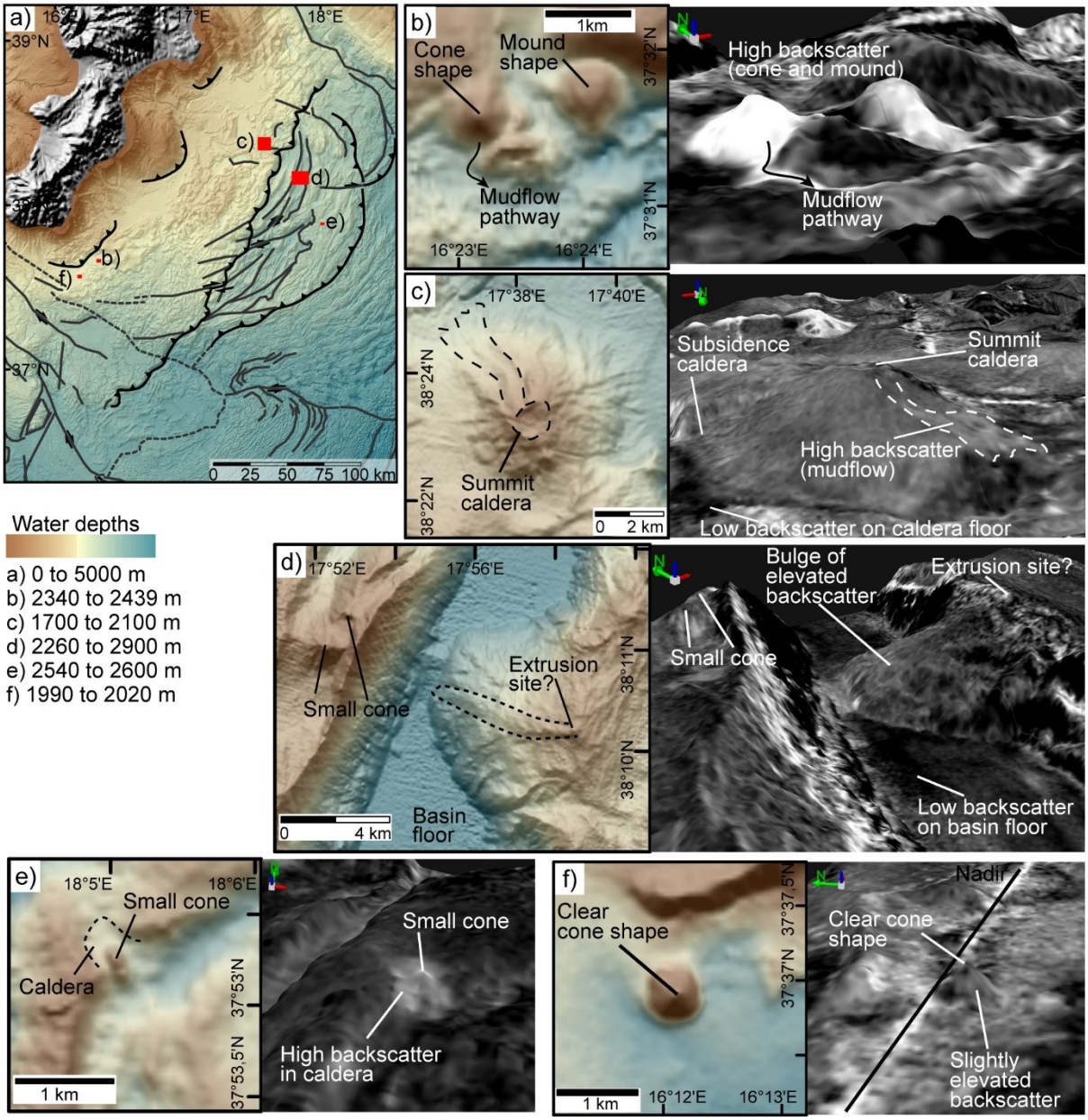


Fig. 9.4. a: Bathymetry map of the study area with tectonic structures after Gutscher et al. (2017); b-f) Pairs of bathymetry (left side) and backscatter (right side) of MVs and annotated features; b-d: MVs identified with high confidence; e: MV classified as low confidence; f: MV classified as medium confidence.

## 9.4. Discussion

Ultimately, only visual observations or ground truthing by geological sampling can confirm or reject an alleged MV but also geophysical evidence can provide a good degree of confidence (Volgin and Woodside, 1996; Mascle et al., 2014). The resulting distribution of MVs across the CAP (Fig. 9.5) clearly confirms the previous finding by Ceramicola et al. (2014b) that most MV (84%) occur in the forearc basins and the inner pre-Messinian prism (i.e. landward of the Calabrian Escarpment) an area referred to as the inner plateau. However, the herein presented results also identified two new regions (Fig. 9.5). The first consists of an area at the SW edge of the inner plateau where previously only the Athena MV and two unnamed MVs had been known (Ceramicola et al., 2014b). A few new but putative MVs in this region are located on what has been referred to as the mid-slope basins of the W lobe of the CAP (Gutscher et al., 2017). The second region lies among the oblique ridges and troughs (fold-and-thrust belt) seaward of the Calabrian Escarpment, and potentially hosts up to 27 MVs (including the newly named Nikolaus MV; Bohrmann et al. (2015)) where previously only one MV had been recognized (Ceramicola et al., 2014b). They are all located on morphological highs (ridges) or on flat plateaus of the fold-and-thrust belt. Interestingly, they do not correlate with the thrust-plane outcrops of the splay faults identified for example by Polonia et al. (2011) and as already noted by Ceramicola et al. (2014b), no MVs occur at the base of the Calabrian Escarpment.

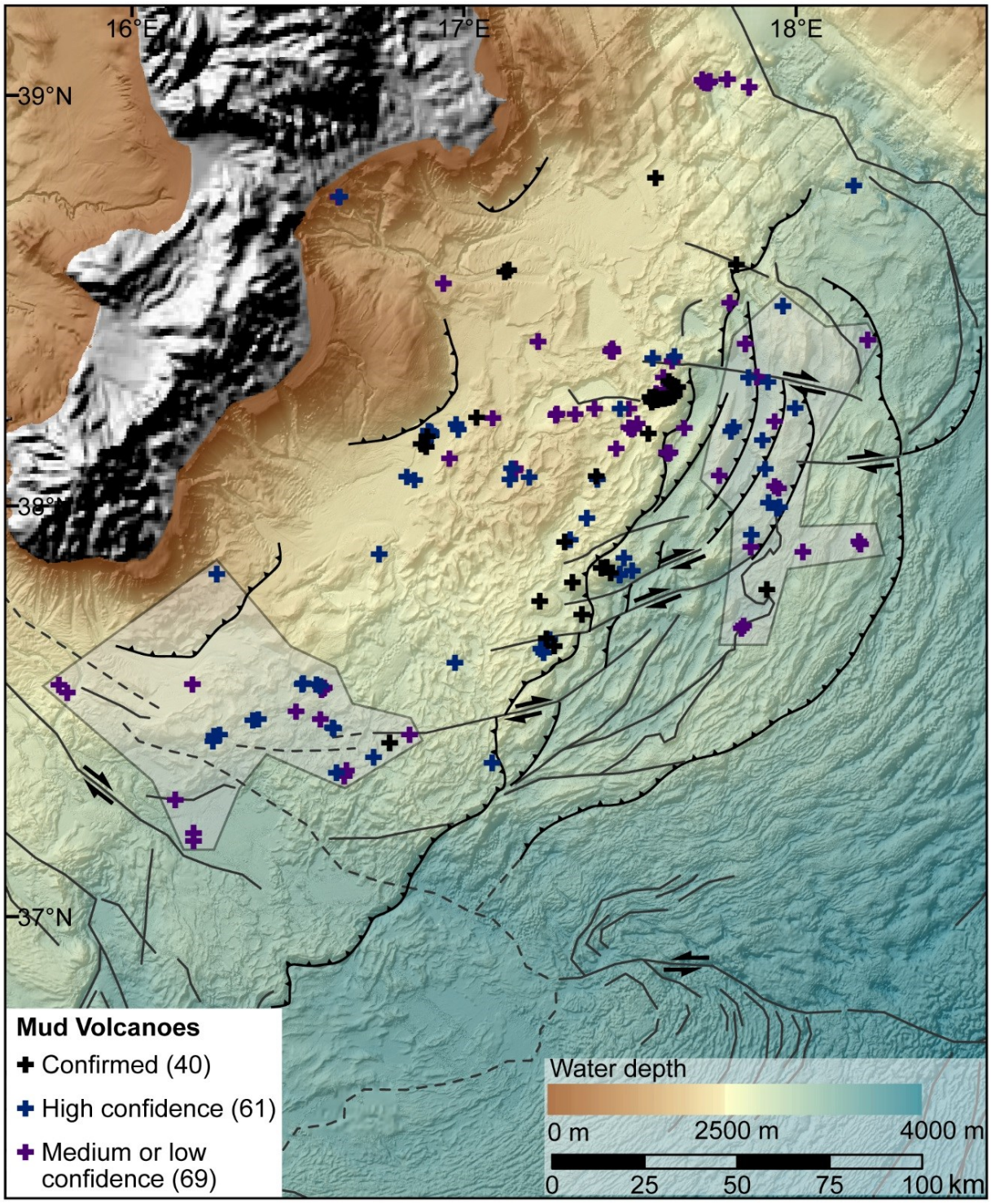


Fig. 9.5. Bathymetry map of the CAP with the location of MVs that are confirmed (black), MVs with a high confidence (blue), and MVs with a medium or low confidence (magenta) on the basis of the analyses of geophysical data and available sediment cores; two shaded areas delineate the aproximate extent of new potential MV regions; thrust faults (black lines with teeth), strike-slip faults (black arrows indicate sense of motion), and structural lineaments (dark grey lines, stippled where unclear) are after Gutscher et al. (2017) and Polonia et al. (2011).

Polonia et al. (2011) noted that the Calabrian Escarpment is characterized by transpressive faults indicating strain partitioning at the transition between the inner plateau and the fold-and-thrust belt. Based on the new bathymetric data and regional seismic investigations, the transpressional ridges and elongate troughs have been attributed to strike-slip deformation affecting this region (Gutscher et al., 2017). In this context, a tentative interpretation of the MV distribution relative to the out-of-sequence thrusts (also “splay faults”) identified by Polonia et al. (2011) and strike-slip faults across the Calabrian Escarpment identified by Gutscher et al. (2017) is presented (Fig. 9.6). At the transition between inner plateau and the fold-and-thrust belt, the MVs appear to be predominantly aligned with the dextral strike-slip faults. This holds true for the case for Pythagoras MV, which has been previously associated with a NW-dipping thrust (Praeg et al., 2009) but can now be seen to be additionally situated in the extension of a major strike-slip fault. Several other MVs, including the Cetus MV investigated during M112 (Bohrmann et al., 2015), are aligned parallel to this transpressive feature. Also the MV Ridge (consisting of a series of up to 21 confirmed and medium-confidence features) shows a clear relation to a strike-slip fault. This fault that has been tentatively extended further seaward by the author, given that there is a clear break in morphology across the fold-and-thrust belt, and connects to several MVs located seaward of the Calabrian Escarpment.

The occurrence of the MVs along major strike-slip faults may explanation why several are located a few km landwards of the Calabrian Escarpment rather than at the thrust-plane outcrop. It can be interpreted that these faults provide more efficient fluid migration pathways than the thrust planes. Given the lack of deeper-reaching subsurface data targeting specifically the MV sites, the exact ascent mechanism or pathways can only be speculated. It is possible, however, that the strike-slip component in the overall transpressive setting provides pathways that are oriented more sub-vertically and are more favorable for the upward migration of fluids and mud breccia than the thrust planes. Whether the strike-slip faults reach deep enough to allow the direct ascent of material from strata as old as the Cretaceous, as for example indicated by mud breccia clast analyses at the Pythagoras MV (Praeg et al., 2009), cannot be currently resolved. The potential interception of sub-vertical conduits as proposed for MVs in the CAP (Praeg et al., 2009) with the thrust or strike-slip faults have, therefore, been labeled with a question mark.

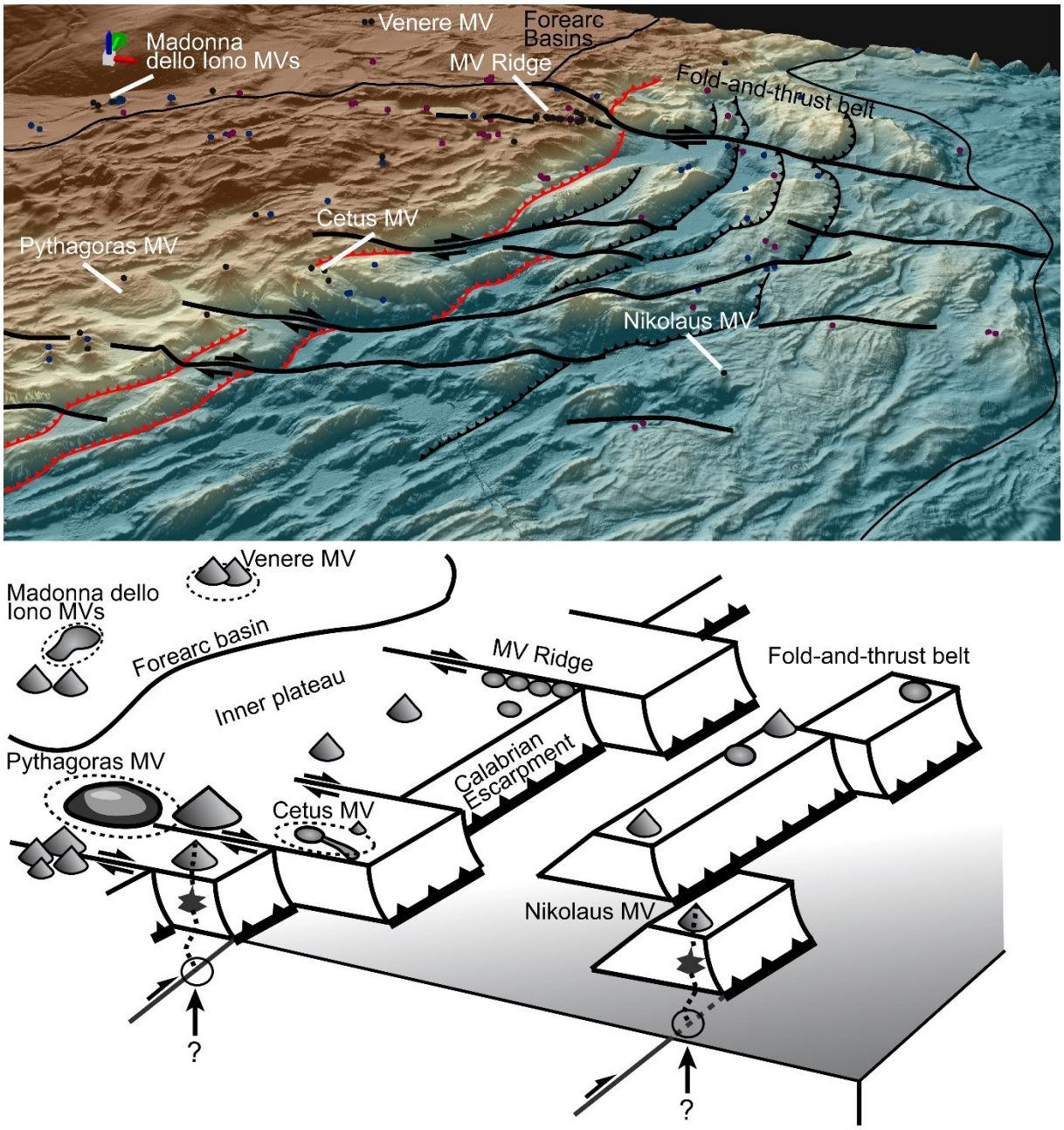


Fig. 9.6. Upper image: 3D-view on the central CAP with fold-and-thrust belt (Calabrian Escarpment thrust with red lie and teeth pointing downdip; seawards thrusts with black lines and teeth) disected by a transpressional system (dextral strike-slip in thick black lines); colored dots indicate MVs (black = confirmed; blue = high confidence; magenta = medium/low confidence; tectonic lineaments after Gutscher et al. (2017) and Polonia et al. (2011)); Lower image: conceptual sketch of the structural setting at the Calabrian Escarpment and one set of the fold-and-thrus belt; MV locations are schematic to show structural alignment with strike-slip features at the Calabrian Escarpment. Question marks indicate that the fluid migration pathway at thrust intersection is unclear but do not follow the thrust plane to the surface.

## 9.5. Conclusions and Outlook

Most MVs in the Mediterranean occur in remote deep-sea environments where geophysical techniques such as mapping by multibeam echosounders or sub-bottom (seismic) profilers has proven to be essential for the efficient and systematic identification of extrusive features

and gas seepage sites (Fusi and Kenyon, 1996; Ceramicola et al., 2014b; Mascle et al., 2014). The preliminary investigations presented here was so far limited to a bathymetry and backscatter dataset but already led to the identification of two new MV areas: 1) seaward of the Calabrian Escarpment (referred to as the fold-and-thrust belt), and 2) in the SW region of the inner plateau. MVs are apparently even more widely distributed across the CAP than previously recognized and activity along strike-slip faults may provide alternative fluid migration pathways to the out-of-sequence thrusts previously favored.

By including analyses of the existing sub-bottom (Parasound) profile data from the survey lines during the M112 cruise (e.g. Fig. 9.7), a more reliable identification of some of the medium-low confidence MVs could be achieved. The study of sub-bottom data may help to identify potentially buried mudflows but careful analyses or even ground truthing are required to differentiate mudflows from mass transport deposits related to the dynamic sediment transport processes known from the area (e.g. Polonia et al. (2013)).

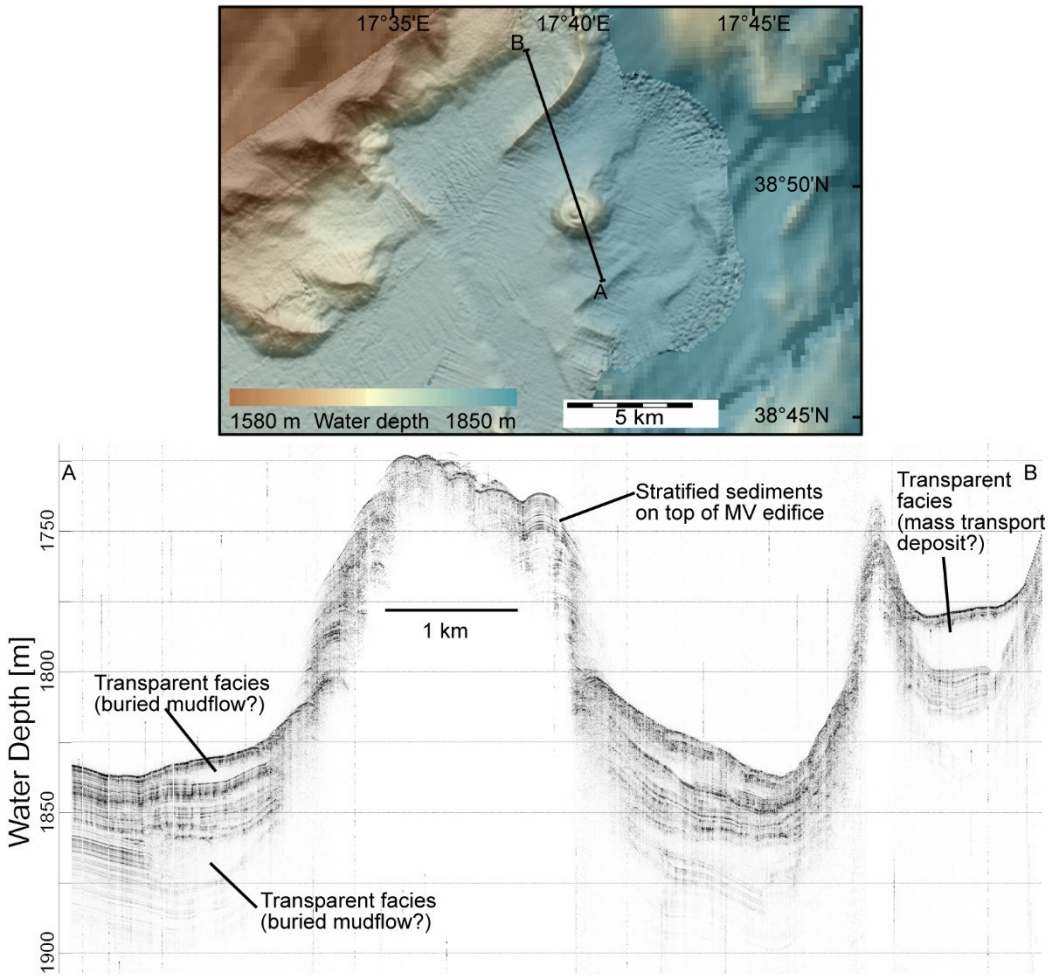


Fig. 9.7. Bathymetry (upper image) and sub-bottom profile (lower image, from A to B in upper image) of Minerva MV located in forearc basin of the CAP (see Fig. 9.1 for location).

It is proposed to follow the approach outlined by Ceramicola et al. (2014b) who suggested a systematic characterization based on the following criteria: 1) MVs geologically proven by sediment cores containing mud breccia; 2) MVs geophysically inferred by a combination of morphology, backscatter, or unstratified acoustic facies in subbottom profiles. Ground truthing of several of the new potential MVs in the newly identified regions will be needed, however. For a more qualitative dataset concerning the so far identified MVs it will be required to systematically measure the height and width of the edifices and potentially even extract their volume from the bathymetry. This information could help to identify relationships between the different morpho-structural regions of the CAP and the appearance of the MVs. The great morphological diversity even at neighboring MVs remains an unresolved question. Given the anomalous backscatter signatures of most MVs the areal extent of the most recent mud breccia extrusions could be obtained by mapping the corresponding backscatter patches. These datasets would complement the already existing but very general age estimates of the most recent MV activity spanning the last 56 ka (Ceramicola et al., 2014b). Estimates of the volumes and rates of mud breccia extrusion could provide first order information on the amount and intensity of mud volcanism across the respective morpho-structural zones of the CAP. Such data are only available for few submarine MV provinces so far (Rabaute and Chamot-Rooke, 2007) and a systematic hydroacoustic mapping approach may even prove to be more feasible than a similar endeavor for terrestrial regions.

# 10. Conclusions and outlook

## 10.1. Summary of conclusions

This cumulative dissertation investigated past and current fluid seepage related to Venere mud volcano (MV) and associated peripheral seeps in the Calabrian Accretionary Prism (CAP, Central Mediterranean). The entire work focused on detailed seafloor mapping at different scales: the regional MV distribution in the CAP (based on bathymetry and backscatter maps at tens of meters resolution), Venere MV as an individual structure (based on bathymetry and backscatter maps at meter-scale resolution), and the extrusion sites of mud breccia and cold seeps with chemosynthesis-based organisms, authigenic carbonates, and sites of gas bubble emissions (based on seafloor images with up to centimeter-scale resolutions). The observations and maps are complemented by sub-bottom profiles and geological samples including sediments, gas, and pore water. These data result from two research cruises: RV METEOR cruise M112 and RV POSEIDON cruise POS499 visiting the CAP in 2014 and 2016, respectively. In a forearc basin of the CAP, active gas bubble emissions and freshly extruded mud breccia were recognized for the first time at Venere MV during M112. AUV- (autonomous underwater vehicle) and ROV- (remotely operated vehicle) investigations revealed the detailed structure of Venere MV. They revealed recent mudflows from one of the two ca. 100 m high cones, peripheral seeps along a ring-fault system of a subsidence caldera ca. 3000 m in diameter, and bedforms in Squillace Canyon in the surrounding of the MV edifice.

The aim of the first manuscript in this work was to deepen the knowledge on processes potentially underlying mud volcanism including the sources, depths, and migration paths of fluids and solids by characterizing the ongoing discharge dynamics at Venere MV. The second manuscript of this work focused on the sediments and detailed morphology and backscatter characteristics of Venere MV, its mudflows, and bedforms in the surrounding canyon. The goal was to unravel the development of the respective surface expressions over time and potentially estimate the amounts of extruded material. In the third manuscript, the aim was to develop an understanding on the processes which led to the formation of the cold seep structures along the periphery of Venere MV by creating photo mosaics and by visually mapping different seafloor facies.

The most important conclusions that can be drawn from the three manuscripts presented in this thesis are summarized and represented in Fig. 10.1. Mud volcanism at Venere MV is characterized by the extrusion of warm mud breccia (up to 13 °C warmer than background temperatures), that contains thermogenic hydrocarbons (2.7 times oversaturated in methane) and strongly freshened pore water. Gas flares occur at the summit and along four peripheral seeps, which are additionally characterized by authigenic carbonate deposits and chemosynthesis-based communities. Methane release at the peripheral seeps occurred along ring faults, clearly associated to caldera formation. The ring faults are interpreted to provide migration pathways for gas (but not mud breccia) which has been diverted from the main conduit at a specific depth–a zone of critical pore fluid pressures where gas an migrate

laterally–to the periphery of the mud volcano. A conceptual model consisting of an upward-branching plumbing system is proposed for Venere MV. Thermogenic organic matter degradation and mineral dehydration processes are interpreted to indicate a deep source (>3.5 km) below the forearc basin of the CAP. The fluids do not indicate interaction with Messinian salts, which seem to be absent or may have been removed during persistent fluid flow over the past.

The surface of Venere MV consists of numerous, elongate, partially overlapping mudflows. Their relative, stratigraphic succession and extent was mapped based on AUV-derived bathymetry and backscatter data. Morphological change that occurred at the western summit of Venere MV between 2014 and 2016 could be evidenced by differential bathymetry. The recent sedimentation rate (0.17–0.19 mm/year) was determined in the study area in addition to the amount of hemipelagic sediments overlying different mudflows. The emplacement ages of investigated mudflows span about 4000 years until present. It could be calculated that flows of 1–10*$10^6$ $m^3$ volume were extruded at average rates estimated to have ranged between 5000–47000 $m^3$/year in the last 882 years. The structure of the mudflows point to a non-explosive, moderate, but persistent extrusive behavior of Venere MV. The twin-cones of Venere MV are large edifices (ca. 178*$10^6$ $m^3$) similar to known MVs offshore or on land (Table 10.1). Such comparisons are difficult, however, since published volumes of MV structures (mainly resulting from seismic investigations) tend to include subsurface deposits (e.g. Kirkham et al. (2017)), which are presently unknown for Venere MV. The extrusion rates estimated for Venere MV, however, are comparable to published values for the pie-shaped Napoli and Milano MVs and the flat Haakon Mosby MV (Table 10.1). Volume estimates from cone-shaped edifices have been lacking in the literature so far and the values obtained in this study for Venere MV, are a valuable addition to the few available datasets, where both a surface-edifice volume and estimates on extrusion rates are available. Erosive scours, cyclic steps, and sediment waves in the surrounding of Venere MV indicate that gravity-driven sediment-transport processes occurred in the canyon and spilled across the canyon levees. They seem to have influenced the overall morphology of the MV but in turn, the MV deflected the sediment flows and acted as an obstacle.

Chemosynthesis-based ecosystem diversity is high at the peripheral seeps of Venere MV and includes the presence of microbial mats, vesicomyid clams, and tubeworms living in close association with authigenic carbonate deposits. The seafloor facies could be well documented and mapped by photo mosaics covering different areas influenced by ongoing or past methane seepage. The benthic organisms depend on methane supply from below and downward diffusion of seawater sulfate that supports the anaerobic oxidation of methane (AOM) and precipitation of authigenic carbonates. Carbonate formation apparently seals off the seafloor, diminishing fluid flow and sulfate supply, by forming extensive pavements. The pavements trap gas in sufficient quantities to support gas hydrate formation. This local gas-saturated reservoir induces an upward buoyancy force on the sediments and carbonates, which eventually causes the carbonates to break. Crater-like collapse structures suggest an instable seafloor in these areas. Along carbonate fractures, seepage and infiltration of

seawater sulfate may occur supporting the re-colonization of carbonate fractures by chemosynthesis-based organisms. In this study, a temporal development from plain seepage to colonized features is proposed, which culminates in rupture formation and possibly seafloor collapse over timescales of decades, centuries, and millennia, respectively.

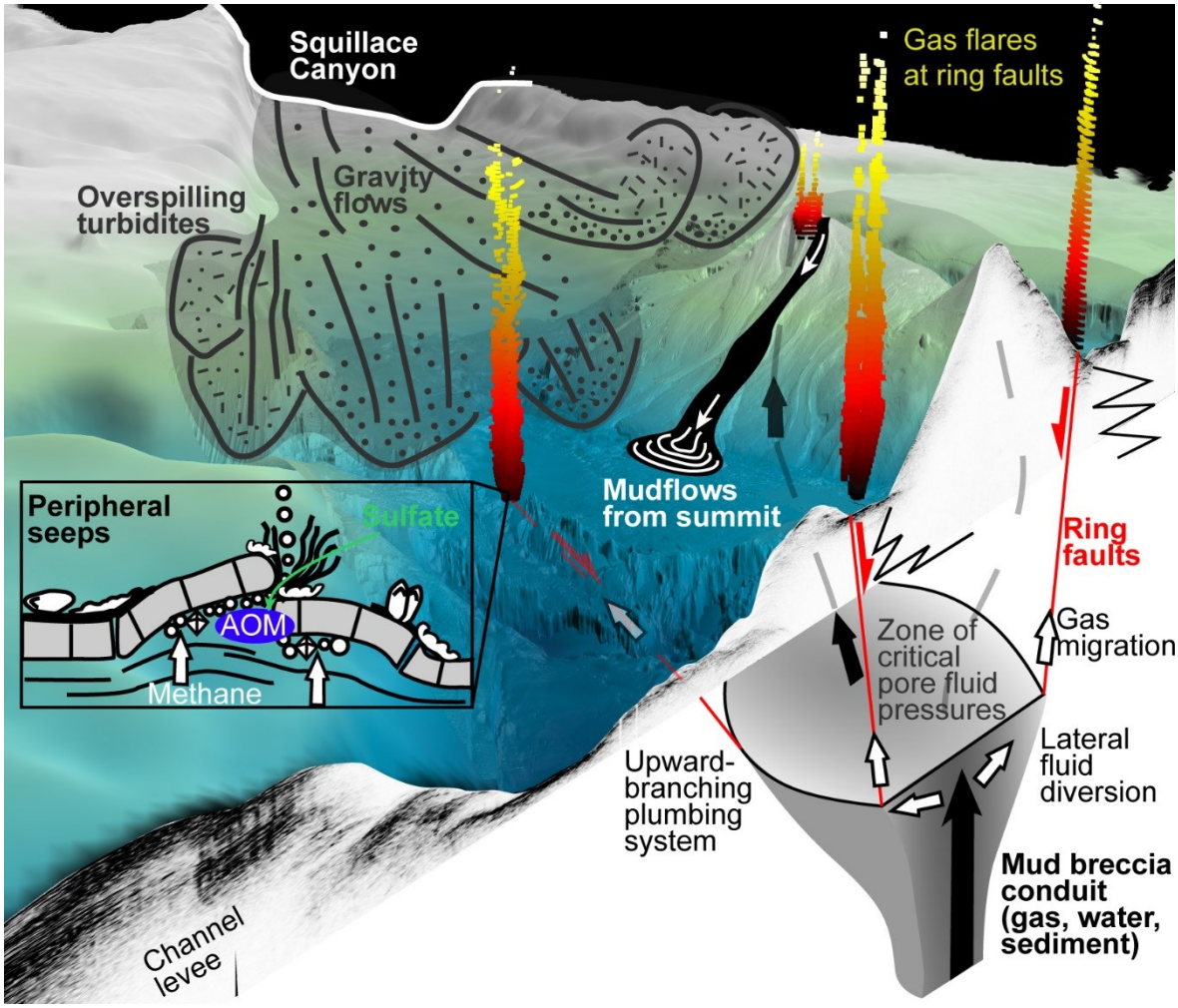


Fig. 10.1. Summary of the main results of this work showing AUV-based bathymetry draped on ship-based bathymetry cut by parasound profile (v.e. ~10x) with gas flares and cartoons (not to scale) of geological processes at Venere MV and Squillace Canyon; Venere MV is sourced by fluid-rich mud breccia (thick, black arrows), which originates at depth and is extruded at the western summit as mudflows (old mudflow deposits indicated by wedge-shape black lines in subsurface of the eastern cone). Gas (thick, white arrows) migrates from a zone of critical pore fluid pressures, along ring faults that constitute an upward-branching plumbing system. Gas emission occurs at peripheral seeps where carbonate mounds and rich chemosynthesis-based ecosystems (dependent on AOM) are sustained. Gravity-driven sediment transport occurs along Squillace Canyon, encounters Venere MV as an obstacle, and overspills the channel levees.

In a separate study, a photo mosaic from the active western summit of Venere MV has been analyzed, which documents the patterns of fresh, elongate mud breccia flows on the seafloor for the first time. The surface structure of these flows shows regular mud-crack patterns that appear to form by degassing and dewatering while the mudflow progressively moves downslope. Crevasses, furrows, and ridges closely resemble structures observed on (rock-) glaciers. The high-resolution images suggest differential motion and variations in mud

breccia composition on the outside compared to the inside to mudflows. Although these results will require additional analyses, they provide insights into the flow behavior of mud breccia at the seafloor.

In a final study, the distribution of MVs across the morpho-structural zones of the CAP was reinvestigated. A detailed analysis of newly acquired ship-based bathymetry and backscatter data of the CAP (with higher resolutions than previously available), not only confirmed most of the MVs known to occur in the inner pre-Messinian prism and the forearc basins, but led to the identification of two new potential MV provinces. The first province is an area in the outer pre-Messinian prism and the second is located in the southwestern part of the inner pre-Messinian prism and forearc basins. Their presence confirms the wide-spread nature and importance of focused fluid flow across large areas such as accretionary prisms. Although not all of the potential MVs have been geologically proven by ground-truthing yet, they may provide a key to address remaining questions regarding the relationship of out-of-sequence thrusting, strain partitioning, and fluid migration pathways along strike-slip faults in the CAP.

In summary, the relevance of the results presented in this work are not geographically restricted to the CAP but deepen our knowledge of fluid-seep systems and mud volcanism in general. Venere MV shows a persistent but moderate extrusive activity and caldera collapse as opposed to short-lived, violent eruptions, which are so far documented or hypothesized for most MVs on land or offshore, respectively. Caldera subsidence and ring faulting are relevant for the potential development of cold-seep ecosystems at the periphery of submarine MVs. It is shown for the first time that MV edifices can influence the flow dynamics of turbidity currents. The evolution of Venere MV highlights long-term interactions between fluid seepage, sediment extrusion, and sediment transport in submarine canyons. Cold-seep ecosystems clearly evolve over time and involve dynamic processes of gas accumulation and bubble release as well as self-sealing by carbonate precipitation, doming, rupturing, and possibly seafloor collapse. The unique insights on submarine mudflows, cold-seep ecosystems, and canyon morphologies document that the use of AUV- and ROV-based seafloor technologies pave the way for new and exciting scientific results. This work has permanently improved our understanding of one of the least explored regions on our planet by bringing light (and sound) for a short time into to a usually dark and remote environment in the deep sea.

Table 10.1. Comparison of MV sizes and extrusion volumes from the literature (grouped by region on- and offshore) and results from this work (dark green shading); most relevant comparisons are shaded in light green.

| Region | Site or MV name | Onshore or offshore | Size of MV ($x10^6$ $m^3$) | Extrusion volume ($m^3$) | Time | Event type | Reference |
|---|---|---|---|---|---|---|---|
| S Caspian Basin | Chirag MV | onshore | 22500 | | | long phases of activity | Stewart and Davies 2006 |
| S Caspian Basin | Azeri MV | onshore | 2750 | | | MV plumbing system | Stewart and Davies 2006 |
| S Caspian Basin | Azeri MV | onshore | 4100 | | | MV plumbing system | Stewart and Davies 2006 |
| S Caspian Basin | Gunashli | onshore | 2100 | | | MV plumbing system | Stewart and Davies 2006 |
| S Caspian Basin | Gunashli | onshore | 2100 | | | MV plumbing system | Stewart and Davies 2006 |
| NDSF (western province) | 386 MVs | offshore (min. value) | 100 | | | MV plumbing system | Kirkham et al. 2017 |
| NDSF (western province) | 386 MVs | offshore (max. value) | 3300 | | | MV plumbing system | Kirkham et al. 2017 |
| Azerbaijan | Airantekyan MV | onshore | 2415 | | | surface edifice vol.? | Kholodov 2002 |
| Azerbaijan | Bol'shoi Kyanizadagh MV | onshore | 735 | | | surface edifice vol.? | Kholodov 2002 |
| Azerbaijan | Touragay MV | onshore | *343 | | | surface edifice vol. | Kholodov 2002 |
| Calabrian Accretionary Prism | Venere MV (both cones) | offshore (min. value) | *178 | 5000 | year | average extrusion rate | This study |
| | | offshore (max. value) | *178 | 47000 | year | average extrusion rate | This study |
| Mediterranean Ridge | Milano MV | offshore (min. value) | 3400 | 2000 | year | average extrusion rate | Kopf 1999; Wallmann et al. 2006 |
| Mediterranean Ridge | Milano MV | offshore (max. value) | 7900 | 8000 | year | average extrusion rate | Kopf 1999; Wallmann et al. 2006 |
| Mediterranean Ridge | Napoli MV | offshore (min. value) | 9500 | 6000 | year | average extrusion rate | Kopf 1999; Wallmann et al. 2006 |
| Mediterranean Ridge | Napoli MV | offshore (max. value) | 14600 | 15000 | year | average extrusion rate | Kopf 1999; Wallmann et al. 2006 |
| Mediterranean Ridge | 215 mudflows | offshore | | 657000000000 | 37-60 kyr activity at backstop | | Rabaute and Chamot-Rooke 2007 |
| | | | | 51000 to 83000 | year | normalized/average of | Rabaute and Chamot-Rooke 2007 |
| Barents Sea | Haakon Mosby MV | offshore (min.) | | 10000 | year | mass outflow | Kaul et al. 2006 |
| Barents Sea | Haakon Mosby MV | offshore (max.) | | 30000 | year | mass outflow | Kaul et al. 2006 |
| Barents Sea | Haakon Mosby MV | offshore | | 128000000 | ca. 30 kyr long activity phase | | Perez-Garcia et al. 2009 |
| | | | | 4267 | year | normalized/average of | Perez-Garcia et al. 2009 |
| Makran | Malan Island | offshore | | 160000 | days | island-forming event | Delisle et al. 2002 |
| Makran | Chandragup I | onshore | | 1.4 | 1 hour | slow mud discharge | Delisle et al. 2002 |
| Timor Island | Waimata Valley volcano | onshore | | 1500000 | <1 h | eruption | Dimitrov 2002 |
| Trinidad | Piparo MV | onshore | | >100000 | days | catastrophic | Deville and Guerlais 2009 |
| Trinidad | Chatham MV | onshore | | 250000 | days | catastrophic | Deville and Guerlais 2009 |
| Trinidad | Tabaquite MV | onshore | | 400000 | 20 min | catastrophic | Deville and Guerlais 2009 |
| Indonesia | Lusi MV | onshore (min.) | | 50000 | day | eruption | Istadi et al. 2009 |
| Indonesia | Lusi MV | onshore (max.) | | 156000 | day | eruption | Istadi et al. 2009 |
| Azerbaijan | Lokbatan | onshore | | 300000 | 30 min | single mudflow | Planke et al. 2003 |
| Azerbaijan | Kotur-Dagh MV | onshore | | 630000000 | 1 year | blowout eruption | Kholodov 2002 |
| Kerch | Bulganak MV | onshore | | 5000 liters | day | fluid mud | Kholodov 2002 |
| *(asterisk) marks values for surface edifice volumes such as determined for Venere MV; MV sizes in the reviewed literature mostly refer to values including buried mud breccia deposits and the plumbing system or it is not clear | | | | | | | |

## 10.2. Outlook

A wealth of data and investigations exist on both terrestrial and offshore MVs globally. The more numerous seafloor MVs and their potentially associated cold-seep ecosystems, however, are only slowly emerging into view with advancements in state-of-the-art MBES mapping technologies. In addition to simply studying their morphology and structure, it is important to improve the constraints on the state and activity in terms of fluid and sediment discharge. In the CAP, for example, estimates of the volumes and rates of mud breccia extrusion will provide first order information on the amount and intensity of mud volcanism in the different morpho-structural zones. Comparable data are only available for few submarine MV provinces (e.g. the Mediterranean Ridge; (Rabaute and Chamot-Rooke, 2007)) and a systematic hydroacoustic mapping approach may even prove to be more feasible than a similar endeavor for terrestrial regions. To investigate MV evolution and dynamics requires detailed morphological analyses, subbottom data, and supporting information about the properties and composition of extrusive products. A large number of parameters possibly influence the appearance of any individual MV and its mudflows and geotechnical properties of mud breccia may help to elucidate flow behavior. Although gas hydrate occurrences have so far only been documented at a few MVs in the warm Mediterranean Sea they represent a natural laboratory to study gas hydrate behavior close to the stability boundary. With this regard, more investigations are needed to test if (and if yes, how) gas hydrate deposits in the subsurface play a role in sustaining cold-seep ecosystems by a consistent methane supply as opposed to intermittent gas pulses observed at many cold seeps today.

## 11. Acknowledgements

Before concluding, I would like to express my thankfulness to all people involved and supportive of my PhD. Without you, writing this thesis would never have gone as smooth as it did and I feel that I would have had a much harder three years than those I experienced.

I thank my doctor father Prof. Dr. Gerhard Bohrmann for all his support and guidance and for always having an open door to take his time for my questions. I greatly appreciated that you shared your ideas and your advice but still let me follow the scientific objectives I was most interested in including the fantastic research expeditions you invited me to join. I also appreciate Prof. Dr. Helmut Weissert for his openness and interest to act as my second thesis reviewer. I am convinced that your guidance in the mountainous Zwinglipass already laid the foundation that I would eventually find my way to science in the deep sea. I would like to thank Dr. Heiko Sahling as my second supervisor for his guidance at any time and his help in finding the best story to tell with a manuscript and his keen eye for details geologically, biologically, and editorially. I greatly appreciate the support of Prof. Dr. Marta Torres, Dr. Miriam Römer, Dr. David Völker, and Dr. Jürgen Pätzold, for their support as my GLOMAR thesis committee.

My thanks also go to the whole working group for the pleasant atmosphere both scientifically and socially during my PhD and specifically during the research cruises. I am greatly thankful to Miriam Römer for sharing her passion about gas bubbles, for all her constructive thoughts, as well as support of my work, and for being a great friend and fellow adventuress. I thank Dr. Thomas Pape for the discussions, his insight, and his always open ear for my questions on gas geochemistry or other on- and off-topic issues. Dr. Susan Mau, Dr. Yann Marcon, Paul Wintersteller, Christian dos Santos Ferreira, Janice Malnati, Angelika Rinkel, and Greta Ohling are thanked for their dedication and help in technical aspects on board the cruises, in the lab, or in the office but also for the many fun experiences we shared during my time in this working group. Specifically, I mention my close friends Patrizia Geprägs and Chieh-Wei (Jeff) Hsu with whom I shared innumerous hours of concentrated work, intense discussions, and boisterous laughter both in the office and on the cruises. I would also like to express my appreciation to now former members of the group, namely Jan-Hendrik Körber, Stefanie Buchheister and Sven Klüber. A special thank you goes to Dr. Daniel Praeg and his multi-facetted insights and critical ideas, which he so enthusiastically and willingly shared with me during numerous exchanges. I also appreciate Dr. Silvia Ceramicola for her hospitality during our visit to Trieste and her support on board cruise POS499. Dr. Andreas Klügel is thanked for his technical help with the tephra analysis and identification.

Lastly, I thank all my friends and family for their whole-hearted support, interest, and appreciation of my work. My Mum and Dad and my grandparents for being such great role models. Most importantly, I appreciate the unconditional support from my future wife Aline Clalüna. She had to share my passion – but not my love – for her with a deep-sea mud volcano for three years but of course she is and always will be the unabated Venus in my eyes.

## 12. References

Abegg, F., Hohnberg, H. J., Pape, T., Bohrmann, G., and Freitag, J., 2008, Development and application of pressure-core-sampling systems for the investigation of gas- and gas-hydrate-bearing sediments: Deep Sea Research Part I: Oceanographic Research Papers, v. 55, no. 11, p. 1590-1599, doi: 10.1016/j.dsr.2008.06.006.

Aloisi, G., Bouloubassi, I., Heijs, S. K., Pancost, R. D., Pierre, C., Damsté, J. S. S., Gottschal, J. C., Forney, L. J., and Rouchy, J.-M., 2002, CH4-consuming microorganisms and the formation of carbonate crusts at cold seeps: Earth and Planetary Science Letters, v. 203, p. 195-203

Aloisi, G., Pierre, C., Rouchy, J.-M., Foucher, J.-P., Woodside, J., and Party, M. S., 2000, Methane-related authigenic carbonates of eastern Mediterranean Sea mud volcanoes and their possible relation to gas hydrate destabilisation: Earth and Planetary Science Letters, v. 184, p. 321-338

Ambrosetti, P., Bosi, C., Carraro, F., Ciaranfi, N., Panizza, M., Papani, G., Vezzani, L., and Zanferrari, A., 1983, Neotectonic map of Italy, scale 1: 500,000 (sheet 6). Consiglio Nazionale delle Ricerche; Quaderni della Ricerca Scientifica vol 4, no 114.

Antonioli, F., Ferranti, L., Lambeck, K., Kershaw, S., Verrubbi, V., and Pra, G. D., 2006, Late Pleistocene to Holocene record of changing uplift rates in southern Calabria and northeastern Sicily (southern italy, Central Mediterranean Sea): Tectonophysics, v. 422, no. 1-4, p. 23-40, doi: 10.1016/j.tecto.2006.05.003.

Archer, D., 2007, Methane hydrate stability and anthropogenic climate change: Biogeosciences, v. 4, no. 4, p. 521-544

Bahr, A., Pape, T., Abegg, F., Bohrmann, G., van Weering, T., and Ivanov, M. K., 2010, Authigenic carbonates from the eastern Black Sea as an archive for shallow gas hydrate dynamics - Results from the combination of CT imaging with mineralogical and stable isotope analyses: Marine and Petroleum Geology, v. 27, no. 9, p. 1819-1829, doi: 10.1016/j.marpetgeo.2010.08.005.

Bahr, A., Pape, T., Bohrmann, G., Mazzini, A., Haeckel, M., Reitz, A., and Ivanov, M., 2007, Authigenic carbonate precipitates from the NE Black Sea: a mineralogical, geochemical, and lipid biomarker study: International Journal of Earth Sciences, v. 98, no. 3, p. 677, doi: 10.1007/s00531-007-0264-1.

Barbieri, F., Morlotti, E., Poerio, L., Raffi, I., and Torelli, L., 1982, Dati geologici preliminari sulbacino di Crotone-Spartivento (Mar Ionio): Acta Naturalia de l'Ateneo Parmense, v. 18, p. 141–155

Barry, M. A., Boudreau, B. P., and Johnson, B. D., 2012, Gas domes in soft cohesive sediments: Geology, v. 40, no. 4, p. 379-382, doi: 10.1130/G32686.1.

Bayon, G., Henderson, G. M., and Bohn, M., 2009, U-Th stratigraphy of a cold seep carbonate crust: Chemical Geology, v. 260, no. 1-2, p. 47-56, doi: 10.1016/j.chemgeo.2008.11.020.

Beal, E. J., House, C. H., and Orphan, V. J., 2009, Manganese- and Iron-Dependent Marine Methane Oxidation: Science, v. 325, no. 5937, p. 184-187, doi: 10.1126/science.1169984.

Bernard, B., Brooks, J. M., and Sackett, W. M., 1977, A Geochemical Model For Characterization Of Hydrocarbon Gas Sources In Marine Sediments, doi: 10.4043/2934-MS.

Biju-Duval, B., Dercourt, J., and Le Pichon, X., 1977, From the tethys ocean to the mediterranean seas: a plate tectonic model of the evolution of the western alpine system: International symposium on the structural history of the Mediterranean basins (Split, 1976), p. 143-164

Blumenberg, M., Pape, T., Seifert, R., Bohrmann, G., and Schlömer, S., 2017, Can hydrocarbons entrapped in seep carbonates serve as gas geochemistry recorder?: Geo-Marine Letters, doi: 10.1007/s00367-017-0522-6.

Boetius, A., et al., 2000, A marine microbial consortium apparently mediating anaerobic oxidation of methane: Nature, v. 407, no. 6804, p. 623-626, doi: 10.1038/35036572.

Bohrmann, G., et al., 2014, Report and Preliminary Results of R/V POSEIDON Cruise P462, Izmir - Izmir, 28 October - 21 November, 2013. Gas Hydrate Dynamics of Mud Volcanoes in the Submarine Anaximander Mountains (Eastern Mediterranean): Berichte, MARUM â Zentrum für Marine Umweltwissenschaften, Fachbereich Geowissenschaften, Universität Bremen, v. 300

Bohrmann, G., et al., 2015, Report and preliminary results of R/V METEOR cruise M112, Dynamic of Mud Volcanoes and Seeps in the Calabrian Accretionary Prism, Ionian Sea, Catania (Italy) – Catania (Italy), November 6 – December 15, 2014: Berichte, MARUM – Zentrum für Marine Umweltwissenschaften, Fachbereich Geowissenschaften, Universität Bremen, v. No. 306, p. 217

Bohrmann, G., et al., 2016, Report and preliminary results of R/V POSEIDON cruise POS499, Calabrian Mud Volcanoes, Catania (Italy) – Catania (Italy), 04 May – 22 May, 2016: Berichte, MARUM – Zentrum für Marine Umweltwissenschaften, Fachbereich Geowissenschaften, Universität Bremen, v. No. 311, p. 76

Bohrmann, G., Greinert, J., Suess, E., and Torres, M., 1998, Authigenic carbonates from the Cascadia subduction zone and their relation to gas hydrate stability: Geology, v. 26, no. 7, p. 647-650, doi: Doi 10.1130/0091-7613(1998)026<0647:Acftcs>2.3.Co;2.

Bohrmann, G., et al., 2003, Mud volcanoes and gas hydrates in the Black Sea: new data from Dvurechenskii and Odessa mud volcanoes: Geo-Marine Letters, v. 23, p. 239-249

Bohrmann, G., and Torres, M. E., 2006, Gas Hydrates in Marine Sediments, *in* Schulz, H. D., and Zabel, M., eds., Marine Geochemistry: Berlin, Heidelberg, Springer Berlin Heidelberg, p. 481-512.

Bonini, M., 2007, Interrelations of mud volcanism, fluid venting, and thrust-anticline folding: Examples from the external northern apennines (emilia-romagna, Italy): Journal of Geophysical Research, v. 112

Bonini, M., 2008, Elliptical mud volcano caldera as stress indicator in an active compressional setting (Nirano, Pede-Apennine margin, northern Italy): Geology, v. 36, no. 2, p. 131-134, doi: 10.1130/G24158a.1.

Boudreau, B. P., et al., 2001, Permeable marine sediments: Overturning an old paradigm: EOS Transactions, v. 82, no. 11, p. 133-136

Boudreau, B. R., 2012, The physics of bubbles in surficial, soft, cohesive sediments: Marine and Petroleum Geology, v. 38, no. 1, p. 1-18, doi: 10.1016/j.marpetgeo.2012.07.002.

Breda, A., Mellere, D., and Massari, F., 2007, Facies and processes in a Gilbert-delta-filled incised valley (Pliocene of Ventimiglia, NW Italy): Sedimentary Geology, v. 200, no. 1-2, p. 31-55, doi: 10.1016/j.sedgeo.2007.02.008.

Brown, K. M., 1990, The nature and hydrogeologic significance of mud diapirs and diatremes for accretionary systems: Journal of Geophysical Research, v. 95, no. B6, p. 8969-8982

Buerk, D., Klaucke, I., Sahling, H., and Weinrebe, W., 2010, Morpho-acoustic variability of cold seeps on the continental slope offshore Nicaragua: Results of fluid flow interaction with sedimentary processes: Marine Geology, v. 275, p. 53-65, doi: 10.1016/j.margeo.2010.04.007.

Camerlenghi, A., Cita, M. B., Dellavedova, B., Fusi, N., Mirabile, L., and Pellis, G., 1995, Geophysical Evidence of Mud Diapirism on the Mediterranean Ridge Accretionary Complex: Marine Geophysical Researches, v. 17, no. 2, p. 115-141, doi: Doi 10.1007/Bf01203423.

Camerlenghi, A., Cita, M. B., Hieke, W., and Ricchiuto, T., 1992, Geological Evidence for Mud Diapirism on the Mediterranean Ridge Accretionary Complex: Earth and Planetary Science Letters, v. 109, no. 3-4, p. 493-504, doi: 10.1016/0012-821x(92)90109-9.

Canals, M., Puig, P., de Madron, X. D., Heussner, S., Palanques, A., and Fabres, J., 2006, Flushing submarine canyons: Nature, v. 444, p. 354-357

Capozzi, R., Artoni, A., Torelli, L., Lorenzini, S., Oppo, D., Mussoni, P., and Polonia, A., 2012, Neogene to Quaternary tectonics and mud diapirism in the Gulf of Squillace (Crotone-Spartivento Basin, Calabrian Arc, Italy): Marine and Petroleum Geology, v. 35, no. 1, p. 219-234, doi: 10.1016/j.marpetgeo.2012.01.007.

Caress, D. W., and Chayes, D. N., 1996, Improved processing of Hydrosweep DS multibeam data on the R/V Maurice Ewing: Marine Geophysical Researches, v. 18, no. 6, p. 631-650, doi: 10.1007/bf00313878.

Carter, L., Carter, R. M., Nelson, C. S., Fulthorpe, C. S., and Neil, H. L., 1990, Evolution of Pliocene to Recent Abyssal Sediment Waves on Bounty Channel Levees, New-Zealand: Marine Geology, v. 95, no. 2, p. 97-109, doi: 10.1016/0025-3227(90)90043-J.

Cartigny, M. J. B., Postma, G., van den Berg, J. H., and Mastbergen, D. R., 2011, A comparative study of sediment waves and cyclic steps based on geometries, internal structures and numerical modeling: Marine Geology, v. 280, no. 1-4, p. 40-56, doi: 10.1016/j.margeo.2010.11.006.

Catalano, S., and De Guidi, G., 2003, Late Quaternary uplift of northeastern Sicily: relation with the active normal faulting deformation: Journal of Geodynamics, v. 36, no. 4, p. 445-467, doi: 10.1016/S0264-3707(02)00035-2.

Ceramicola, S., Dupré, S., Somoza, L., and Woodside, J., 2018, Cold Seep Systems, *in* Micallef, A., Krastel, S., and Savini, A., eds., Submarine Geomorphology: Cham, Springer International Publishing, p. 367-387.

Ceramicola, S., Praeg, D., Coste, M., Forlin, E., Cova, A., Colizza, E., and Critelli, S., 2014a, Submarine Mass-Movements Along the Slopes of the Active Ionian Continental Margins and Their Consequences for Marine Geohazards (Mediterranean Sea): In: Krastel S, Behrmann J-H, Völker D, Stipp M, Berndt C, Urgeles R, Chaytor J, Huhn K, Strasser M, Bonnevie Harbitz C (eds) Submarine mass movements and their consequences, 6th International Symposium. Advances in Natural and Technological Hazards Research,, v. 37, no. Springer, Heidelberg, p. 295-306, doi: 10.1007/978-3-319-00972-8_26.

Ceramicola, S., Praeg, D., Cova, A., Accettella, D., and Zecchin, M., 2014b, Seafloor distribution and last glacial to postglacial activity of mud volcanoes on the Calabrian accretionary prism, Ionian Sea: Geo-Marine Letters, v. 34, no. 2-3, p. 111-129, doi: 10.1007/s00367-013-0354-y.

Cernobori, L., Hirn, A., McBride, J. H., Nicolich, R., Petronio, L., and Romanelli, M., 1996, Crustal image of the Ionian basin and its Calabrian margins: Tectonophysics, v. 264, no. 1-4, p. 175-189, doi: 10.1016/S0040-1951(96)00125-4.

Chamot-Rooke, N., Rangin, C., Le Pichon, X., and DOTMED Working Group, 2005, DOTMED: A Synthesis of Deep Marine Data in the Eastern Mediterranean: Mémoires de la Société géologique de France, v. 177, no. Portfolio of maps, p. 64 pp, 69 plates and CD

Charlou, J. L., Donval, J. P., Zitter, T., Roy, N., Jean-Baptiste, P., Foucher, J. P., Woodside, J., and Party, M. S., 2003, Evidence of methane venting and geochemistry of brines on mud volcanoes of the eastern Mediterranean Sea: Deep-Sea Research I, v. 50, p. 941-958

Cita, M., Ryan, W., and Paggi, L., 1981, Prometheus mud breccia: an example of shale diapirism in the Western Mediterranean Ridge: Ann Géol Pays Helléniques, v. 30, p. 543–557

Claypool, G. E., and Kvenvolden, K. A., 1983, Methane and Other Hydrocarbon Gases in Marine Sediment: Annual Review of Earth and Planetary Sciences, v. 11, p. 299-327, doi: 10.1146/annurev.ea.11.050183.001503.

Clayton, C., 1991, Carbon Isotope Fractionation during Natural-Gas Generation from Kerogen: Marine and Petroleum Geology, v. 8, no. 2, p. 232-240, doi: Doi 10.1016/0264-8172(91)90010-X.

Cordes, E. E., Arthur, M. A., Shea, K., Arvidson, R. S., and Fisher, C. R., 2005, Modeling the mutualistic interactions between tubeworms and microbial consortia: PLOS Biology, v. 3, no. 3, p. e77

Cordes, E. E., Bergquist, D. C., Shea, K., and Fisher, C. R., 2003, Hydrogen sulphide demand of long-lived vestimentiferan tube worm aggregations modifies the chemical environment at deep-sea hydrocarbon seeps: Ecology Letters, v. 6, p. 212-219

Coste, M., 2014, Les processus sédimentaires, depuis la pente continentale jusqu'au bassin, en contexte de tectonique active : analyse comparée entre la Marge Calabro-Ionienne et la Marge Ligure durant les derniers 5 Ma: Thèse de doctorat Géologie marine Nice, no. 2014NICE4021

D'Agostino, N., D'Anastasio, E., Gervasi, A., Guerra, I., Nedimovic, M. R., Seeber, L., and Steckler, M., 2011, Forearc extension and slow rollback of the Calabrian

Arc from GPS measurements: Geophysical Research Letters, v. 38, doi: 10.1029/2011gl048270.

Dählmann, A., and De Lange, G., 2003, Fluid-sediment interactions at Eastern Mediterranean mud volcanoes: a stable isotope study from ODP Leg 160: Earth and Planetary Science Letters, v. 212, p. 377-391, doi: 10.1016/S0012-821X(03)00227-9.

Dale, A. W., Van Cappellen, P., Aguilera, D. R., and Regnier, P., 2008, Methane efflux from marine sediments in passive and active margins: Estimations from bioenergetig reaction-transport simulations: Earth and Planetary Science Letters, v. 265, p. 329-344 doi: 10.1016/j.epsl.2007.09.026.

Damuth, J. E., 1979, Migrating Sediment Waves Created by Turbidity Currents in the Northern South China Basin: Geology, v. 7, no. 11, p. 520-523, doi: 10.1130/0091-7613(1979)7<520:Mswcbt>2.0.Co;2.

Dattagupta, S., Arthur, M. A., and Fisher, C. R., 2008, Modification of sediment geochemistry by the hydrocarbon seep tubeworm Lamellibrachia luymesi: A combined empirical and modeling approach: Geochimica Et Cosmochimica Acta, v. 72, no. 9, p. 2298-2315, doi: 10.1016/j.gca.2008.02.016.

Davidson, D. W., Leaist, D. G., and Hesse, R., 1983, Oxygen-18 enrichment in the water of a clathrate hydrate: Geochimica et Cosmochimica Acta, v. 47, p. 2293-2295, doi: 10.1016/0016-7037(83)90053-4.

Davies, R. J., and Stewart, S. A., 2005, Emplacement of giant mud volcanoes in the South Caspian Basin: 3D seismic refelction imaging of their root zones: Journal of the Geological Society, v. 162, p. 1-4

De Beer, D., Sauter, E., Niemann, H., Kaul, N., Foucher, J.-P., Witte, U., Schlüter, M., and Boetius, A., 2006, In situ fluxes and zonation of microbial activity in surface sediments of the Håkon Mosby Mud Volcano: Limnology and Oceanography, v. 51, no. 3, p. 1315-1331

de Voogd, B., Truffert, C., Chamot-Rooke, N., Huchon, P., Lallemant, S., and Le Pichon, X., 1992, Two-ship deep seismic soundings in the basins of the Eastern Mediterranean Sea (Pasiphae cruise): Geophysical Journal International, v. 109, no. 3, p. 536-552, doi: 10.1111/j.1365-246X.1992.tb00116.x.

Delisle, G., von Rad, U., Andruleit, H., von Daniels, C. H., Tabrez, A. R., and Inam, A., 2002, Active mud volcanoes on- and offshore eastern Makran, Pakistan: International Journal of Earth Sciences, v. 91, p. 93-110, doi: 10.1007/s005310100203.

Deville, É., Battani, A., Griboulard, R., Guerlais, S., Herbin, J. P., Houzay, J. P., Muller, C., and Prinzhofer, A., 2003, The origin and processes of mud volcanism: New insights from Trinidad: Subsurface Sediment Mobilization, v. 216, p. 475-490, doi: 10.1144/Gsl.Sp.2003.216.01.31.

Deville, É., Guerlais, S.-H., Lallemant, S., and Schneider, F., 2010, Fluid dynamics and subsurface sediment mobilization processes: an overview from Southeast Caribbean: Basin Research, v. 22, no. 4, p. 361-379, doi: 10.1111/j.1365-2117.2010.00474.x.

Deville, É., and Guerlais, S. H., 2009, Cyclic activity of mud volcanoes: Evidences from Trinidad (SE Caribbean): Marine and Petroleum Geology, v. 26, no. 9, p. 1681-1691

Devoti, R., Riguzzi, F., Cuffaro, M., and Doglioni, C., 2008, New GPS constraints on the kinematics of the Apennines subduction: Earth and Planetary Science Letters, v. 273, no. 1-2, p. 163-174, doi: 10.1016/j.epsl.2008.06.031.

Dewey, J. F., Helman, M. L., Knott, S. D., Turco, E., and Hutton, D. H. W., 1989, Kinematics of the western Mediterranean: Geological Society, London, Special Publications, v. 45, no. 1, p. 265-283, doi: 10.1144/gsl.sp.1989.045.01.15.

Dickens, G. R., 2003, Rethinking the global carbon cycle with a large, dynamic and microbially mediated gas hydrate capacitor: Earth and Planetary Science Letters, v. 213, p. 169-183

Dillon, W. P., Nealon, J. W., Taylor, M. H., Lee, M. W., Drury, R. M., and Anton, C. H., 2001, Seafloor Collapse and Methane Venting Associated with Gas Hydrate on the Blake Ridge: Causes and Implications to Seafloor Stability and Methanerelease, Natural Gas Hydrates: Occurrence, Distribution, and Detection, American Geophysical Union, p. 211-233.

Dimitrov, L. I., 2002, Mud volcanoes - the most important pathway for degassing deeply buried sediments: Earth-Science Reviews, v. 59, no. 1-4, p. 49-76, doi: 10.1016/S0012-8252(02)00069-7, Pii S0012-8252(02)00069-7.

Dubilier, N., Bergin, C., and Lott, C., 2008, Symbiotic diversity in marine animals: the art of harnessing chemosynthesis: Nat Rev Micro, v. 6, no. 10, p. 725-740

Dupré, S., et al., 2008, High-resolution mapping of large gas emitting mud volcanoes on the Egyptian continental margin (Nile Deep Sea Fan) by AUV surveys: Marine Geophysical Researches, v. 29, no. 4, p. 275-290, doi: 10.1007/s11001-009-9063-3.

Dupré, S., Mascle, J., Foucher, J.-P., Harmegnies, F., Woodside, J., and Pierre, C., 2014, Warm brine lakes in craters of active mud volcanoes, Menes caldera off NW Egypt: evidence for deep-rooted thermogenic processes: Geo-Marine Letters, p. 1-16, doi: 10.1007/s00367-014-0367-1.

Dupré, S., et al., 2007, Seafloor geological studies above active gas chimneys off Egypt (Central Nile Deep Sea Fan): Deep Sea Research Part I: Oceanographic Research Papers, v. 54, no. 7, p. 1146-1172

Eason, D. E., Dunn, R. A., Canales, J. P., and Sohn, R. A., 2016, Segment-scale variations in seafloor volcanic and tectonic processes from multibeam sonar imaging, Mid-Atlantic Ridge Rainbow region (35 degrees 45-36 degrees 35N): Geochemistry Geophysics Geosystems, v. 17, no. 9, p. 3560-3579, doi: 10.1002/2016gc006433.

Eddy Lee, Y. D., and George, R. A. T., 2004, High-resolution geological AUV survey results across a portion of the eastern Sigsbee Escarpment: Aapg Bulletin, v. 88, no. 6, p. 747-764

Egorov, A. V., Crane, K., Vogt, P. R., and Rozhkov, A. N., 1999, Gas hydrates that outcrop the sea floor: stability models: Geo-Marine Letters, v. 19, p. 89-96

Etiope, G., and Ciccioli, P., 2009, Earth´s Degassing: A Missing Ethane and Propane Source: Science, v. 323, p. 478, doi: 10.1126/science.1165904.

Etiope, G., Feyzullayev, A., and Baciu, C. L., 2009, Terrestrial methane seeps and mud volcanoes: A global perspective of gas origin: Marine and Petroleum Geology, v. 26, no. 3, p. 333-344, doi: 10.1016/j.marpetgeo.2008.03.001.

Etiope, G., Lassey, K. R., Klusman, R. W., and Boschi, E., 2008, Reappraisal of the fossil methane budget and related emission from geologic sources: Geophysical Research Letters, v. 35, no. 9, doi: 10.1029/2008gl033623.

Etiope, G., and Milkov, A. V., 2004, A new estimate of global methane flux from onshore and shallow submarine mud volcanoes to the atmosphere: Environmental Geology, v. 46, no. 8, p. 997-1002, doi: 10.1007/s00254-004-1085-1.

Evans, R. J., Stewart, S. A., and Davies, R. J., 2008, The structure and formation of mud volcano summit calderas: Journal of the Geological Society, v. 165, p. 769-780, doi: 10.1144/0016-76492007-118.

Faccenna, C., Becker, T. W., Lucente, F. P., Jolivet, L., and Rossetti, F., 2001, History of subduction and back-arc extension in the Central Mediterranean: Geophysical Journal International, v. 145, no. 3, p. 809-820, doi: 10.1046/j.0956-540x.2001.01435.x.

Faccenna, C., Funiciello, F., Civetta, L., D'Antonio, M., Moroni, M., and Piromallo, C., 2007, Slab disruption, mantle circulation, and the opening of the Tyrrhenian basins: Geological Society of America Special Paper, v. 418, doi: 10.1130/2007.2418(08).

Ferranti, L., Monaco, C., Antonioli, F., Maschio, L., Kershaw, S., and Verrubbi, V., 2007, The contribution of regional uplift and coseismic slip to the vertical crustal motion in the Messina Straits, southern Italy: Evidence from raised Late Holocene shorelines: Journal of Geophysical Research-Solid Earth, v. 112, no. B6, doi: 10.1029/2006jb004473.

Feseker, T., Boetius, A., Wenzhofer, F., Blandin, J., Olu, K., Yoerger, D. R., Camilli, R., German, C. R., and de Beer, D., 2014, Eruption of a deep-sea mud volcano triggers rapid sediment movement: Nat Commun, v. 5, p. 5385, doi: 10.1038/ncomms6385.

Feseker, T., Dählmann, A., Foucher, J. P., and Harmegnies, F., 2009a, In-situ sediment temperature measurements and geochemical porewater data suggest highly dynamic fluid flow at Isis mud volcano, eastern Mediterranean Sea: Marine Geology, v. 261, p. 128-137, doi: 10.1016/j.margeo.2008.09.003.

Feseker, T., Foucher, J. P., and Harmegnies, F., 2008, Fluid flow or mud eruptions? Sediment temperature distributions on Håkon Mosby mud volcano, SW Barents Sea slope: Marine Geology, v. 247, p. 194-207

Feseker, T., Pape, T., Wallmann, K., Klapp, S. A., Schmidt-Schierhorn, F., and Bohrmann, G., 2009b, The thermal structure of the Dvurechenskii mud volcano and its implications for gas hydrate stability and eruption dynamics: Marine and Petroleum Geology, v. 26, p. 1812-1823, doi: 10.1016/j.marpetgeo.2009.01.021.

Feseker, T., Wetzel, G., and Heesemann, B., 2012, Introducing the T-Stick: A new device for high precision in situ sediment temperature profile measurements: Limnology and Oceanography: Methods, v. 10, p. 31-40, doi: 10.4319/lom.2012.10.31.

Fildani, A., Normark, W. R., Kostic, S., and Parker, G., 2006, Channel formation by flow stripping: large-scale scour features along the Monterey East Channel and their relation to sediment waves: Sedimentology, v. 53, no. 6, p. 1265-1287, doi: 10.1111/j.1365-3091.2006.00812.x.

Fisher, C. R., Urcuyo, I. A., Simpkins, M. A., and Nix, E., 1997, Life in the slow lane: growth and longevity of cold-seep Vestimentiferans: Marine Ecology, v. 18, no. 1, p. 83-94

Flood, R. D., 1983, Classification of Sedimentary Furrows and a Model for Furrow Initiation and Evolution: Geological Society of America Bulletin, v. 94, no. 5, p. 630-639, doi: 10.1130/0016-7606(1983)94<630:Cosfaa>2.0.Co;2.

Flood, R. D., 1994, Abyssal Bedforms as Indicators of Changing Bottom Current Flow - Examples from the Us East-Coast Continental Rise: Paleoceanography, v. 9, no. 6, p. 1049-1060, doi: 10.1029/94pa01801.

Floodgate, G. D., and Judd, A. G., 1992, The origins of shallow gas: Continental Shelf Research, v. 12, no. 10, p. 1145-1156

Formolo, M. J., Lyons, T. W., Zhang, C., Kelley, C. A., Sassen, R., Horita, J., and Cole, D. R., 2004, Quantifying carbon sources in the formation of authigenic carbonates at gas hydrate sites in the Gulf of Mexico: Chemical Geology, v. 205, p. 253-264

Foucher, J.-P., Dupré, S., Scalabrin, C., Feseker, T., Harmegnies, F., and Nouzé, H., 2010, Changes in seabed morphology, mud temperature and free gas venting at the Håkon Mosby mud volcano, offshore northern Norway, over the time period 2003–2006: Geo-Marine Letters, v. 30, no. 3, p. 157-167, doi: 10.1007/s00367-010-0193-z.

Foucher, J.-P., et al., 2009, Structure and Drivers of Cold Seep Ecosystems: Oceanography, v. 22, no. 1, p. 92-109

Frehner, M., Ling, A. H. M., and Gartner-Roer, I., 2015, Furrow-and-Ridge Morphology on Rockglaciers Explained by Gravity- Driven Buckle Folding: A Case Study From the Murtel Rockglacier (Switzerland): Permafrost and Periglacial Processes, v. 26, no. 1, p. 57-66, doi: 10.1002/ppp.1831.

Friedman, I., and O'Neil, J. R., 1977, Compilation of stable isotope fractionation factors of geochemical interest: U. S. Geol. Surv. Prof. Pap. 440-KK. U.S. Geological Survey, Reston, VA.

Fukushima, Y., Mori, J., Hashimoto, M., and Kano, Y., 2009, Subsidence associated with the LUSI mud eruption, East Java, investigated by SAR interferometry: Marine and Petroleum Geology, v. 26, no. 9, p. 1740-1750

Fusi, N., and Kenyon, N. H., 1996, Distribution of mud diapirism and other geological structures from long-range sidescan sonar (GLORIA) data, in the Eastern Mediterranean Sea: Marine Geology, v. 132, p. 21-38

Fusi, N., Savini, A., and Corselli, C., 2006, Evidence of mud diapirism and coral colonies in the Ionian Sea (Central Mediterranean) from high resultion chirp sonar survey: Annals of Geophysics, v. 49, no. 2-3, p. 751-765

Galindo-Zaldivar, J., Nieto, L., and Woodside, J., 1996, Structural features of mud volcanoes and the fold system of the Mediterranean Ridge, south of Crete: Marine Geology, v. 132, p. 95-112

Gay, A., Lopez, M., Berndt, C., and Seranne, M., 2007, Geological controls on focused fluid flow associated with seafloor seeps in the Lower Congo Basin: Marine Geology, v. 244, no. 1-4, p. 68-92, doi: 10.1016/j.margeo.2007.06.003.

Ge, Z., Nemec, W., Gawthorpe, R. L., and Hansen, E. W. M., 2017, Response of unconfined turbidity current to normal-fault topography: Sedimentology, v. 64, no. 4, p. 932-959, doi: 10.1111/sed.12333.

Gennari, G., Spezzaferri, S., Comas, M. C., Rüggeberg, A., Lopez-Rodriguez, C., and Pinheiro, L. M., 2013, Sedimentary sources of the mud-breccia and mud volcanic activity in the Western Alboran Basin: Marine Geology, v. 339, p. 83-95, doi: 10.1016/j.margeo.2013.04.002.

Gennesseaux, M., and Winnock, E., 1993, Thickness of Mediterranean Plio-Quaternary sediments: Intergovernmental Oceanographic Commission (UNESCO), International Bathymetric Chart of the Mediterranean, Geological-Geophysical Series, IBCM-PQ, scale 1:5,000,000, St. Petersburg, Russia

Geprägs, P., 2016, Methane environment around cold seeps - examples from Antarctica and the Mediterranean [PhD Thesis]: Universität Bremen, 141 p.

Ginsburg, G., Milkov, A. V., Soloviev, V. A., Egorov, A. V., Cherkashev, G. A., Vogt, P. R., Crane, K., Lorenson, T. D., and Khutorskoy, M. D., 1999, Gas hydrate accumulation at the Håkon Mosby Mud Volcano: Geo-Marine Letters, v. 19, p. 57-67

Goes, S., Giardini, D., Jenny, S., Hollenstein, C., Kahle, H. G., and Geiger, A., 2004, A recent tectonic reorganization in the south-central Mediterranean: Earth and Planetary Science Letters, v. 226, no. 3-4, p. 335-345, doi: 10.1016/j.epsl.2004.07.038.

Goldsmith, J. R., Graf, D. L., and Heard, H. C., 1961, Lattice Constants of the Calcium-Magnesium Carbonates: American Mineralogist, v. 46, no. 3-4, p. 453-457

Gontharet, S., et al., 2007, Nature and origin of diagenetic carbonate crusts and concretions from mud volcanoes and pockmarks of the Nile deep-sea fan: Deep-Sea Reseach II, v. 54, p. 1292-1311

Granot, R., 2016, Palaeozoic oceanic crust preserved beneath the eastern Mediterranean: Nature Geoscience, v. 9, no. 9, p. 701-+, doi: 10.1038/Ngeo2784.

Graue, K., 2000, Mud volcanoes in deepwater Nigeria: Marine and Petroleum Geology, v. 17, no. 8, p. 959-974, doi: Doi 10.1016/S0264-8172(00)00016-7.

Greinert, J., Artemov, Y., Egorov, V., De Batist, M., and McGinnis, D., 2006, 1300-m-high rising bubbles from mud volcanoes at 2028m in the Black Sea: Hydroacoustic characteristics and temporal variability: Earth and Planetary Science Letters, v. 244, p. 1-15

Greinert, J., Bohrmann, G., and Suess, E., 2001, Gas hydrate-associated carbonates and methane-venting at Hydrate Ridge: Classification, distribution, and origin of authigenic lithologies, Natural Gas Hydrates: Occurence, Distribution, and Detection, Volume 124, Geophysical Monograph, p. 99-113.

Greinert, J., Bollwerk, S. M., Derkachev, A., Bohrmann, G., and Suess, E., 2002, Massive barite deposits and carbonate mineralization in the Derugin Basin, Sea of Okhotsk: Precipitation process at cold seep sites: Earth and Planetary Science Letters, v. 203, p. 165-180

Greinert, J., Lewis, K.-B., Bialas, J., Pecher, I. A., Rowden, A., Bowden, D.-A., De Batist, M., and Linke, P., 2010, Methane seepage along the Hikurangi Margin,

New Zealand: Overview of studies in 2006 and 2007 and new evidence from visual, bathymetric and hydroacoustic investigations: Marine Geology, v. 272, no. 1-4, p. 6-25, doi: 10.1016/j.margeo.2010.01.017.

Grossman, E., and Ku, T., 1986, Oxygen and carbon isotope fractionation in biogenic aragonite: Temperature effects, 59-74 p.:

Gueguen, E., Doglioni, C., and Fernandez, M., 1998, On the post-25 Ma geodynamic evolution of the western Mediterranean: Tectonophysics, v. 298, no. 1-3, p. 259-269, doi: 10.1016/S0040-1951(98)00189-9.

Guliyev, I., and Feizullayev, A., 1997, All about mud volcanoes: Nafta Press, Baku

Gutscher, M.-A., et al., 2017, Active tectonics of the Calabrian subduction revealed by new multi-beam bathymetric data and high-resolution seismic profiles in the Ionian Sea (Central Mediterranean): Earth and Planetary Science Letters, v. 461, p. 61-72, doi: 10.1016/j.epsl.2016.12.020.

Haase, K. M., et al., 2007, Young volcanism and related hydrothermal activity at 5°S on the slow-spreading southern Mid-Atlantic Ridge: Geochemistry, Geophysics, Geosystems, v. 8, no. 11, p. n/a-n/a, doi: 10.1029/2006GC001509.

Han, X., Suess, E., Sahling, H., and Wallmann, K., 2004, Fluid venting activity on the Costa Rica Margin: new results from authigenic carbonates: International Journal of Earth Sciences, v. 93, p. 596-611 doi: 10.1007/s00531-004-0402-y.

Hantschel, T., and Kauerauf, A. I., 2009, Pore Pressure, Compaction and Tectonics; In: Fundamentals of Basin and Petroleum Systems Modeling, Springer-Verlag Berlin Heidelberg.

Harper, J. T., Humphrey, N. F., and Pfeffer, W. T., 1998, Crevasse patterns and the strain-rate tensor: a high-resolution comparison: Journal of Glaciology, v. 44, no. 146, p. 68-76

Head, I. M., Jones, D. M., and Larter, S. R., 2003, Biological activity in the deep subsurface and the origin of heavy oil: Nature, v. 426, no. 6964, p. 344-352, doi: 10.1038/nature02134.

Henry, P., Le Pichon, X., Lallemant, S., Foucher, J.-P., Westbrook, G., and Hobart, M., 1990, Mud volcano field seaward of the Barbados accretionary complex: a deep-towed side scan sonar survey: Journal of Geophysical Research, v. 95, no. B6, p. 8917

Hensen, C., et al., 2015, Strike-slip faults mediate the rise of crustal-derived fluids and mud volcanism in the deep sea: Geology, v. 43, no. 4, p. 339-342, doi: 10.1130/G36359.1.

Hensen, C., Wallmann, K., Schmidt, M., Ranero, C. R., and Suess, E., 2004, Fluid expulsion related to mud extrusions off Costa Rica - A window to the suducting slab: Geology, v. 32, no. 3, p. 201-204

Hesse, R., Lebel, J., and Gieskes, J., 1985, Interstitial Water Chemistry of Gas-Hydrate-Bearing Sections on the Middle America Trench Slope, Deep Sea Drilling Project Leg 84, in: R. von Huene, J. Aubouin et al. (Eds.), Init. Rep. Deep Sea Drill. Proj., U.S. Government Printing Office, Washington, DC, LVXXX, doi: 10.2973/dsdp.proc.84.130.1985.

Hesselbo, S. P., Grocke, D. R., Jenkyns, H. C., Bjerrum, C. J., Farrimond, P., Bell, H. S. M., and Green, O. R., 2000, Massive dissociation of gas hydrate during a

Jurassic oceanic anoxic event: Nature, v. 406, no. 6794, p. 392-395, doi: Doi 10.1038/35019044.

Higgins, G. E., and Saunders, J. B., 1974, Mud volcanoes – Their nature and origin: Verh. Naturforsch. Ges. Basel, v. 84, p. 101–152

Himmler, T., Birgel, D., Bayon, G., Pape, T., Ge, L., Bohrmann, G., and Peckmann, J., 2015, Formation of seep carbonates along the Makran convergent margin, northern Arabian Sea and amolecular and isotopic approach to constrain the carbon isotopic composition of parent methane: Chemical Geology, v. 415, p. 102-117, doi: 10.1016/j.chemgeo.2015.09.016.

Himmler, T., Brinkmann, F., Bohrmann, G., and Peckmann, J., 2011, Corrosion patterns of seep-carbonates from the eastern Mediterranean Sea: Terra Nova, v. 23, p. 206-212, doi: 10.1111/j.1365-3121.2011.01000.x.

Hinrichs, K.-U., Hayes, J. M., Sylva, S. P., Brewer, P. G., and DeLong, E. F., 1999, Methane-consuming archaebacteria in marine sediments: Nature, v. 398, p. 802-805

Hong, W. L., Torres, M. E., Kim, J. H., Choi, J., and Bahk, J. J., 2013, Carbon cycling within the sulfate-methane-transition-zone in marine sediments from the Ulleung Basin: Biogeochemistry, v. 115, no. 1-3, p. 129-148, doi: 10.1007/s10533-012-9824-y.

Hovland, M., 2002, On the self-sealing nature of marine seeps: Continental Shelf Research, v. 22, no. 16, p. 2387-2394, doi: Doi 10.1016/S0278-4343(02)00063-8.

Hovland, M., Heggland, R., De Vries, M. H., and Tjelta, T. I., 2010, Unit-pockmarks and their potential significance for predicting fluid flow: Marine and Petroleum Geology, v. 27, no. 6, p. 1190-1199, doi: 10.1016/j.marpetgeo.2010.02.005.

Hovland, M., Hill, A., and Stokes, D., 1997, The structure and geomorphology of the Dashgil mud volcano, Azerbaijan: Geomorphology, v. 21, p. 1-15

Hovland, M., Judd, A. G., and Burke, R. A., 1993, The Global Flux of Methane from Shallow Submarine Sediments: Chemosphere, v. 26, no. 1-4, p. 559-578, doi: Doi 10.1016/0045-6535(93)90442-8.

Hovland, M., Judd, A. G., and King, L. H., 1984, Characteristic features of pockmarks on the North Sea floor and Scotian shelf: Sedimentology, v. 31, p. 471-480

Hovland, M., and Svensen, H., 2006, Submarine pingoes: Indicators of shallow gas hydrates in a pockmark at Nyegga, Nrowegian Sea: Marine Geology, v. 228, p. 15-23

Hovland, M., Talbot, M. R., Qvale, H., Olaussen, S., and Aasberg, L., 1987, Methane-related carbonate cements in pockmarks of the North Sea: Journal of Sedimentary Petrology, v. 57, no. 2, p. 881-892

Hsü, K. J., Cita, M. B., and Ryan, W. B. F., 1973, The origin of the Mediterranean evaporite: Initial Reports of the Deep Sea Drilling Project, p. 1203

Huguen, C., et al., 2009, Menes caldera, a highly active site of brine seepage in the Eastern Mediterranean sea: "In situ" observations from the NAUTINIL expedition (2003): Marine Geology, v. 261, no. 1-4, p. 138-152, doi: 10.1016/j.margeo.2009.02.005.

Huguen, C., Mascle, J., Chaumillon, E., Kopf, A. J., Woodside, J., and Zitter, T., 2004, Structural setting and tectonic control of mud volcanoes from the Central

Mediterranean Ridge (Eastern Mediterranean): Marine Geology, v. 209, p. 245-263

Huguen, C., Mascle, J., Woodside, J., Zitter, T., and Foucher, J. P., 2005, Mud volcanoes and mud domes of the Central Mediterranean Ridge: Near-bottom and in-situ observations: Deep-Sea Research Part 1, v. 52, p. 1911-1931

Hunt, J. M., 1996, Petroleum Geochemistry and Geology: W. H. Freeman and Company, New York

Huseynov, D. A., and Guliyev, I. S., 2004, Mud volcanic natural phenomena in the South Caspian Basin: geology, fluid dynamics and environmental impact: Environmental Geology, v. 46, no. 8, p. 1012-1023, doi: 10.1007/s00254-004-1088-y.

Iannace, A., et al., 2007, The carbonate tectonic units of northern Calabria (Italy): a record of Apulian palaeomargin evolution and Miocene convergence, continental crust subduction, and exhumation of HP-LT rocks: Journal of the Geological Society, v. 164, p. 1165-1186, doi: 10.1144/0016-76492007-017.

IPCC, 2014, Climate Change 2014: Synthesis Report. Contribution of Working Groups I, II and III to the Fifth Assessment Report of the Intergovernmental Panel on Climate Change [Core Writing Team, R.K. Pachauri and L.A. Meyer (eds.)]: IPCC, Geneva, Switzerland, p. 151 pp

Istadi, B. P., Pramono, G. H., Sumintadireja, P., and Alam, S., 2009, Modeling study of growth and potential geohazard for LUSI mud volcano: East Java, Indonesia: Marine and Petroleum Geology, v. 26, no. 9, p. 1724-1739

Ivanov, M. K., Limonov, A. F., and Cronin, B. T., 1996a, Mud volcanism and fluid venting in the eastern part of the Mediterranean Ridge, Unesco reports in marine science, Volume 68: Paris, UNESCO, p. 126.

Ivanov, M. K., Limonov, A. F., and van Weering, T. C. E., 1996b, Comparative characteristics of the Black Sea and Mediterranean Ridge mud volcanoes: Marine Geology, v. 132, p. 253-271

Iversen, N., and Jorgensen, B. B., 1985, Anaerobic Methane Oxidation Rates at the Sulfate Methane Transition in Marine-Sediments from Kattegat and Skagerrak (Denmark): Limnology and Oceanography, v. 30, no. 5, p. 944-955

Jain, A. K., and Juanes, R., 2009, Preferential Mode of gas invasion in sediments: Grain-scale mechanistic model of coupled multiphase fluid flow and sediment mechanics: Journal of Geophysical Research-Solid Earth, v. 114, doi: 10.1029/2008jb006002.

Jarosewich, E., Nelen, J. A., and Norberg, J. A., 1980, Reference Samples for Electron Microprobe Analysis: Geostandards Newsletter, v. 4, no. 1, p. 43-47, doi: 10.1111/j.1751-908X.1980.tb00273.x.

Jerosch, K., Schlüter, M., Foucher, J.-P., Allais, A.-G., Klages, M., and Edy, C., 2007, Spatial distribution of mud flows, chemoautotrophic communities, and biogeochemical habitats at Håkon Mosby Mud Volcano: Marine Geology, v. 243, p. 1-17

Johnson, H. P., and Helferty, M., 1990, The geological interpretation of side-scan sonar: Review of Geophysics, v. 28, no. 4, p. 357-380

Jolivet, L., Frizon de Lamotte, D., Mascle, A., and Séranne, M., 1999, The Mediterranean Basins: Tertiary Extension within the Alpine Orogen — an

introduction: Geological Society, London, Special Publications, v. 156, no. 1, p. 1

Joye, S. B., Boetius, A., Orcutt, B. N., Montoya, J. P., Schulz, H. N., Erickson, M. J., and Lugo, S. K., 2004, The anaerobic oxidation of methane and sulfate reduction in sediments from Gulf of Mexico cold seeps: Chemical Geology, v. 205, p. 219-238

Judd, A. G., and Hovland, M., 2007, Seabed fluid flow. The impact on geology, biology and marine environment, p. 475 pp.

Kääb, A., and Weber, M., 2004, Development of transverse ridges on rock glaciers: Field measurements and laboratory experiments: Permafrost and Periglacial Processes, v. 15, no. 4, p. 379-391, doi: 10.1002/ppp.506.

Karpen, V., Thomsen, L., and Suess, E., 2004, A new 'schlieren' technique application for fluid flow visualization at cold seep sites: Marine Geology, v. 204, p. 149-159

Kastens, K. A., 1984, Earthquakes as a Triggering Mechanism for Debris Flows and Turbidites on the Calabrian Ridge: Marine Geology, v. 55, no. 1-2, p. 13-33, doi: 10.1016/0025-3227(84)90130-0.

Kastner, M., Solomon, E. A., Harris, R. N., and Torres, M. E., 2014, Chapter 4.4.3 - Fluid Origins, Thermal Regimes, and Fluid and Solute Fluxes in the Forearc of Subduction Zones, *in* Ruediger Stein, D. K. B. F. I., and Hans-Christian, L., eds., Developments in Marine Geology, Volume Volume 7, Elsevier, p. 671-733.

Kaul, N., Foucher, J.-P., and Heesemann, M., 2006, Estimating mud expulsion rates from temperature measurements on Håkon Mosby Mud Volcano, SW Barents Sea: Marine Geology, v. 229, p. 1-14

Keller, J., Ryan, W. B. F., Ninkovich, D., and Altherr, R., 1978, Explosive volcanic activity in the Mediterranean over the past 200,000 yr as recorded in deep-sea sediments: Geological Society of America Bulletin, v. 89, no. 4, p. 591-604, doi: 10.1130/0016-7606(1978)89<591:evaitm>2.0.co;2.

Kennett, J. P., Cannariato, K. G., Hendy, I. L., and Behl, R. J., 2000, Carbon isotopic evidence for methane hydrate instability during Quaternary interstadials: Science, v. 288, p. 128-133

Kholodov, V. N., 2002, Mud Volcanoes, Their Distribution Regularities and Genesis: Communication 1. Mud Volcanic Provinces and Morphology of Mud Volcanoes: Lithology and Mineral Resources, v. 37, no. 3, p. 197-209, doi: 10.1023/A:1015425612749.

King, L. H., and MacLean, B., 1970, Pockmarks on the Scotian shelf: Geological Society of America Bulletin, v. 81, p. 3141-3148

Kioka, A., and Ashi, J., 2015, Episodic massive mud eruptions from submarine mud volcanoes examined through topographical signatures: Geophysical Research Letters, v. 42, no. 20, p. 8406-8414, doi: 10.1002/2015gl065713.

Kirkham, C., Cartwright, J., Hermanrud, C., and Jebsen, C., 2017, The spatial, temporal and volumetric analysis of a large mud volcano province within the Eastern Mediterranean: Marine and Petroleum Geology, v. 81, p. 1-16, doi: 10.1016/j.marpetgeo.2016.12.026.

Klaucke, I., Sahling, H., Weinrebe, W., Blinova, V., Bürk, D., Lursmanashvili, N., and Bohrmann, G., 2006, Acoustic investigations of cold seeps offshore Georgia, eastern Black Sea: Marine Geology, v. 231, no. 1-4, p. 51-67

Klaucke, I., Weinrebe, W., Petersen, C.-J., and Bowden, D., 2010, Temporal variability of gas seeps offshore New Zealand: Multi-frequency geoacoustic imaging of the Wairarapa area, Hikurangi margin: Marine Geology, v. 272, no. 1-4, p. 49-58, doi: 10.1016/j.margeo.2009.02.009.

Knittel, K., and Boetius, A., 2009, Anaerobic oxidation of methane: Progress with unknown process: Annual Review of Microbiology, v. 63, p. 311-334, doi: 10.1146/annurev.micro.61.080706.093130.

Koch, S., Berndt, C., Bialas, J., Haeckel, M., Crutchley, G., Papenberg, C., Klaeschen, D., and Greinert, J., 2015, Gas-controlled seafloor doming: Geology, v. 43, no. 7, p. 571-574, doi: 10.1130/G36596.1.

Komar, P. D., 1973, Continuity of Turbidity Current Flow and Systematic Variations in Deep-Sea Channel Morphology: Geological Society of America Bulletin, v. 84, no. 10, p. 3329-3334, doi: 10.1130/0016-7606(1973)84<3329:Cotcfa>2.0.Co;2.

Kopf, A., Robertson, A. H. F., Clennell, M. B., and Flecker, R., 1998, Mechanisms of mud extrusion on the Mediterranean Ridge Accretionary Complex: Geo-Marine Letters, v. 18, no. 2, p. 97-114, doi: 10.1007/s003670050058.

Kopf, A., Sample, J. C., Bauer, P., Behrmann, J. H., and Erlenkheuser, H., 1995, Diagenetic carbonates from Cascadia Margin: Textures, chemical composition, and oxygen and carbon stabile isotope signatures. In: Carson, B. et al. (eds.) (1995), Proc. ODP, Sci. Results, 146 (Pt. 1): College Station, TX (Ocean Drilling Program), p. 117-136

Kopf, A. J., 1999, Fate of sediment during plate convergence at the Mediterranean Ridge accretionary complex: Volume balance of mud extrusion versus subduction and/or accretion: Geology, v. 27, no. 1, p. 87-30

Kopf, A. J., 2002, Significance of mud volcanism: Reviews of Geophysics, v. 40, no. 2, doi: 10.1029/2000rg000093.

Kopf, A. J., 2003, Global methane emission through mud volcanoes and its past and present impact on the Earth's climate: International Journal of Earth Sciences, v. 92, p. 806-816

Kopf, A. J., 2008, Volcanoes - Making calderas from mud: Nature Geoscience, v. 1, no. 8, p. 500-501, doi: Doi 10.1038/Ngeo256.

Kopf, A. J., Klaeschen, D., and Mascle, J., 2001, Extreme efficiency of mud volcanism in dewatering accretionary prisms: Earth and Planetary Science Letters, v. 189, p. 295-313, doi: 10.1016/S0012-821X(01)00278-3.

Körber, J. H., Sahling, H., Pape, T., Ferreira, C. D. S., MacDonald, I., and Bohrmann, G., 2014, Natural oil seepage at Kobuleti Ridge, eastern Black Sea: Marine and Petroleum Geology, v. 50, no. 0, p. 68-82, doi: 10.1016/j.marpetgeo.2013.11.007.

Kostic, S., 2011, Modeling of submarine cyclic steps: Controls on their formation, migration, and architecture: Geosphere, v. 7, no. 2, p. 294-304, doi: 10.1130/Ges00601.1.

Kostic, S., Sequeiros, O., Spinewine, B., and Parker, G., 2010, Cyclic steps: A phenomenon of supercritical shallow flow from the high mountains to the

bottom of the ocean: Journal of Hydro-Environment Research, v. 3, no. 4, p. 167-172, doi: 10.1016/j.jher.2009.10.002.

Kvenvolden, K. A., 1988, Methane hydrate - a major reservoir of carbon in the shallow geosphere?: Chemical Geology, v. 71, p. 41-51

Kvenvolden, K. A., 1993, Gas Hydrates - Geological Perspective and Global Change: Reviews of Geophysics, v. 31, no. 2, p. 173-187, doi: Doi 10.1029/93rg00268.

Kvenvolden, K. A., and McMenamin, M. A., 1980, Hydrates of natural gas; a review of their geologic occurrence, 825.

Kvenvolden, K. A., and Rogers, B. W., 2005, Gaia's breath - global methane exhalations: Marine and Petroleum Geology, v. 22, p. 579-590

Lamb, M. P., Parsons, J. D., Mullenbach, B. L., Finlayson, D. P., Orange, D. L., and Nittrouer, C. A., 2008, Evidence for superelevation, channel incision, and formation of cyclic steps by turbidity currents in Eel Canyon, California: Geological Society of America Bulletin, v. 120, no. 3-4, p. 463-475, doi: 10.1130/B26184.1.

Lance, S., Henry, P., Pichon, X. L., Lallemant, S., Chamley, H., Rostek, F., Faugères, J.-C., Gonthier, E., and Olu, K., 1998, Submersible study of mud volcanoes seaward of the Barbados accretionary wedge: sedimentology, structure and rheology: Marine Geology, v. 145, p. 255-292

Lastras, G., Arzola, R. G., Masson, D. G., Wynn, R. B., Huvenne, V. A. I., Huhnerbach, V., and Canals, M., 2009, Geomorphology and sedimentary features in the Central Portuguese submarine canyons, Western Iberian margin: Geomorphology, v. 103, no. 3, p. 310-329, doi: 10.1016/j.geomorph.2008.06.013.

Le Pichon, X., Foucher, J.-P., Boulègue, J., Henry, P., Lallemant, S., Benedetti, M., Avedik, F., and Mariotti, A., 1990, Mud volcano field seaward of the Barbados accretionary complex: a submersible survey: Journal of Geophysical Research, v. 95, no. B6, p. 8931-8943

Lee, S. E., Talling, P. J., Ernst, G. G. J., and Hogg, A. J., 2002, Occurrence and origin of submarine plunge pools at the base of the US continental slope: Marine Geology, v. 185, no. 3-4, p. 363-377, doi: 10.1016/S0025-3227(01)00298-5.

Leifer, I., Luyendyk, B. P., Boles, J., and Clark, J. F., 2006, Natural marine seepage blowout: Contribution to atmospheric methane: Global Biogeochemical Cycles, v. 20, doi: 10.1029/2005GB002668.

Lelieveld, J., Crutzen, P. J., and Dentener, F. J., 1998, Changing concentration, lifetime and climate forcing of atmospheric methane: Tellus Series B-Chemical and Physical Meteorology, v. 50, no. 2, p. 128-150, doi: DOI 10.1034/j.1600-0889.1998.t01-1-00002.x.

León, R., Somoza, L., Medialdena, T., González, F. J., Díaz-del-Rio, V., Fernández-Puga, M. C., Maestro, A., and Mata, M. P., 2007, Sea-floor features related to hydrocarbon seeps in deepwater carbonate-mud mounds of the Gulf of Cádiz: from mud flows to carbonate precipitation: Geo-Mar Letters, v. 27, p. 237-247

Limonov, A. F., Woodside, J. M., Cita, M. B., and Ivanov, M. K., 1996, The Mediterranean Ridge and related mud diapirism: a background: Marine Geology, v. 132, p. 7-19

Loher, M., Ceramicola, S., Wintersteller, P., Meinecke, G., Sahling, H., and Bohrmann, G., in review (G3), Mud volcanism in a canyon: Morpho-dynamic evolution of the active Venere mud volcano and its interplay with Squillace Canyon, Central Mediterranean: Geochemistry Geophysics Geosystems

Loher, M., Pape, T., Marcon, Y., Römer, M., Wintersteller, P., Praeg, D., Torres, M., Sahling, H., and Bohrmann, G., in review (JMPG), Mud extrusion and ring-fault gas seepage – upward branching fluid discharge at the deep-sea Venere mud volcano (Central Mediterranean Sea): Marine and Petroleum Geology

Loher, M., Reusch, A., and Strasser, M., 2016, Long-term pockmark maintenance by fluid seepage and subsurface sediment mobilization – sedimentological investigations in Lake Neuchâtel: Sedimentology, v. 63, no. 5, p. 1168-1186, doi: 10.1111/sed.12255.

Luff, R., and Wallmann, K., 2003, Fluid flow, methane fluxes, carbonate precipitation and biogeochemical turnover in gas hydrate-bearing sediments at Hydrate Ridge, Cascadia Margin: Numerical modeling and mass balances: Geochimica et Cosmochimica Acta, v. 67, no. 18, p. 3403-3421

Luff, R., Wallmann, K., and Aloisi, G., 2004, Numerical modeling of carbonate crust formation at cold vent sites:significance for fluid and methane budgets and chemosynthetic biological communities: Earth and Planetary Science Letters, v. 221, p. 337-353

Lumsden, D. N., 1979, Discrepancy between Thin-Section and X-Ray Estimates of Dolomite in Limestone: Journal of Sedimentary Petrology, v. 49, no. 2, p. 429-436

Lurton, X., and Lamarche, G., 2015, Backscatter measurements by seafloor ‐ mapping sonars. Guidelines and Recommendations: http://geohab.org/wp ‐ content/uploads/2014/05/BSWGREPORT ‐ MAY2015.pdf, p. 200p

Lykousis, V., et al., 2009, Mud volcanoes and gas hydrates in the Anaximander mountains (Eastern Mediterranean Sea): Marine and Petroleum Geology, v. 26, no. 6, p. 854-872, doi: 10.1016/j.marpetgeo.2008.05.002.

Macdonald, H. A., Wynn, R. B., Huvenne, V. A. I., Peakall, J., Masson, D. G., Weaver, P. P. E., and McPhail, S. D., 2011, New insights into the morphology, fill, and remarkable longevity (> 0.2 m.y.) of modern deep-water erosional scours along the northeast Atlantic margin: Geosphere, v. 7, no. 4, p. 845-867, doi: 10.1130/Ges00611.1.

MacDonald, I. R., and Peccini, M. B., 2009, Distinct activity phases during the recent geologic history of a Gulf of Mexico mud volcano: Marine and Petroleum Geology, v. 26, no. 9, p. 1824-1830

Malinverno, A., and Ryan, W. B. F., 1986, Extension in the Tyrrhenian Sea and shortening in the Apennines as result of arc migration driven by sinking of the lithosphere: Tectonics, v. 5, no. 2, p. 227-245, doi: 10.1029/TC005i002p00227.

Maltman, A. J., and Bolton, A., 2003, How sediments become mobilized: Subsurface Sediment Mobilization, v. 216, p. 9-20, doi: 10.1144/Gsl.Sp.2003.216.01.02.

Manga, M., Brumm, M., and Rudolph, M. L., 2009, Earthquake triggering of mud volcanoes: Marine and Petroleum Geology, v. 26, no. 9, p. 1785-1798

Marcon, Y., Ondréas, H., Sahling, H., Bohrmann, G., and Olu, K., 2014a, Fluid flow regimes and growth of a giant pockmark: Geology, v. 42, no. 1, p. 63-66, doi: 10.1130/g34801.1.

Marcon, Y., Sahling, H., Allais, A.-G., Bohrmann, G., and Olu, K., 2014b, Distribution and temporal variation of mega-fauna at the Regab pockmark (Northern Congo Fan), based on a comparison of videomosaics and geographic information systems analyses: Marine Ecology, v. 35, no. 1, p. 77-95, doi: 10.1111/maec.12056.

Marcon, Y., Sahling, H., and Bohrmann, G., 2013, LAPM: a tool for underwater large-area photo-mosaicking: Geosci. Instrum. Method. Data Syst., v. 2, no. 2, p. 189-198, doi: 10.5194/gi-2-189-2013.

Martens, C. S., and Berner, R. A., 1974, Methane Production in Interstitial Waters of Sulfate-Depleted Marine Sediments: Science, v. 185, no. 4157, p. 1167-1169, doi: 10.1126/science.185.4157.1167.

Martin, J. B., Kastner, M., Henry, P., Pichon, X. L., and Lallement, S., 1996, Chemical and isotopic evidence for sources of fluids in a mud volcano field seaward of the Barbados accretionary wedge: Journal of geophysical research, v. 101, no. B9, p. 20325-20345

Mascle, J., Mary, F., Praeg, D., Brosolo, L., Camera, L., Ceramicola, S., and Dupré, S., 2014, Distribution and geological control of mud volcanoes and other fluid/free gas seepage features in the Mediterranean Sea and nearby Gulf of Cadiz: Geo-Marine Letters, p. 1-22, doi: 10.1007/s00367-014-0356-4.

Masoudi, R., and Tohidi, B., 2005, Estimating the hydrate zone in the presence of salts and/or organic inhibitors using water partial pressure: Journal of Petroleum Science and Engineering, v. 46, no. 1-2, p. 23-36, doi: 10.1016/j.petrol.2004.10.002.

Mastalerz, V., de Lange, G. J., and Dählmann, A., 2009, Differential aerobic and anaerobic oxidation of hydrocarbon gases discharged at mud volcanoes in the Nile deep-sea fan: Geochimica et Cosmochimica Acta, v. 73, p. 3849-3863, doi: 10.1016/j.gca.2008.12.030.

Matsumoto, R., 1990, Vuggy Carbonate Crust Formed by Hydrocarbon Seepage on the Continental-Shelf of Baffin Island, Northeast Canada: Geochemical Journal, v. 24, no. 3, p. 143-158

Mattavelli, L., and Novelli, L., 1988, Geochemistry and Habitat of Natural Gases in Italy: Organic Geochemistry, v. 13, no. 1-3, p. 1-13, doi: 10.1016/0146-6380(88)90021-6.

Mattei, M., Cifelli, F., and D'Agostino, N., 2007, The evolution of the Calabrian Arc: Evidence from paleomagnetic and GPS observations: Earth and Planetary Science Letters, v. 263, no. 3-4, p. 259-274, doi: 10.1016/j.epsl.2007.08.034.

Mau, S., et al., 2017, Widespread methane seepage along the continental margin off Svalbard - from Bjornoya to Kongsfjorden: Scientific Reports, v. 7, doi: 10.1038/srep42997.

Mazzini, A., and Etiope, G., 2017, Mud volcanism: An updated review: Earth-Science Reviews, v. 168, p. 81-112, doi: 10.1016/j.earscirev.2017.03.001.

Mazzini, A., Etiope, G., and Svensen, H., 2012, A new hydrothermal scenario for the 2006 Lusi eruption, Indonesia. Insights from gas geochemistry: Earth and Planetary Science Letters, v. 317, p. 305-318, doi: 10.1016/j.epsl.2011.11.016.

Mazzini, A., Ivanov, M. K., Nermoen, A., Bahr, A., Bohrmann, G., Svensen, H., and Planke, S., 2008, Complex plumbing systems in the near subsurface: Geometries of authigenic carbonates from Dolgovskoy Mound (Black Sea) constrained by analogue experiments: Marine and Petroleum Geology, v. 25, no. 6, p. 457-472

Mazzini, A., Nermoen, A., Krotkiewski, M., Podladchikov, Y., Planke, S., and Svensen, H., 2009a, Strike-slip faulting as a trigger mechanism for overpressure release through piercement structures. Implications for the Lusi mud volcano, Indonesia: Marine and Petroleum Geology, v. 26, no. 9, p. 1751-1765, doi: 10.1016/j.marpetgeo.2009.03.001.

Mazzini, A., Svensen, H., Akhmanov, G. G., Aloisi, G., Planke, S., Malthe-Sorenssen, A., and Istadi, B., 2007, Triggering and dynamic evolution of the LUSI mud volcano, Indonesia: Earth and Planetary Science Letters, v. 261, no. 3-4, p. 375-388, doi: 10.1016/j.epsl.2007.07.001.

Mazzini, A., Svensen, H., Planke, S., Guliyev, I., Akhmanov, G. G., Fallik, T., and Banks, D., 2009b, When mud volcanoes sleep: Insight from seep geochemistry at the Dashgil mud volcano, Azerbaijan: Marine and Petroleum Geology, v. 26, no. 9, p. 1704-1715, doi: 10.1016/j.marpetgeo.2008.11.003.

Mellors, R., Kilb, D., Aliyev, A., Gasanov, A., and Yetirmishli, G., 2007, Correlations between earthquakes and large mud volcano eruptions: Journal of Geophysical Research-Solid Earth, v. 112, no. B4, doi: 10.1029/2006jb004489.

Migeon, S., Savoye, B., and Faugeres, J. C., 2000, Quaternary development of migrating sediment waves in the Var deep-sea fan: distribution, growth pattern, and implication for levee evolution: Sedimentary Geology, v. 133, no. 3-4, p. 265-293, doi: Doi 10.1016/S0037-0738(00)00043-9.

Migeon, S., Savoye, B., Zanella, E., Mulder, T., Faugeres, J. C., and Weber, O., 2001, Detailed seismic-reflection and sedimentary study of turbidite sediment waves on the Var Sedimentary Ridge (SE France): significance for sediment transport and deposition and for the mechanisms of sediment-wave construction: Marine and Petroleum Geology, v. 18, no. 2, p. 179-208, doi: 10.1016/S0264-8172(00)00060-X.

Milkov, A. V., 2000, Worldwide distribution of submarine mud volcanoes and associated gas hydrates: Marine Geology, v. 167, no. 1-2, p. 29-42, doi: 10.1016/S0025-3227(00)00022-0.

Milkov, A. V., Sassen, R., Apanasovich, T. V., and Dadashev, F. G., 2003, Global gas flux from mud volcanoes: A significant source of fossil methane in the atmosphere and the ocean: Geophysical Research Letters, v. 30, no. 2, p. 1037, doi: 10.1029/2002GLO16358.

Miller, S. A., and Mazzini, A., 2017, More than ten years of Lusi: A review of facts, coincidences, and past and future studies: Marine and Petroleum Geology, doi: 10.1016/j.marpetgeo.2017.06.019.

Minelli, L., and Faccenna, C., 2010, Evolution of the Calabrian accretionary wedge (central Mediterranean): Tectonics, v. 29, no. 4, doi: 10.1029/2009tc002562.

Mitchell, N. C., 1993, A Model for Attenuation of Backscatter Due to Sediment Accumulations and Its Application to Determine Sediment Thicknesses with Gloria Sidescan Sonar: Journal of Geophysical Research-Solid Earth, v. 98, no. B12, p. 22477-22493, doi: 10.1029/93jb02217.

Monaco, C., and Tortorici, L., 2000, Active faulting in the Calabrian arc and eastern Sicily: Journal of Geodynamics, v. 29, no. 3-5, p. 407-424, doi: 10.1016/S0264-3707(99)00052-6.

Moore, J. M., et al., 2016, The geology of Pluto and Charon through the eyes of New Horizons: Science, v. 351, no. 6279, p. 1284-1293, doi: 10.1126/science.aad7055.

Morelli, D., Cuppari, A., Colizza, E., and Fanucci, F., 2011, Geomorphic setting and geohazard-related features along the Ionian Calabrian margin between Capo Spartivento and Capo Rizzuto (Italy): Marine Geophysical Research, v. 32, no. 1-2, p. 139-149, doi: 10.1007/s11001-011-9130-4.

Morlotti, E., Sartori, R., Torelli, L., Barbieri, F., and Raffi, I., 1982, Chaotic deposits fromthe external Calabrian Arc (Ionian Sea, easternMediterranean): Mem Soc Geol Ital, v. 24, p. 261–275

Mozley, P. S., and Burns, S. J., 1993, Oxygen and Carbon Isotopic Composition of Marine Carbonate Concretions - an Overview: Journal of Sedimentary Petrology, v. 63, no. 1, p. 73-83

Murton, B. J., and Biggs, J., 2003, Numerical modelling of mud volcanoes and their flows using constraints from the Gulf of Cadiz: Marine Geology, v. 195, no. 1-4, p. 223-236, doi: 10.1016/S0025-3227(02)00690-4.

Naehr, T. H., Eichhubl, P., Orphan, V. J., Hovland, M., Paull, C. K., Ussler, W., Lorenson, T. D., and Greene, H. G., 2007, Authigenic carbonate formation at hydrocarbon seeps in continental margin sediments: A comparative study: Deep-Sea Research Part Ii-Topical Studies in Oceanography, v. 54, no. 11-13, p. 1268-1291, doi: 10.1016/j.dsr2.2007.04.010.

Naudts, L., Greinert, J., Artemov, Y., Beaubien, S. E., Borowski, C., and Batist, M. D., 2008, Anomalous sea-floor backscatter patterns in methane venting areas, Dnepr paleo-delta, NW Black Sea: Marine Geology, v. 251, no. 3-4, p. 253-267

Naudts, L., Greinert, J., Poort, J., Belza, J., Vangampelaere, E., Boone, D., Linke, P., Henriet, J.-P., and De Batist, M., 2010, Active venting sites on the gas-hydrate-bearing Hikurangi Margin, off New Zealand: Diffusive- versus bubble-released methane: Marine Geology, v. 272, no. 1-4, p. 233-250, doi: 10.1016/j.margeo.2009.08.002.

Neri, G., Orecchio, B., Totaro, C., Falcone, G., and Presti, D., 2009, Subduction Beneath Southern Italy Close the Ending: Results from Seismic Tomography: Seismological Research Letters, v. 80, no. 1, p. 63-70, doi: 10.1785/gssrl.80.1.63.

Neurauter, T. W., and Bryant, W. R., 1990, Seismic Expression of Sedimentary Volcanism on the Continental-Slope, Northern Gulf-of-Mexico: Geo-Marine Letters, v. 10, no. 4, p. 225-231, doi: 10.1007/Bf02431069.

Niemann, H., et al., 2006, Novel microbial communities of the Haakon Mosby mud volcano and their role as a methane sink: Nature, v. 443, p. 854-858

Nikolovska, A., Sahling, H., and Bohrmann, G., 2008, Hydroacoustic methodology for detection, localization, and quantification of gas bubbles rising from the seafloor at gas seeps from the Black Sea: Geochemistry Geophysics Geosystems, v. 9, no. 10, p. Q10010, doi: 10.1029/2008GC002118.

Nix, E. R., Fisher, C. R., Vodenichar, J., and Scott, K. M., 1995, Physiological ecology of a mussel with methanotrophic endosymbionts at three hydrocarbon seep sites in the Gulf of Mexico: Marine Biology, v. 122, p. 605-617

Normark, W. R., Hess, G. R., Stow, D. A. V., and Bowen, A. J., 1980, Sediment Waves on the Monterey Fan Levee - a Preliminary Physical Interpretation: Marine Geology, v. 37, no. 1-2, p. 1-18, doi: Doi 10.1016/0025-3227(80)90009-2.

Normark, W. R., Piper, D. J. W., Posamentier, H., Pirmez, C., and Migeon, S., 2002, Variability in form and growth of sediment waves on turbidite channel levees: Marine Geology, v. 192, no. 1-3, p. 23-58, doi: 10.1016/S0025-3227(02)00548-0.

Nye, J. F., 1952, The Mechanics of Glacier Flow: Journal of Glaciology, v. 2, no. 12, p. 82-93, doi: 10.1017/S0022143000033967.

O'Regan, M., Forwick, M., Jakobsson, M., Moran, K., and Mosher, D., 2015, Seafloor cratering and sediment remolding at sites of fluid escape: Geology, v. 43, no. 10, p. 895-898, doi: 10.1130/G36945.1.

Olu-Le Roy, K., Sibuet, M., Fiala-Médioni, A., Gofas, S., Salas, C., Mariotti, A., Foucher, J. P., and Woodside, J., 2004, Cold seep communities in the deep eastern Mediterranean Sea: composition, symbiosis and spatial distribution on mud volcanoes: Deep-Sea Research I, v. 51, p. 1915-1936

Orphan, V. J., Ussler III, W., Naehr, T. H., House, C. H., Hinrichs, K.-U., and Paull, C. K., 2004, Geological, geochemical, and microbiological heterogeneity of the seafloor around methane vents in the Eel River Basin, offshore California: Chemical Geology, v. 205, p. 265-289

Padden, M., Weissert, H., and de Rafelis, M., 2001, Evidence for Late Jurassic release of methane from gas hydrate: Geology, v. 29, no. 3, p. 223-226, doi: Doi 10.1130/0091-7613(2001)029<0223:Efljro>2.0.Co;2.

Pallasser, R. J., 2000, Recognising biodegradation in gas/oil accumulations through the delta C-13 compositions of gas components: Organic Geochemistry, v. 31, no. 12, p. 1363-1373, doi: 10.1016/S0146-6380(00)00101-7.

Panieri, G., et al., 2017, An integrated view of the methane system in the pockmarks at Vestnesa Ridge, 79°N: Marine Geology, v. 390, p. 282-300, doi: 10.1016/j.margeo.2017.06.006.

Panieri, G., Polonia, A., Lucchi, R. G., Zironi, S., Capotondi, L., Negri, A., and Torelli, L., 2013, Mud volcanoes along the inner deformation front of the Calabrian Arc accretionary wedge (Ionian Sea): Marine Geology, v. 336, p. 84-98, doi: 10.1016/j.margeo.2012.11.003.

Pape, T., Bahr, A., Klapp, S. A., Abegg, F., and Bohrmann, G., 2011a, High-intensity gas seepage causes rafting of shallow gas hydrates in the southeastern Black Sea: Earth and Planetary Science Letters, v. 307, no. 1-2, p. 35-46, doi: 10.1016/j.epsl.2011.04.030.

Pape, T., Feseker, T., Kasten, S., Fischer, D., and Bohrmann, G., 2011b, Distribution and abundance of gas hydrates in near-surface deposits of the Hakon Mosby Mud Volcano, SW Barents Sea: Geochemistry Geophysics Geosystems, v. 12, doi: 10.1029/2011gc003575.

Pape, T., Geprags, P., Hammerschmidt, S., Wintersteller, P., Wei, J. G., Fleischmann, T., Bohrmann, G., and Kopf, A. J., 2014, Hydrocarbon seepage and its sources at mud volcanoes of the Kumano forearc basin, Nankai Trough subduction zone: Geochemistry Geophysics Geosystems, v. 15, no. 6, p. 2180-2194, doi: 10.1002/2013gc005057.

Pape, T., Kasten, S., Zabel, M., Bahr, A., Abegg, F., Hohnberg, H.-J., and Bohrmann, G., 2010, Gas hydrates in shallow deposits of the Amsterdam mud volcano, Anaximander Mountains, Northeastern Mediterranean Sea: Geo-Marine Letters, v. 30, no. 3, p. 187-206, doi: 10.1007/s00367-010-0197-8.

Parnell, J., 2002, Fluid seeps at continental margins: Towards an integrated plumbing system: Geofluids, v. 2, no. 2, p. 57-61, doi: DOI 10.1046/j.1468-8123.2002.00035.x.

Paterne, M., Guichard, F., and Labeyrie, J., 1988, Explosive Activity of the South Italian Volcanos during the Past 80,000 Years as Determined by Marine Tephrochronology: Journal of Volcanology and Geothermal Research, v. 34, no. 3-4, p. 153-172, doi: 10.1016/0377-0273(88)90030-3.

Patterson, W. P., Smith, G. R., and Lohmann, K. C., 1993, Continental Paleothermometry and Seasonality Using the Isotopic Composition of Aragonitic Otoliths of Freshwater Fishes, Climate Change in Continental Isotopic Records, American Geophysical Union, p. 191-202.

Paull, C. K., Caress, D. W., Lundsten, E., Gwiazda, R., Anderson, K., McGann, M., Conrad, J., Edwards, B., and Sumner, E. J., 2013, Anatomy of the La Jolla Submarine Canyon system; offshore southern California: Marine Geology, v. 335, p. 16-34, doi: 10.1016/j.margeo.2012.10.003.

Paull, C. K., Caress, D. W., Thomas, H., Lundsten, E., Anderson, K., Gwiazda, R., Riedel, M., McGann, M., and Herguera, J. C., 2015a, Seafloor geomorphic manifestations of gas venting and shallow subbottom gas hydrate occurrences: Geosphere, v. 11, no. 2, p. 491-513, doi: 10.1130/Ges01012.1.

Paull, C. K., et al., 2015b, Active mud volcanoes on the continental slope of the Canadian Beaufort Sea: Geochemistry Geophysics Geosystems, v. 16, no. 9, p. 3160-3181, doi: 10.1002/2015gc005928.

Paull, C. K., et al., 1984, Biological communities at the Florida Escarpment resemble hydrothermal vent taxa: Science, v. 226, p. 965-967

Paull, C. K., Ussler, W., Caress, D. W., Lundsten, E., Covault, J. A., Maier, K. L., Xu, J. P., and Augenstein, S., 2010, Origins of large crescent-shaped bedforms within the axial channel of Monterey Canyon, offshore California: Geosphere, v. 6, no. 6, p. 755-774, doi: 10.1130/Ges00527.1.

Peakall, J., McCaffrey, B., and Kneller, B., 2000, A process model for the evolution, morphology, and architecture of sinuous submarine channels: Journal of Sedimentary Research, v. 70, no. 3, p. 434-448, doi: 10.1306/2dc4091c-0e47-11d7-8643000102c1865d.

Perez-Garcia, C., Feseker, T., Mienert, J., and Berndt, C., 2009, The Hakon Mosby mud volcano: 330 000 years of focused fluid flow activity at the SW Barents

Sea slope: Marine Geology, v. 262, no. 1-4, p. 105-115, doi: 10.1016/j.margeo.2009.03.022.

Pettinga, J. R., 2003, Mud volcano eruption within the emergent accretionary Hikurangi margin, southern Hawke's Bay, New Zealand: New Zealand Journal of Geology and Geophysics, v. 46, no. 1, p. 107-121

Philip, B. T., Denny, A. R., Solomon, E. A., and Kelley, D. S., 2016, Time-series measurements of bubble plume variability and water column methane distribution above Southern Hydrate Ridge, Oregon: Geochemistry Geophysics Geosystems, v. 17, no. 3, p. 1182-1196, doi: 10.1002/2016gc006250.

Pierre, C., 1999, The oxygen and carbon isotope distribution in the Mediterranean water masses: Marine Geology, v. 153, no. 1-4, p. 41-55, doi: Doi 10.1016/S0025-3227(98)00090-5.

Pierre, C., Bayon, G., Blanc-Valleron, M. M., Mascle, J., and Dupre, S., 2014, Authigenic carbonates related to active seepage of methane-rich hot brines at the Cheops mud volcano, Menes caldera (Nile deep-sea fan, eastern Mediterranean Sea): Geo-Marine Letters, v. 34, no. 2-3, p. 253-267, doi: 10.1007/s00367-014-0362-6.

Piper, D. J. W., and Normark, W. R., 1983, Turbidite Depositional Patterns and Flow Characteristics, Navy Submarine Fan, California Borderland: Sedimentology, v. 30, no. 5, p. 681-694, doi: 10.1111/j.1365-3091.1983.tb00702.x.

Planke, S., Svensen, H., Hovland, M., Banks, D. A., and Jamtveit, B., 2003, Mud and fluid migration in active mud volcanoes in Azerbaijan: Geo-Marine Letters, v. 23, p. 258-268, doi: 10.1007/s00367-003-0152-z.

Pollack, H. N., Hurter, S. J., and Johnson, J. R., 1991, A New Global Heat Flow Compilation. International Heat Flow Commission database: available via the IHFC website, http://www.heatflow.und.edu/ (10/2016)

Polonia, A., Panieri, G., Gasperini, L., Gasparotto, G., Bellucci, L. G., and Torelli, L., 2013, Turbidite paleoseismology in the Calabrian Arc Subduction Complex (Ionian Sea): Geochemistry Geophysics Geosystems, v. 14, no. 1, p. 112-140, doi: 10.1029/2012gc004402.

Polonia, A., Romano, S., Cagatay, M. N., Capotondi, L., Gasparotto, G., Gasperini, L., Panieri, G., and Torelli, L., 2015, Are repetitive slumpings during sapropel S1 related to paleo-earthquakes?: Marine Geology, v. 361, p. 41-52, doi: 10.1016/j.margeo.2015.01.001.

Polonia, A., Torelli, L., Mussoni, P., Gasperini, L., Artoni, A., and Klaeschen, D., 2011, The Calabrian Arc subduction complex in the Ionian Sea: Regional architecture, active deformation, and seismic hazard: Tectonics, v. 30, no. 5, doi: 10.1029/2010tc002821.

Posamentier, H. W., and Kolla, V., 2003, Seismic geomorphology and stratigraphy of depositional elements in deep-water settings: Journal of Sedimentary Research, v. 73, no. 3, p. 367-388, doi: 10.1306/111302730367.

Praeg, D., Ceramicola, S., Barbieri, R., Unnithan, V., and Wardell, N., 2009, Tectonically-driven mud volcanism since the late Pliocene on the Calabrian accretionary prism, central Mediterranean Sea: Marine and Petroleum Geology, v. 26, no. 9, p. 1849-1865, doi: 10.1016/j.marpetgeo.2009.03.008.

Prinzhofer, A., Mello, M. R., and Takaki, T., 2000, Geochemical characterization of natural gas: A physical multivariable approach and its applications in maturity and migration estimates: AAPG Bulletin-American Association of Petroleum Geologists, v. 84, no. 8, p. 1152-1172, doi: 10.1306/A9673C66-1738-11D7-8645000102C1865D.

Prior, D. B., Doyle, E. H., and Kaluza, M. J., 1989, Evidence for Sediment Eruption on Deep-Sea Floor, Gulf of Mexico: Science, v. 243, no. 4890, p. 517-519, doi: 10.1126/science.243.4890.517.

Quigley, T. M., and Mackenzie, A. S., 1988, The Temperatures of Oil and Gas-Formation in the Sub-Surface: Nature, v. 333, no. 6173, p. 549-552, doi: 10.1038/333549a0.

Rabaute, A., and Chamot-Rooke, N., 2007, Quantitative mapping of active mud volcanism at the western Mediterranean Ridge-backstop contact: Marine Geophysical Researches, v. 28, no. 3, p. 271-295, doi: 10.1007/s11001-007-9031-8.

Reusch, A., et al., 2015, Giant lacustrine pockmarks with subaqueous groundwater discharge and subsurface sediment mobilization: Geophysical Research Letters, v. 42, no. 9, p. 3465-3473, doi: 10.1002/2015gl064179.

Ritger, S., Carson, B., and Suess, E., 1987, Methane-derived authigenic carbonates formed by subduction-induced pore-water expulsion along the Oregon/Washington margin: Geological Society of America Bulletin, v. 98, p. 147-156

Roberts, H. H., and Carney, R. S., 1997, Evidence of episodic fluid, gas, and sediment venting on the northern Gulf of Mexico continental slope: Economic Geology, v. 92, p. 863-879

Roberts, K. S., Davies, R. J., and Stewart, S. A., 2010, Structure of exhumed mud volcano feeder complexes, Azerbaijan: Basin Research, v. 22, no. 4, p. 439-451, doi: 10.1111/j.1365-2117.2009.00441.x.

Roberts, K. S., Davies, R. J., Stewart, S. A., and Tingay, M., 2011a, Structural controls on mud volcano vent distributions: examples from Azerbaijan and Lusi, east Java: Journal of the Geological Society, v. 168, no. 4, p. 1013-1030, doi: 10.1144/0016-76492010-158.

Roberts, K. S., Stewart, S. A., Davies, R. J., and Evans, R. J., 2011b, Sector collapse of mud volcanoes, Azerbaijan: Journal of the Geological Society, v. 168, no. 1, p. 49-60, doi: 10.1144/0016-76492010-115.

Robertson, A., et al., 1996, Mud volcanism on the Mediterranean Ridge: Initial results of Ocean Drilling Program Leg 160: Geology, v. 24, no. 3, p. 239-242, doi: 10.1130/0091-7613(1996)024<0239:Mvotmr>2.3.Co;2.

Robertson, A. H. F., and Kopf, A., 1998, Tectonic setting and processes of mud volcanism on the Mediterranean ridge accretionary complex: Evidence from Leg 160, In Robertson, A.H.F., Emeis, K.-C., Richter, C., and Camerlenghi, A. (Eds.): Proceedings of the Ocean Drilling Program, Scientific Results, v. 160: College Station, TX (Ocean Drilling Program), p. 665-680, doi: 10.2973/odp.proc.sr.160.062.1998.

Roda, C., 1964, Distribuzione e facies dei sedimenti Neogenici nel Bacino Crotonese: Geol. Romana, v. 3, p. 319–366

Römer, M., Riedel, M., Scherwath, M., Heesemann, M., and Spence, G. D., 2016, Tidally controlled gas bubble emissions: A comprehensive study using long-term monitoring data from the NEPTUNE cabled observatory offshore Vancouver Island: Geochemistry Geophysics Geosystems, v. 17, no. 9, p. 3797-3814, doi: 10.1002/2016gc006528.

Römer, M., Sahling, H., Pape, T., Bahr, A., Feseker, T., Wintersteller, P., and Bohrmann, G., 2012a, Geological control and quantity of methane ebullition from a high-flux seep area in the Black Sea - the Kerch seep area: Marine Geology, v. 319-322, p. 57-74, doi: 10.1016/j.margeo.2012.07.005.

Römer, M., Sahling, H., Pape, T., Bohrmann, G., and Spiess, V., 2012b, Quantification of gas bubble emissions from submarine hydrocarbon seeps at the Makran continental margin (offshore Pakistan): Jounal of geophysical Research, v. 117, p. C10015, doi: 10.1029/2011JC007424.

Römer, M., Sahling, H., Pape, T., Ferreira, C. D., Wenzhofer, F., Boetius, A., and Bohrmann, G., 2014, Methane fluxes and carbonate deposits at a cold seep area of the Central Nile Deep Sea Fan, Eastern Mediterranean Sea: Marine Geology, v. 347, no. 0, p. 27-42, doi: 10.1016/j.margeo.2013.10.011.

Römer, M., Wenau, S., Mau, S., Veloso, M., Greinert, J., Schlüter, M., and Bohrmann, G., 2017, Assessing marine gas emission activity and contribution to the atmospheric methane inventory: A multidisciplinary approach from the Dutch Dogger Bank seep area (North Sea): Geochemistry, Geophysics, Geosystems, v. 18, no. 7, p. 2617-2633, doi: 10.1002/2017GC006995.

Rosenbaum, G., Lister, G. S., and Duboz, C., 2002, Reconstruction of the tectonic evolution of the western Mediterranean since the Oligocene: In: Rosenbaum, G. and Lister, G. S. 2002. Reconstruction of the evolution of the Alpine-Himalayan Orogen, v. Journal of the Virtual Explorer, no. 8, p. 107 - 130

Rossi, S., and Sartori, R., 1981, A Seismic-Reflection Study of the External Calabrian Arc in the Northern Ionian Sea (Eastern Mediterranean): Marine Geophysical Researches, v. 4, no. 4, p. 403-426, doi: 10.1007/Bf00286036.

Roveri, M., Bernasconi, A., Rossi, M., and Visentin, C., 1992, Sedimentary evolution of the Luna Field area, Calabria, Southern Italy: In: Generation Accumulation and Production of Europe's Hydrocarbons II (Spencer AM, Ed.); Special Publication of the European Association of Petroleum Geoscientists No. 2, Springer-Verlag, Berlin, p. 217-224

Roveri, M., et al., 2014, The Messinian Salinity Crisis: Past and future of a great challenge for marine sciences: Marine Geology, v. 352, p. 25-58, doi: 10.1016/j.margeo.2014.02.002.

Rubin-Blum, M., et al., 2017, Short-chain alkanes fuel mussel and sponge Cycloclasticus symbionts from deep-sea gas and oil seeps, v. 2, p. 17093, doi: 10.1038/nmicrobiol.2017.93.

Rubin-Blum, M., Tsadok, R., Shemesh, E., Goodman-Tchernov, B. N., Austin, J. A., Coleman, D. F., Ben-Avraham, Z., Gruber, D. F., and Tchernov, D., 2014, Distribution of the Lamellibrachia spp. (Siboglinidae, Annelida) and their trophosome endosymbiont phylotypes in the Mediterranean Sea: Marine Biology, v. 161, no. 6, p. 1229-1239, doi: 10.1007/s00227-014-2413-y.

Ryan, W. B. F., et al., 2009, Global Multi-Resolution Topography synthesis: Geochemistry Geophysics Geosystems, v. 10, no. 3, p. n/a-n/a, doi: 10.1029/2008gc002332.

Sahling, H., et al., 2009, Vodyanitskii mud volcano, Sorokin trough, Black Sea: Geological characterization and quantification of gas bubble streams: Marine and Petroleum Geology, v. 26, no. 9, p. 1799-1811

Sahling, H., Bohrmann, G., Spiess, V., Bialas, J., Breitzke, M., Ivanov, M., Kasten, S., Krastel, S., and Schneider, R., 2008a, Pockmarks in the Northern Congo Fan area, SW Africa: Complex seafloor features shaped by fluid flow: Marine Geology, v. 249, no. 3-4, p. 206-225

Sahling, H., et al., 2016, Massive asphalt deposits, oil seepage, and gas venting support abundant chemosynthetic communities at the Campeche Knolls, southern Gulf of Mexico: Biogeosciences, v. 13, no. 15, p. 4491-4512, doi: 10.5194/bg-13-4491-2016.

Sahling, H., Masson, D. G., Ranero, C. R., Hühnerbach, V., Weinrebe, W., Klaucke, I., Bürk, D., Brückmann, W., and Suess, E., 2008b, Fluid seepage at the continental margin offshore Costa Rica and southern Nicaragua: Geochemistry Geophysics Geosystems, v. 9, no. 5, doi: 10.1029/2008GC001978.

Sahling, H., Rickert, D., Lee, R. W., Linke, P., and Suess, E., 2002, Macrofaunal community structure and sulfide flux at gas hydrate deposits from the Cascadia convergent margin, NE Pacific: Marine Ecology Progress Series, v. 231, p. 121-138

Sahling, H., Wallmann, K., Dählmann, A., Schmaljohann, R., and Petersen, S., 2005, The physicochemical habitat of *Sclerolinum* sp. at Hook Ridge hydrothermal vent, Bransfield Strait, Antarctica: Limnology and Oceanography, v. 50, no. 2, p. 598-606

Sandwell, D. T., Muller, R. D., Smith, W. H. F., Garcia, E., and Francis, R., 2014, New global marine gravity model from CryoSat-2 and Jason-1 reveals buried tectonic structure: Science, v. 346, no. 6205, p. 65-67, doi: 10.1126/science.1258213.

Sartori, R., 2003, The Tyrrhenian back-arc basin and subduction of the Ionian lithosphere: Episodes, v. 26, no. 3, p. 217-221

Sassen, R., Roberts, H. H., Aharon, P., Larkin, J., Chinn, E. W., and Carney, R., 1993, Chemosynthetic bacterial mats at cold hydrocarbon seeps, Gulf of Mexico continetal slope: Organic Geochemistry, v. 20, no. 1, p. 77-89

Sassen, R., Roberts, H. H., Carney, R., Milkov, A. V., DeFreitas, D. A., Lanoil, B. D., and Zhang, C. L., 2004, Free hydrocarbon gas, gas hydrate, and authigenic minerals in chemosynthetic communities of the northern Gulf of Mexico continental slope: relation to microbial processes: Chemical Geology, v. 205, p. 195-217

Sauter, E. J., Muyakshin, S. I., Charlou, J.-L., Schlüter, M., Boetius, A., Jerosch, K., Damm, E., Foucher, J.-P., and Klages, M., 2006, Methane discharge from a deep-sea submarine mud volcano into the upper water column by gas hydrate-coated methane bubbles: Earth and Planetary Science Letters, v. 243, p. 354-365

Schoell, M., 1983, Genetic-Characterization of Natural Gases: Aapg Bulletin-American Association of Petroleum Geologists, v. 67, no. 12, p. 2225-2238

Shanmugam, G., 2000, 50 years of the turbidite paradigm (1950s-1990s): deep-water processes and facies models - a critical perspective: Marine and Petroleum Geology, v. 17, no. 2, p. 285-342, doi: 10.1016/S0264-8172(99)00011-2.

Sibuet, M., and Olu, K., 1998, Biogeography, biodiversity and fluid dependence of deep-sea cold-seep communities at active and passive margins: Deep-Sea Research II, v. 45, p. 517-567

Skarke, A., Ruppel, C., Kodis, M., Brothers, D., and Lobecker, E., 2014, Widespread methane leakage from the sea floor on the northern US Atlantic margin: Nature Geosci, v. advance online publication, doi: 10.1038/ngeo2232.

Sloan, E. D., and Koh, C., 2008, Clathrate Hydrates of Natural Gases, Third Edition, CRC Press.

Smith, E. B., Scott, K. M., Nix, E. R., Korte, C., and Fisher, C. R., 2000, Growth and condition of seep mussels (Bathymodiolus childressi) at a Gulf of Mexico brine pool: Ecology, v. 81, no. 9, p. 2392-2403

Sommer, S., et al., 2006, Efficiency of the benthic filter: Biological control of the emission of dissolved methane from sediments containing shallow gas hydrates at Hydrate Ridge: Global Biogeochemical Cycles, v. 20, doi: 10.1029/2004GB002389.

Somoza, L., et al., 2012, Structure of mud volcano systems and pockmarks in the region of the Ceuta Contourite Depositional System (Western Alborán Sea): Marine Geology, v. 332-334, p. 4-26, doi: 10.1016/j.margeo.2012.06.002.

Southward, E. C., Andersen, A. C., and Hourdez, S., 2011, Lamellibrachia anaximandri n. sp., a new vestimentiferan tubeworm (Annelida) from the Mediterranean, with notes on frenulate tubeworms from the same habitat: Zoosystema, v. 33, no. 3, p. 245-279, doi: doi:10.5252/z2011n3a1.

Spakman, W., 1986, Subduction beneath Eurasia in connection with the Mesozoic Tethys: Geologie en Mijnbouw, v. 65, no. 2, p. 145-153

Spakman, W., and Wortel, M., 2004, A Tomographic View on Western Mediterranean Geodynamics, in: The TRANSMED Atlas, The Mediterranean Region from Crust to Mantle, Edited by: Cavazza W, Roure F, Spakman W., Stampfli GM, Ziegler P.

Stadnitskaia, A., Ivanov, M. K., Poludetkina, E. N., Kreulen, R., and van Weering, T. C. E., 2008, Sources of hydrocarbon gases in mud volcanoes from the Sorokin Trough, NE Black Sea, based on molecular and carbon isotopic compositions: Marine and Petroleum Geology, v. 25, no. 10, p. 1040-1057

Stakes, D. S., Tréhu, A. M., Goffredi, S. K., Naehr, T. H., and Duncan, R. A., 2002, Mass wasting, methane venting, and biological communities on the Mendocino transform fault: Geology, v. 30, no. 5, p. 407-410

Stewart, S. A., and Davies, R. J., 2006, Structure and emplacement of mud volcano systems in the South Caspian Basin: Aapg Bulletin, v. 90, no. 5, p. 771-786, doi: Doi 10.1306/11220505045.

Stolper, D. A., et al., 2014, Formation temperatures of thermogenic and biogenic methane: Science, v. 344, no. 6191, p. 1500-1503, doi: 10.1126/science.1254509.

Suess, E., 2014, Marine cold seeps and their manifestations: geological control, biogeochemical criteria and environmental conditions: International Journal of Earth Sciences, v. 103, no. 7, p. 1889-1916, doi: 10.1007/s00531-014-1010-0.

Suess, E., et al., 1999, Gas hydrate destabilization: enhanced dewatering, benthic material turnover and large methane plumes at the Cascadia convergent margin: Earth and Planetary Science Letters, v. 170, p. 1-15

Sultan, N., et al., 2014, Pockmark formation and evolution in deep water Nigeria: Rapid hydrate growth versus slow hydrate dissolution: Journal of Geophysical Research-Solid Earth, v. 119, no. 4, p. 2679-2694, doi: 10.1002/2013jb010546.

Symons, W. O., Sumner, E. J., Tailing, P. J., Cartigny, M. J. S., and Clare, M. A., 2016, Large-scale sediment waves and scours on the modern seafloor and their implications for the prevalence of supercritical flows: Marine Geology, v. 371, p. 130-148, doi: 10.1016/j.margeo.2015.11.009.

Taki, K., and Parker, G., 2005, Transportational cyclic steps created by flow over an erodible bed. Part 1. Experiments: Journal of Hydraulic Research, v. 43, no. 5, p. 488-501

Teichert, B. M. A., Bohrmann, G., and Suess, E., 2005, Chemoherms on Hydrate Ridge: Unique microbially-mediated carbonate build-ups growing into the water column: Palaeogeography, Palaeoclimatology, Palaeoecology, v. 227, no. 1-3, p. 67-85

Teichert, B. M. A., Eisenhauer, A., Bohrmann, G., Haase-Schramm, A., Bock, B., and Linke, P., 2003, U/Th systematics and ages of authigenic carbonates from Hydrate Ridge, Cascadia Margin: Recorders of fluid flow variations: Geochimica Et Cosmochimica Acta, v. 67, no. 20, p. 3845-3857, doi: 10.1016/S0016-7037(03)00128-5.

Tingay, M., 2015, Initial pore pressures under the Lusi mud volcano, Indonesia: Interpretation-a Journal of Subsurface Characterization, v. 3, no. 1, p. Se33-Se49, doi: 10.1190/Int-2014-0092.1.

Tinivella, U., and Giustiniani, M., 2012, An Overview of Mud Volcanoes Associated to Gas Hydrate System.

Torres, M. E., Kim, J.-H., Choi, J.-Y., Ryu, B.-J., Bahk, J.-J., Riedel, M., Collett, T. S., Hong, W.-L., and Kastner, M., Occurrence of high salinity fluids associated with massive near-seafloor gas hydrate deposits, *in* Proceedings Proceedings of the 7th International Conference on Gas Hydrates (ICGH 2011), Edinburgh, Scotland, United Kingdom2011.

Torres, M. E., Teichert, B. M. A., Tréhu, A., Borowski, W., and Tomaru, H., 2004a, Relationship of pore water freshening to accretionary processes in the Cascadia margin: Fluid sources and gas hydrate abundance: Geophysical Research Letters, v. 31, doi: 10.1029/2004GL021219.

Torres, M. E., Wallmann, K., Tréhu, A. M., Bohrmann, G., Borowski, W. S., and Tomaru, H., 2004b, Gas hydrate growth, methane transport, and chloride enrichment at the southern summit of Hydrate Ridge, Cascadia margin off Oregon: Earth and Planetary Science Letters, v. 226, p. 225-241

Treude, T., Knittel, K., Blumenberg, M., Seifert, R., and Boetius, A., 2005, Subsurface microbial methanotrophic mats in the Black Sea: Applied and Environmental Microbiology, v. 71, no. 10, p. 6375-6378, doi: 10.1128/Aem.71.10.6375-6378.2005.

Trincardi, F., Verdicchio, G., and Miserocchi, S., 2007, Seafloor evidence for the interaction between cascading and along-slope bottom water masses: Journal of Geophysical Research-Earth Surface, v. 112, no. F3, doi: 10.1029/2006jf000620.

Troll, V. R., Walter, T. R., and Schmincke, H. U., 2002, Cyclic caldera collapse: Piston or piecemeal subsidence? Field and experimental evidence: Geology, v. 30, no. 2, p. 135-138, doi: Doi 10.1130/0091-7613(2002)030<0135:Cccpop>2.0.Co;2.

Ussler, W., and Paull, C. K., 1995, Effects of Ion-Exclusion and Isotopic Fractionation on Pore-Water Geochemistry during Gas Hydrate Formation and Decomposition: Geo-Marine Letters, v. 15, no. 1, p. 37-44, doi: 10.1007/Bf01204496.

Van Dijk, J. P., et al., 2000, A regional structural model for the northern sector of the Calabrian Arc (southern Italy): Tectonophysics, v. 324, no. 4, p. 267-320, doi: 10.1016/S0040-1951(00)00139-6.

van Loon, A. J., 2010, Sedimentary volcanoes: Overview and implications for the definition of a volcano on Earth, *in* Cañón-Tapia, E., and Szakács, A., eds., What Is a Volcano?, Geological Society of America.

Van Rensbergen, P., Depreiter, D., Pannemans, B., and Henriet, J., 2005a, Seafloor expression of sediment extrusion and intrusion at the El Arraiche mud volcano field, Gulf of Cadiz: Journal of Geophysical Research, v. 110, doi: 10.1029/2004JF000165.

Van Rensbergen, P., et al., 2005b, The El Arraiche mud volcano field at the Moroccan Atlantic slope, Gulf of Cadiz: Marine Geology, v. 219, p. 1-17

Van Rensbergen, P., Hillis, R. R., Maltman, A. J., and Morley, C. K., 2003, Subsurface sediment mobilization: introduction: Subsurface Sediment Mobilization, v. 216, p. 1-8, doi: Doi 10.1144/Gsl.Sp.2003.216.01.01.

Vandorpe, T., Martins, I., Vitorino, J., Hebbeln, D., Garcia, M., and Van Rooij, D., 2016, Bottom currents and their influence on the sedimentation pattern in the El Arraiche mud volcano province, southern Gulf of Cadiz: Marine Geology, v. 378, p. 114-126, doi: 10.1016/j.margeo.2015.11.012.

Vogt, C., Lauterjung, J., and Fischer, R. X., 2002, Investigation of the clay fraction (< 2 µm) of the Clay Minerals Society reference clays: Clays and Clay Minerals, v. 50, no. 3, p. 388-400, doi: 10.1346/000986002760833765.

Vogt, P. R., Gardner, J., Crane, K., Sundvor, E., Bowles, F., and Cherkashev, G., 1999, Ground-truthing 11- to 12-kHz side-scan sonar imagery in the Norwegian-Greenland Sea: Part I: Pockmarks on the Vestnesa Ridge and Storegga slide margin: Geo-Marine Letters, v. 19, p. 97-110

Volgin, A. V., and Woodside, J. M., 1996, Sidescan sonar images of mud volcnoes from the Mediterranean Ridge: possible causes of variations in backscatter intensity: Marine Geology, v. 132, p. 39-53

Vornberger, P. L., and Whillans, I. M., 1990, Crevasse Deformation and Examples from Ice Stream-B, Antarctica: Journal of Glaciology, v. 36, no. 122, p. 3-10

Wallmann, K., Drews, M., Aloisi, G., and Bohrmann, G., 2006, Methane discharge into the Black Sea and the global ocean via fluid flow through submarine mud volcanoes: Earth and Planetary Science Letters, v. 248, no. 1-2, p. 545-560, doi: 10.1016/j.epsl.2006.06.026.

Weinberger, J. L., Brown, K. M., and Long, P. E., 2005, Painting a picture of gas hydrate distribution with thermal images: Geophysical Research Letters, v. 32, no. L04609, doi: 10.1029/2004GL021437.

Westaway, R., 1993, Quaternary Uplift of Southern Italy: Journal of Geophysical Research-Solid Earth, v. 98, no. B12, p. 21741-21772, doi: 10.1029/93jb01566.

Whiticar, M. J., 1999, Carbon and hydrogen isotope systematics of bacterial formation and oxidation of methane: Chemical Geology, v. 161, no. 1-3, p. 291-314, doi: 10.1016/S0009-2541(99)00092-3.

Whiticar, M. J., Faber, E., and Schoell, M., 1986, Biogenic methane formation in marine and freshwater environments: CO2 reduction vs. Acetate fermentation - Isotope evidence: Geochimica et Cosmochimica Acta, v. 50, p. 693-709

Woodside, J. M., Ivanov, M. K., Limonov, A. F., and expedition, S. s. o. t. a., 1998, Shallow gas and gas hydrates in the Anaximander Mountain region, eastern Mediterranean Sea, *in* Henriet, J. P., and Mienert, J., eds., Gas Hydrates: Relevance to World Margin Stability and Climate Change, Volume 137: London, Geological Society, p. 177-193.

Woodside, J. M., and Volgin, A. V., 1996, Brine pools associated with Mediterranean Ridge mud diapirs: An interpretation of echo-free patches in deep tow sidescan sonar data: Marine Geology, v. 132, no. 1-4, p. 55-61, doi: Doi 10.1016/0025-3227(95)00153-0.

Wortel, M. J. R., and Spakman, W., 2000, Subduction and slab detachment in the Mediterranean-Carpathian region: Science, v. 290, no. 5498, p. 1910-1917, doi: DOI 10.1126/science.290.5498.1910.

Wulf, S., Kraml, M., and Keller, J., 2008, Towards a detailed distal tephrostratigraphy in the Central Mediterranean: The last 20,000 yrs record of Lago Grande di Monticchio: Journal of Volcanology and Geothermal Research, v. 177, no. 1, p. 118-132, doi: 10.1016/j.jvolgeores.2007.10.009.

Wynn, R. B., et al., 2014, Autonomous Underwater Vehicles (AUVs): Their past, present and future contributions to the advancement of marine geoscience: Marine Geology, v. 352, no. 0, p. 451-468, doi: 10.1016/j.margeo.2014.03.012.

Yang, D. H., and Xu, W. Y., 2007, Effects of salinity on methane gas hydrate system: Science in China Series D-Earth Sciences, v. 50, no. 11, p. 1733-1745, doi: 10.1007/s11430-007-0126-5.

Yassir, N. A., 1989, Mud volcanoes and the behaviour of overpressured clays and silts: University of London.

Yusifov, M., and Rabinowitz, P. D., 2004, Classification of mud volcanoes in the South Caspian Basin, offshore Azerbijan: Marine and Petroleum Geology, v. 21, p. 965-975

Zanchetta, G., Sulpizio, R., Roberts, N., Cioni, R., Eastwood, W. J., Siani, G., Caron, B., Paterne, M., and Santacroce, R., 2011, Tephrostratigraphy, chronology and climatic events of the Mediterranean basin during the Holocene: An overview: Holocene, v. 21, no. 1, p. 33-52, doi: 10.1177/0959683610377531.

Zecchin, M., Caffau, M., and Ceramicola, S., 2016, Interplay between regional uplift and glacio-eustasy in the Crotone Basin (Calabria, southern Italy) since 0.45 Ma: A review: Global and Planetary Change, v. 143, p. 196-213, doi: 10.1016/j.gloplacha.2016.06.013.

Zecchin, M., Caffau, M., Civile, D., Critelli, S., Di Stefano, A., Maniscalco, R., Muto, F., Sturiale, G., and Roda, C., 2012, The Plio-Pleistocene evolution of the Crotone Basin (southern Italy): Interplay between sedimentation, tectonics and eustasy in the frame of Calabrian Arc migration: Earth-Science Reviews, v. 115, no. 4, p. 273-303, doi: 10.1016/j.earscirev.2012.10.005.

Zecchin, M., Caffau, M., and Roda, C., 2011, Relationships between high-magnitude relative sea-level changes and filling of a coarse-grained submarine canyon (Pleistocene, Ionian Calabria, Southern Italy): Sedimentology, v. 58, no. 4, p. 1030-1064, doi: 10.1111/j.1365-3091.2010.01194.x.

Zecchin, M., Massari, F., Mellere, D., and Prosser, G., 2003, Architectural styles of prograding wedges in a tectonically active setting, Crotone Basin, Southern Italy: Journal of the Geological Society, v. 160, p. 863-880, doi: 10.1144/0016-764902-099.

Zecchin, M., Praeg, D., Ceramicola, S., and Muto, F., 2015, Onshore to offshore correlation of regional unconformities in the Plio-Pleistocene sedimentary successions of the Calabrian Arc (central Mediterranean): Earth-Science Reviews, v. 142, p. 60-78, doi: 10.1016/j.earscirev.2015.01.006.

Zeebe, R. E., 2001, Seawater pH and isotopic paleotemperatures of Cretaceous oceans: Palaeogeography Palaeoclimatology Palaeoecology, v. 170, no. 1-2, p. 49-57, doi: 10.1016/S0031-0182(01)00226-7.

Zitter, T. A. C., Huguen, C., and Woodside, J. M., 2005, Geology of mud volcanoes in the eastern Mediterranean from combined sidescan sonar and submersible surveys: Deep-Sea Research I, v. 52, p. 457-475

# 13. Appendix

## 13.1. Supporting information for manuscript I

### Mud extrusion and ring-fault gas seepage – upward branching fluid discharge at the deep-sea Venere mud volcano (Central Mediterranean Sea)

M. Loher[1]*, T. Pape 1, Y. Marcon [1,2], M. Römer[1], P. Wintersteller[1], D. Praeg[3], M. Torres[4], H. Sahling[1], G. Bohrmann[1]

[1]MARUM - Center for Marine Environmental Sciences and Department of Geosciences at University of Bremen, Klagenfurter Str., 28359 Bremen, Germany

[2]Alfred Wegener Institute, Helmholtz Centre for Polar and Marine Research, Am Handelshafen 12, 27570 Bremerhaven, Germany

[3]Géoazur, UMR7329 CNRS, 250 rue Albert Einstein, 06560 Valbonne, France AND Institute of Petroleum and Natural Resources, PUCRS, Av. Ipiranga, 6681, 90619-900 Porto Alegre, RS, Brazil

*corresponding author e-mail: mloher@marum.de

Submitted to the journal of *Marine and Petroleum Geology* on 21 May 2017. We provide tables containing pore fluid data (Tables 13.1-11) used in the figures and main text (cmbsf = centimeters below sea floor).

Table 13.1. Depth indication, chloride and sulfate concentrations of pore water analyses of GeoB19230-5.

| Depth / cmbsf | Chloride / mmol/L | Sulfate / mmol/L |
|---|---|---|
| 4.5 | 603.2 | 19.1 |
| 8.5 | 623.0 | 4.8 |
| 12.5 | 607.5 | 0.8 |
| 16.5 | 592.9 | 0.9 |
| 20.5 | 612.9 | 0.3 |
| 24.5 | 612.5 | 3.3 |

Table 13.2. Depth indication, chloride and sulfate concentrations of pore water analyses of GeoB19236-1.

| Depth / cmbsf | Chloride / mmol/L | Sulfate / mmol/L |
|---|---|---|
| 3 | 601.6 | 25.7 |
| 8 | 601.0 | 16.0 |
| 14 | 600.8 | 10.2 |
| 25 | 601.2 | 1.3 |
| 35 | 593.9 | 1.9 |
| 55 | 593.6 | 2.2 |
| 75 | 599.7 | 4.0 |
| 99 | 597.2 | 1.8 |
| 125 | 607.1 | 1.3 |
| 155 | 601.6 | 0.7 |
| 178 | 600.4 | 0.9 |
| 190 | 603.2 | 0.5 |

Table 13.3. Depth indication, chloride and sulfate concentrations of pore water analyses of GeoB19267-4.

| Depth / cmbsf | Chloride / mmol/L | Sulfate / mmol/L |
|---|---|---|
| 3 | 613.9 | 27.13 |
| 7 | 610.8 | 12.83 |
| 11 | 615.1 | 1.52 |
| 15 | 618.8 | 0.13 |
| 19 | 610.6 | 1.27 |

Table 13.4. Depth indication, chloride and sulfate concentrations of pore water analyses of GeoB19249-7.

| Depth / cmbsf | Chloride / mmol/L | Sulfate / mmol/L |
|---|---|---|
| 3 | 644.7 | 18.7 |
| 7 | 604.6 | 4.6 |
| 11 | 605.7 | 2.9 |
| 15 | 607.1 | 1.8 |
| 19 | 607.6 | 1.4 |

Table 13.5. Depth indication, chloride and sulfate concentrations of pore water analyses of GeoB192340-10.

| Depth / cmbsf | Chloride / mmol/L | Sulfate / mmol/L |
|---|---|---|
| 1.5 | 613.0 | 28.1 |
| 5.5 | 609.6 | 24.0 |
| 9.5 | 611.3 | 22.0 |
| 13.5 | 609.7 | 24.8 |
| 17.5 | 611.2 | 21.3 |

Table 13.6. Depth indication, chloride and sulfate concentrations of pore water analyses of GeoB19242-6.

| Depth / cmbsf | Chloride / mmol/L | Sulfate / mmol/L |
|---|---|---|
| 1 | 573.5 | 26.1 |
| 5 | 542.4 | 22.7 |
| 9 | 506.1 | 21.7 |
| 13 | 416.8 | 18.2 |
| 17 | 314.3 | 9.4 |

Table 13.7. Depth indication, chloride and sulfate concentrations of pore water analyses of GeoB19242-10.

| Depth / cmbsf | Chloride / mmol/L | Sulfate / mmol/L |
|---|---|---|
| 1.5 | 587.9 | 27.1 |
| 5.5 | 546.5 | 22.6 |
| 9.5 | 521.0 | 22.6 |
| 13.5 | 471.3 | 18.3 |
| 17.5 | 419.8 | 14.1 |

Table 13.8. Depth indication, chloride and sulfate concentrations of pore water analyses of GeoB19242-11.

| Depth / cmbsf | Chloride / mmol/L | Sulfate / mmol/L |
|---|---|---|
| 2 | 525.3 | 23.5 |
| 6 | 414.7 | 14.9 |
| 10 | 292.8 | 7.0 |
| 14 | 185.7 | 1.4 |
| 18 | 145.9 | 0.3 |

Table 13.9. Depth indication, chloride and sulfate concentrations of pore water analyses of GeoB19242-14.

| Depth / cmbsf | Chloride / mmol/L | Sulfate / mmol/L |
|---|---|---|
| 1.5 | 539.4 | 25.8 |
| 5.5 | 438.3 | 17.5 |
| 13.5 | 171.5 | 0.9 |
| 17.5 | 169.2 | 1.1 |

Table 13.10. Depth indication, chloride and sulfate concentrations of pore water analyses of GeoB19242-17.

| Depth / cmbsf | Chloride / mmol/L | Sulfate / mmol/L |
|---|---|---|
| 2 | 243.3 | 4.5 |
| 10 | 160.2 | 1.0 |
| 14 | 128.2 | 0.3 |
| 18 | 160.9 | 0.7 |

Table 13.11. Depth indication, chloride and sulfate concentrations of pore water analyses of GeoB19245-1.

| Depth / cmbsf | Chloride / mmol/L | Sulfate / mmol/L |
|---|---|---|
| 22 | 274.8 | 7.7 |
| 70 | 130.5 | 0.4 |
| 89 | 137.6 | 0.6 |
| 107 | 130.0 | 0.3 |
| 127 | 133.7 | 0.4 |
| 147 | 132.7 | 0.3 |
| 197 | 127.9 | 0.1 |
| 260 | 149.8 | 1.0 |
| 325 | 138.5 | 0.5 |
| 395 | 125.7 | 0.0 |
| 447 | 128.8 | 0.0 |
| 498 | 125.4 | 0.0 |

## 13.2. Supporting information for manuscript II

### Mud volcanism in a canyon: Morpho-dynamic evolution of the active Venere mud volcano and its interplay with Squillace Canyon, Central Mediterranean

Markus Loher[1], Silvia Ceramicola[2], Paul Wintersteller[1], Gerrit Meinecke[1], Heiko Sahling[1], Gerhard Bohrmann[1]

[1]MARUM – Center for Marine Environmental Sciences and Faculty of Geosciences, University of Bremen, Klagenfurter Str., 28359 Bremen, Germany

[2]OGS (Istituto Nazionale di Oceanografia e di Geofisica Sperimentale), Borgo Grotta Gigante 42/c, Sgonico, 34010 Trieste, Italy

Submitted to the journal of *Geochemistry, Geophysics, Geosystems* on 31 July 2017. In the supplementary data we provide two figures (13.1 and 13.2) with core photos and interpretations of the gravity- as well as the mini-cores used in this study. Fig. 13.3 is complementary to Fig. 6.3 in the main manuscript showing the slope-map of the same areal extent. Table 13.12 gives the results of the WDS analyses used in this study.

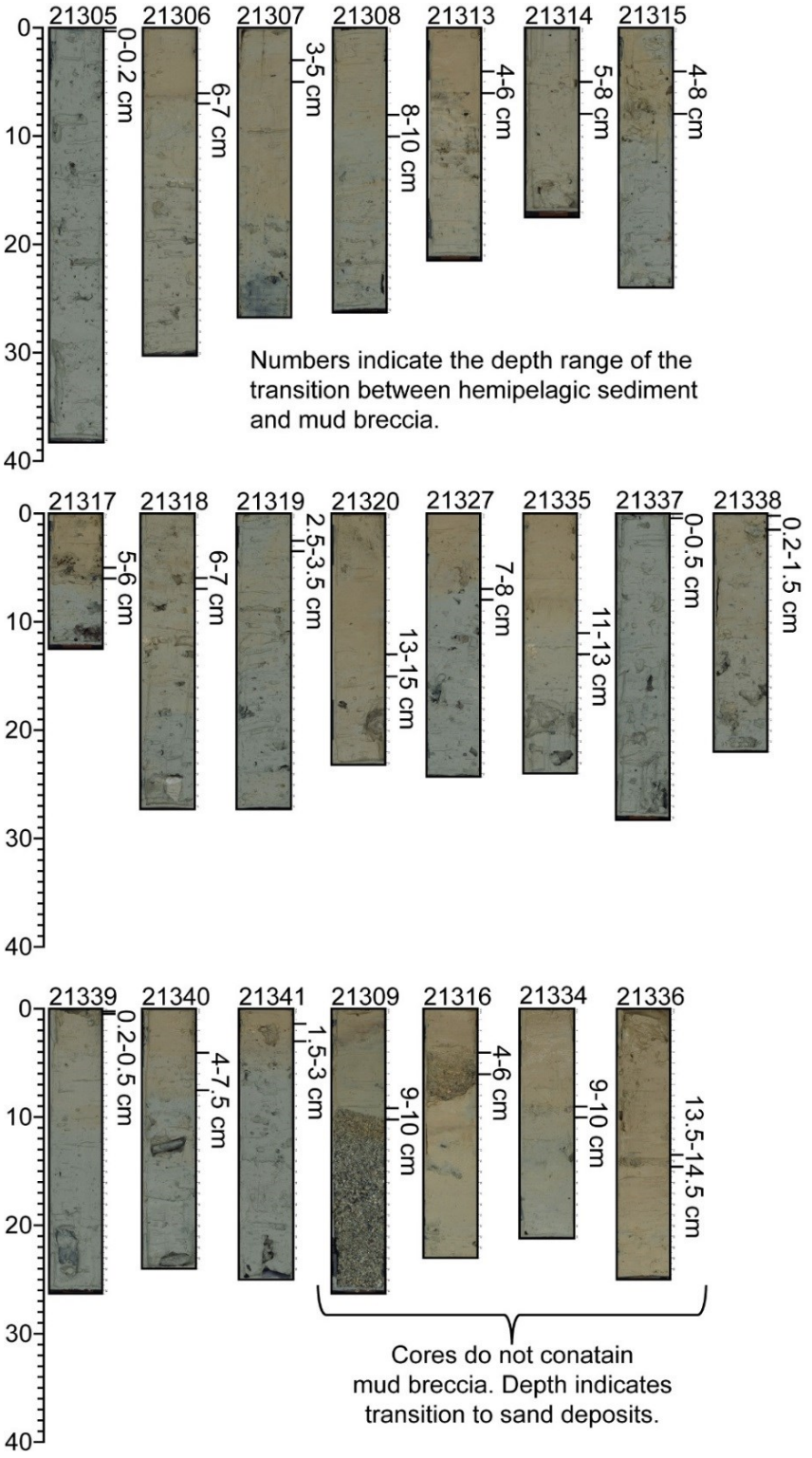


Figure 13.1. Core photos of all mini-cores (numbers above indicate GeoB-identifier) used in this study; the amount of hemipelagic burial of mud breccia is indicated by numbers next to cores.

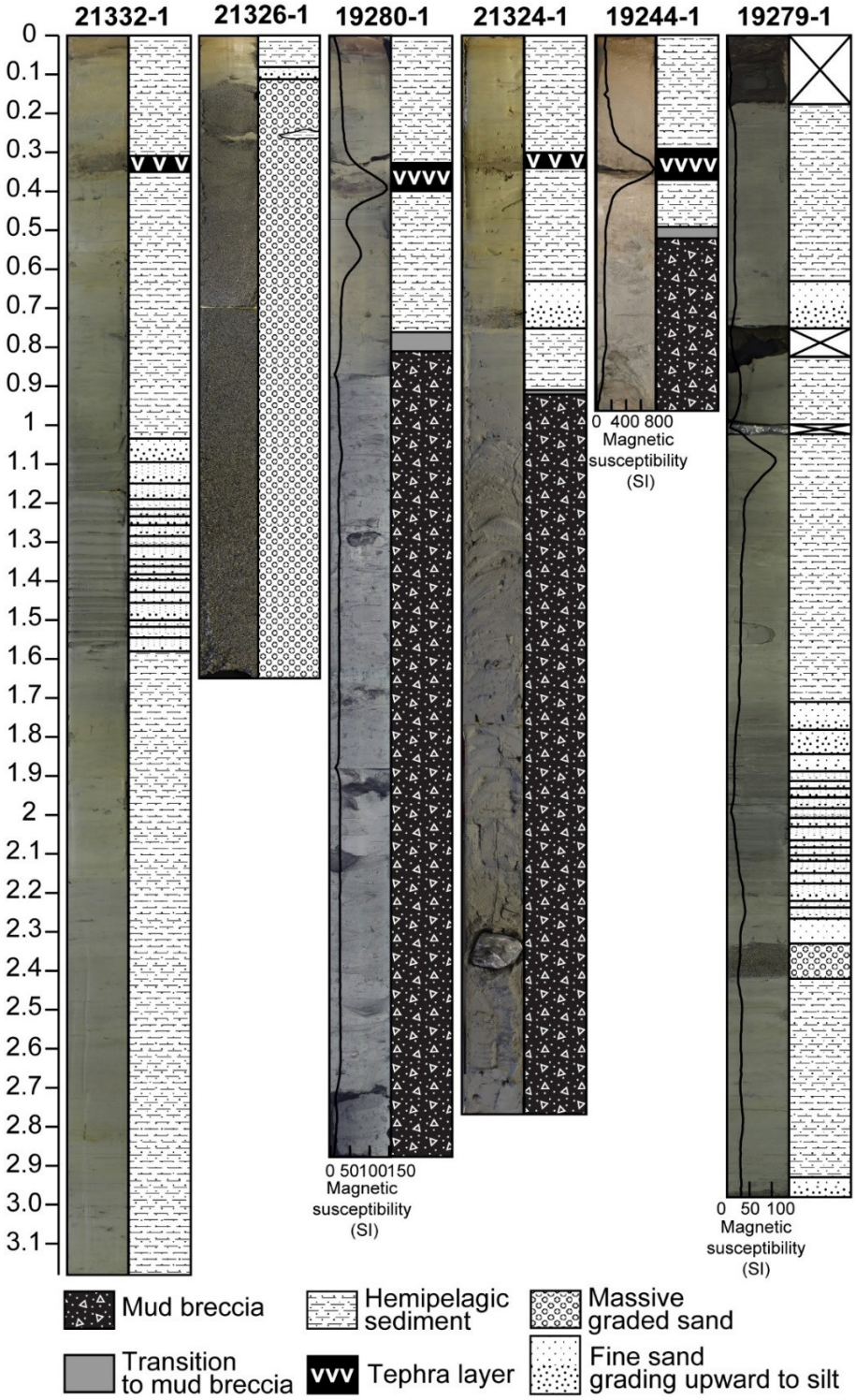


Figure 13.2. Core photos, lithology, and selected magnetic susceptibility profiles for gravity cores used in this study; numbers above cores represent GeoB-identifier, depth axis in m. Magnetic susceptibility of GeoB19279-1 and -19280-1 was acquired at MARUM–University of Bremen by a Geotek multi sensor core logger (MSCL; Geotek Limited, Daventry, UK).

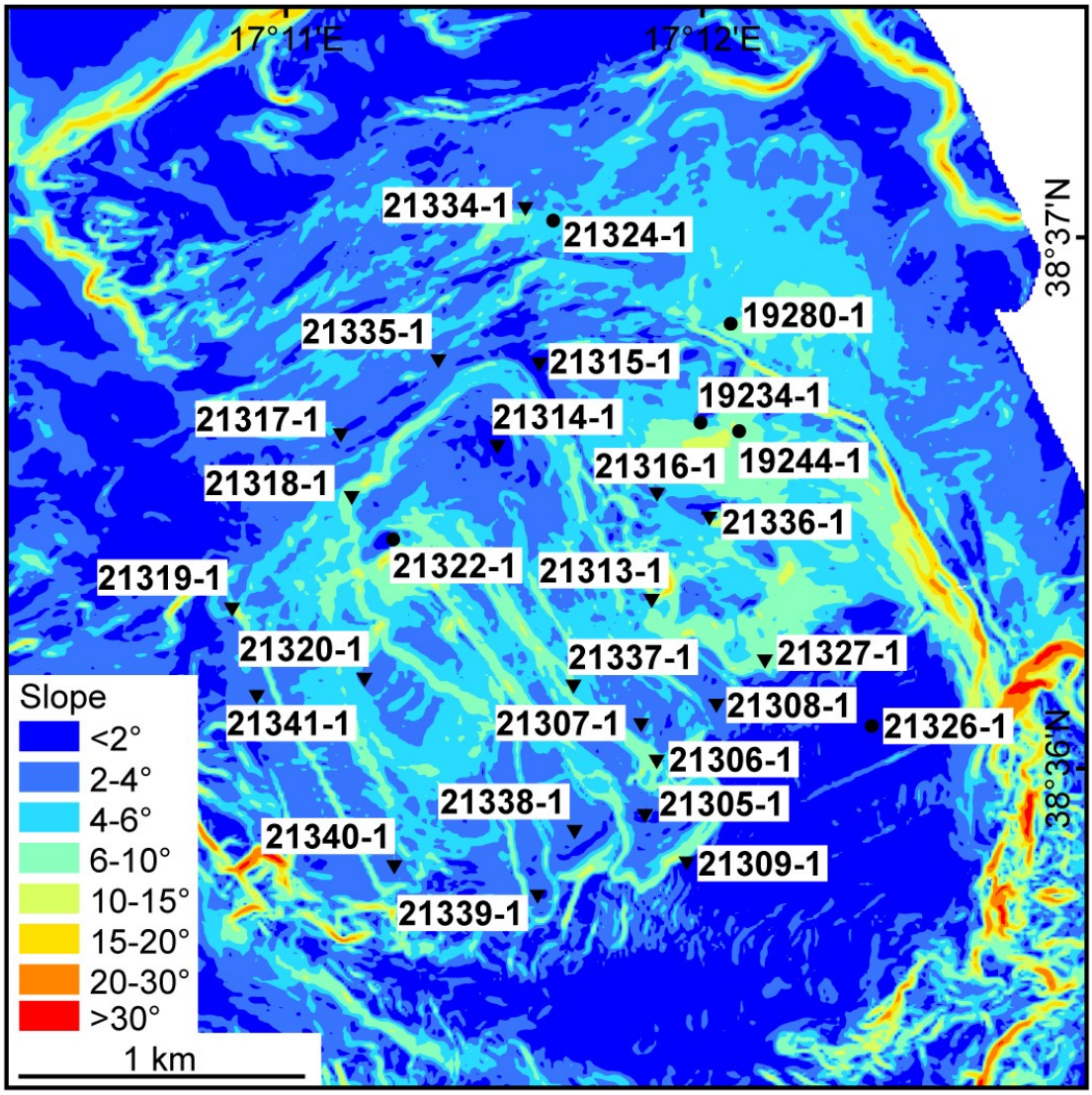


Figure 13.3. AUV-derived slope map (5 m cell size, same extent as in Fig. 6.3) for Venere MV indicating locations of mini-cores (triangles) and gravity cores (circles), numbers refer to GeoB-identifier.

Table 13.12. Results of the WDS analyses from selected glass shards from Core GeoB19234-1 (43–44 cm depth) in normalized weight-% of each compound; note the phonolitic composition of the upper group, the leucite micro-crystal in Ash3 (see also Fig. 4b in main manuscript), the rhyolitic composition of the lower group, standard rhyolite (VG-568) and basalt (VG-A99) materials, and literature values from Polonia et al. (2015), Wulf et al. (2008), and Paterne et al. (1988) used for comparison and tephra identification.

| | | | | Normalized compound weight-% | | | | | | | | |
|---|---|---|---|---|---|---|---|---|---|---|---|---|
| Analysis | $Na_2O$ | MgO | $P_2O_5$ | $K_2O$ | $SO_2$ | FeO | MnO | CaO | $TiO_2$ | $SiO_2$ | $Al_2O_3$ | Original-Total |
| Ash1 | 6.58 | 0.53 | 0.13 | 9.11 | 0.05 | 3.67 | 0.11 | 4.02 | 0.46 | 54.42 | 20.92 | 95.65 |
| Ash1 | 4.83 | 1.05 | 0.22 | 7.77 | 0.00 | 4.02 | 0.00 | 5.19 | 0.51 | 55.35 | 21.06 | 101.46 |
| Ash10 | 5.03 | 0.04 | 0.02 | 11.20 | 0.01 | 1.67 | 0.15 | 2.07 | 0.13 | 58.15 | 21.53 | 99.56 |
| Ash10 | 5.39 | 0.01 | 0.03 | 10.86 | 0.05 | 1.55 | 0.13 | 2.61 | 0.17 | 56.27 | 22.92 | 99.60 |
| Ash2 | 5.76 | 0.12 | 0.01 | 9.86 | 0.06 | 2.29 | 0.15 | 2.56 | 0.22 | 55.94 | 23.03 | 100.38 |
| Ash3 | 7.55 | 0.09 | 0.05 | 7.31 | 0.02 | 1.85 | 0.21 | 3.37 | 0.19 | 56.15 | 23.21 | 98.67 |
| Ash3 | 7.80 | 0.10 | 0.03 | 7.16 | 0.01 | 1.90 | 0.03 | 3.35 | 0.27 | 56.33 | 22.99 | 98.51 |
| Ash4 | 5.98 | 0.03 | 0.00 | 8.92 | 0.05 | 2.14 | 0.28 | 2.47 | 0.17 | 57.06 | 22.90 | 101.80 |
| Ash4 | 7.55 | 0.06 | 0.03 | 8.66 | 0.00 | 1.76 | 0.00 | 2.38 | 0.18 | 56.23 | 23.14 | 102.81 |
| Ash5 | 5.51 | 0.53 | 0.09 | 8.69 | 0.09 | 3.79 | 0.14 | 4.56 | 0.42 | 55.40 | 20.79 | 99.89 |
| Ash5 | 4.85 | 0.57 | 0.30 | 8.80 | 0.08 | 3.75 | 0.21 | 4.55 | 0.48 | 55.54 | 20.87 | 100.33 |
| Ash6 | 5.99 | 0.07 | 0.03 | 10.46 | 0.02 | 2.02 | 0.09 | 2.39 | 0.24 | 55.94 | 22.73 | 98.57 |
| Ash6 | 6.05 | 0.05 | 0.05 | 10.11 | 0.04 | 1.73 | 0.10 | 2.37 | 0.18 | 56.05 | 23.25 | 97.90 |
| Ash7 | 6.01 | 0.42 | 0.17 | 8.59 | 0.04 | 3.07 | 0.15 | 4.21 | 0.38 | 55.99 | 20.97 | 99.71 |
| Average | 6.06 | 0.26 | 0.08 | 9.11 | 0.04 | 2.52 | 0.13 | 3.29 | 0.29 | 56.06 | 22.17 | **Phonolitic** |
| st.dev | 0.99 | 0.31 | 0.09 | 1.25 | 0.03 | 0.92 | 0.08 | 1.03 | 0.13 | 0.85 | 1.05 | |
| Ash3 (Leucite micro-crystal) | 0.76 | 0.00 | 0.04 | 20.59 | 0.01 | 0.65 | 0.00 | 0.04 | 0.08 | 55.00 | 22.83 | 99.58 |
| Ash8 | 3.17 | 0.02 | 0.03 | 5.14 | 0.03 | 1.64 | 0.01 | 0.76 | 0.05 | 75.77 | 13.36 | 97.44 |
| Ash8 | 3.30 | 0.03 | 0.00 | 5.23 | 0.00 | 1.44 | 0.06 | 0.71 | 0.06 | 76.06 | 13.09 | 99.10 |
| Ash9 | 3.01 | 0.03 | 0.05 | 5.37 | 0.00 | 1.78 | 0.07 | 0.81 | 0.05 | 75.76 | 13.07 | 96.18 |
| Ash9 | 2.91 | 0.01 | 0.00 | 5.13 | 0.00 | 1.31 | 0.03 | 0.75 | 0.11 | 76.26 | 13.49 | 96.18 |
| Average | 3.10 | 0.02 | 0.02 | 5.22 | 0.01 | 1.54 | 0.04 | 0.76 | 0.07 | 75.96 | 13.25 | **Rhyolitic** |
| st.dev | 0.18 | 0.01 | 0.03 | 0.11 | 0.02 | 0.21 | 0.03 | 0.04 | 0.03 | 0.24 | 0.21 | |
| **Analyses of standards (Jarosewich et al., 1980)** | | | | | | | | | | | | |
| VG-568 | 3.61 | 0.00 | 0.01 | 5.04 | 0.01 | 0.98 | 0.00 | 0.48 | 0.04 | 77.85 | 12.07 | 100.09 |
| VG-568 | 3.45 | 0.05 | 0.03 | 5.05 | 0.03 | 1.41 | 0.04 | 0.41 | 0.07 | 78.00 | 11.91 | 100.43 |
| Average | 3.53 | 0.03 | 0.02 | 5.04 | 0.02 | 1.19 | 0.02 | 0.45 | 0.05 | 77.93 | 11.99 | **Rhyolite** |
| st.dev. | 0.11 | 0.04 | 0.01 | 0.00 | 0.01 | 0.30 | 0.02 | 0.05 | 0.02 | 0.10 | 0.11 | |
| VG-A99 | 2.74 | 5.17 | 0.56 | 0.86 | 0.00 | 13.86 | 0.05 | 9.40 | 4.00 | 51.44 | 12.41 | 100.50 |
| VG-A99 | 2.69 | 5.15 | 0.56 | 0.89 | 0.00 | 13.43 | 0.16 | 9.13 | 4.21 | 51.52 | 12.57 | 100.31 |
| Average | 2.72 | 5.16 | 0.56 | 0.88 | 0.00 | 13.65 | 0.11 | 9.26 | 4.11 | 51.48 | 12.49 | **Basalt** |
| st.dev. | 0.04 | 0.01 | 0.00 | 0.02 | 0.00 | 0.31 | 0.08 | 0.19 | 0.15 | 0.06 | 0.11 | |
| **Literature values for comparison** | | | | | | | | | | | | |
| Cala 21 (15.5-16.5, mean)* | 6.66 | 0.30 | nr | 8.05 | nr | 3.02 | 0.08 | 3.67 | 0.30 | 55.57 | 21.57 | nr |
| st.dev. | 0.85 | 0.14 | nr | 0.94 | nr | 0.60 | 0.05 | 0.72 | 0.13 | 0.95 | 0.88 | nr |
| Cala 21 (20-21, mean)* | 7.00 | 0.23 | nr | 7.95 | nr | 2.69 | 0.09 | 3.56 | 0.22 | 55.50 | 21.97 | nr |
| st.dev. | 0.87 | 0.15 | nr | 1.08 | nr | 0.73 | 0.07 | 0.89 | 0.15 | 0.49 | 0.77 | nr |
| Z1** | 5.91 | 0.50 | nr | 6.57 | nr | 3.78 | 0.15 | 4.68 | 0.41 | 55.54 | 21.52 | 100.03 |
| 1 sigma | 0.42 | 0.11 | nr | 1.08 | nr | 0.79 | 0.04 | 0.60 | 0.13 | 0.82 | 0.53 | |
| KET8003*** | 3.68 | 0 | nr | 5.4 | nr | 1.68 | nr | 0.67 | 0.09 | 74.77 | 13.7 | 99.99 |
| LIP8206*** | 3.89 | 0.03 | nr | 4.99 | nr | 1.34 | nr | 0.87 | 0.06 | 75.56 | 13.24 | 99.98 |
| *Polonia et al. 2015 | | | ***Paterne et al. 1988 | | | | | | | | | |
| **Wulf et al. 2008 | | | nr = not reported | | | | | | | | | |

## 13.3. Supporting information for manuscript III

### Seafloor sealing, doming, and collapse associated with gas seeps and authigenic carbonate structures at Venere mud volcano, Central Mediterranean

Markus Loher[1,*]; Yann Marcon[1,2]; Thomas Pape[1]; Miriam Römer[1]; Paul Wintersteller[1], Christian dos Santos Ferreira[1]; Marta Torres[3]; Daniel Praeg[4]; Heiko Sahling[1]; Gerhard Bohrmann[1]

[1]MARUM – Center for Marine Environmental Sciences and Department of Geosciences at University of Bremen, Klagenfurter Str., 28359 Bremen, Germany

[2]Alfred Wegener Institute, Helmholtz Centre for Polar and Marine Research, Am Handelshafen 12, 27570 Bremerhaven, Germany

[3]OGS (Istituto Nazionale di Oceanografia e di Geofisica Sperimentale), Borgo Grotta Gigante 42/c, Sgonico, 34010 Trieste, Italy; present address: Institute of Petroleum and Natural Resources, PUCRS, Av. Ipiranga, 6681, 90619-900 Porto Alegre, RS, Brazil
AND Géoazur (UMR7329 CNRS), 250 Rue Albert Einstein,06560 Valbonne, France

[4]College of Earth, Ocean, and Atmospheric Sciences, Oregon State University, 104 CEOAS Administration Building, Corvallis, OR 97331-5503, USA

*corresponding author e-mail: mloher@marum.de

In preparation for submission to *Geo-Marine Letters*. The supplementary data consists of four video files, which can be found on the CD-ROM accompanying this thesis document.

Representative screenshots are shown here.

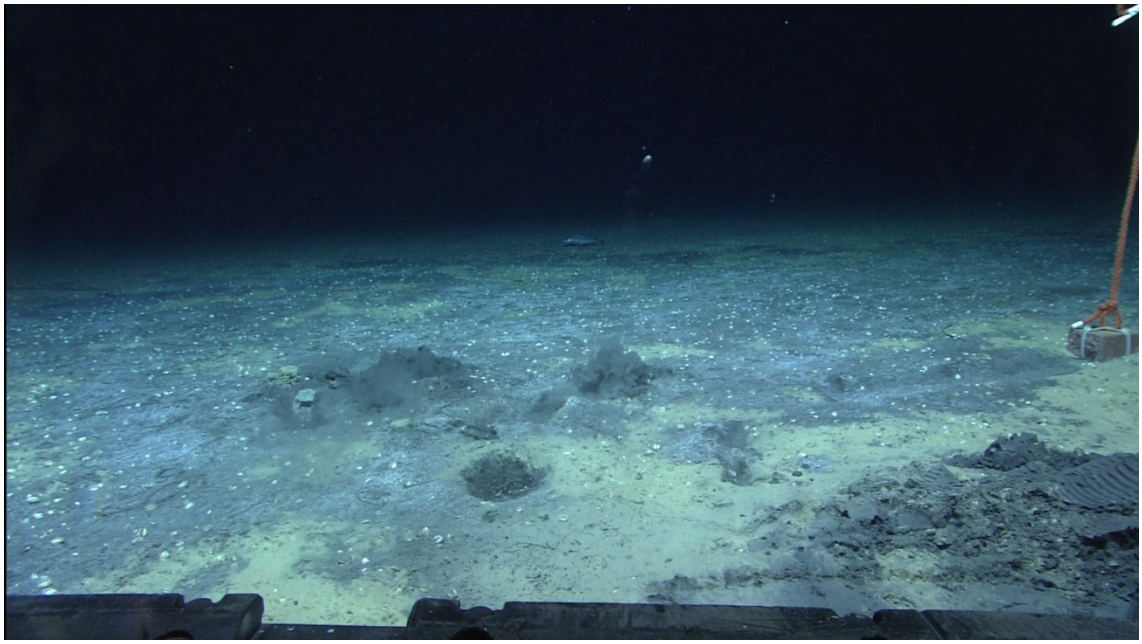

Figure 13.1. Screenshot of movie S1 (see CD-ROM) showing a push-coring location at Site 1 in soft sediments with intense black patches and white microbial mats. An up-floating flake of white material (at the center of the screenshot) is interpreted as a piece gas hydrate.

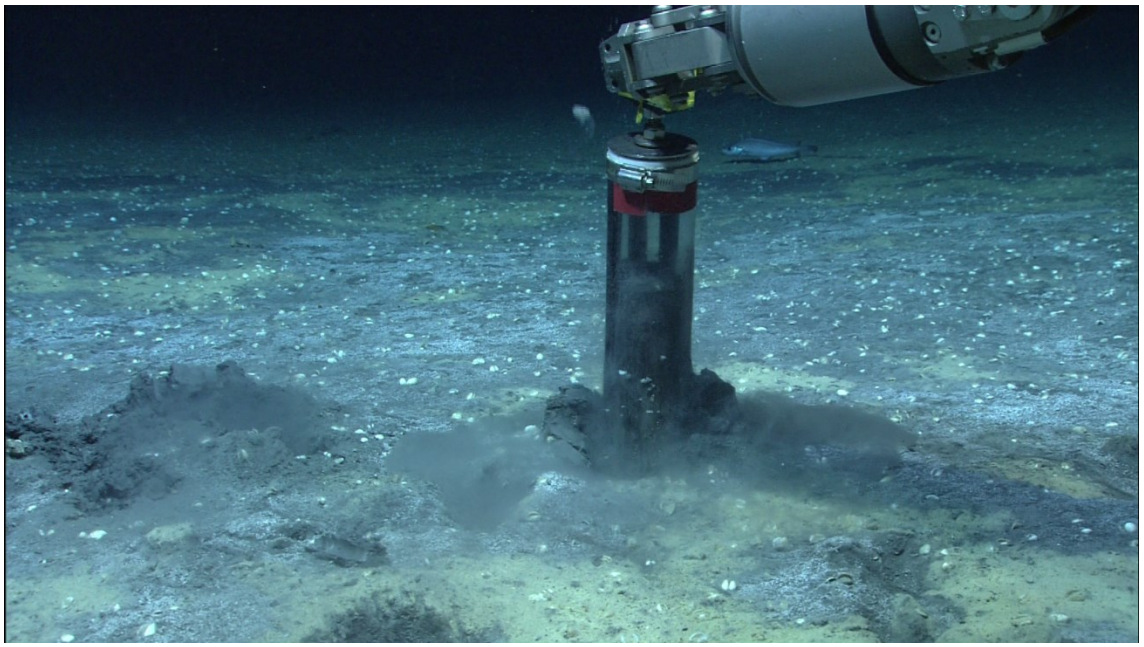

Figure 13.2. Screenshot of movie S2 (see CD-ROM) showing a push-coring location in soft sediment with black patches and white microbial mats at Site 1. An up-floating flake of white material (near the top of the push core in screenshot) is interpreted as a piece gas hydrate.

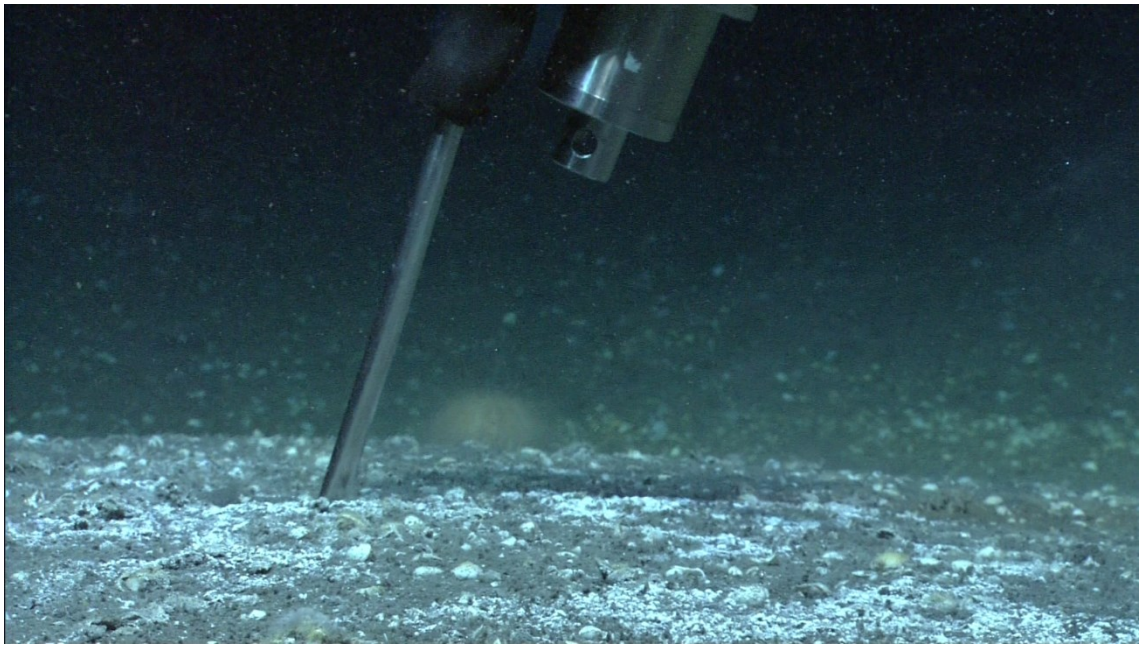

Figure 13.3. Screenshot of movie S3 (see CD-ROM) showing T-stick penetrating a mound at Site 4. Near the site of penetration of the metal rod, disturbances in the water by fluid flow (“Schlieren”) can be made out.

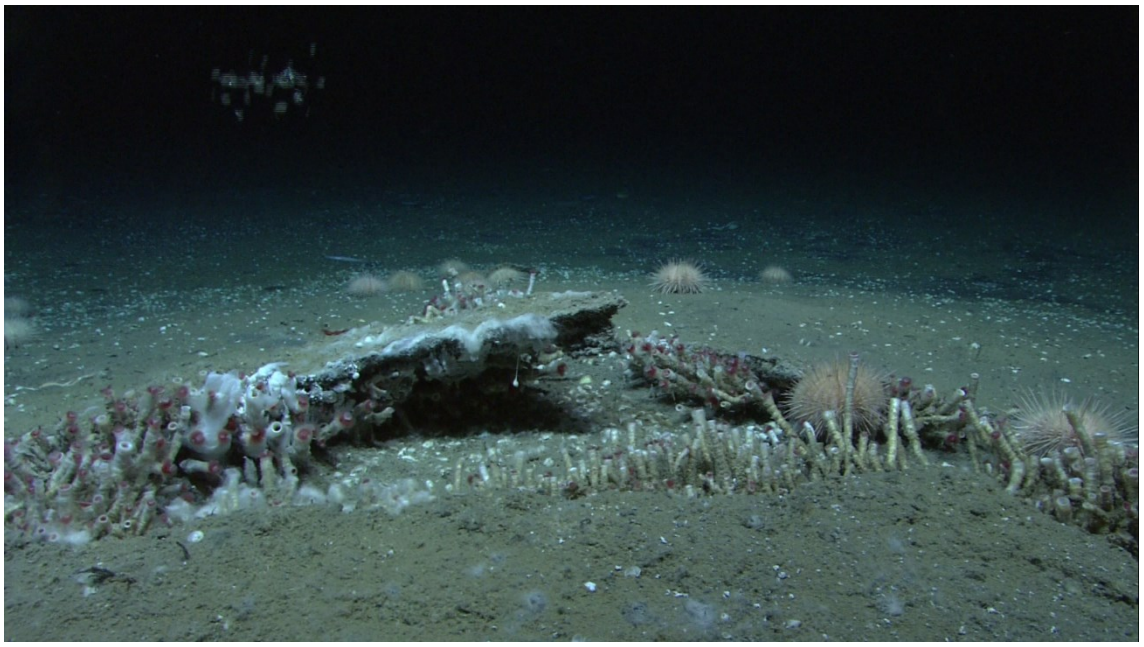

Figure 13.4. Screenshot of movie S4 (see CD-ROM) showing Site 5. An outcropping carbonate slab is colonized by tubeworms and filamentous white microbial mats and forms a ledge that retains ascending gas (not long enough for gas hydrate formation) before releasing it as a pulse of bubbles (upper left) into the water column.

## 13.4. Conference contributions

Poster and oral contribution to the *Gordon Research Conference (GRC) and the Gordon Research Seminar (GRS) – Natural Gas Hydrate Systems*, 27 February to 4 March 2016, Galveston, Texas, USA. The MARUM graduate school GLOMAR is thanked for funding to attend this conference.

### Gas hydrates fueling methane seepage at Venere mud volcano in the Calabrian Arc (Central Mediterranean)

M. Loher, M. Römer, T. Pape, H. Sahling, G. Bohrmann

MARUM - Center for Marine Environmental Sciences, University of Bremen, Department of Geosciences, Klagenfurter Str., 28359 Bremen, Germany

Interactions of gas and gas hydrates in shallow sediments and influences of methane seepage on the seafloor expression were investigated at cold seeps, situated at 1580 to 1625 meters water depth near the Venere mud volcano (Central Mediterranean). The study of these seeps, situated within the gas hydrate stability zone, will help to understand fluid seepage in comparable Mediterranean environments.

Multiple ROV dives explored sub-circular patches of high backscatter which are located at the outer rim of the Venere mud volcano, showing extents of up to several tens of meters. Active gas bubble emissions, a chemosynthetic community of organisms (filamentous bacteria, seep-typical bivalves and vestimentiferans) and cm to dm thick slabs of authigenic carbonate, characterize the cold seeps. Different morphological expressions of the carbonate crusts include domed, ruptured and convex-down structures. The presence of shallow gas hydrates was indicated by methane concentrations exceeding solubilities determined by pressure coring, gravity cores showing intervals of mousse-like sediment texture and up-floating hydrate chips during ROV-based push coring. Moreover, instantaneous gas hydrate precipitation was observed along the funnel of a gas bubble sampler during near-seafloor gas collection. We conclude that gas hydrate is finely dispersed within sediments in the proximity of the active seeps, the extent of which coincide with the high backscatter patches. Similar, such sub-circular patches of high intensity on backscatter maps are known for numerous sites around the world indicating the presence of seep-related features such as authigenic methane-derived carbonates.

We propose a conceptual model in which gas rising from depth accumulates in shallow subsurface sediments and forms fine precipitates of gas hydrate within a certain area of influence of the emission site. The diffusive release of dissolved methane initially fuels the development of active seep communities and over time leads to the growth of authigenic carbonate crusts. Increased buoyancy through gas and / or gas hydrate in the subsurface may cause doming and rupturing of carbonate crusts. In case gas supply from depth ceases, the local gas hydrate accumulation dissolves, the carbonate crusts sag and form a negative morphology as a relic of the former seep site.

Oral contribution to the *13th International Conference on Gas in Marine Sediments (GIMS13)*, 19–22 September 2016, Tromsø, Norway. The MARUM graduate school GLOMAR is thanked for funding to attend this conference.

**Deep-seated fluid seepage at the Venere mud volcano, Calabrian accretionary wedge**

M. Loher[1,*], T. Pape[1], M. Torres[2], M. Römer[1], H. Sahling[1], G. Bohrmann[1]

[1]MARUM - Center for Marine Environmental Sciences and Department of Geosciences at University of Bremen, Klagenfurter Str., 28359 Bremen, Germany

[2]College of Earth, Ocean, and Atmospheric Sciences, Oregon State University, 104 CEOAS Administration Building, Corvallis, OR 97331-5503, USA

*corresponding author e-mail: mloher@marum.de

Deep-seated reactions in accretionary convergent continental margins leads to the generation of hydrocarbons and excess water from mineral dehydration reactions. Mud volcanoes expel sediments and fluids at the seafloor of the accretionary wedge, and the upward migrating fluids provide insights on geochemical processes at depth. The Venere mud volcano is located in ~1600 m water depth in the forearc basin of the Calabrian accretionary wedge, central Mediterranean.

Warm sediment (> 24°C compared to 13.8°C of the ambient bottom water) is currently being extruded from the summit of a ca. 100 m-high mud cone. Fluids in the freshly extruded mud contain high concentrations of methane (up to 4500 µmol/L), show $C_1/C_2$ hydrocarbon ratios in the range of 91-130, and are depleted in chloride to values as low as 125 mmol/L compared to 610 mmol/L of the ambient bottom water. Bathymetric mapping by an autonomous underwater vehicle (AUV) revealed that ring faults structurally control the periphery of the mud volcano cone and seem to provide secondary fluid migration pathways. Exploration by a remotely operated vehicle (ROV) discovered four sites where the ascent of methane-rich fluids has led to the establishment of active chemosynthetic communities, the precipitation of methane-derived authigenic carbonates, and the release of gas bubbles into the water column. At these peripheral sites, the $C_1/C_2$ ratio ranges from 895 to 2370 and porewater freshening is very weak (< 5% that of normal seawater) compared to fluids from the mud volcano summit.

The low $C_1/C_2$ ratios in the Venere summit samples are indicative of a thermogenic hydrocarbon origin whereas the peripheral cold seeps record an admixture of gas sources with a higher fraction of microbial methane. Furthermore, the highly freshened samples (depletion in chloride) point to porewater formation by mineral dehydration processes deep within the accretionary wedge and characterize the end-member fluid involved in sediment mobilization and mud volcanism on the Calabrian accretionary wedge.

In summary, the Venere mud volcano hosts at least two contrasting sedimentological environments, influenced by different modes of fluid migration: the mud volcano summit and the peripheral cold seeps. The fluids provide evidence for geochemical processes responsible for their generation at remote depths and for the mechanisms that drive dewatering and gas seepage processes through this accretionary system.

### 13.5. Additional theses related to this PhD work

The following studies are related to the general scientific context of this PhD thesis and were conducted in the frame of BSc or MSc theses. I gave technical as well as scientific input to this studies and supported the students by providing map figures and by discussing or reviewing their results and writing.

| **Thesis title** | **Name of student and type of thesis** |
|---|---|
| Gas seepage and magnetic susceptibility in sediment cores from Venere mud volcano, Calabrian arc, southern Italy | Rubén Alvarez Gajardo; Master thesis (2016) |
| Kartierung und Interpretation des Aufbaus des Satori-Schlammvulkans vor Kalabrien anhand von Fächerlot-Daten, aufgenommen mit einem autonomen Unterwasserfahrzeug | Sven Kleiner; Bachelor thesis (2017) |
| Bestimmung der Aktivität des Amsterdam Schlammvulkans im Anaximander Gebirge anhand chronologischer Einordnung der Schlammflüsse | Viola Bihler; Bachelor thesis (2016) |
| Stratigraphische Datierung der Schlammflüsse des Venere-Schlammvulkans im kalabrischen Akkretionskeil | Marc Kevin Brand; Bachelor thesis (2016) |
| Geochemische und mineralogische Untersuchungen an authigenen Karbonaten des Venere Schlammvulkans, südöstlich von Kalabrien | Jonas Brünjes; Bachelor thesis (2016) |
| Analyse eines Sedimentkernes vor der Südküste Kalabriens | Denise Knebel; Bachelor thesis (2015) |

## 13.6. Cruise participation

The following gives an overview of all cruises which I participated during my PhD thesis. Although not all of the cruises relate to mud volcanism in the CAP directly (i.e. no specific data contributed to the studies), they were nevertheless important to deepen my understanding of fluid flow systems. In addition, all cruises provided invaluable experiences for practical work on research vessels and a better familiarity with the acquisition of samples, measurements, and workflows for post-processing of data.

| Date | Expedition | Study area | Chief scientists | Tasks |
|---|---|---|---|---|
| 12/02/15 – 28/03/15 | RV METEOR M114 | Southern Gulf of Mexico | Dr. Heiko Sahling<br>Prof. Dr. Gerhard Bohrmann | Hydroacoustics; Sediment sampling and core descriptions; photo mosaicking; ROV dives |
| 25/08/15 – 08/09/15 | FS HEINCKE HE450 | Svalbard Continental Margin | Prof. Dr. Gerhard Bohrmann | Hydroacoustics; Core descriptions |
| 18/04/16 – 01/05/16 | FS POSEIDON POS498 | Anaximander Mud Volcanoes (Eastern Mediterranean) | Dr. Heiko Sahling | Hydroacoustics; Sediment sampling; core descriptions |
| 04/05/16 – 22/05/16 | FS POSEIDON POS499 | Calabrian Accretionary Prism (Central Mediterranean) | Prof. Dr. Gerhard Bohrmann | Hydroacoustics; Sediment sampling; core descriptions |
| 16/01/17 – 18/02/17 | RV METEOR M134 | South Georgia | Prof. Dr. Gerhard Bohrmann | Sediment core logging and description |

## 13.7. Co-author papers

In the following, the title, co-author list and abstract of two manuscripts are presented, which do not count to the cumulative thesis presented above but to which I contributed as a co-author.

The first is published as Sahling et al. (2016) in the journal *Biogeosciences.*

### Massive asphalt deposits, oil seepage, and gas venting support abundant chemosynthetic communities at the Campeche Knolls, southern Gulf of Mexico

Heiko Sahling[1,2], Christian Borowski[2,3], Elva Escobar-Briones[4], Adriana Gaytán-Caballero[4], Chieh-Wei Hsu[1], Markus Loher[2], Ian MacDonald[5], Yann Marcon[6], Thomas Pape[1,2], Miriam Römer[1,2], Maxim Rubin-Blum[3], Florence Schubotz[2], Daniel Smrzka[7], Gunter Wegener[2,3], and Gerhard Bohrmann[1,2]

**Abstract**

Hydrocarbon seepage is a widespread process at the continental margins of the Gulf of Mexico. We used a multidisciplinary approach, including multibeam mapping and visual seafloor observations with different underwater vehicles to study the extent and character of complex hydrocarbon seepage in the Bay of Campeche, southern Gulf of Mexico. Our observations showed that seafloor asphalt deposits previously only known from the Chapopote Knoll also occur at numerous other knolls and ridges in water depths from 1230 to 3150 m. In particular the deeper sites (Chapopopte and Mictlan knolls) were characterized by asphalt deposits accompanied by extrusion of liquid oil in form of whips or sheets, and in some places (Tsanyao Yang, Mictlan, and Chapopote knolls) by gas emission and the presence of gas hydrates in addition. Molecular and stable carbon isotopic compositions of gaseous hydrocarbons suggest their primarily thermogenic origin. Relatively fresh asphalt structures were settled by chemosynthetic communities including bacterial mats and vestimentiferan tube worms, whereas older flows appeared largely inert and devoid of corals and anemones at the deep sites. The gas hydrates at Tsanyao Yang and Mictlan Knolls were covered by a 5-to-10 cm-thick reaction zone composed of authigenic carbonates, detritus, and microbial mats, and were densely colonized by 1–2 m long tube worms, bivalves, snails, and shrimps. This study increased knowledge on the occurrences and dimensions of asphalt fields and associated gas hydrates at the Campeche Knolls. The extent of all discovered seepage structure areas indicates that emission of complex hydrocarbons is a widespread, thus important feature of the southern Gulf of Mexico.

[1]Department of Geosciences at the University of Bremen, Klagenfurter Str., 28359 Bremen, Germany; [2]MARUM Center for Marine Environmental Sciences, Leobener Str., 28359 Bremen, Germany; [3]Max-Planck Institute for Marine Microbiology, Celsiusstr. 1, 28359 Bremen, Germany : [4]Universidad Nacional Autónoma de México, Instituto de Ciencias del Mar y Limnología, A. P. 70-305 Ciudad Universitaria, 04510 Mexico City, México; [5]Florida State University, P.O. Box 3064326, Tallahassee, FL 32306, USA; [6]Alfred Wegener Institute Helmholz Centre for Polar and Marine Research, HGF-MPG Group for Deep Sea Ecology and Technology, Am Handelshafen 12, 27570 Bremerhaven, Germany; [7]Center for Earth Sciences, University of Vienna, Althanstr. 14, 1090 Vienna, Austria.

The second is published as Mau et al. (2017) in the journal *Nature Scientific Reports.*

## Widespread methane seepage along the continental margin off Svalbard - from Bjørnøya to Kongsfjorden

S. Mau[1], M. Römer[1], M. E. Torres[2], I. Bussmann[3], T. Pape[1], E. Damm[3], P. Geprägs[1], P. Wintersteller[1], C.-W. Hsu[1], M. Loher[1] & G. Bohrmann[1]

**Abstract**

Numerous articles have recently reported on gas seepage offshore Svalbard, because the gas emission from these Arctic sediments was thought to result from gas hydrate dissociation, possibly triggered by anthropogenic ocean warming. We report on findings of a much broader seepage area, extending from 74° to 79°, where more than a thousand gas discharge sites were imaged as acoustic flares. The gas discharge occurs in water depths at and shallower than the upper edge of the gas hydrate stability zone and generates a dissolved methane plume that is hundreds of kilometer in length. Data collected in the summer of 2015 revealed that 0.02–7.7% of the dissolved methane was aerobically oxidized by microbes and a minor fraction (0.07%) was transferred to the atmosphere during periods of low wind speeds. Most flares were detected in the vicinity of the Hornsund Fracture Zone, leading us to postulate that the gas ascends along this fracture zone. The methane discharges on bathymetric highs characterized by sonic hard grounds, whereas glaciomarine and Holocene sediments in the troughs apparently limit seepage. The large scale seepage reported here is not caused by anthropogenic warming.

[1]MARUM – Center for Marine Environmental Sciences and Department of Geosciences, University of Bremen, Klagenfurter Str., 28359 Bremen, Germany. [2]College of Oceanic and Atmospheric Sciences, Oregon State University, 104 Ocean Admin Building, Corvallis, Oregon 97331–5503, USA. [3]Alfred Wegener Institute Helmholtz Centre for Polar and Marine Research, Am Handelshafen 12, 27570 Bremerhaven, Germany. Correspondence and requests for materials should be addressed to S.M. (email: smau@marum.de).

## 13.8. Versicherung an Eides Statt

### Versicherung an Eides Statt / *Affirmation in lieu of an oath*

**gem. § 5 Abs. 5 der Promotionsordnung vom 15.07.2015 /**
***according to § 5 (5) of the Doctoral Degree Rules and Regulations of 15 July, 2015***

Ich / I, Markus Loher, Karolinastrasse 8, 28195 Bremen, 3018969
(Vorname / First *Name*, Name / *Name*, Anschrift / *Address*, ggf. Matr.-Nr. / *student ID no., if applicable)*

versichere an Eides Statt durch meine Unterschrift, dass ich die vorliegende Dissertation selbständig und ohne fremde Hilfe angefertigt und alle Stellen, die ich wörtlich dem Sinne nach aus Veröffentlichungen entnommen habe, als solche kenntlich gemacht habe, mich auch keiner anderen als der angegebenen Literatur oder sonstiger Hilfsmittel bedient habe und die zu Prüfungszwecken beigelegte elektronische Version (PDF) der Dissertation mit der abgegebenen gedruckten Version identisch ist. / *With my signature I affirm in lieu of an oath that I prepared the submitted dissertation independently and without illicit assistance from third parties, that I appropriately referenced any text or content from other sources, that I used only literature and resources listed in the dissertation, and that the electronic (PDF) and printed versions of the dissertation are identical.*

Ich versichere an Eides Statt, dass ich die vorgenannten Angaben nach bestem Wissen und Gewissen gemacht habe und dass die Angaben der Wahrheit entsprechen und ich nichts verschwiegen habe*. / I affirm in lieu of an oath that the information provided herein to the best of my knowledge is true and complete.*

Die Strafbarkeit einer falschen eidesstattlichen Versicherung ist mir bekannt, namentlich die Strafandrohung gemäß § 156 StGB bis zu drei Jahren Freiheitsstrafe oder Geldstrafe bei vorsätzlicher Begehung der Tat bzw. gemäß § 161 Abs. 1 StGB bis zu einem Jahr Freiheitsstrafe oder Geldstrafe bei fahrlässiger Begehung. / *I am aware that a false affidavit is a criminal offence which is punishable by law in accordance with § 156 of the German Criminal Code (StGB) with up to three years imprisonment or a fine in case of intention, or in accordance with § 161 (1) of the German Criminal Code with up to one year imprisonment or a fine in case of negligence.*

Bremen, den
Ort / *Place*, Datum / *Date*

Unterschrift / *Signature*